University of Southern Queensland
Faculty of Engineering and Surveying

A Conprehensive Study of Footing on c-ϕ Soil Slopes - Numerical and Physical Modelling

A dissertation submitted by

Andrew James Shorten Cole

In fulfilment of the requirements of

Courses ENG4111 and ENG4112 Research Project

towards the degree of

Bachelor of Engineering (CIVIL)

Submitted: November, 2009

Abstract

The problem of a footing being located on a slope is one which is encountered regularly and must be understood so that catastrophic failure of structures causing death or injury does not occur. This research project is split into two different but still related sections aimed at providing a greater understanding of the footing on slope problem.

This project will initially undertake a numerical study to see what effect geometrical and material properties have on the bearing capacity of a footing located on a slope, with non-dimensional parameters used to highlight these effects. These parameters include dimensionless strength ratio, footing distance ratio, slope height ratio and soil internal friction angle which in this paper have been analysed more comprehensively then previously done before. FLAC will be used as the analysing software with the results obtained from these analyses are presented in design charts making the information easy to understand and use.

A number of physical modelling cases will then be performed, in an attempt to validate the results produced from FLAC for a purely cohesive soil against real-world testing. A number of test samples will be set up for a range of slope specifications and tested. The results will be analysed and compared with previously derived FLAC results to see if a common result is produced between the two very different methods whilst allowing for an acceptable amount of variation. Once the physical modelling is completed it will open the door for a larger range of modelling scenarios to be attempted in both the footing on slope problem area and in other geotechnical areas such as piles and anchors.

University of Southern Queensland

Faculty of Engineering and Surveying

ENG4111 Research Project Part 1 & ENG4112 Research Project Part 2

Limitations of Use

The Council of the University of Southern Queensland, its Faculty of Engineering and Surveying, and the staff of the University of Southern Queensland, do not accept any responsibility for the truth, accuracy or completeness of material contained within or associated with this dissertation.

Persons using all or any part of this material do so at their own risk, and not at the risk of the Council of the University of Southern Queensland, its Faculty of Engineering and Surveying or the staff of the University of Southern Queensland.

This dissertation reports an educational exercise and has no purpose or validity beyond this exercise. The sole purpose of the course ”Project and Dissertation” is to contribute to the overall education within the student’s chosen degree programme. This document, the associated hardware, software, drawings, and other material set out in the associated appendices should not be used for any other purpose: if they are so used, it is entirely at the risk of the user.

Prof Frank Bullen
Dean
Faculty of Engineering and Surveying

Certification

I certify that the ideas, designs and experimental work, results, analyses and conclusions set out in this dessertation are entirely my own effort, exept where otherwise indicated and acknowledged.

I further certify that the work is original and has not been previously submitted for assessment in any other course of institution, except where specifically stated.

Andrew James Shorten Cole

Student Number: 0050057529

Signature

Date

Acknowledgements

I would like to thank Dr. Jim Shiau for his support and professional advice whilst I undertook this project. His expert knowledge in the geomechanics field was always available for any problems encountered and his guidance was greatly appreciated throughout the year.

I would also like the thank Dean Beliveau for his time and effort put into the software used with the physical modelling. His input ensured a reliable program was created which proved very easy to use, and if any problems in the software were found he was more then happy to help rectify the situation.

Finally I would like to thank my family and friends for their help during this project. In particular I would like to thank Nathan Lyle and Joseph Marstella for their help throughout the physical modelling stage.

Table of Contents

List of Figures

List of Tables

Nomenclature

The principal symbols used are presented in the following list. Other symbols used within this paper not mentioned in this list are less common and defined in their relevant sections.

B	footing width
H	slope height
D	distance of footing from edge of slope
D/B	footing distance ratio
H/B	slope height ratio
D_f	depth of footing embedment
c	soil cohesion
ϕ	friction angle of soil
γ	unit weight of soil
β	slope angle
$c/\gamma B$	dimensionless strength ratio, also referred to as SR
$p/\gamma B$	normalised bearing capacity
p	average pressure beneath footing
q_u	ultimate bearing capacity
q_a	allowable bearing capacity
FLAC	Fast Lagrangian Analysis of Continua

Project Introduction

1

1.1 Footing on Slope Problem Statement

The footing on slope problem is encountered extremely often within the engineering field. This can be in the form of a bridge abutment, construction of an underground carpark alongside an existing building, a building placed on the side of a hill to take advantage of the views, or anywhere where a footing is located near a slope due to area restraints.

The bearing capacity of a particular slope is the main focus in this study, and is effected by many factors including the height of the slope, the distance the footing is from the edge of the slope and the material the slope is made of. It is these factors that need to be looked into in order to gain a better understanding of the problem and be able to provide reliable information so that future footing on slope situations can be more easily and accurately analysed.

1.2 Research Aims and Objectives

The research work involved in this project is comprised of two related, but yet still very different areas.

The aim of the first part involves using FLAC analysis software (explained in section 1.4) and is based on soils of a cohesive-granular nature, known as $c - \phi$ soils. These soils are known as sandy soils and unlike clay, which has a high internal cohesion force but zero internal friction, have lower internal cohesive force but positive internal friction. They are not completely sand soils though as these have high internal friction but almost zero cohesive force.

FLAC will be used to study the effects of the slope height, the distance of the footing from the edge of the slope, and the internal specifications of the slope material to determine what the maximum bearing capacity of a slope is before failure will occur. There has been some work done in this area however in the past most study has been performed on clay based slopes due to the easier analysis involved with one less parameter (internal friction) needing to be incorporated in the script file used to obtain results. The work that has been done is far from comprehensive though so this project will aim to develop a more comprehensive set of results for cohesive-granular soils. These results will then be used to develop a set of design charts that could be used to approximate the bearing capacity of a particular slope.

The aim of the second part of the project is to perform physical modelling using clay material samples. These clay samples would be created to represent slopes of specific dimensions and tested using a loading rig to determine the maximum capacity values reached before slope failure occurred. These results will then be compared with results from numerical analysis obtained from FLAC that have been derived previously to see whether or not the computer modelling results can be replicated using physical modelling and vice versa.

The main objectives of this project to fulfill the intended aims are:

- researching background information on the footing on slope problem.
- reviewing previous studies on the problem.
- performing the numerical analysis on cohesive-granular material.
- creating design charts using this data.
- performing to physical modelling and comparing these results with the relevant numerical results.

1.3 Clay and Sand Numerical Model Differences

As mentioned in the previous section there are a number of differences between using pure clay and sandy material in a slope analysis due to the different parameters if each material.

As mentioned previously, clay has a very high cohesive force and zero internal friction angle. This cohesive force is due to the cementation of the clay particles and the greater the concentration of clay particles in a soil the larger the cohesive force will be. The magnitude of the cohesive force can also be attributed to the size of each individual particle as smaller particles will have more surface area able to bond with adjacent particles, with less air voids within the material to act as weak zones. The zero internal friction angle of clay is due to the shape of each individual particle. Clay particles are considered to be perfectly round and as such have great difficulty stacking on top of each other. This could be best demonstrated by trying to stack a number of basketballs on top of each other, which we know would be very unstable. This zero friction angle is why when clay is poured in a pile it does not maintain a cone formation.

As mentioned sand on the other hand has low cohesive force but very high internal friction. Unlike clay, sand has a larger particle size as therefore has less surface area of each particle able to bond with adjacent particles. This larger particle size also results in greater concentration of air voids within the material creating weak zones around each particle. The high internal friction of sand is again related to the shape of each particle but is high for sand due to the angular surface of each particle. This does not allow particles to roll freely past each other and is the reason why when poured in a pile sand will hold a cone formation. This would be best demonstrated by stacking broken brick pieces on top of each other, which while not rectangular and able to create a vertical surface, they are much more easily stacked then basketballs.

Within the FLAC program this creates boundary problems due to the different friction angles of the two materials (the effect of different friction angles is discussed in a later chapter) which means the same numerical model cannot be used for clay as for sand. The extra friction within a sand soil model means a larger slope size needs to be analysed creating longer run times to obtain the same type of results. It also means that a slightly different script file needs to be created (purpose of script file explained in section 1.4).

1.4 Brief Introduction to FLAC

FLAC stands for Fast Lagrangian Analysis of Continua and is a software program designed to analyse the effect of a footing on a slope (or flat ground for that matter). To do this it utilises a script file that tells the program the values of the parameters that are needed such as the height of the slope, the distance of the footing from the edge of the slope, the strength of the slope material, the coarseness (internal friction) of the material and the angle of the slope from the horizontal.

Using these parameter values FLAC creates the appropriate model that satisfies all the conditions set out in the script file. These conditions are created to ensure there are no boundary problems which can cause unreliable results and include such things as a footing placed far away from a slope on a high friction angle material will have slope dimensions larger then that of a footing placed at the same location on a slope of low friction angle material.

The script file also includes the types of output from the program required by the user. These include both text files and jpeg images, with each output demonstrating a different result that is useful when analysing footings on slopes. The text files output include the maximum normalised bearing capacity of the slope that was reached, the CPU time that was taken to analyse the slope and the general information about the slope that was analysed. The jpeg images also include the normalised bearing capacity and CPU time expressed in a graphical form, as well as diagrams showing the deformed shape after the load was applied as well as the strain recorded in the soil along the failure surface. An example jpeg that is output is shown in Figure 1.1. This jpeg is of the strain in the soil along the failure plane and will be used throughout the numerical analysis of this project.

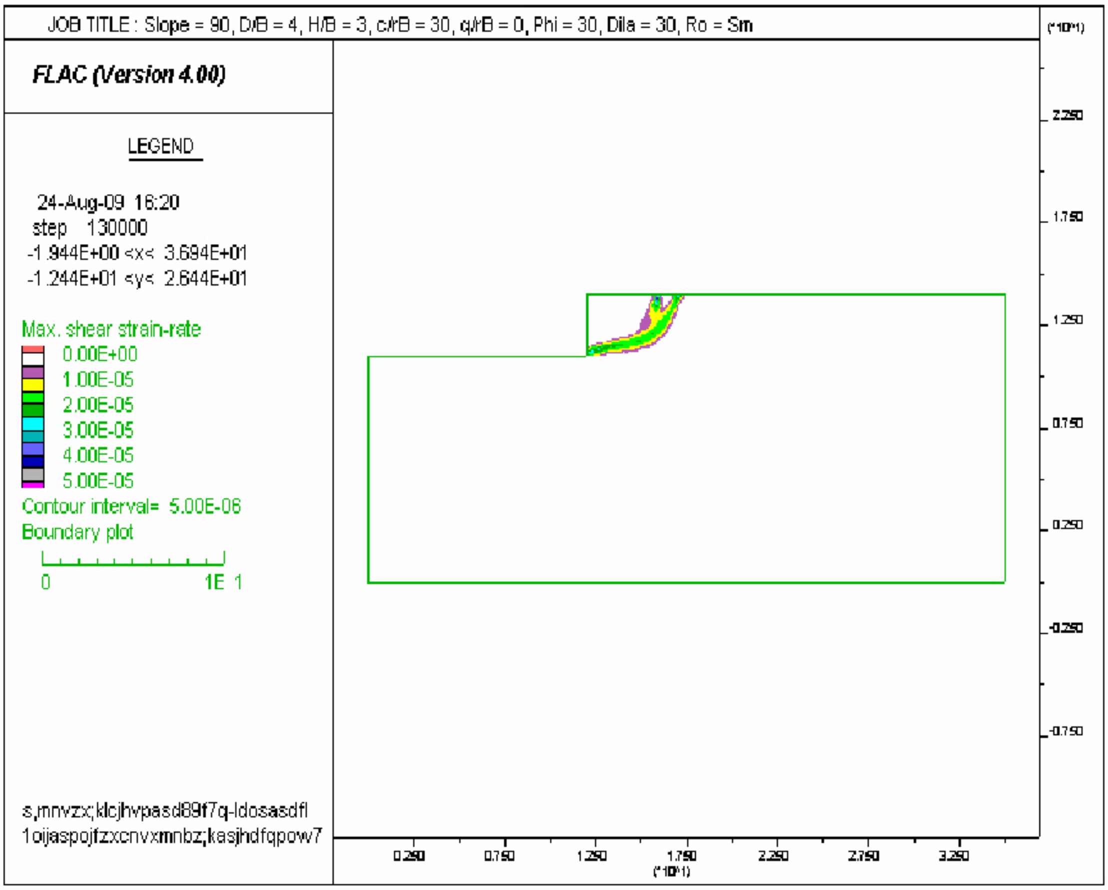

Figure 1.1: Typical jpeg output from FLAC

While there are many options and possible variables within the FLAC script file, only a few were required to be changed for each different slope case for this study. As this project is not focussed a great deal on how the software works but rather the results it outputs, the complex sections of the script which enable results to be obtained were not learnt, rather only the important sections were focussed on to ensure reliable results.

Figure 1.2 shows a screenshot of the FLAC program when running as it is analysing a slope case.

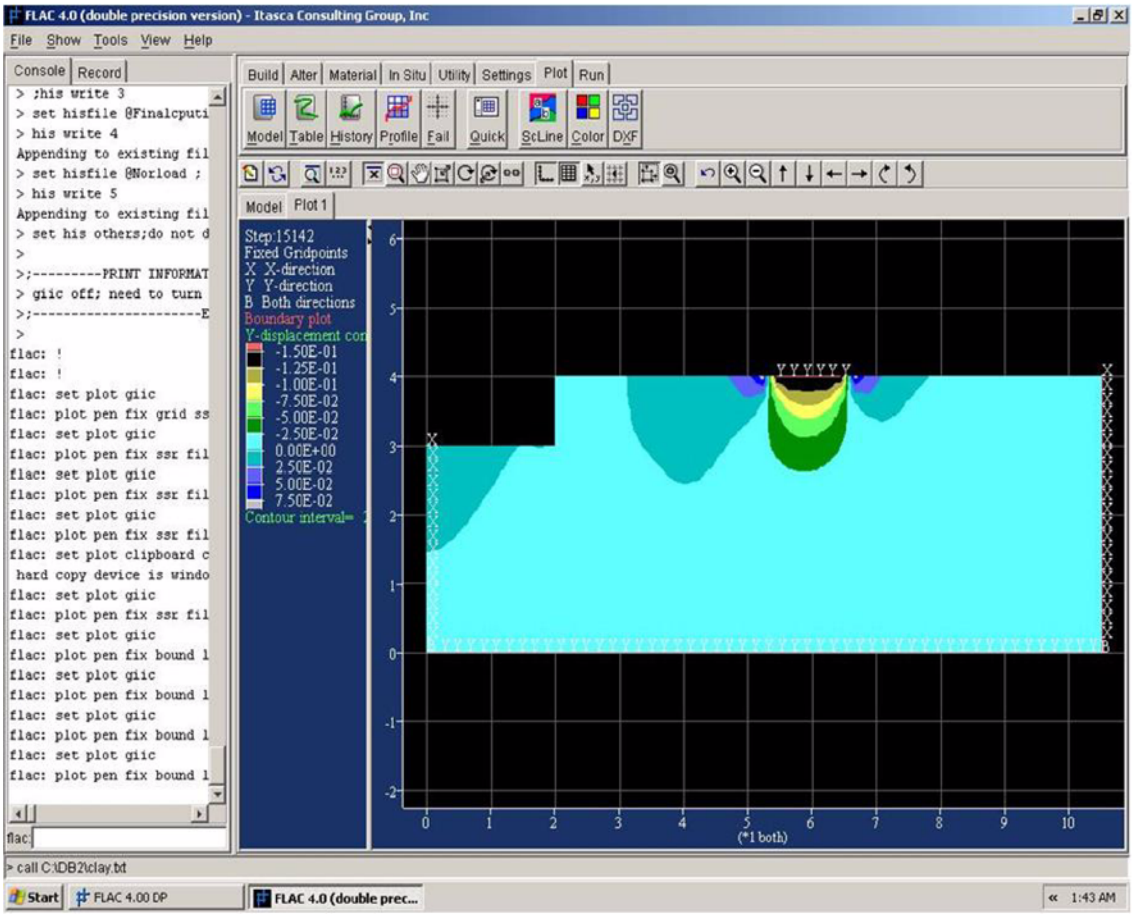

Figure 1.2: Screenshot of FLAC software program

Literature Review

2

2.1 Introduction

The footing on slope problem has been around for many years and as such there have been a number of theories developed to try and determine what the bearing capacity of a particular slope is. These theories have eventuated due to the complex nature of the footing on slope problem so each researcher has developed a method that they find the best for approximating bearing capacity.

This chapter will take a look at the various theories that have been developed over the years, as well as important terms to understand such as failure modes and the types of capacity terms that are regularly used. Finally it will take a look at work that has been completed by previous USQ students.

2.2 Shallow Foundations

The foundations of a building is what transfers the load of the building to the material lying underneath. This underlying material is what the building relies on to ensure that is does not collapse or topple over. When the material is weak very large foundations need to be used to make certain that enough resistance will be able to be provided by the material so that the building load will be supported and a failure will not occur.

These shallow foundations are also known as footings, such as what is referred to throughout this paper. The main requirement to classify a footing as a shallow foundation is for the depth of embedded footing to be less then the width of the footing, or $D_f/B \leq 1$.

As this study places the footing on the top of the underlying material this requirement is obviously satisfied.

2.3 Bearing Capacities

There are 2 types of bearing capacities when referring to a footing on a slope– ultimate bearing capacity and allowable bearing capacity.

2.3.1 Ultimate Bearing Capacity

Ultimate bearing capacity refers to the force that is being applied when a failure occurs. This failure usually occurs as a shear failure however excessive settlement cause also be experienced. Even without immediate shear failure the effects of settlement can be noticed with doors that wont shut or open, cracks forming in brickwork or plaster, or if in a workshop machinery may not function as it should such as a railway mounted hoist. The shear failure that occurs can be of three forms– general, local or punching shear failure. The ultimate bearing capacity corresponding to each shear mechanism will be varied due to different magnitudes of shear force required to generate each failure. The shear failures will be discussed in section 2.4. Throughout this paper all bearing capacities recorded, be they dimensionless or not, will be ultimate bearing capacities unless stated otherwise to indicate the load at which failure would occur.

2.3.2 Allowable Bearing Capacity

Allowable bearing capacities are obtained by using the ultimate bearing capacity for a material underlying a foundation and applying a safety factor to it. This reduces the bearing capacity value in an attempt to ensure that failure will not occur. The calculation to determine allowable bearing capacity is as simple as $q_{all} = q_{ult}/FS$ where FS equals the safety factor. The purpose of applying a safety factor is to account for inconsistencies within the foundation supporting material, such as variations in the strength of the natural material, the effects of weathering that may have occurred, or even the simple case of cracking within the soil due to dry weather creating zones of little resistance to movement.

2.4 Failure Modes

2.4.1 General Shear Failure

General shear failure occurs when rupturing of the material underneath the footing takes place. This rupturing is due to the underlying soil having little compressibility, and as such is usually found occurring in dense sand or hard clay soils. This rupturing causes heaving to be observed on either side of the footing. The heaving is due to the triangle section of soil beneath the footing moving with the footing as it settles and forcing soil either side of this triangle section to move horizontally and towards the surface. When failure occurs it is usually only on one side of the footing causing the footing to tilt and leading to catastrophic failures such as toppling. Figure 2.1 shows the prominent heaving associated with general shear failure and the load-displacement curve that is produced.

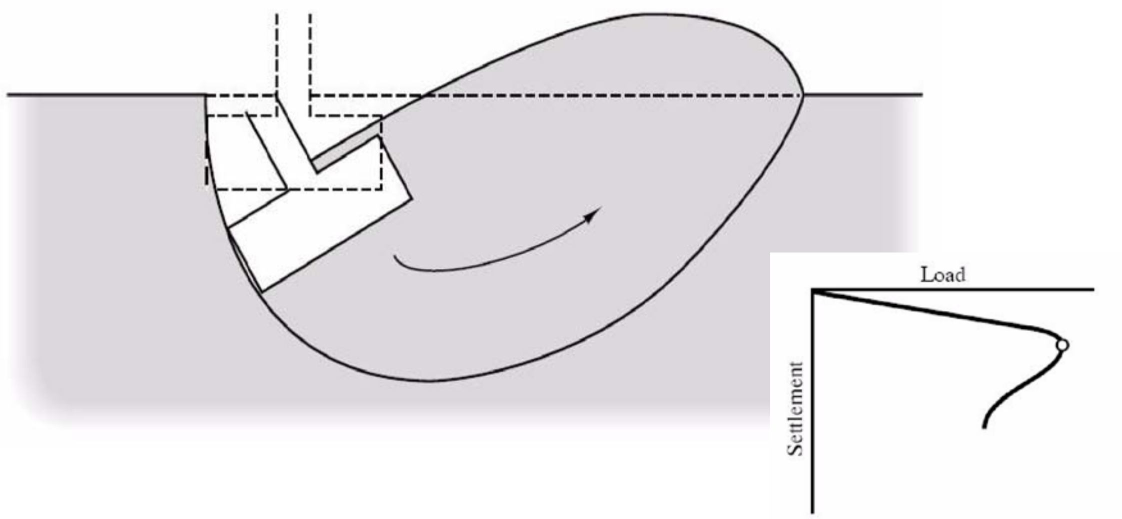

Figure 2.1: General shear failure plane and load-displacement curve

2.4.2 Local Shear Failure

This type of failure is typically found in soils of a compressible nature. This leads to large settlement of the footing with very little heaving of the surface being observed and is most likely to occur in loose sandy soils, silty sands and weak clays. In the case of local shear failure no tilting of the footing is expected rather only settlement should occur. This can be attributed to an undefined shear path except for directly underneath the footing and results in only partial plastic equilibrium. Figure 2.2 shows how slight heaving occurs for local shear failure and the load-displacement curve associated with it.

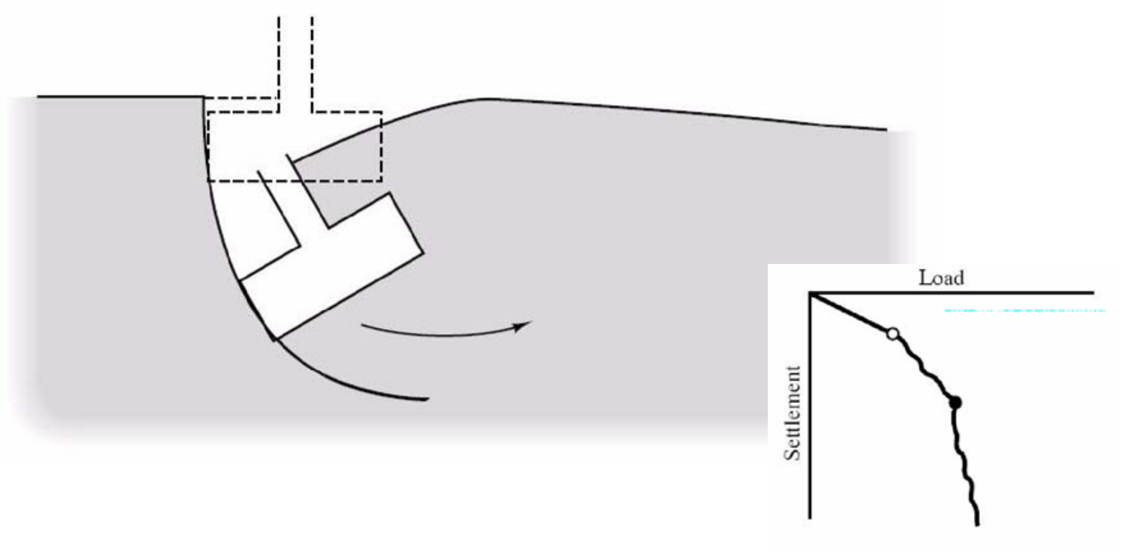

Figure 2.2: Local shear failure plane and load-displacement curve

2.4.3 Punching Shear Failure

Punching shear failure usually occurs in soils of high compressibility such as loose sands. The soil beneath the footing compacts as settlement occurs with no heaving or horizontal displacement of material happening. A vertical shear plane between the edge of the footing and the soil is developed with insignificant plastic equilibrium being developed. A catastrophic failure will not occur however the settlement that does eventuate is usually unacceptable. Figure 2.3 shows the settlement of the footing with no heaving occurring and the load-displacement curve that occurs.

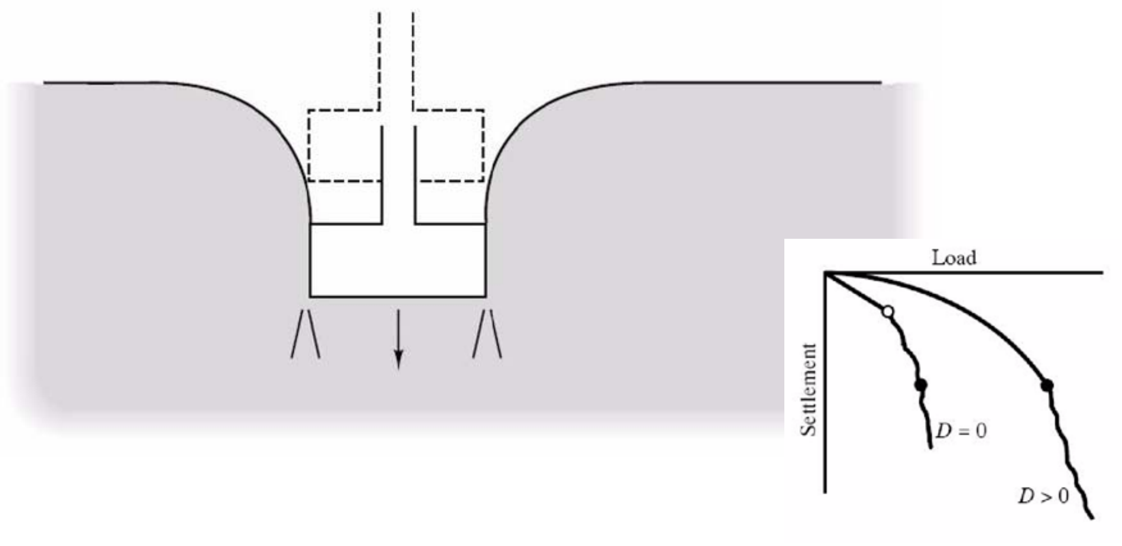

Figure 2.3: Punching shear failure plane and load-displacement curve

2.5 Footing on Flat Ground Theories

2.5.1 Terzaghi's Level Ground Bearing Capacity Theory

Terzaghi (1943) was the first to suggest a theory for predicting the bearing capacity of footings. These footings were considered shallow foundations with an embedment depth of $D_f/B \leq 1$ and as a strip footing of infinite length. Terzaghi's equation is shown in equation 1.1.

$$q_u = cN_c + qN_q + 1/2\,\gamma BN_\gamma \tag{1.1}$$

where:
- c = soil cohesion
- q = surcharge loading (γD_f)
- γ = unit weight of soil
- B = footing width
- N_c, N_q, N_γ = non-dimensional bearing capacity factors related to the friction angle of the soil.

Examples of Terzaghi's bearing capacity factors (N_c, N_q, N_γ) are shown in Table 2.1.

Table 2.1: Example Terzaghi factor values

ϕ	N_c	N_q	N_γ
0	5.7	1	0
5	7.3	1.6	0.5
10	9.6	2.7	1.2
15	12.9	4.4	2.5
20	17.7	7.4	5
25	25.1	12.7	9.7
30	37.2	22.5	19.7
35	57.8	41.4	42.4
40	95.7	81.3	100.4

Terzaghi's theory utilises the idea that the structure load (P) being applied to the footing is supported by 3 shear zones within the soil beneath the footing, shown in Figure 2.4.

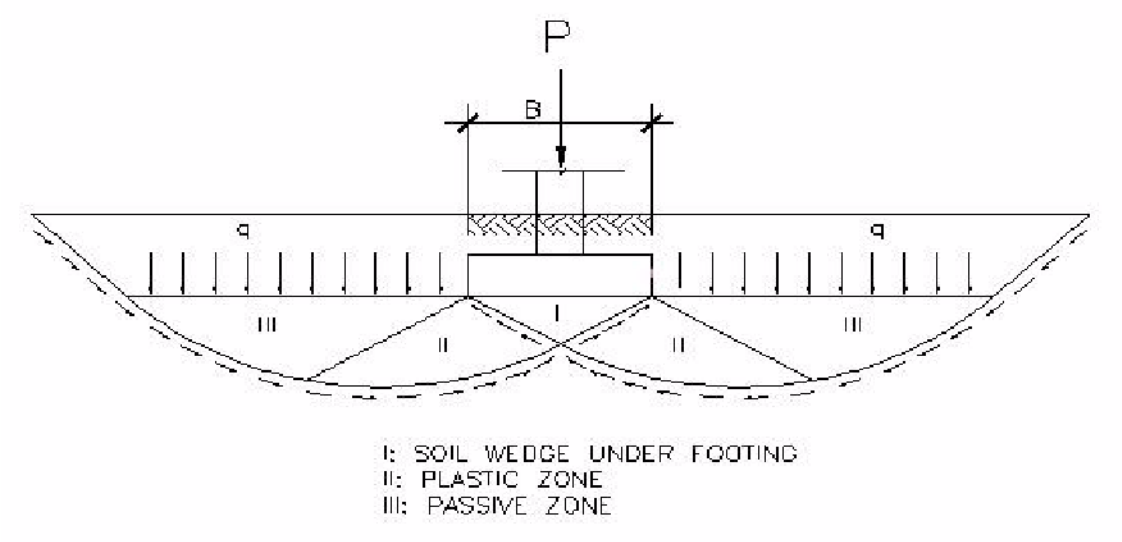

Figure 2.4: Shear zones based on Terzaghi's theory

Terzaghi made a number of assumptions when creating his theory which included:

• the footing was continuous.

• the soil mass above the footing was replaced with an equivalent surcharge.

• the shear resistance of the soil above the footing is neglected.

• the soil wedge beneath the footing moves with the footing and is in an elastic state.

• the base of the footing is rough to stop the soil directly beneath the footing from moving horizontally.

2.5.2 Meyerhof's Level Ground Bearing Capacity Theory

The theory developed by Meyerhof (1963) came about as he (Meyerhof) believed Terzaghi's theory was over-conservative and could be improved. Meyerhof also believed that the friction and resistance of the soil above the footing, which was previously replaced by Terzaghi with a simple surcharge, did have an effect on the bearing capacity. As well as this, Meyerhof felt there was a need to allow for the effects of the shape and depth of the footing, as well as an allowance for an inclined load being applied. With these new factors being included Meyerhof came up with a revised equation shown in equation 1.2.

$$q_u = cN_cF_{cs}F_{cd}F_{ci} + qN_qF_{qs}F_{qd}F_{qi} + 1/2\,\gamma BN_\gamma F_{\gamma s}F_{\gamma d}F_{\gamma i} \qquad (1.2)$$

where: • c = soil cohesion

• q = surcharge loading (γD_f)

- γ = unit weight of soil
- B = footing width
- N_c, N_q, N_γ = non-dimensional bearing capacity factors related to the friction angle of the soil.
- $F_{cs}, F_{qs}, F_{\gamma s}$ = footing shape factors
- $F_{cd}, F_{qd}, F_{\gamma d}$ = footing depth factors
- $F_{ci}, F_{qi}, F_{\gamma i}$ = load inclination factors

Meyerhof also determined new bearing capacity factor values for N_c, N_q, N_γ which are shown compared to Terzaghi's values for the friction angles used in this project in Table 2.2.

Table 2.2: Example Meyerhof factor values compared with Terzaghi values

	Terzaghi			Meyerhof		
ϕ	N_c	N_q	N_γ	N_c	N_q	N_γ
0	5.7	1.00	0.00	5.14	1.00	0.00
10	9.6	2.69	1.2	8.34	2.47	0.37
20	17.69	7.44	5.00	14.83	6.4	2.87
30	37.16	22.46	19.7	30.14	18.4	15.67
40	95.66	81.27	100.4	75.31	64.2	93.69

2.5.3 Additional Researchers

The footing on level ground bearing capacity equation has also been modified by other researchers such as Skempton (1951), Hansen (1961), Vesic (1973). Skempton's research revised the shape and depth factors for footings located on the surface of clay soils. Hansen's theory introduced a factor for a footing that was tilted or not parallel to the soil surface and was built on Meyerhof's theory for footings on slopes. Vesic's model accounted for footings that experience large settlement by recommending factors for rigidity. Each of these theories aimed to improve the bearing capacity prediction to produce a less conservative and more accurate solution.

2.6 Footing on Slope Theories

2.6.1 Meyerhof's Footing Near Slope Bearing Capacity Theory

Meyerhof proposed his theory for the bearing capacity of a footing located on a slope in 1953. The equation that eventuated as a result of this theory was again a modified version of Terzaghi's initial bearing capacity equation and is shown in equation 1.3.

$$q_u = cN_{cq} + 1/2\,\gamma BN_{\gamma q} \tag{1.3}$$

This theory was developed to only consider purely cohesive soils ($\phi = 0^\circ$) which in the above equation is cN_{cq}, and for purely granular soils ($c = 0\ kPa$) which in equation 1.3 is $1/2\,\gamma BN_{\gamma q}$.

To find the value of $N_{\gamma q}$ and N_{cq} Meyerhof created a range of design charts that included the effects of slope angle and the internal friction angle of the material for footings that were located either on the surface or at a depth equal to the footing width. To account for the effect of the height of the slope a stability number, taken as $N_s = \gamma H/c$, was used.

2.6.2 Graham et. al. Footing Near Slope Bearing Capacity Theory

In 1988 Graham et. al. proposed new values for Meyerhof's $N_{\gamma q}$ bearing capacity factor for soils of purely granular material. These new values were the result of analyses using the stress characteristics method on a cohesionless soil slope. The ultimate bearing capacity values produced using the Graham et.al theory are larger then those obtained using other methods, as unlike the other methods which use factors to obtain a bearing capacity, Graham et. al. uses slip line analysis to determine capacities.

2.6.3 Shiau et. al. Footing Near Slope Bearing Capacity Theory

The study performed by Shiau et. al. in 2007 used non-linear programming to examine the effects of many parameters associated with footings on slopes. These parameters were converted into dimensionless values to allow easier analysis and included the strength ratio of the soil, footing distance ratio, slope height ratio, slope angle relative to the horizontal, surcharge applied to the slope top surface and the effect of the footing roughness.

This study encapsulated many parameters making it very comprehensive in this aspect, however the depth that it looked in to parameter was not sufficient to create a range of design charts that may be used in the geotechnical field.

2.6.4 Additional Researchers

There have been a number of other researchers who have contributed to the footing on slope problem in a number of ways using various analysis techniques. Kusakabe, Kimura and Yamaguchi were the first to use dimensionless strength ratio in 1981 using upper and lower bound analysis. Narita and Yamaguchi used log-spiral analysis in 1990 that had been originally developed for footing on flat ground cases and were able to closely replicate results produced previously for purely cohesive (clay) material.

2.7 Previous Research Work Done

2.7.1 Biopuso Samuel (2005)

In 2005 Samuel conducted a project to study consolidation settlement and the bearing capacity of shallow foundations near a slope. Small scaled physical models were constructed for both areas of the project. For the consolidation settlement study oedometer tests were conducted with a spreadsheet then developed to assist in the calculations required for foundation settlement design.

For the bearing capacity section of the project two models were constructed at two different slope angles. The bearing capacity values that were gained from these two models were then compared against the results using other methods.

2.7.2 Catherine Smith (2006)

In 2006 Catherine Smith undertook a project to determine if the geotechnical modelling program FLAC was suitable for analysing bearing capacities of footings and producing results comparable with methods such as Terzaghi, Meyerhof and Shiau et. al. While this study was mainly to validate the FLAC software program, footing on slope problems did make up a component of this validation.

A purely granular material was selected within the FLAC program to compare with results based on Meyerhof's theory as well as the upper bound-lower bound methods of Davis &

Booker and Shiau et. al. Smith also used a purely cohesive material, with zero internal friction, to study the effect of the footing distance from the edge of the slope (footing distance ratio), the height of the slope (slope height ratio) and the strength of the soil making up the slope (dimensionless strength ratio) on the bearing capacity the slope was capable of.

This project was important to the footing on slope problem as it verified that FLAC is a reliable tool to use for obtaining results. While this initial validation was for clay soils, it did provide a direction for sandy soils as discussed in this paper for parameters such as mesh size, applied velocity and stepping number.

2.7.3 Joshua Watson (2008)

This project was undertaken as a continuation of the work of Catherine Smith and was a more in depth study specifically of the footing on slope problem. This involved analysing the effects of a greater range of soil strength ratios, as well as slope height and footing distance ratios. Watson also studied the effect slope angle had on the bearing capacity. This study was an attempt to provide a better understanding of the bearing capacities of different slopes of a two dimensional nature, that is, slopes with footings of infinite length located on top.

Watson also made a number of improvements to the FLAC script file, the major improvement being to the mesh grid used in each analysis. The mesh was redesigned so only the mesh beneath the angle was inclined, compared to Catherine Smith who inclined the entire mesh that was located between the bottom and the top of the slope for all slope angles less than 90°. This improvement resulted in more accurate results being produced.

2.7.4 Matthew Arnold (2008)

The study conducted by Matthew Arnold in 2008 involved similar work to that performed by Joshua Watson however Arnold's concentration was on cohesive-granular (sandy) soil materials whereas Watson focussed on pure clay materials. Arnold studied the usual slope dimension parameters of slope height ratio and footing distance ratio as well as the material parameters of dimensionless strength ratio and internal friction angle. This internal friction angle is the key difference between pure clay and cohesive-granular materials and has a significant effect of the bearing capacity associated with a slope. Each parameter was only looked into lightly with a small number of cases used to base the analysis on however the results produced still appeared to be reliable.

As has been done in this paper, Arnold created a number of design charts using the software program Surfer. This program creates contour plots to display the information required but only example charts were created to demonstrate what was possible. Arnold also briefly looked into the effect of surcharge loading, combination shear failure and two-way shear mechanism for footing on slope situation and presented the trends that were noticed. This last section of study was introduced as a possible area of interest for further study by another student.

2.7.5 Nathan Lyle (2009)

In 2009 Nathan Lyle set out to create a complete set of design charts for the footing on slope problem based on pure clay material. In his study he looked at each of the common slope problem parameters of slope height ratio, footing distance ratio and dimensionless strength ratio in depth for various slope angles to create a very comprehensive set of geotechnical charts.

Lyle also performed a validation of the FLAC software specifically for the footing on slope problem which had not been completed with considerable detail before. As well as this, Lyle discussed the program interface to identify its strengths and weaknesses.

Validation of FLAC Software for c–ϕ Soil Analysis

3

3.1 Introduction

The purpose of this chapter is to validate the FLAC model used for c/ϕ soil analysis, to ensure that any results obtained form this software program are reliable and credible.

In validating the software it is necessary to determine the values of key factors relating to the deformation of the slope by applying a load. These key factors are element size, applied velocity and stepping number, and are related to each other in that they affect the accuracy of the model. Element size and stepping number are very closely related because they determine how much and how quickly penetration is applied to the slope. Element size refers to the size of the mesh grid used on the model. All of these factors are discussed in greater detail following this introduction.

The final section of validation involves fixing H/B, D/B, β and ϕ changing only $c/\gamma B$. These results are then compared with results from other methods with the same parameters to determine if the FLAC results are within an acceptable range. If the difference in results is acceptable then any FLAC values obtained during research will be considered as satisfactory for the purpose of this project.

3.2 Effect of Applied Velocity

Applied velocity (or y-velocity as the velocity is applied in the y-axis direction) is an important factor in verifying the FLAC model. It is closely linked to the the stepping number input in the FLAC script file as together they determine the depth of penetration performed in the analysis of a slope.

Applied velocity relates to the speed at which the slope is deformed in numerical analysis. Whereas in real world testing we apply a load to a surface to obtain deformation, FLAC applies a set velocity which combines with a stepping number to create a deformation to gain results.

Previous studies have used a total penetration of 1.3 metres (y-velocity = $1e^{-5}$, stepping number = 130000) when analysing a sandy soil however no proof that this velocity was acceptable had been researched. As this section is dealing with changing the applied velocity, it was decided that after changing each applied velocity, the stepping number would also be changed to keep the 1.3 metre penetration otherwise penetration depths up to 1300 metres may have eventuated. (Changing only the stepping number to give greater and lesser penetration then 1.3 metres is examined in the next section)

It was determined that applied velocities of $1e^{-2}$, $1e^{-3}$, $1e^{-4}$, $1e^{-5}$ and $1e^{-6}$ would be used in conjunction with stepping numbers 130, 1300, 13000, 130000 and 1300000 respectively. Each of these combinations of applied velocity and stepping number would give the 1.3 metres penetration required to properly analyse the soil slope. In all of these models the key parameters were kept the same, them namely being $\beta = 90^\circ$, $H/B = 5$, $D/B = 2$, $c/\gamma B = 20$ and $\phi = 20^\circ$.

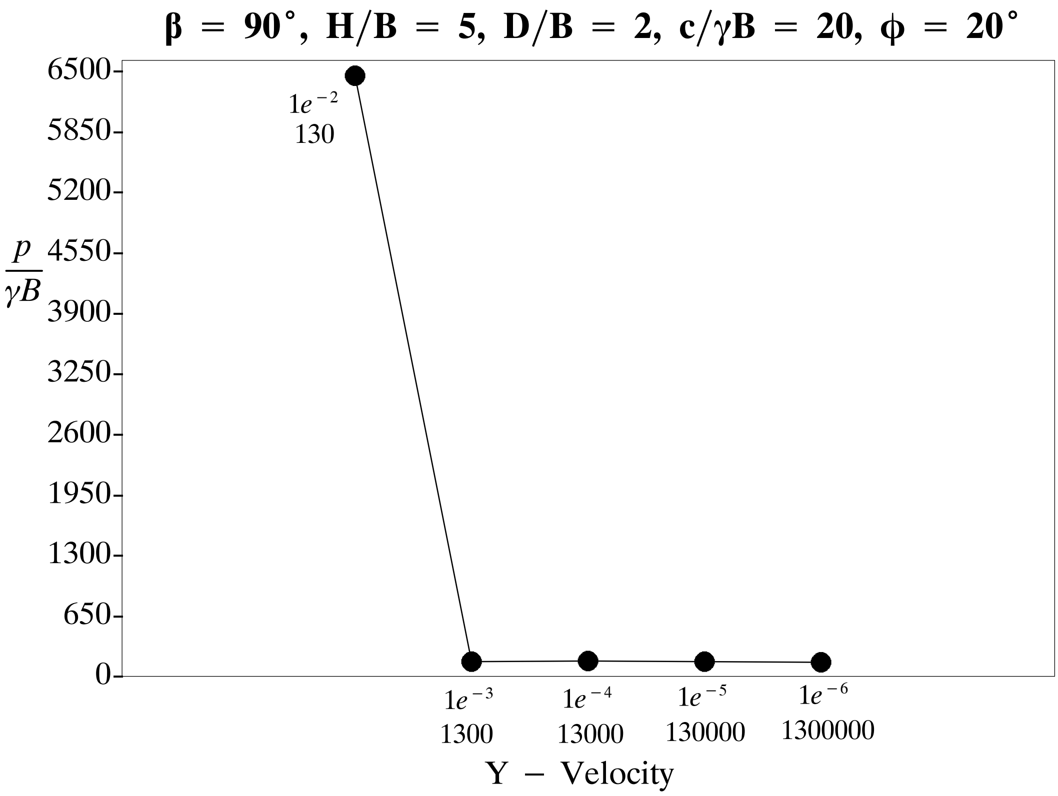

Figure 3.1: Validation for increasing y-velocity

Figure 3.1 shows the results of the validation files for applied velocity. It can be clearly seen that a velocity of $1e^{-2}$ results in a highly inaccurate bearing capacity value, while all other values of applied velocity appear to give similar values. Due to the extreme variance in bearing capacity values, the applied velocity, stepping number used, bearing capacity at failure and computational time are included in Table 3.1.

Table 3.1: Applied velocity, stepping number, bearing capacity, CPU time

Applied Velocity	**1e-2**	**1e-3**	**1e-4**	**1e-5**	**1e-6**
Stepping Number	130	1300	13000	130000	1300000
Bearing capacity	6439.28	159.34	156.29	149.18	143.00
CPU time (min)	0.041	8.63	2.21	21.90	300+

It can be seen after looking at this table the inaccuracy of using an applied velocity greater then $1e^{-4}$. Using anything larger then this yields results all within 10% of each other which is not quite within an acceptable range, so before choosing a final value for applied velocity the computational time taken to analyse the slope must be considered. We can see that a velocity of $1e^{-4}$ requires 2.21 minutes, while $1e^{-5}$ requires 21.9 minutes which is still an acceptable amount of time taken to improve the accuracy of the final answer by 5%. 300+ minutes though, as used by $1e^{-6}$, is undesirable as obtaining a set of values would take considerable time.

Now with the chosen applied velocity set as $1e^{-5}$ we can determine the optimum desirable stepping number.

3.3 Effect of Stepping Number

Now with the applied velocity decided, taking into account result accuracy and computational time, we need to find the stepping number value to use. As mentioned earlier, changing the stepping number while keeping applied velocity fixed simply changes the depth of penetration in the numerical model. This section is aimed at determining if the depth of penetration is critical and the optimum value to use that will ensure reliable results, while also again taking into account CPU time.

Stepping number refers to how many iterations of the applied velocity are applied onto the slope surface. This results in a set penetration length which needs to be sufficient to make the slope structure deform sufficiently and ensure the maximum bearing capacity be found. Without a sufficient penetration depth the maximum capacity of a slope may not be found resulting in unreliable results.

As mentioned in the previous section a depth of 1.3 metres penetration has been used before however this has never been validated as being acceptable or not. In this verification we will use stepping numbers of 25000, 50000, 100000, 130000 and 150000 which when combined with the chosen value for applied velocity ($1e^{-5}$) gives penetration depths of 0.25 m, 0.5 m, 1 m, 1.3 m and 1.5 m respectively.

The key parameters were set the same as previously used to eliminate and variation and make the results more valid, these being $\beta = 90^\circ$, $H/B = 5$, $D/B = 2$, $c/\gamma B = 20$ and $\phi = 20^\circ$.

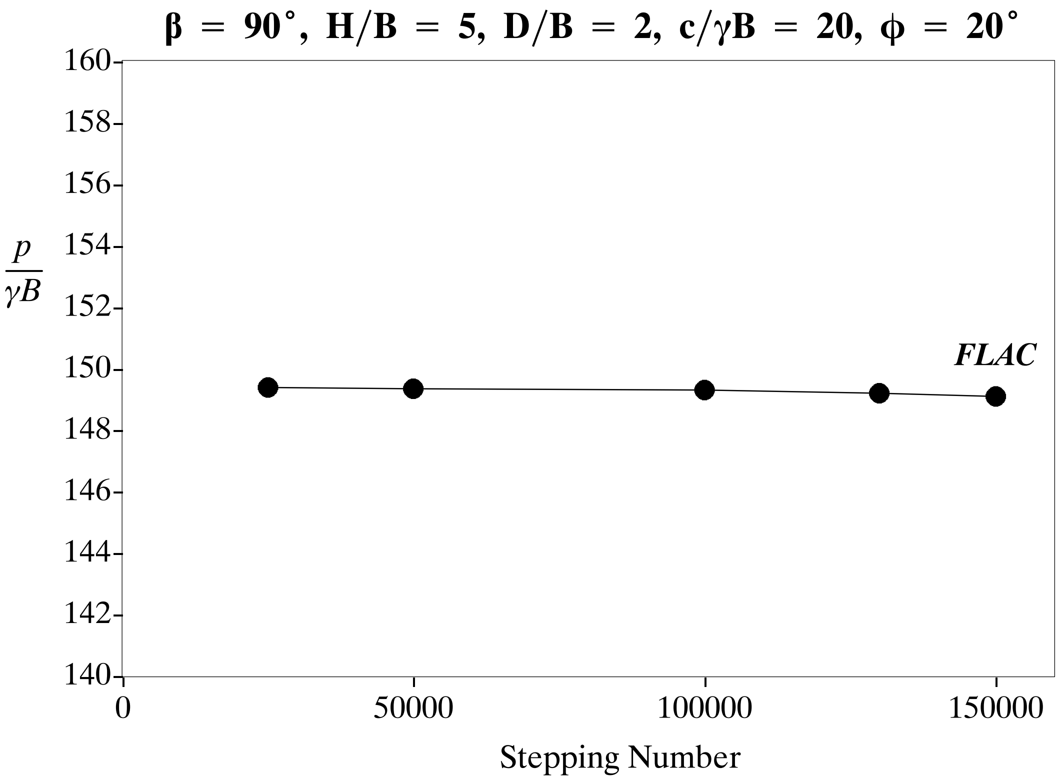

Figure 3.2: Validation for increasing stepping number

Figure 3.2 shows the results obtained when only stepping number was varied. By inspection of the chart it appears that there is minimal difference between the values suggesting that stepping number, and therefore penetration depth, is not critical. To decide upon the stepping number to use the stepping numbers versus bearing capacities and CPU times are shown in Table 3.2.

Table 3.2: Stepping number, penetration depth, bearing capacity, CPU time

Stepping Number	**25000**	**50000**	**100000**	**130000**	**150000**
Penetration Depth (m)	0.25	0.5	1.0	1.3	1.5
Bearing Capacity	149.37	149.34	149.30	149.18	149.09
CPU Time (min)	4.27	8.57	17.16	22.29	25.70

We can see that between the stepping numbers, there is less then 1% difference in result values. When we examine the computational time taken, we can see that the analysis varies between almost 4.5 minutes and just over 25.5 minutes, all of which are acceptable. On first inspection of these results it would seem logical to use a stepping number of 25000 as it takes the least amount of time, however the dimensions of the slope need to be considered in this case.

Since the footing from edge of slope ratio has been specified at D/B=2, which is very close to the edge, it will not require much penetration depth to create slope failure. Should the D/B ratio be equal to 10 however, then it is highly likely that a greater penetration depth would be needed to initiate failure in the slope in order to be able to obtain the bearing capacity of the soil. It is for this reason that we will use a stepping number of 130000 and stick with the 1.3 metres penetration, as CPU time is still very reasonable, the results are slightly more accurate and the fact that is has been used before and appears to give reliable results no matter what the key slope parameters are.

3.4 Effect of Element Size

With applied velocity and stepping number values validated and chosen, the next step is determining the element size for the slope model.

Element size (or mesh size) refers to the size of the mesh grid used in the numerical analysis, and determines how many square elements there will be in the slope model. The value of the element size used must be able to be evenly divided into the footing width. With a footing width equal to 1 (one), element sizes of 0.05, 0.1, 0.2 and 0.5 were tested as they all satisfied this requirement. Figure 3.3 and Figure 3.4 below show the difference in mesh size between 0.1 and 0.5.

These figures show the deformed shape of the slopes after being subjected to analysis, but show very well the difference in mesh sizes. The most noticeable difference is at the edges of the footing where we can see a difference in the angles of the mesh between the two sizes.

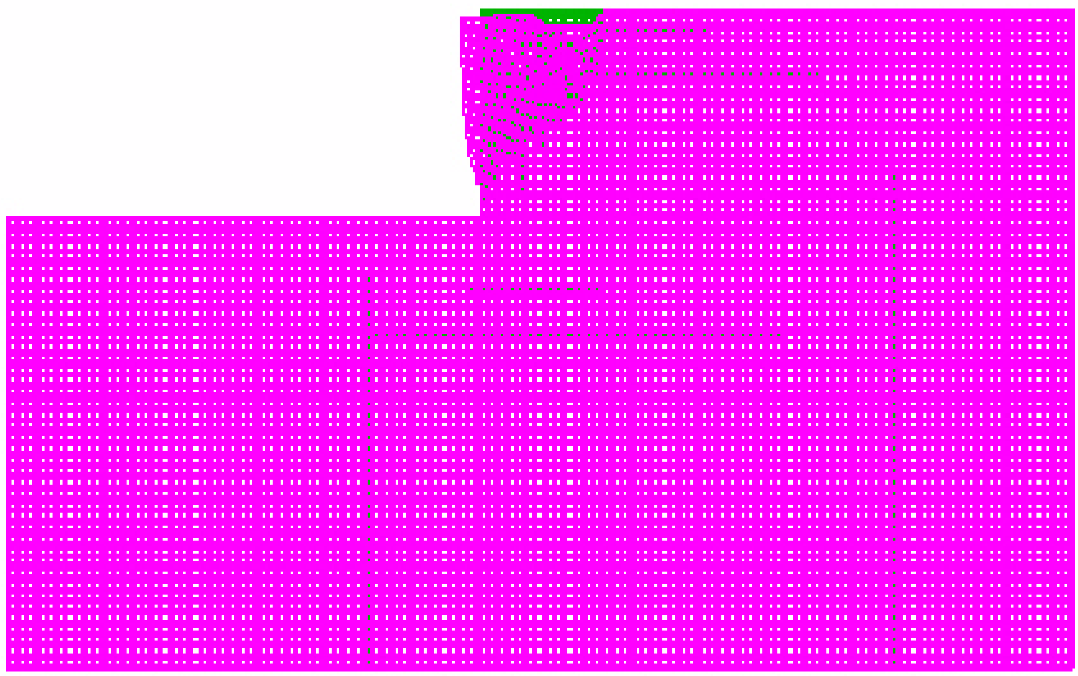

Figure 3.3: 0.1 mesh size

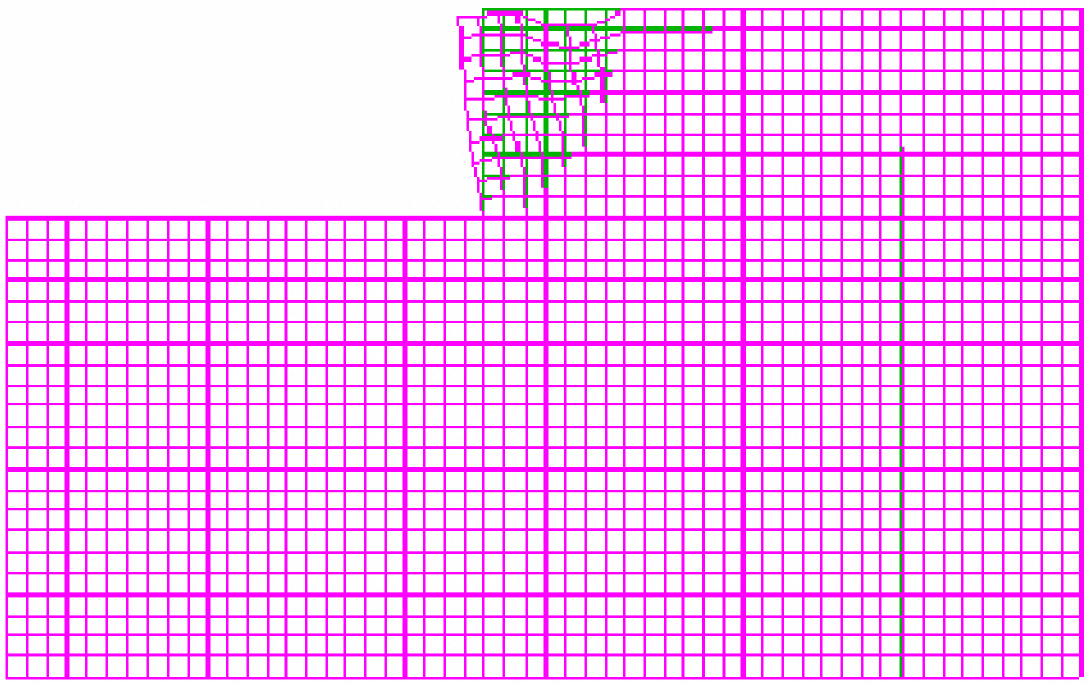

Figure 3.4: 0.5 mesh size

For the validation the key parameters were again set as $\beta = 90^\circ$, $H/B = 5$, $D/B = 2$, $c/\gamma B = 20$, and $\phi = 20^\circ$, as well as including the applied velocity and stepping number values determined in the previous sections. FLAC was then used to obtain results for the varying element sizes with these results shown in Figure 3.5.

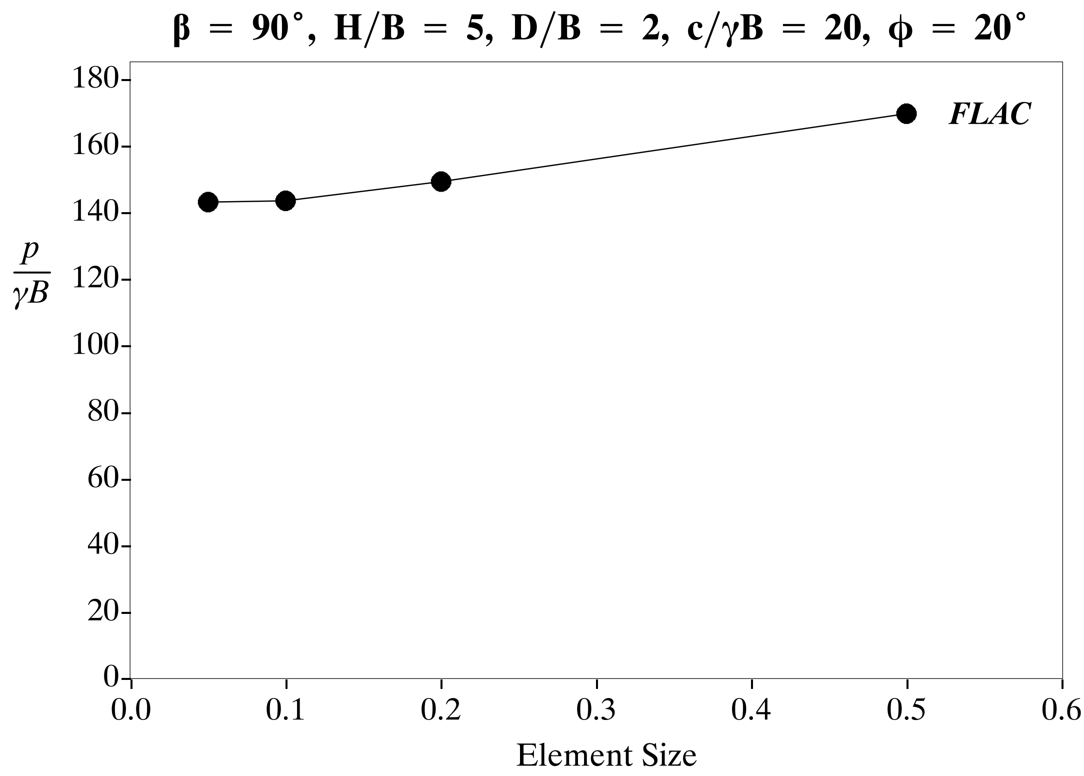

Figure 3.5: Validation for increasing element size

In Figure 3.5 we can see the difference in final values between the different element sizes. An element size of 0.5 appears to overestimate the bearing capacity of the slope, which we would expect after observing Figure 3.4. By inspection of this figure we can conclude even before bearing capacity results are known that this mesh size is unlikely to yield accurate results due to it being so large. The difference in results between an element size of 0.2, 0.1 and 0.05 is considerably less, with 0.1 and 0.05 mesh sizes returning values almost identical. A mesh size of 0.2 yields results only 4% different to those obtained for 0.1 and 0.05 which is within an acceptable range. Now we know the result values using the various element sizes we must now examine the CPU times to find the optimal value. These values are most easily compared in a tabular form (Table 3.3).

Table 3.3: Applied velocity, stepping number, bearing capacity, CPU time

Element Size	0.05	0.1	0.2	0.5
Bearing Capacity	143.00	143.37	149.18	169.48
CPU Time	337.38	81.5	18.15	2.51

Since we know a mesh size of 0.2 gives a result only 4% different to 0.1 and 0.05, but can be obtained in a quarter of the time of 0.1 size mesh, it is the mesh size we will use. This enables us to obtain data in acceptable time with the data accuracy also within a tolerable range.

3.5 Comparison with Other Existing Solutions

The last check we need to perform is to see whether the results output by FLAC are comparable to that derived using other methods. This will allow us to see the difference in values from various methods and determine whether the FLAC results are acceptable.

A research paper that was compiled by members of the Civil Engineering Department at the Tokyo Institute of Technology was used to obtain some results to compare with, as the parameters that were used in the paper mirrored that which can be varied in the FLAC script file. Once these parameters were known FLAC cases were set up and run which produced results shown in Figure 3.6.

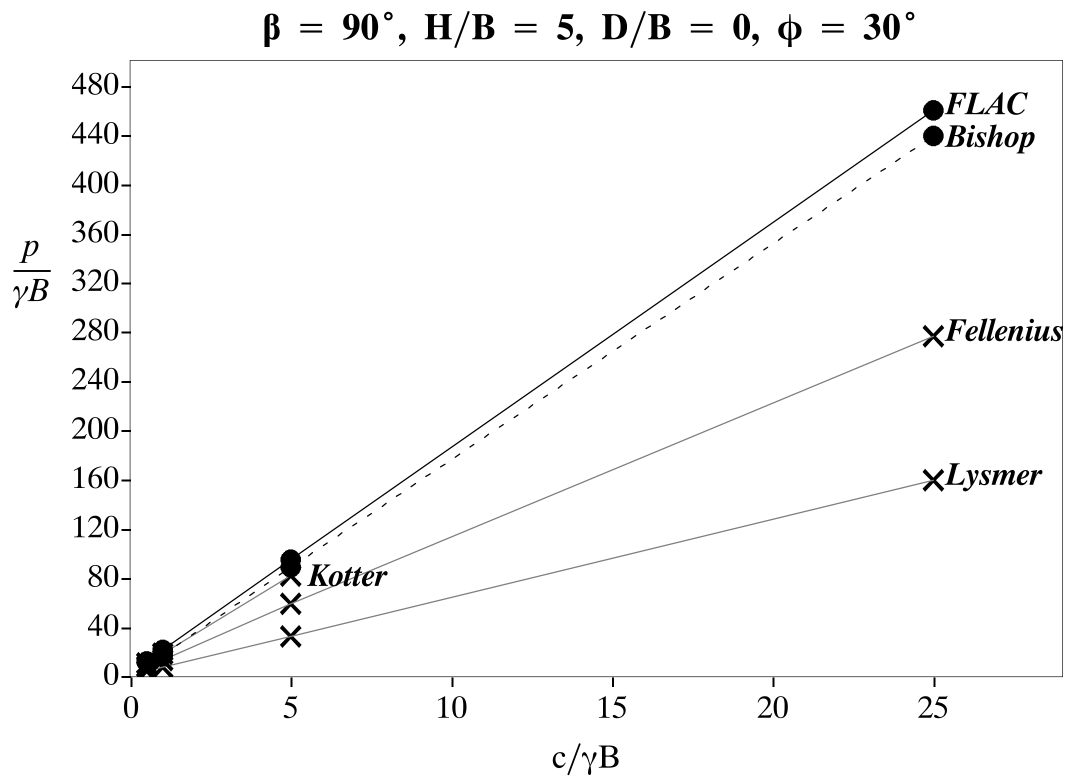

Figure 3.6: Comparison against other results

From this diagram we can see that the trend displayed for each analysis method is the same with a linear increase in normalised bearing capacity with an increase is dimensionless strength ratio. What is interesting to note is the difference is bearing capacity values between each of the methods. The Lysmer (lower bound) method is less then half of that obtained from FLAC, however we expect this method to return low capacity values due to it being the lower bound method which finds the lowest possible bearing capacity for a given case.

We can see the difference between the FLAC derived results and those obtained using Bishops method is very small, and if results had been available for a dimensionless strength ratio of 25 using Kotter's method then it is believed that there would also be little difference between FLAC and Kotter based results.

If the results for Lysmer method are ignored as it is known that this method will always produce low values, then the results produced from FLAC are within an acceptable range of two out of three other methods. Thus we can classify FLAC as producing reliable results. Of course as the normalised bearing capacity values from FLAC are the highest out of all the methods compared, it would be wise to apply a safety factor if using FLAC which is common practice in industry anyway.

The values used in Figure 3.6 are shown below in Table 3.4.

Table 3.4: Results from comparison of methods (after Kusakabe, Kimura and Yamaguchi, 1981)

Soil Strength Ratio	Bishop Method	Fellenius Method	Kotter Method	Lysmer (lower bound) Method	FLAC Method
25	439.0	276.0	N/A	159.2	459.62
5	88.0	58.3	81.2	32.11	94.46
1	17.1	12.9	18.2	6.86	21.14
0.5	10.3	7.45	10.2	3.84	11.7

From this table we can see that the FLAC method compares well against the slice method of Bishop (Fellenius is also a slice method), and Kotter's stress characteristic equations.

Numerical Analysis – 90° Slope

4

4.1 Introduction

This chapter will investigate the effect of slope material properties, as well as the effect the slope dimensions have on the bearing capacity of a footing near slope.

The slope material properties that will be varied are dimensionless strength ratio and internal friction angle. The dimensionless strength ratio ($c/\gamma B$) will be varied with values of 1, 10, 20 and 30. The internal friction angle (ϕ) will have the values of 10°, 20°, 30° and 40°.

As this chapter is focussed with cohesive-granular slope materials it is necessary to vary the values of strength ratio and friction angle as shown above. This is in contrast to sand where cohesion ($c/\gamma B$) equals zero, or clay where friction angle (ϕ) equals zero.

The slope dimension parameters that will be examined are footing distance ratio (D/B) and slope height ratio (H/B). It is possible to also study the effect that slope angle has on bearing capacity however this chapter will focus solely on 90° slope rather then take a brief look at a number of slope angles. The footing distance ratio values to be used will be 0, 1, 2, 3, 4, 5, 6, 8, 10, 15, 20 and 25 while the slope height ratio values will be 0, 1, 2, 3, 4, 5, 6, 8, 10, 13 and 16.

Different trends will be experienced when using various combinations of these parameters which will each give a different bearing capacity value. This is due to the stability of the slope changing and making failure less or more easily occurring.

The analysis software FLAC will be used to obtain results relevant to this chapter, which was validated as an acceptable program in chapter 3 of this dissertation.

4.2 Effect of Dimensionless Strength Ratio, $c/\gamma B$

The strength of a soil will determine the magnitude of the loads it is able to sustain before it becomes susceptible to deformation or failure. The factors that affect this strength of a soil are the internal cohesive force and the density of the material. In FLAC based analysis the strength of a soil is taken to be dimensionless, thus creating the dimensionless strength ratio for a soil. This is done as the cohesive force and density are unknown parameters, but by using a dimensionless strength value, analysis is still able to take place.

Dimensionless strength ratio is known as $c/\gamma B$ where c = cohesion, γ= material density and B = width of the footing. Within the FLAC script files it is simply given a numerical value which can be used later on to find the value of one of the parameters if the other is known.

As the strength of a soil increases, it is expected that the bearing capacity will also increase. This is due to the larger cohesive force holding the soil particles together and resisting deformation as higher cohesion = higher force needed to break each particle bond. In the case of FLAC analysis a higher dimensionless strength ratio equals a stronger soil. This is better explained with an example: Assume a material has a density (γ) of $20kN/m^2$, and a footing width (B) of 1. With a strength ratio of $c/\gamma B$= 10, the cohesive strength (c) of that soil: $10 = c/(20 \times 1)$ therefore c = 200 kPa. With a strength ratio of 20 the cohesive strength is: $20 = c/(20 \times 1)$ therefore c = 400 kPa.

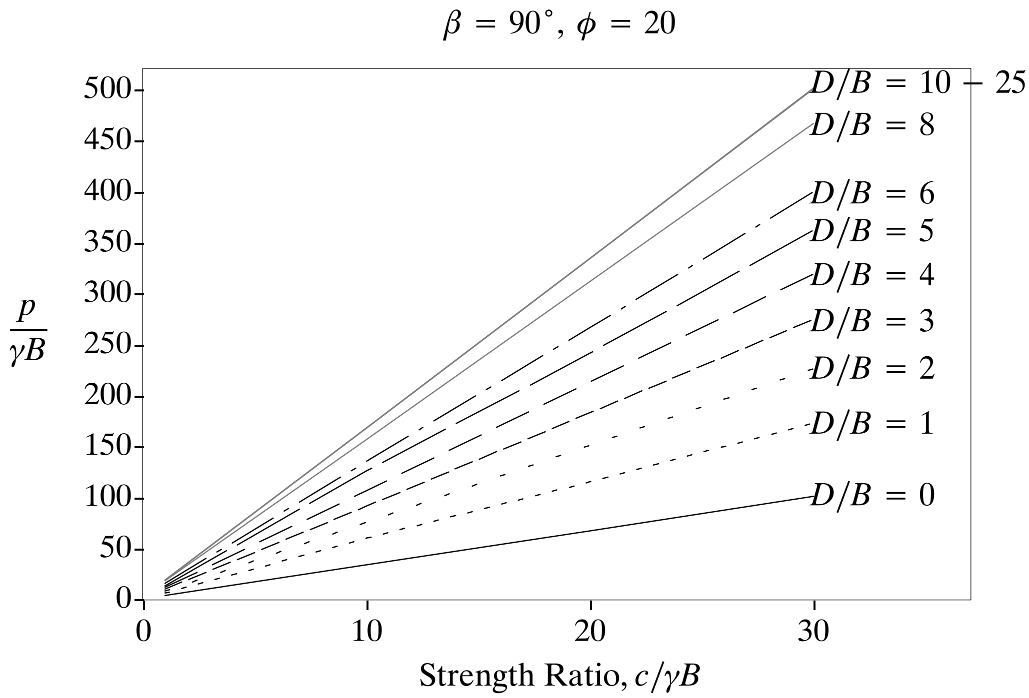

Figure 4.1: Increasing bearing capacity with increased strength ratio

Figure 4.1 shows the bearing capacity of an example slope with the dimensions of H/B = 4, $\phi = 20^\circ$ (effects of friction angle ϕ will be discussed later) and varying D/B values. It can be seen that as the strength ratio of the soil increases so does the bearing capacity which is as expected. It is also noted that for small strength ratios converging of the results occurs, meaning that with weaker materials the distance of the footing from the edge of the slope is not such a major factor as the bearing capacity is very similar even for large footing distances.

4.2.1 Comparison With Footing Distance Ratio

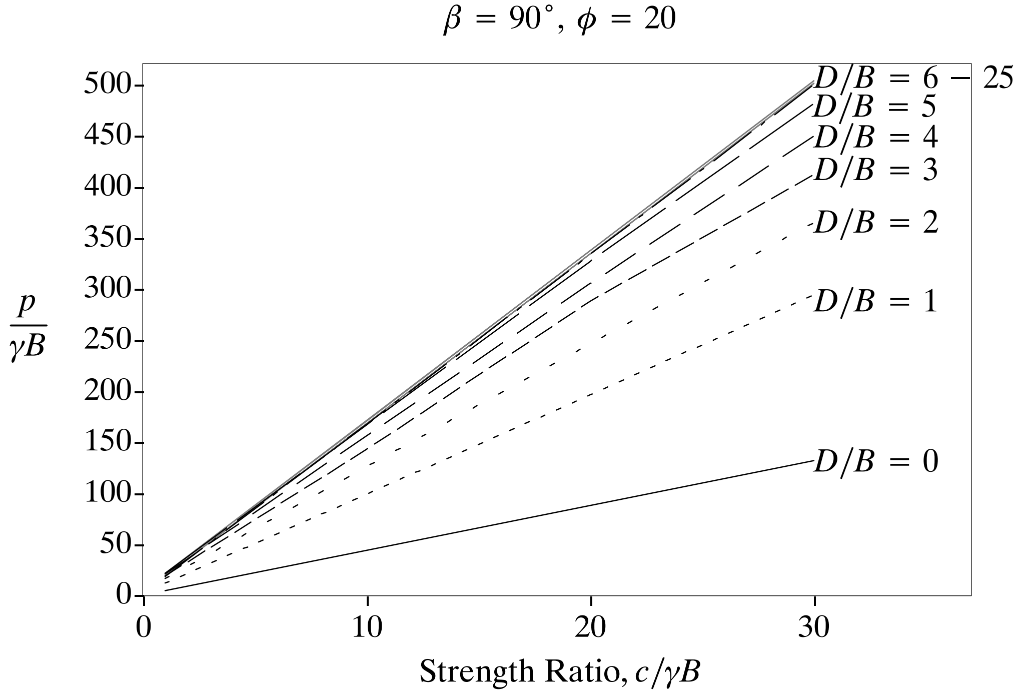

Figure 4.2: Effect of dimensionless strength ratio with footing distance ratio

Observing Figure 4.2 we can see the relationship between footing distance ratio and dimensionless strength ratio. From section 4.1 we know that increasing dimensionless strength ratio will give an increased bearing capacity, but we can also see in this figure that an increase in footing distance will also an increase on normalised bearing capacity. We can also note the large difference between a footing distance ratio of D/B = 0 and D/B = 1 showing that even a little increase in this ratio can greatly increase the bearing capacity when the footing is located so close to the slope edge. As the footing distance ratio increase though this difference becomes lessened as flat ground behaviour is approached. Flat ground behaviour is reached with large footing distance ratios as indicated by the single result line for D/B =6–25.

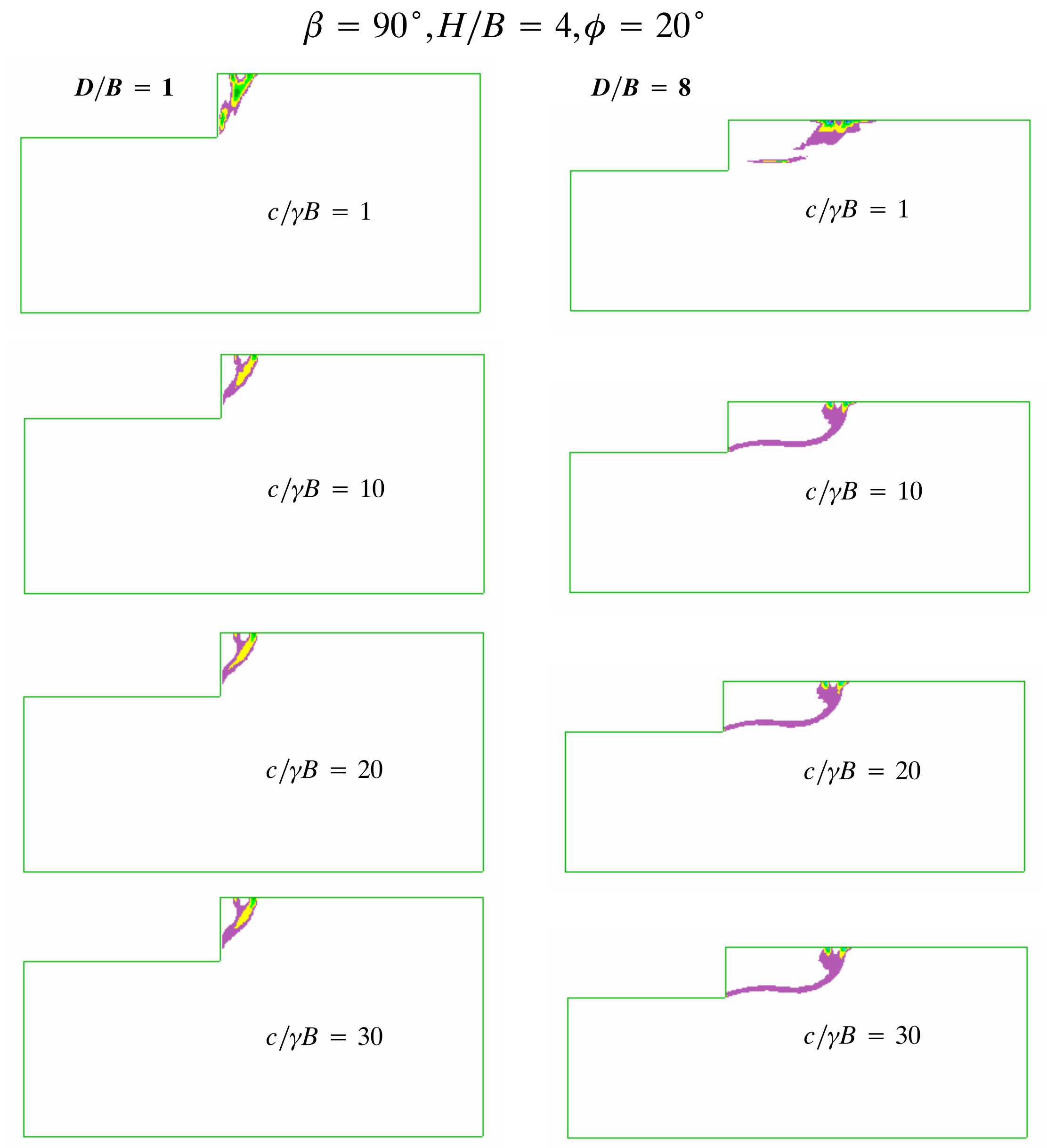

Figure 4.3: Contour plots for dimensionless strength ratio with varied footing distance ratio

Note in the contour plots Figure 4.3 and the trends which they display. It can be seen that even with a varied dimensionless strength ratio, the failure planes will be very similar for a slope of the same dimensions and when the footing is in the same location. This is because the strength of a soil only affects the bearing capacity it is capable of and not the failure plane that will occur. The break in failure plane that can be seen in the top right image ($c/\gamma B = 1$, D/B = 8) is due to the resolution of the jpeg produced not showing up the very small shear stresses.

4.2.2 Comparison With Slope Height Ratio

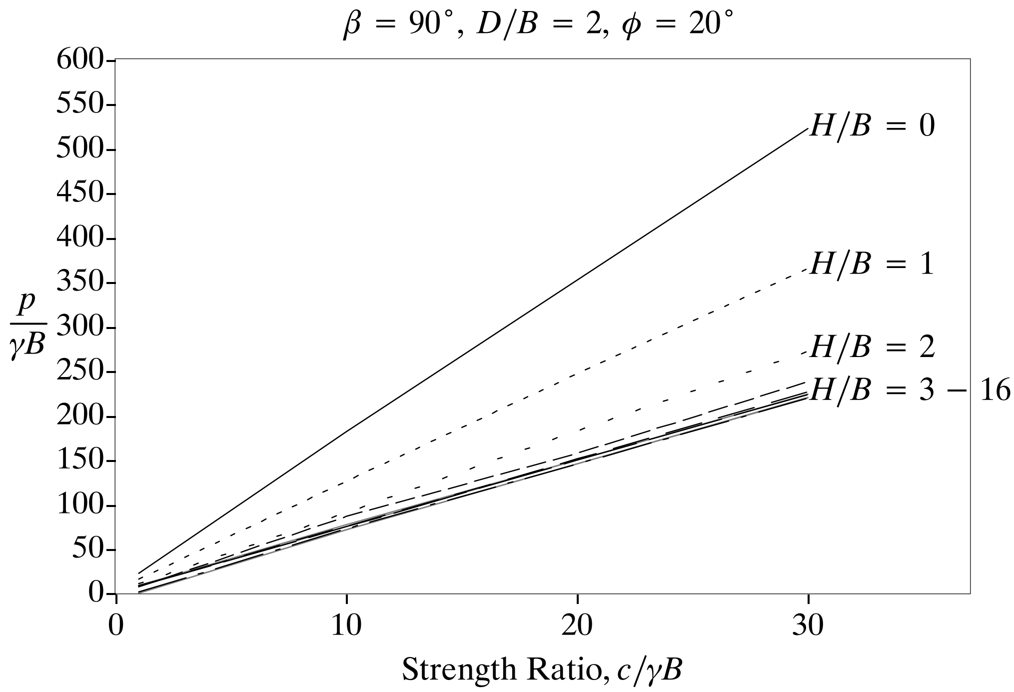

Figure 4.4: Effect of dimensionless strength ratio with slope height ratio

In Figure 4.4 we can see the correct assumption that as the slope height ratio increases the bearing capacity decreases, and bearing capacity increases as dimensionless strength ratio increases. We can see that a significantly higher bearing capacity is achieved with a small slope height ratio then with a large slope height ratio. H/B = 0 is included to show the capacity of this particular material for a flat ground situation so it can be seen how much change even a small increase in slope height has. Note how the normalised bearing capacities change very little once a slope height of H/B = 3 is reached suggesting that above toe failure has occurred for this particular case.

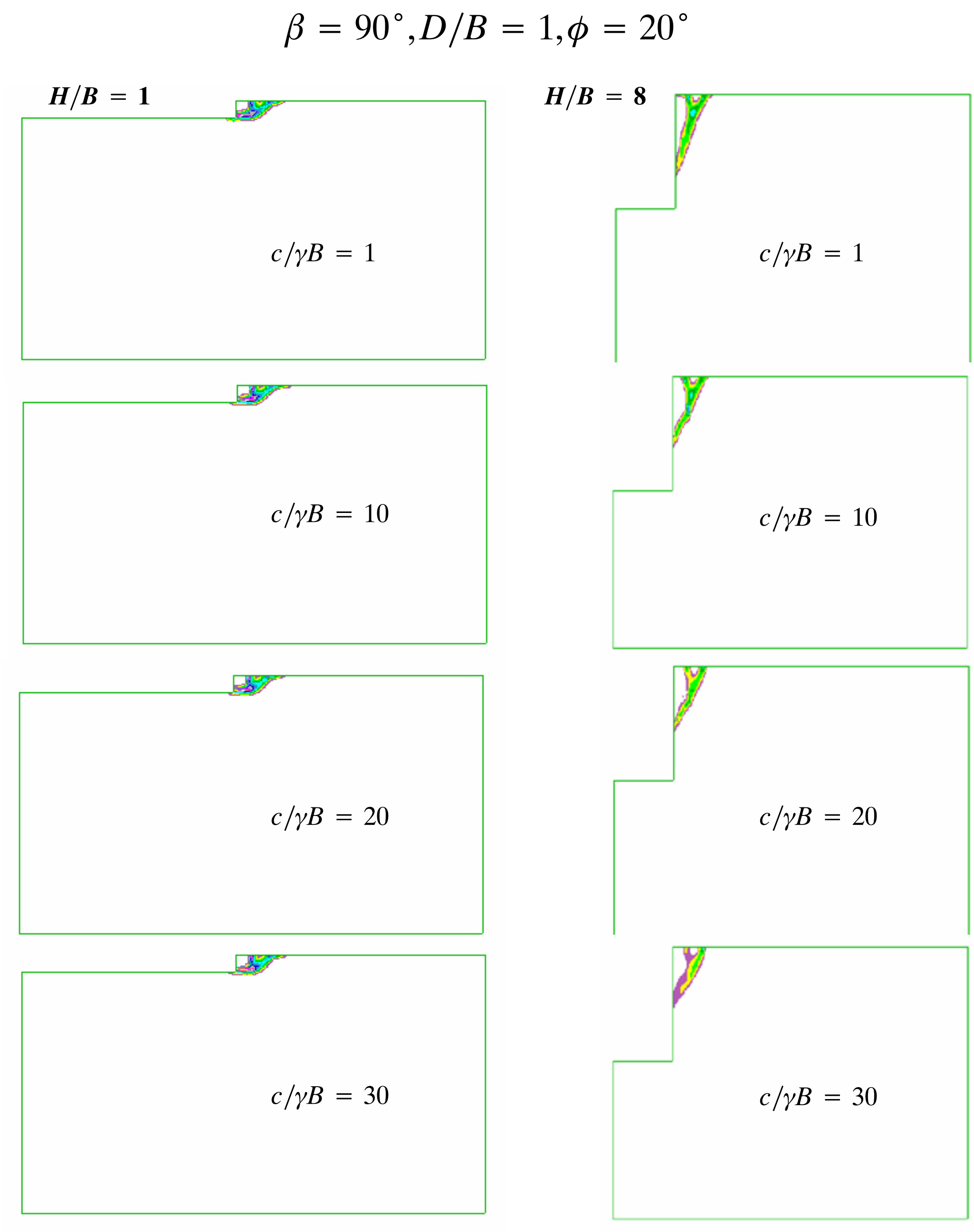

Figure 4.5: Contour plots for dimensionless strength ratio with varied slope height ratio

In Figure 4.5 we can see the below and above toe failures occurring for the low and high slope height ratios respectively. The below toe failure plane demonstrated by the H/B = 1 contours is the reason for the larger difference in bearing capacities compared to the H/B = 8 contours and above toe failure planes as the below toe failures have more slope material to provide resistance so a larger force can be supported. Once the failure plane is above toe it does not matter how much higher a slope becomes (until it becomes so high it is unstable with no load) the bearing capacity will be the same due to the common failure plane (indicated by flat lining of capacity in Figure 4.20). Again note the very similar failure planes that have occurred for a slope of the same dimensions even with different strength soils.

4.2.3 Comparison With Friction Angle

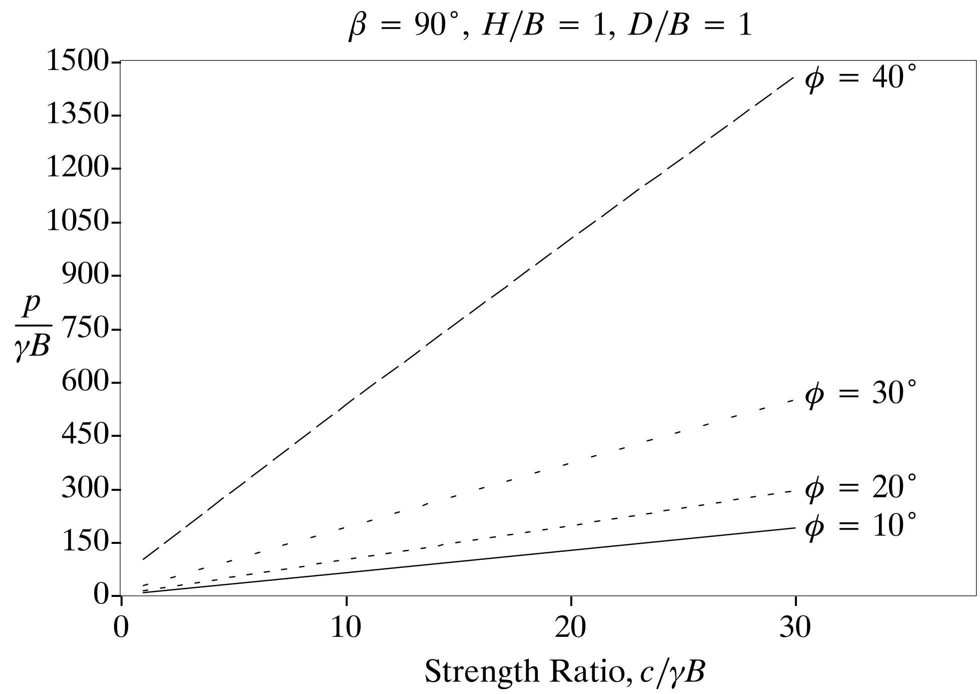

Figure 4.6: Effect of dimensionless strength ratio with friction angle

The results in Figure 4.6 highlight the effect of dimensionless strength ratio when combined with friction angle. Just as it is seen when the dimensionless strength ratio is decreased, when the friction angle is decreased the normalised bearing capacities converge. Also note the difference in bearing capacity values occurring between the different friction angles. The trend in the results suggests that as friction angle is increased the bearing capacity increases exponentially. The effect of friction angle is very well highlighted if we examine the results relating to a dimensionless strength ratio of 1: a soil with friction angle of 10° has a normalised bearing capacity of roughly 7, while a soil with friction angle of 40° has a capacity of approximately 100.

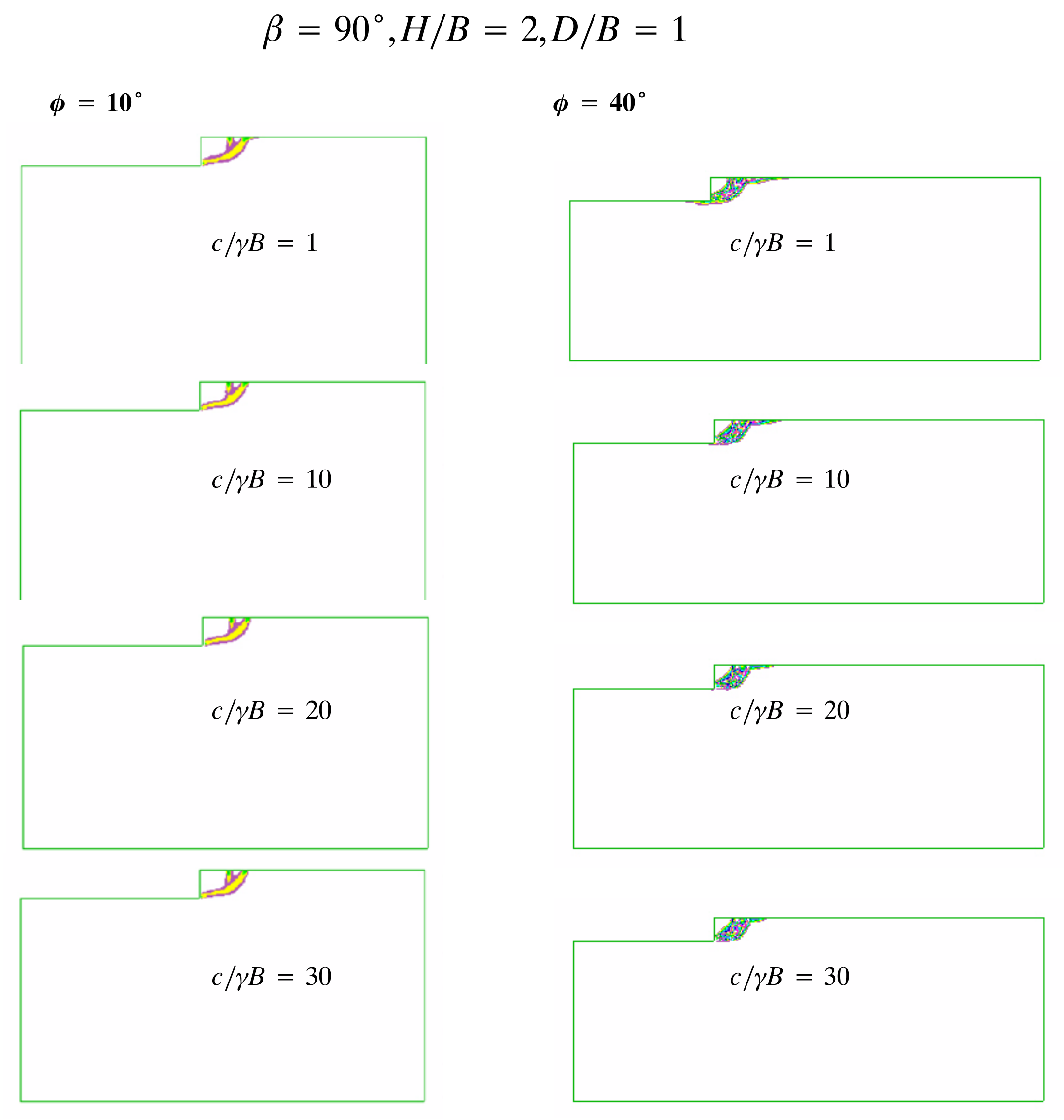

Figure 4.7: Contour plots for dimensionless strength ratio with varied internal friction

In Figure 4.7 we can once again see the similarities in failure planes between the different dimensionless strength ratios for the same friction angle. The differences in the failure planes is not significant once again proving that the strength of the slope material does not determine the failure plane that occurs. Note the larger contour plot surface for friction angle 40° which suggests more material is involved in supporting the load applied to the slope. The effect of friction angle on bearing capacity will be explained in the next section (4.3).

4.2.4 Conclusion

The purpose of this sub-section was to make clear the effect dimensionless strength ratio has on normalised bearing capacity. The assumed knowledge that a higher dimensionless strength ratio will produce a higher bearing capacity has been proven by comparing it against all the main parameters that have an effect of the ultimate bearing capacity of a slope. From the results shown we know that there will be larger differences in bearing capacities between each strength ratio when the slope is stable- that is either below toe failure or flat ground behaviour- and that once the slope becomes unstable this difference becomes lessened. From the contour plots we have also gathered that dimensionless strength ratio does not have a noteworthy effect on the failure surface that occurs.

4.3 Effect of Internal Friction Angle, ϕ

The friction angle of a soil relates to the shape of each particle that makes up the foundation material. The magnitude of the friction angle of a soil is also a key parameter when determining the bearing capacity of a slope, along with its strength ratio.

The internal friction angle of soil is what determines the amount of material that will be involved in supporting a footing as it affects the interference of one particle on another. A material with zero or extremely low internal friction, such as clay, means each particle is perfectly round or close to it so the particles are unable to stack up on each other, similar to how it is hard to stack a group of basketballs on top of each other due to their round shape. A material with a large friction angle however, such as sand, will stack on top of itself due to the irregularity of each particle binding on adjacent particles.

Given that the friction angle of a material affects how the particles interact within a soil mass, it is expected that a larger friction angle would result in a larger bearing capacity. This theory will be now be discussed by comparing the effects of friction angle with dimensionless strength ratio, footing distance ratio and slope height ratio.

4.3.1 Comparison With Dimensionless Strength Ratio

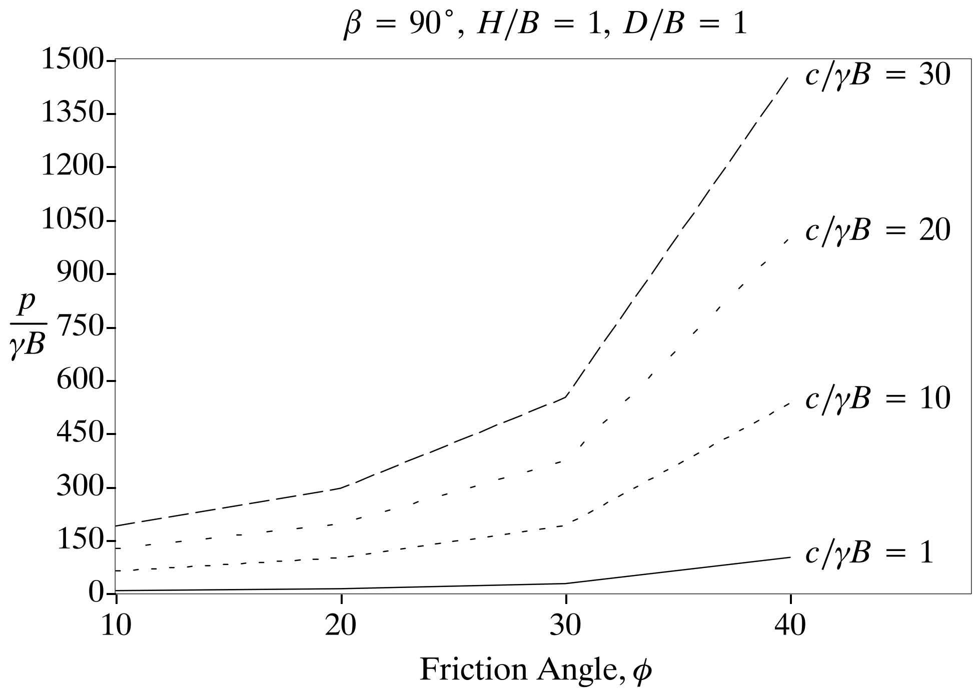

Figure 4.8: Effect of friction angle with dimensionless strength ratio

When we observe friction angle with dimensionless strength ratio, such as in Figure 4.8, we again see the expected trend of increased bearing capacity with a larger strength ratio material. We can also see that the difference in bearing capacity becomes larger between each dimensionless strength ratio as the internal friction angle of the soil increases. It is also interesting to note that as friction angle decreases the normalised bearing capacities converge indicating that friction angle greatly affects the strength of a slope just like strength ratio does.

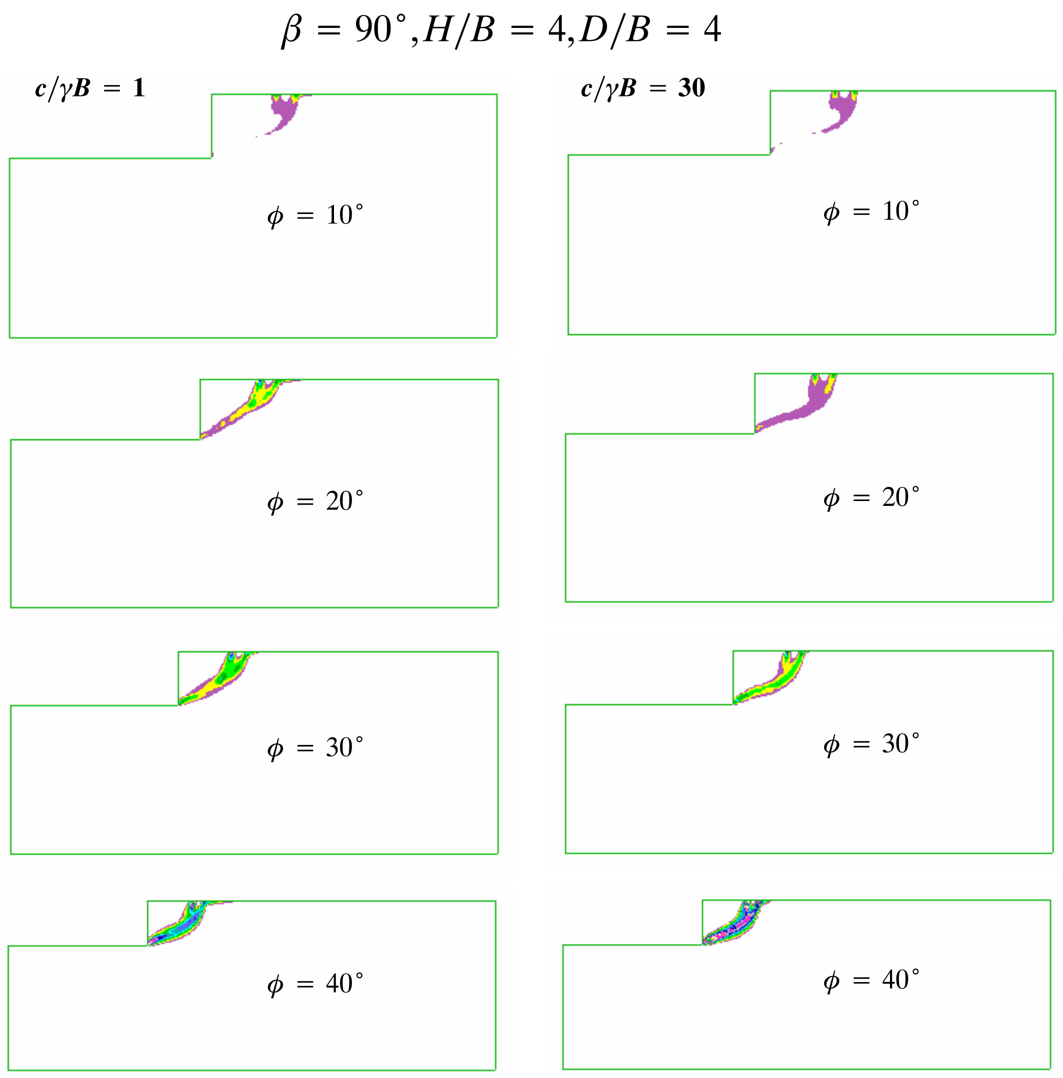

Figure 4.9: Contour plots for friction angle with varied dimensionless strength ratio

Examining Figure 4.9 we can see the area of affected material increasing with each larger friction angle which helps prove why a larger bearing capacity is obtained on slopes that consist of a material with high internal friction, as more material provides resistance to the footing force. Note how each slip plane shown consists of basically the same lower extremity, with more soil becoming affected above this line as the friction angle increases. It should also be noted how the failure surface is the same for each value of ϕ again proving that dimensionless strength ratio does not change the failure plane as stated in the previous section. The abnormality in failure surface in the tope two images is again due to the resolution not showing the very small shear stresses.

4.3.2 Comparison With Footing Distance Ratio

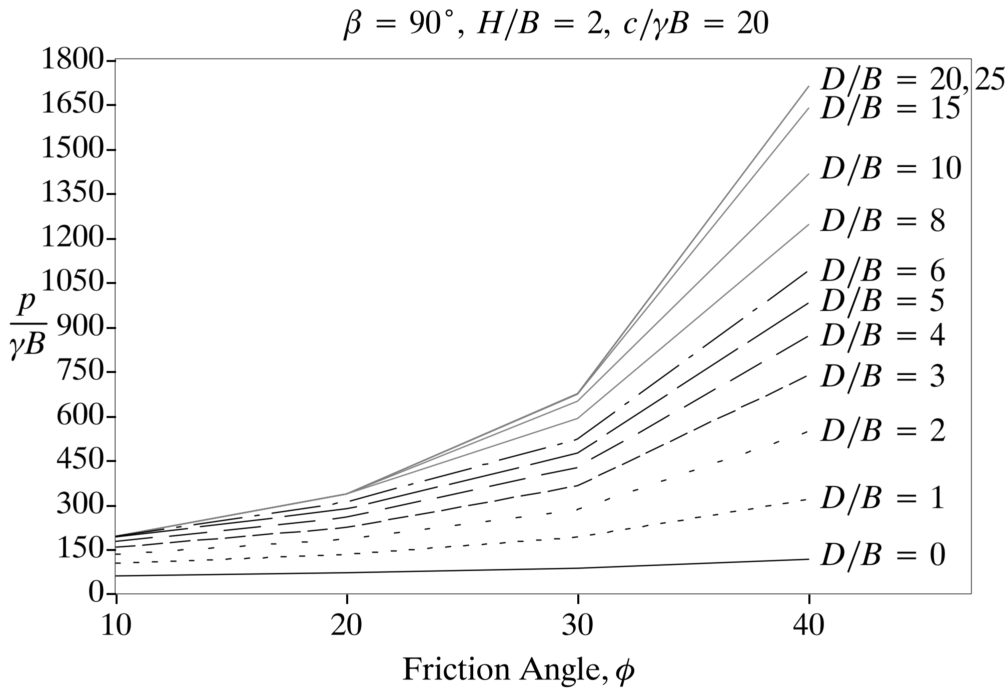

Figure 4.10: Effect of friction angle with footing distance ratio

Figure 4.10 again confirms that increasing friction angle ratio increases the bearing capacity of a slope by. We can see the differences in bearing capacity become more noticeable with a higher friction angle as more slope material becomes available to provide resistance to the footing force. We can also again see that the results converge with a smaller friction angle as there will not be as much interaction between the soil particles no matter what the footing distance ratio is. A footing situated at D/B = 2 for a material with $\phi = 40^\circ$ friction angle will have a higher bearing capacity then a footing situated much further away from the slope face at D/B = 25 for a material with $\phi = 20^\circ$ friction angle.

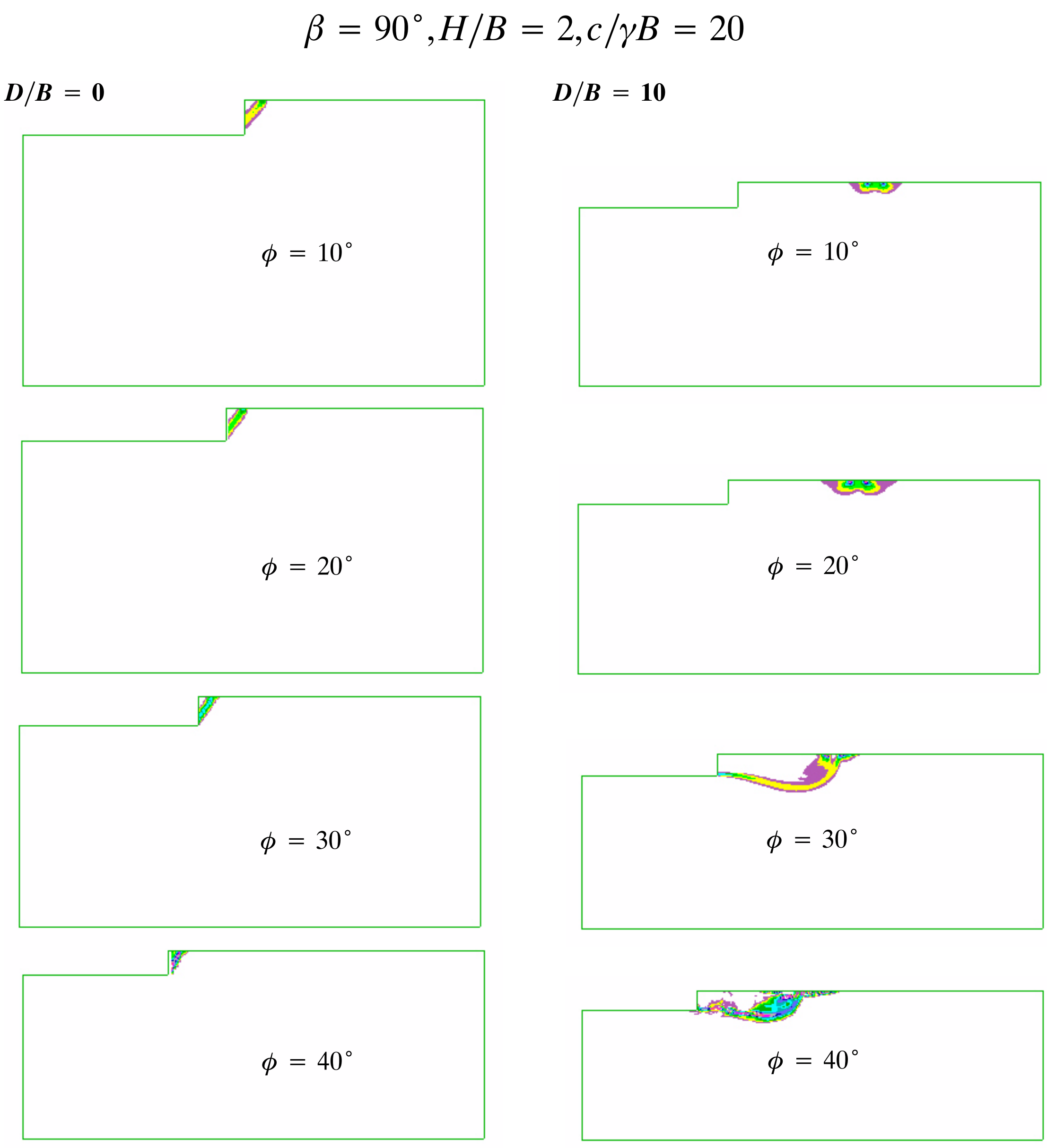

Figure 4.11: Contour plots for friction angle with varied footing distance ratio

Figure 4.11 demonstrates the effect friction angle has on the failure plane for a particular slope. We can observe that for friction angles of $\phi = 10^\circ$ and $\phi = 20^\circ$ footing on slope situation occurs for the smaller footing distance ratio and footing on flat ground situation occurs for the large footing distance ratio as expected. However for friction angles of $\phi = 30^\circ$ and $\phi = 40^\circ$ for the larger footing distance ratio, we can see that the failure plane has once again become a footing on slope problem. It can be gathered from these contour plots that while bearing capacity of a slope increases with increased friction angle, the footing on slope problem can re-emerge even for large footing distance ratios.

4.3.3 Comparison With Slope Height Ratio

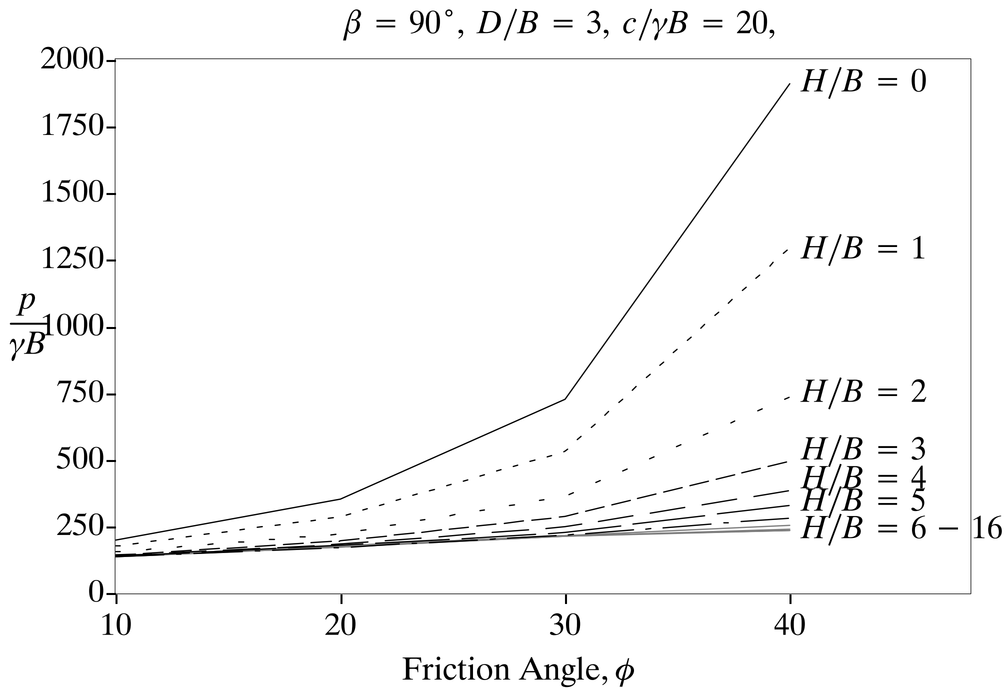

Figure 4.12: Effect of friction angle with slope height ratio

Examining Figure 4.12 we can the expected trend of increaseing bearing capacity with increasing friction angle. What we can also again see though, is the normalising of results above approximately H/B = 6. We have come to expect that as friction angle of a material increases so too will the bearing capacity, however for H/B > 6 we can see that there is very little increase in bearing capacity between $\phi = 10^\circ$ and $\phi = 40^\circ$. This tends to suggest that above this slope height ratio, there is not enough extra material available for high friction angle soils to be at an advantage. It could be assumed from this that the failure plane for slope height ratios greater then H/B = 6 would be the same.

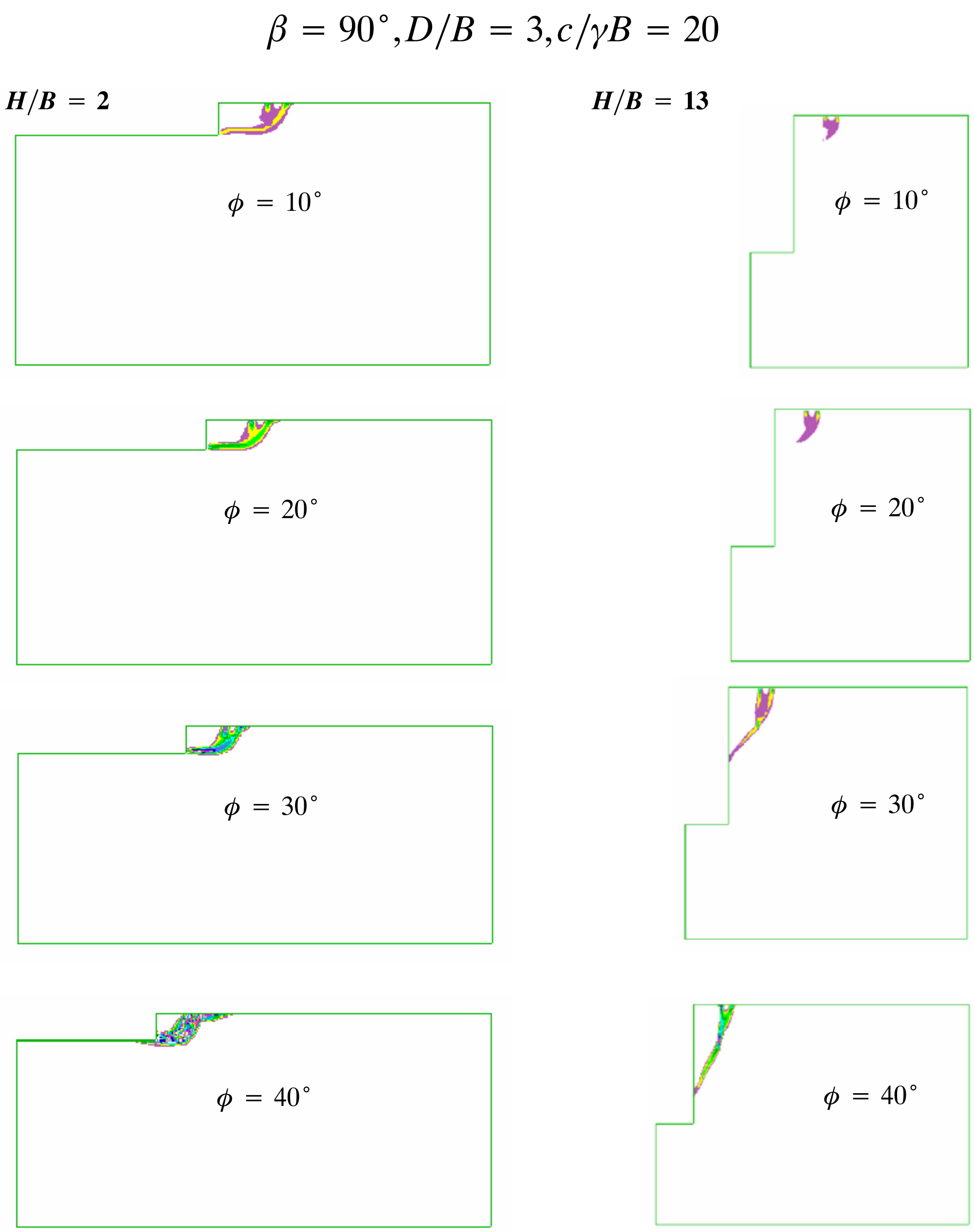

Figure 4.13: Contour plots for friction angle with varied slope height ratio

For the small slope height ratio for the case shown in Figure 4.13, we can see the insignificant changes in the failure plane between each of the friction angles with only the size of the failure surface changing as it is now expected. For the larger slope height ratio, the slopes with smaller values of friction angle do not appear to have failed as normally seen for a footing on flat ground behaviour however the failure planes have not reached the slope face. If we compare this with the failure surfaces for the larger friction angles we can see that their failure planes have reached the slope face due to the greater interaction between the material particles.

4.3.4 Conclusion

From the results analysed it has been determined that friction angle does have a large effect on the normalised bearing capacity of a slope. In each of the comparisons that were made the higher friction angles always produced the higher bearing capacities. In the contour plots shown we can see that this higher bearing capacity is due to the increased mass of material that is involved for a higher friction angled material in supporting the footing load. It could be concluded then that for a material with very low friction angle a change in any of the other main parameters would only result in a marginal increase in bearing capacity, and the best material for construction purposes is one with a high friction angle as it will always produce a higher bearing capacity.

4.4 Effect of Footing Distance Ratio, D/B

Footing distance ratio refers to the distance from the edge of the slope to the face of the footing and is relative to the footing width. This ratio is important to slope analysis as it is a key factor that affects whether a footing is judged as a footing on slope problem or a footing on flat ground problem. This is because as the footing moves away from the slope edge, the instability that may be associated with a particular slope plays a lesser role in the bearing capacity of the slope.

With this knowledge in mind, it can be expected that as a footing moves further away from a slope edge the bearing capacity of the slope material will be increased. What is not known however is the combined effect footing distance ratio with dimensionless strength ratio, slope height ratio and friction angle or the material. This section will look into this and attempt to note any trends encountered.

4.4.1 Comparison With Dimensionless Strength Ratio

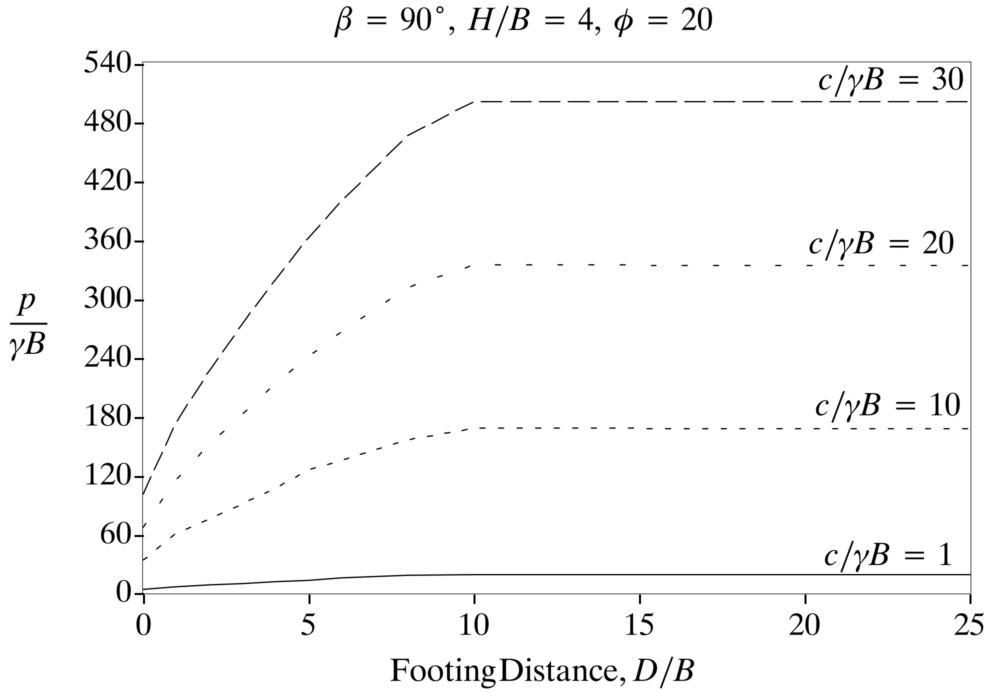

Figure 4.14: Effect of footing distance ratio with dimensionless strength ratio

In Figure 4.14 we can observe the effects of footing distance ratio on bearing capacity when combined with dimensionless strength ratio. When can see the trend that for varying strengths of soil flat ground behaviour will be experienced at the same footing distance ratio value, where anything further from the slope edge then this is a footing on flat ground situation. We can also see the trend that the bearing capacities converge as the footing distance decreases for all the strength ratios. It is these footing distance ratios where the failure plane is above toe and still a slope problem so each soil strength ratio will have a similar failure plane for a particular footing distance.

$$\beta = 90^\circ, H/B = 2, \phi = 20^\circ$$

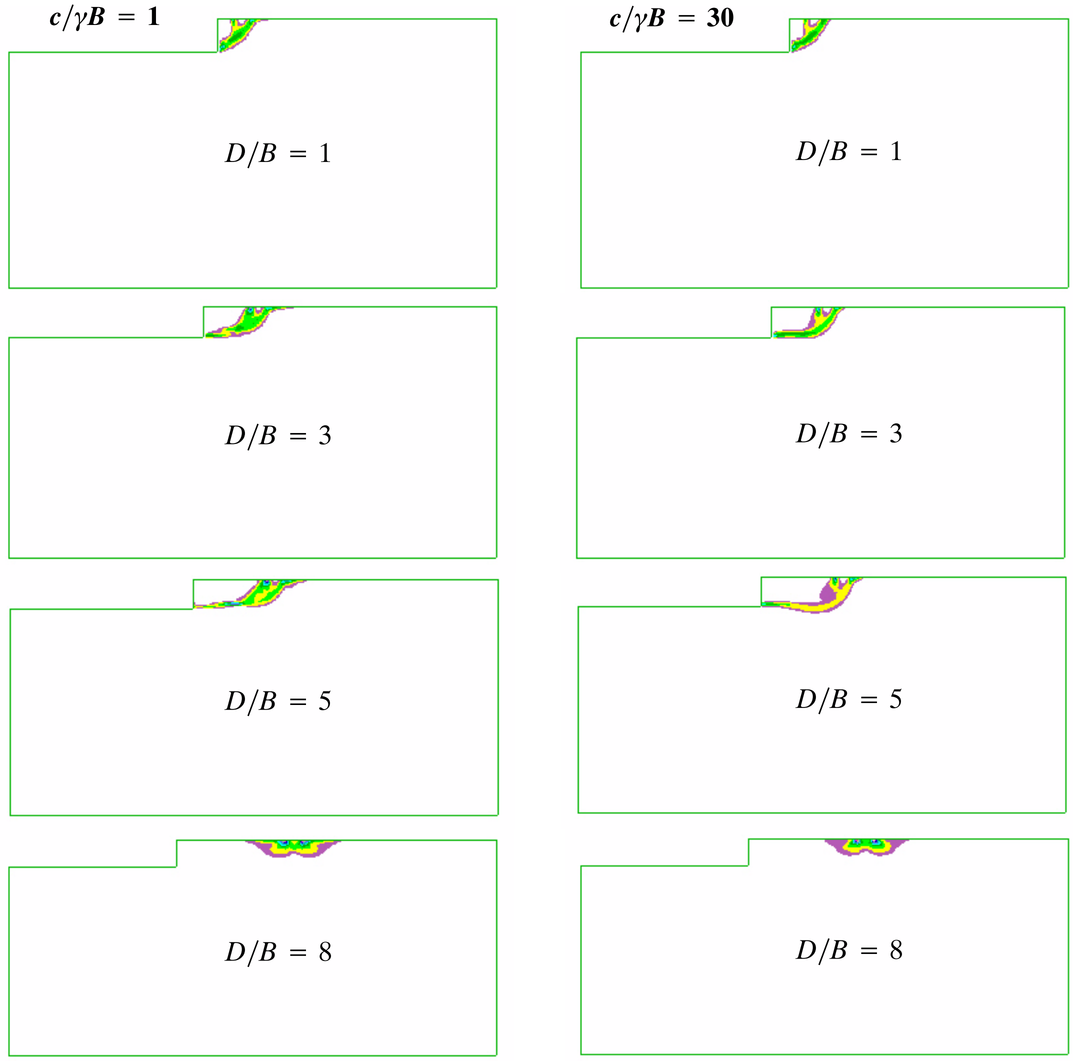

Figure 4.15: Contour plots for footing distance ratio with varied dimensionless strength ratio

If we examine Figure 4.15 we can see as the footing distance ratio increases the failure surface changes from a slope failure to a flat ground failure. We can also see the extent to which a failure plane can reach for the particular case shown, with the vertical plane becoming horizontal as it approaches the slope face the for footing distance ratio of D/B = 5. Even though this section is concerned with the effect of footing distance ratio also note the very similar failure surfaces for each footing distance ratio, again proving that dimensionless strength ratio relates to the strength of the material and has little to no effect on the failure plane that occurs.

4.4.2 Comparison With Slope Height Ratio

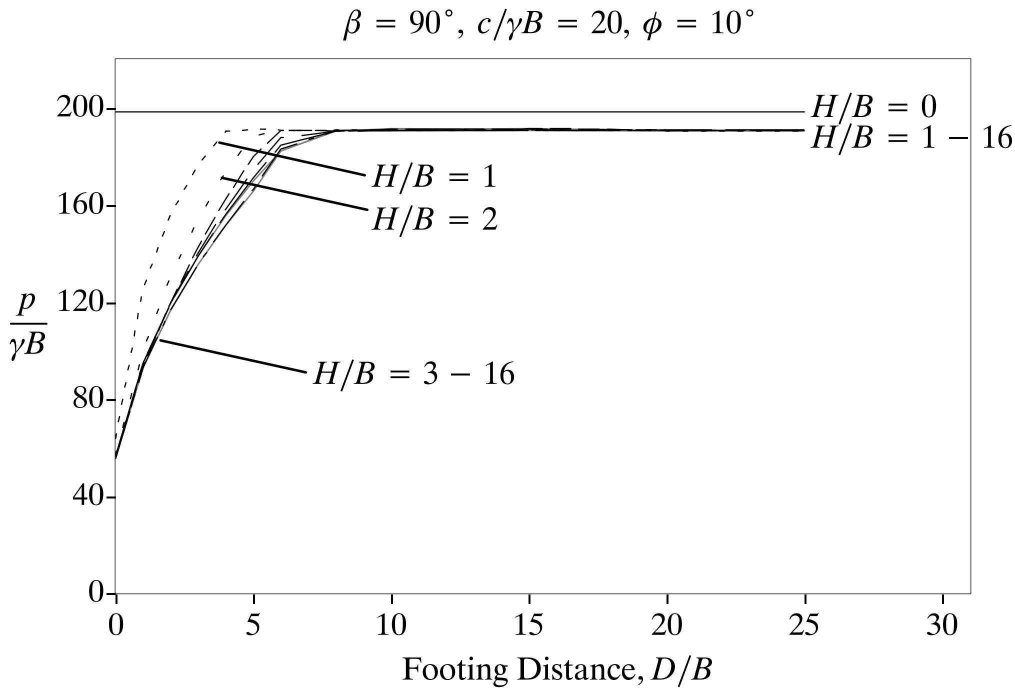

Figure 4.16: Effect of footing distance ratio with slope height ratio

H/B = 0 has been included in Figure 4.16 to show the flat ground bearing capacity for the material in this particular case. We can again see the higher bearing capacities associated with the higher footing distance ratios, with a common line for H/B = 3–16 showing that the failure plane occurs above toe immediately. We can also again see flat ground behaviour occurring at approximately D/B = 9 for this case, which due to the single results line for any footing distance ratio higher then this indicates that the footing is no longer a footing on slope problem even for the largest slope height ratio.

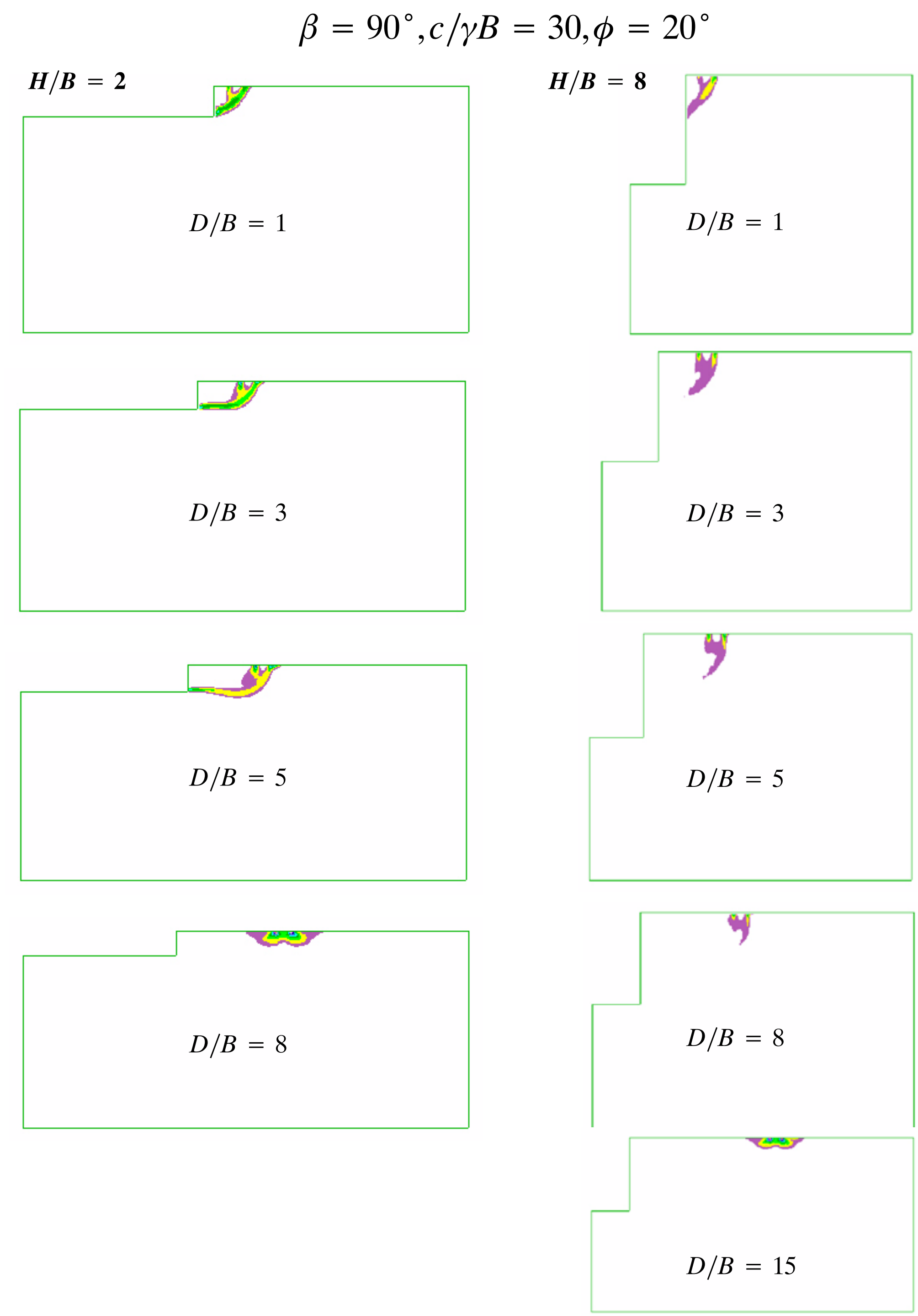

Figure 4.17: Contour plots for footing distance ratio with varied slope height ratio

Figure 4.17 shows the contour plots that occur with increasing values of footing distance ratio. Interesting to note is the failure planes that have occurred between to two different slope height ratios used. We can see on the H/B = 2 images that the failure plane extends from the footing location to the toe of the slope for each footing distance ratio until it becomes flat ground behaviour at D/B = 8, while for the H/B = 8 images only the lowest footing distance ratio has failed through to the slope face. For all the other cases for H/B = 8 the failure surfaces are on the verge of failing through the slope face but it didn't eventuate which could be attributed to the larger soil mass of the slope. We can also see that for the higher slope height ratio flat ground behaviour is not experienced until D/B = 15 while for the lower slope height it occurs at D/B = 8.

4.4.3 Comparison With Friction Angle

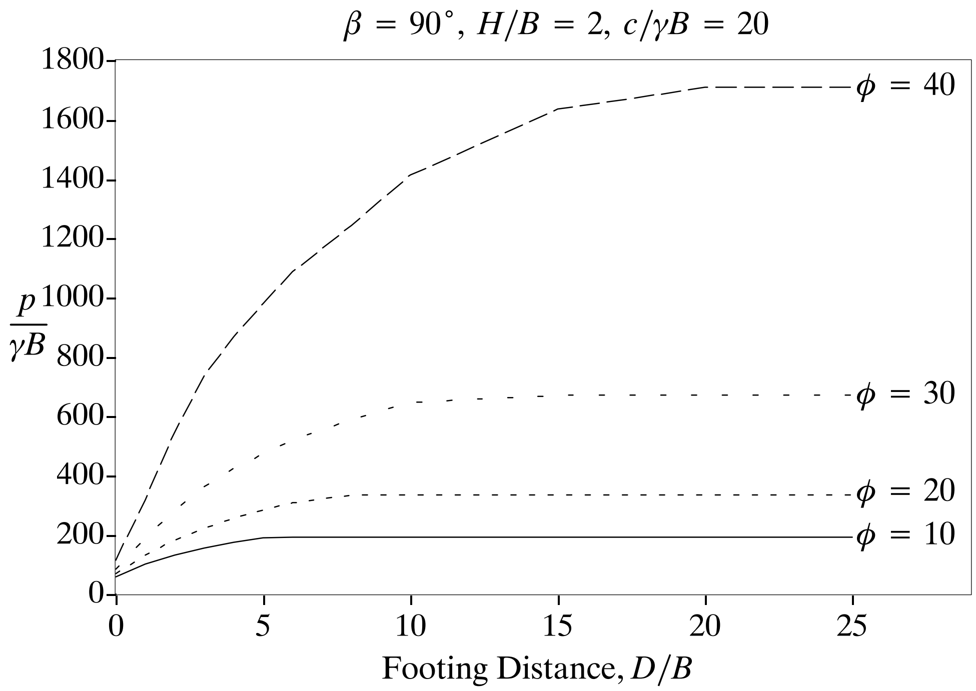

Figure 4.18: Effect of footing distance ratio with friction angle

In Figure 4.18 it can be seen what effects footing distance ratio has with friction angle on the normalised bearing capacity of a slope. If we observe bearing capacity values for small footing distance ratios, we can see that the results converge, meaning that when the footing is located close to the slope edge the internal friction angle of the slope material plays a less critical role in overall bearing capacity of a slope. Another interesting point to note is when flat behaviour is experienced for each of the friction angles. If we consider $\phi = 10^\circ$ we can see that flat ground behaviour occurs at D/B = 6, while for $\phi = 40^\circ$ it occurs at D/B = 24 approximately. This supports the idea that a larger friction angle creates a larger interaction mass of soil producing higher bearing capacities as suggested earlier.

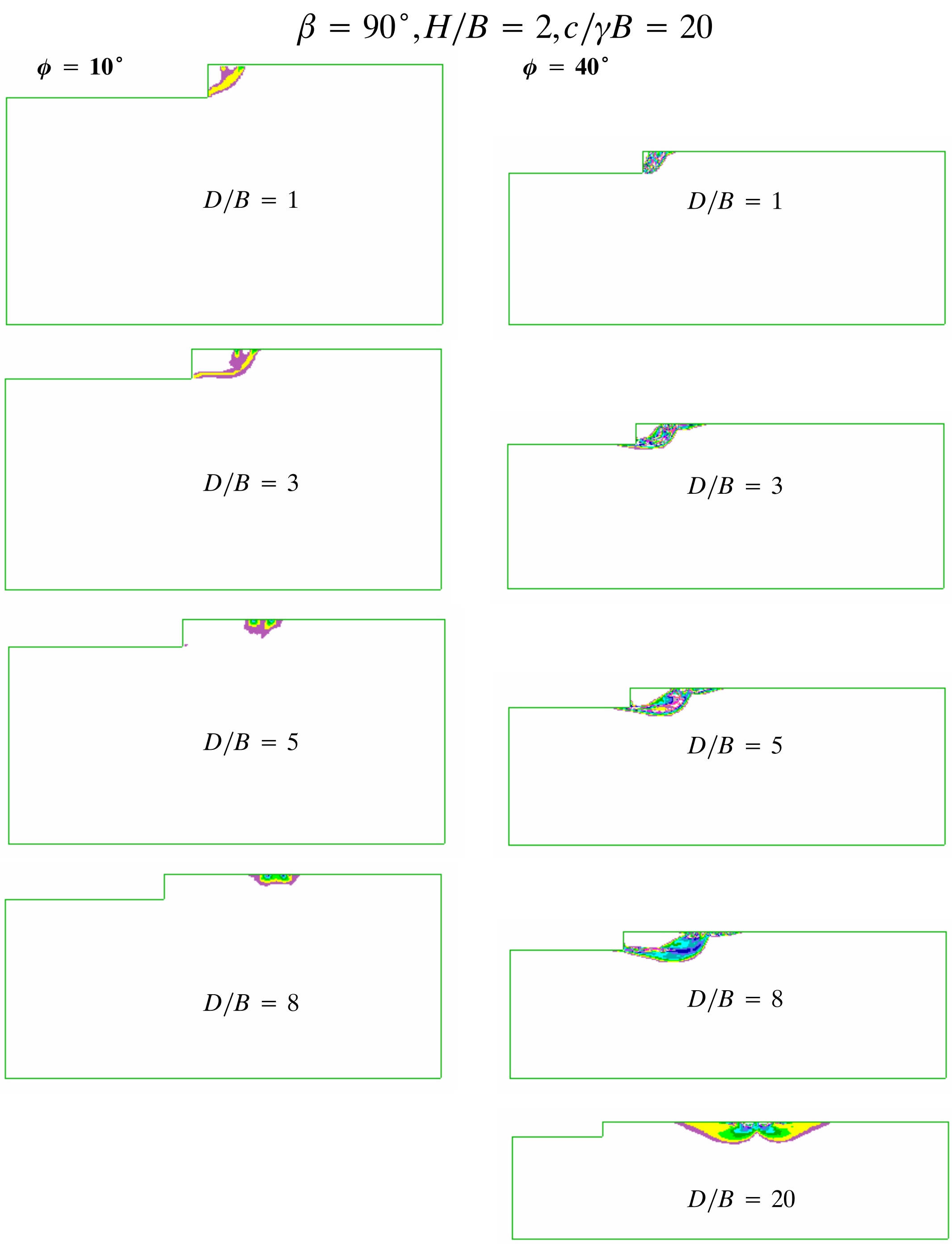

Figure 4.19: Contour plots for footing distance ratio with varied friction angle

In Figure 4.19 it is clearly seen the effect of footing distance ratio and friction angle combined. We can see that for a friction angle of $\phi = 10^\circ$ flat ground behaviour is on the verge of occurring at D/B=5, while for a friction angle of $\phi = 40^\circ$ the failure plane is still occurring below toe for the same situation. For the material with $\phi = 40^\circ$ flat ground behaviour isn't experiences until D/B = 20 which is significantly further from the slope face. Thus we can gather from these images that footing distance ratio combined with friction angle will have a very considerable effect on the where flat ground behaviour is reached which in turn will affect the bearing capacity.

4.4.4 Conclusion

Footing distance ratio plays a significant role in where footing on flat ground behaviour will occur, however it is also affected by many of the other parameters that were combined with it in this section. We found that dimensionless strength ratio did not affect where flat ground behaviour occurred, rather it simply changes the bearing capacity that was reached. However the parameters of slope height ratio and friction angle did have an effect on this transition from footing on slope to footing on flat ground problem. It was noted that a higher slope height required a greater footing distance for flat ground behaviour which could be attributed to the greater natural instability of a higher slope. We also determined that an increased friction angle effected the occurrence of flat ground behaviour, due to the greater interaction between the soil particles transferring the effects of a footing load further.

4.5 Effect of Slope Height Ratio, H/B

Slope height ratio refers to the distance between the top of the slope and the bottom of the slope and is again relative to the footing width just as is the case for footing distance ratio. The slope height ratio plays in important part in a slopes bearing capacity due to a number of reasons. Firstly, the slope height ratio can affect whether footing on flat ground behaviour occurs or not, as with a small slope height ratio for a particular footing distance ratio a footing on flat ground situation may occur. If we however increase the slope height ratio while keeping the footing distance ratio constant, the footing may again become classified as a footing on slope problem. This is related to the slope's stability which is another reason why slope height ratio has in important role in bearing capacity.

The stability of a slope will affect the bearing capacity that is possible for that particular slope. If a slope is unstable then it will be unable to support as much load as a stable slope, due to the fact that some of the slope's strength will be involved in simply keeping the slope from failing due to its own weight and dimensions.

Knowing this information, we could expect that as the height of a slope is increased its bearing capacity will be decreased. What we don't know is what effect dimensionless strength ratio, footing distance ratio and the friction angle of the soil combined with slope height ratio have on the bearing capacity of a slope. It is these parameter relationships that will be looked into in this section.

4.5.1 Comparison With Dimensionless Strength Ratio

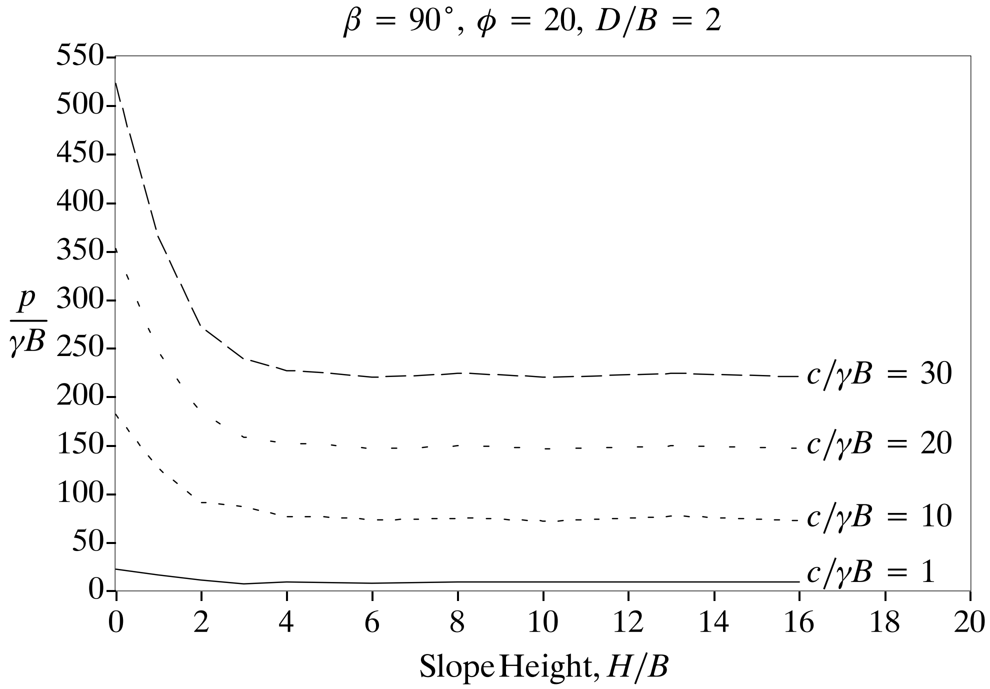

Figure 4.20: Effect of slope height ratio with dimensionless strength ratio

In Figure 4.20 we can again see a trend that as the slope height ratio increases the bearing capacity decreases. We can also again see that with a larger dimensionless strength ratio a higher bearing capacity is obtained. As with the results for dimensionless strength ratio and footing distance, flat ground behaviour is again experienced at the same position on a particular slope for all strength ratios. We can also see that for small slope height ratios, the strength ratio of the material does have a significant effect while the failure plane is below toe. However, as the slope height increases the effect of soil strength is less severe as failure becomes above toe and similar failure planes begin to occur.

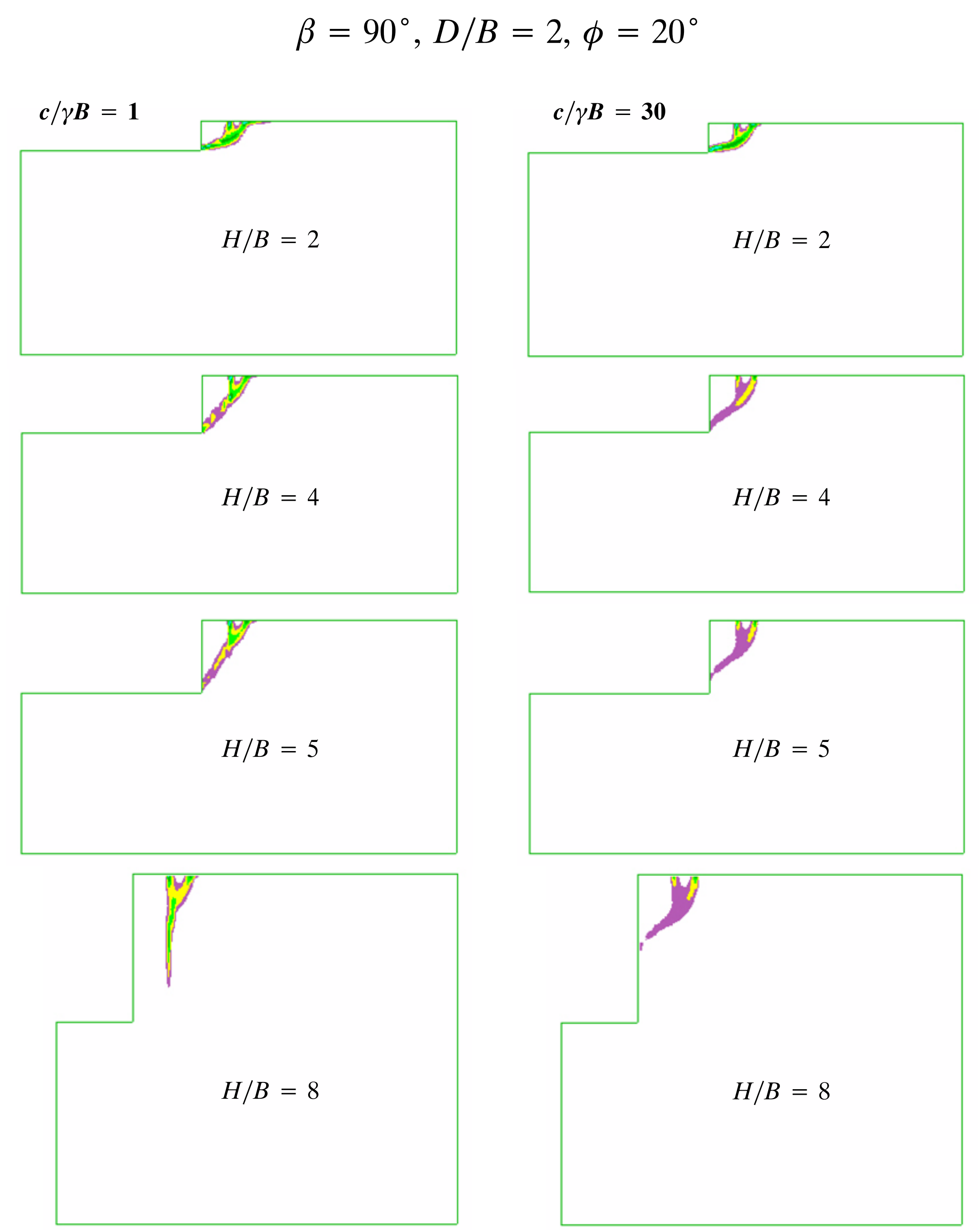

Figure 4.21: Contour plots for slope height ratio with varied dimensionless strength ratio

Figure 4.21 shows the effect of slope height ratio and dimensionless strength ratio on the failure surfaces that occur. We can see that the failure planes are the same for corresponding values of slope height ratio except for the case of H/B = 8. It is unclear why this has happened as different strength ratios should still give the same failure planes as discussed in previous sections. Note that for all cases above H/B = 2 the failure has occurred above the toe indicating that the maximum bearing capacity has been reached.

4.5.2 Comparison With Footing Distance Ratio

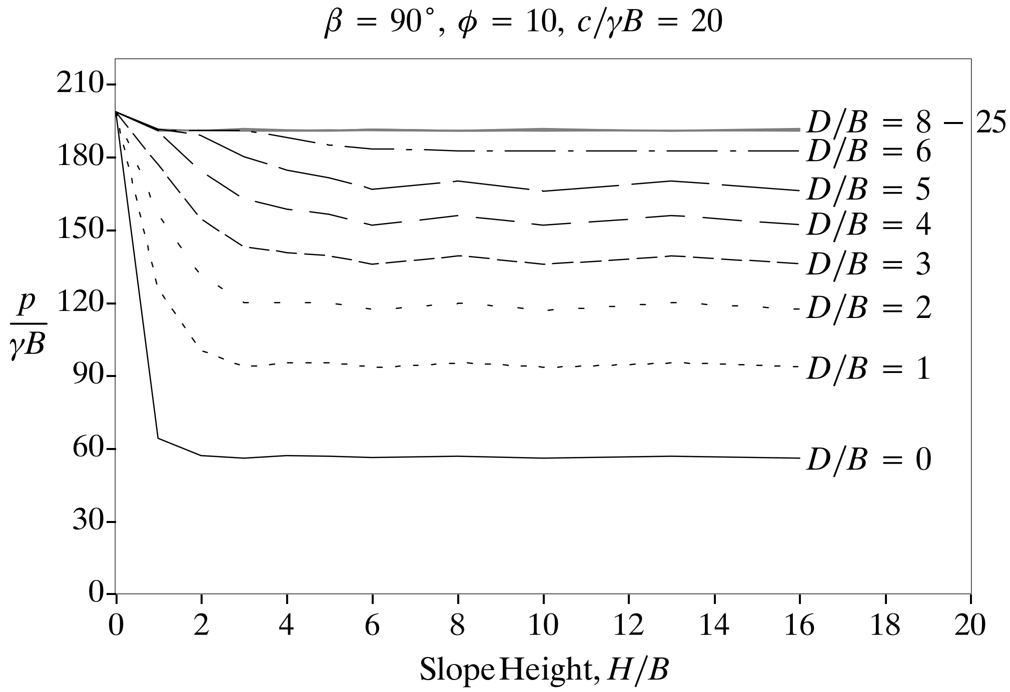

Figure 4.22: Effect of slope height ratio with footing distance ratio

Figure 4.22 shows the effect of slope height ratio combined with footing distance ratio. While the effects of slope height ratio on bearing capacity have already been established in previous sections, the remarkable effect of footing distance ratio combined with slope height ratio can be clearly seen in the above figure. It is particularly noticeable for the lowest values of footing distance ratio where even a slight increase in this distance can produce a far better bearing capacity for a given slope height. We should also note the convergence of capacities related to a slope height of H/B = 0 which is due to footing distance ratio having no effect on the bearing capacity due to flat ground behaviour being experienced.

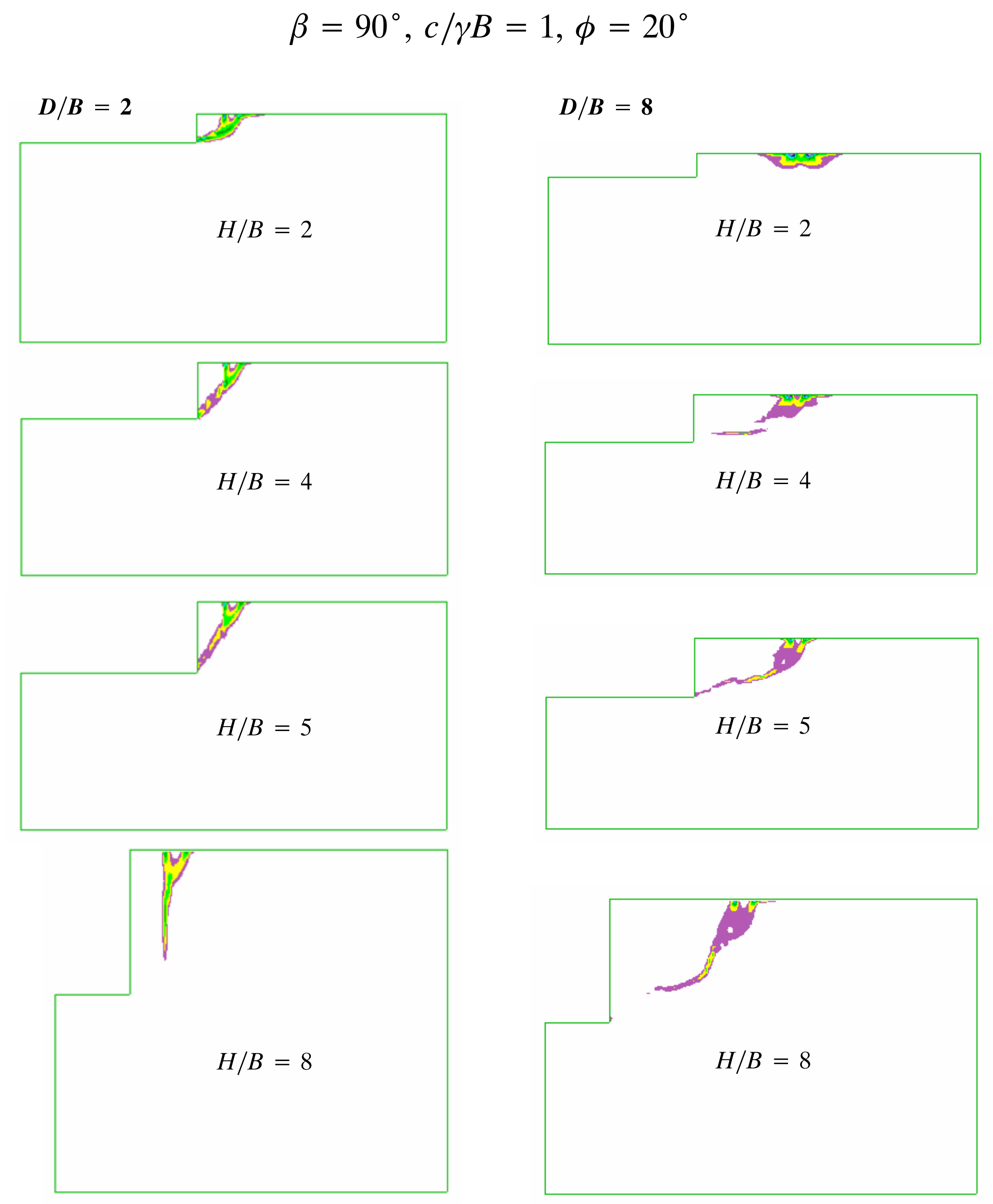

Figure 4.23: Contour plots for slope height ratio with varied footing distance ratio

Figure 4.23 clearly demonstrates the effect of increasing slope height ratio. We can see that for a small footing distance ratio where the footing is located close to the slope edge, that above toe failure occurs each time. However for a larger footing distance ratio where flat ground behaviour has initially occurred, we can see that as the slope height increases the results have reverted back and the footing has become a footing on slope problem once again.

4.5.3 Comparison With Friction Angle

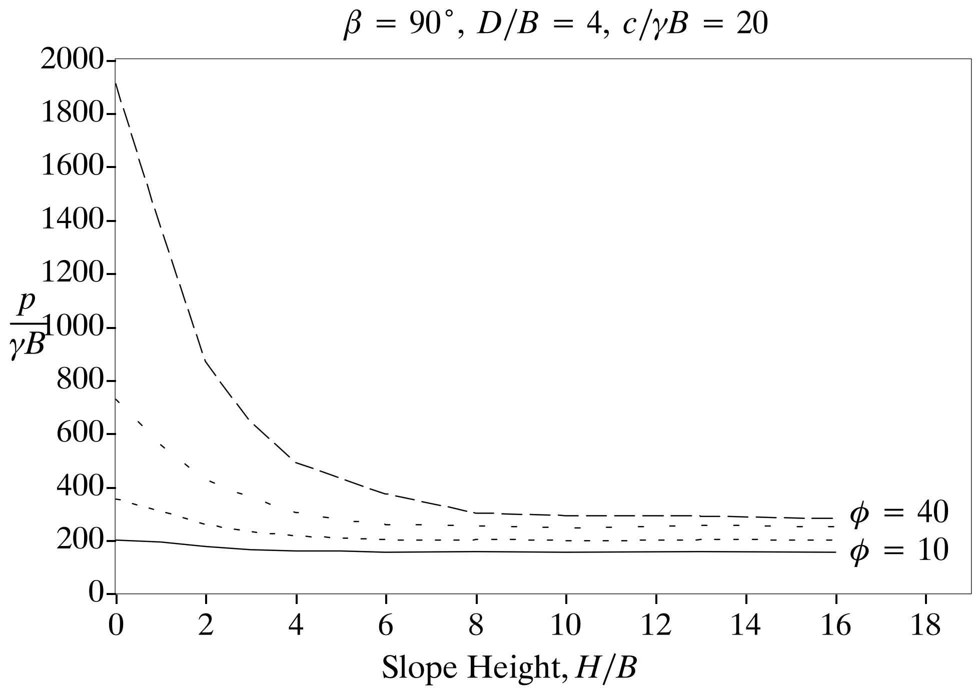

Figure 4.24: Effect of slope height ratio with friction angle

Figure 4.24 again shows the effect friction angle has on the bearing capacity of a slope. For small slope height ratios we can see the large difference in bearing capacities between the friction angles due to the initial below toe failure surfaces and the different areas of material that are involved. While for large slope height ratios we can see that once the failure plane is above toe there is not enough extra soil mass able to be involved in supporting the footing force so the results converge and become relatively close. It should also be noted how the bearing capacity for each friction angle decreases to a limit, and that this limit is different for each friction angle.

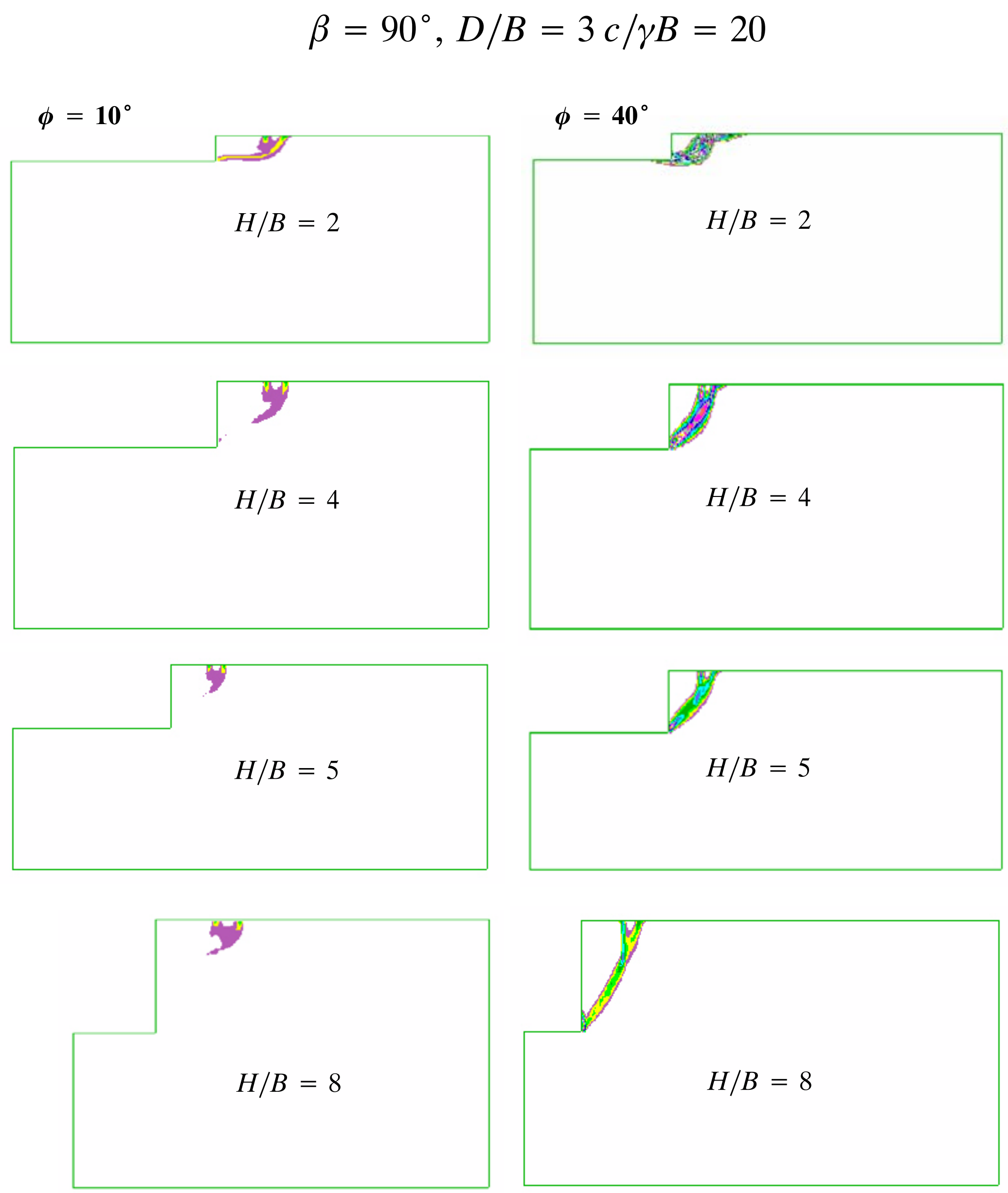

Figure 4.25: Contour plots for slope height ratio with varied friction angle

When we observe Figure 4.25 we can now see why the results in Figure 4.12 display the trend that they do. While it was initally believed that results above a slope height ratio of H/B = 6 were the same due to insufficient extra material to utilise the soil's friction angle and create a larger bearing capacity, we can now see that is not the case. We can see that for a low friction angle there is less interaction between the soil particles and footing on flat ground behaviour is experienced while for a soil with a large friction angle the interaction is greater which actually creates a footing on slope problem. This was an unexpected result but very interesting to note as it means that a slope with high friction angle would suffer slope failure while a slope with low friction angle would suffer from localised footing failure.

4.5.4 Conclusion

In analysing the effect of slope height ratio we found that increasing the slope height ratio reduced the normalised bearing capacity that was obtained. It was also observed that having a higher friction angle combined with a large slope height ratio can cause a change from a localised footing failure to a footing on slope failure. The higher slopes also resulted in similar failure lines once failure had become above toe which produced a bearing capacity limit. Slopes of weaker material such as low friction angles or of small dimensionless strength ratio were affected less by increasing slope height ratio.

4.6 Effect of Stability Number, $N = c/\gamma HF$

Stability number is a measure of how stable a slope is. The stability of a slope can mainly be attributed to two parameters– dimensionless strength ratio and slope height ratio. The combination of these factors determine how well a slope is able to support itself and therefore also the load that it can sustain and is infact how stability number is derived.

The purpose of including stability number in this analysis is due to its common use within the geotechnical field. This means if the stability number of a slope is obtained from another method or source, then it is able to be compared with these analytical results so a bearing capacity can be found.

Due to the involvement of both slope height ratio and dimensionless strength ratio this section will only look at how footing distance ratio and friction angle effect a slope's bearing capacity combined with stability number.

Stability number also considers safety factor when obtaining a bearing capacity value. In the comparisons that will value a safety factor (F) of one was used. For a larger safety factor it is simply necessary to divide the stability number found by the safety factor and use this new value with the chart.

4.6.1 Comparison With Footing Distance Ratio

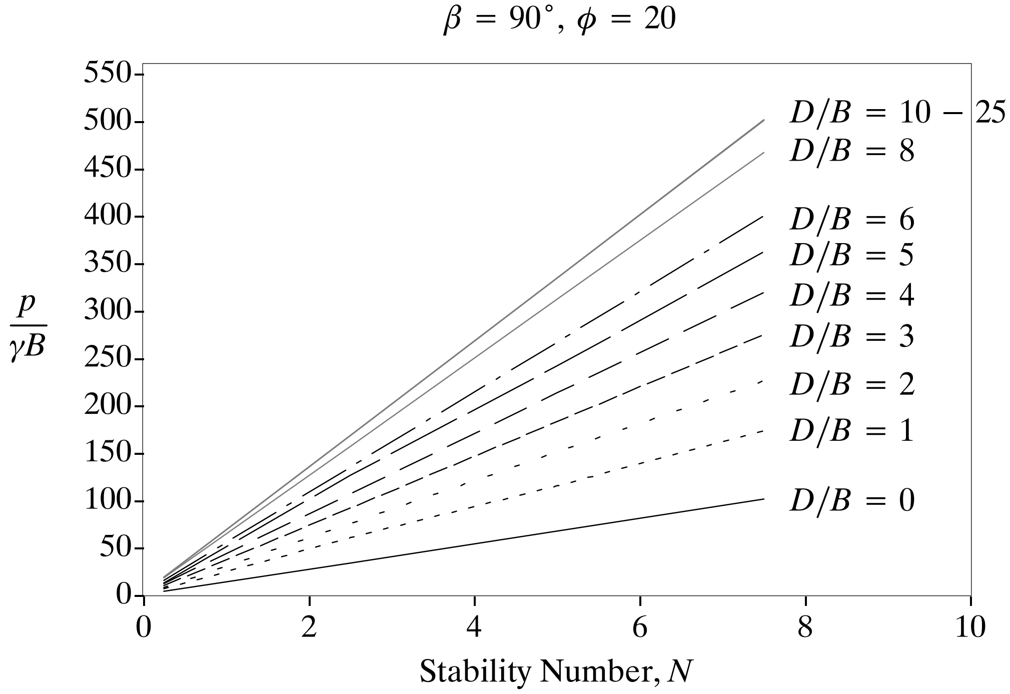

Figure 4.26: Effect of stability number with footing distance ratio

In Figure 4.26 we can see the similarity in the results with dimensionless strength ratio, due to the relationship between stability number and dimensionless strength ratio. However this does re-affirm that a higher stability number will equal a larger bearing capacity. We can also observe that as the footing distance ratio increases higher bearing capacities and flat ground behaviour is reached as expected. This is due to the slope becoming less likely to failure due to a footing load being placed close to its edge and results in a maximum bearing capacity limit.

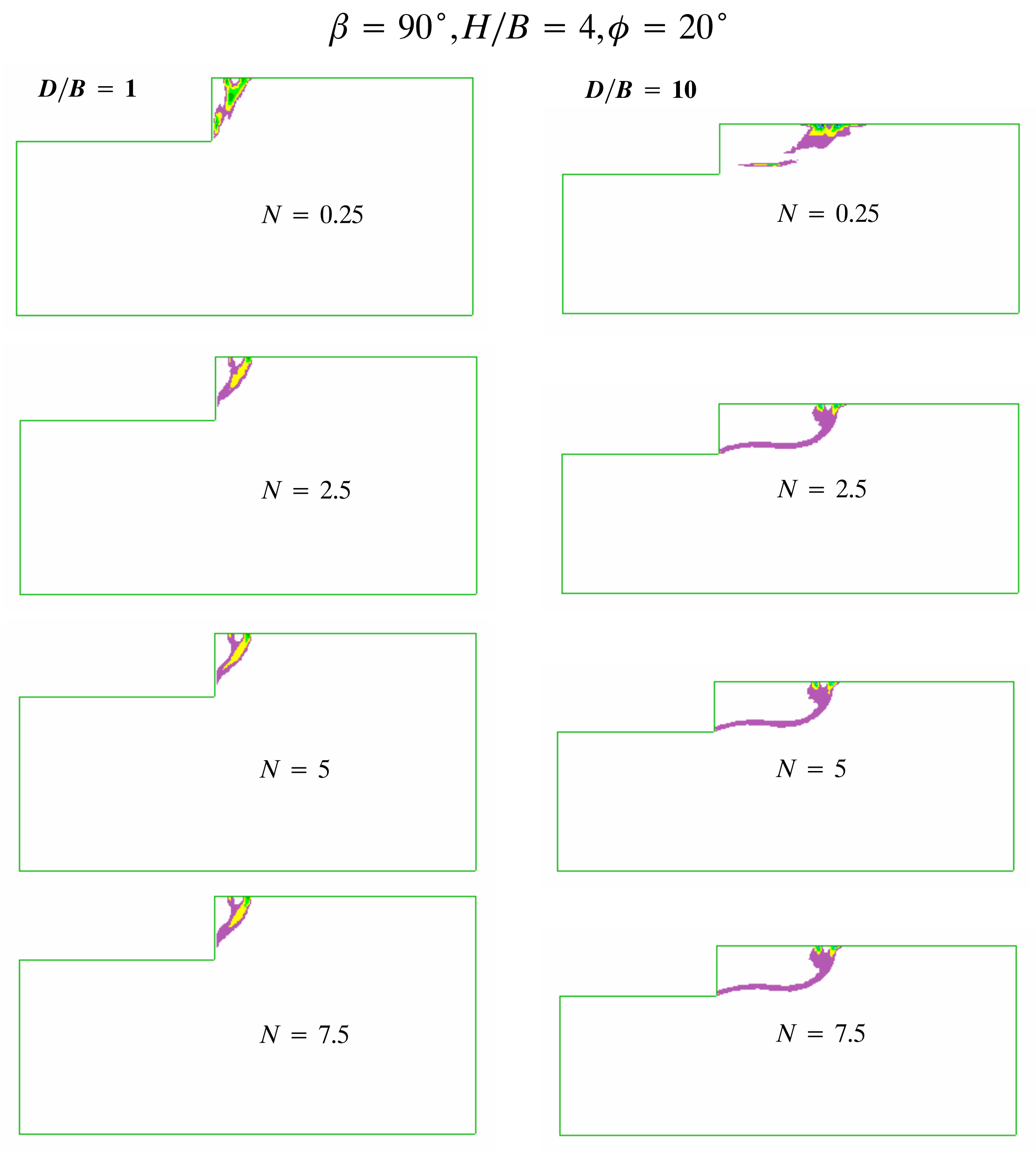

Figure 4.27: Contour plots for stability number with varied footing distance ratio

Again we can see in Figure 4.27 the similarity in results like that obtained for dimensionless strength ratio combined with footing distance ratio. Note the similar failure planes that have occurred indicating that stability number does not affect the failure planes rather it simply influences the strength of the foundation material.

4.6.2 Comparison With Friction Angle

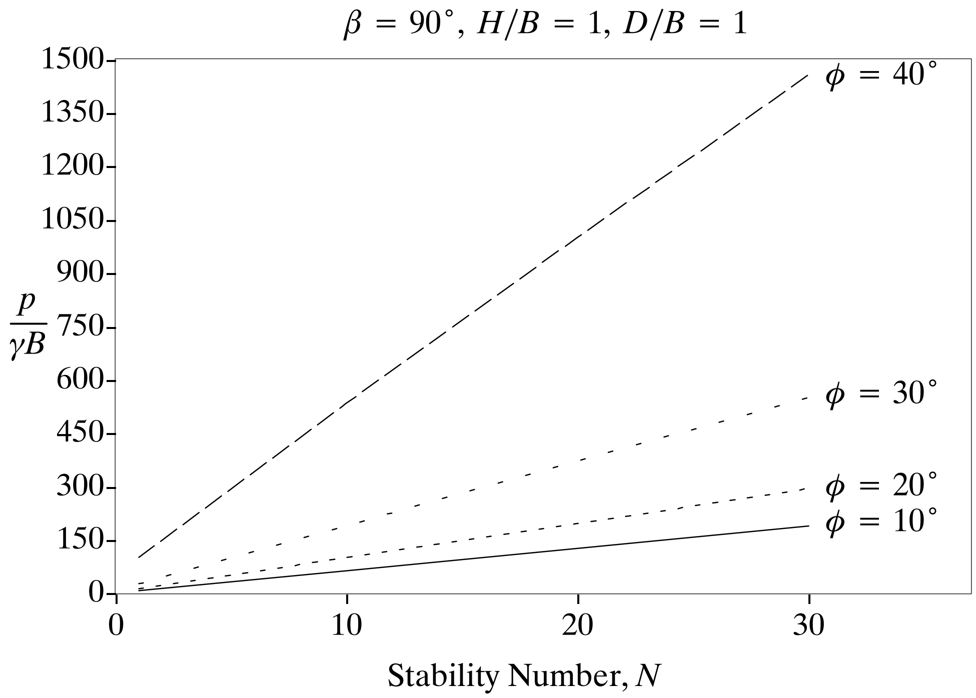

Figure 4.28: Effect of stability number with friction angle

In Figure 4.28 we can once again see the same trend displayed for the effect of stability number with friction ratio as was seen for dimensionless strength ratio and friction angle. Friction angle we know increases the bearing capacity of a slope, with the best combination being a soil of friction angle $\phi = 40^\circ$ and stability number N = 30. Note the smaller difference in bearing capacities between the stability numbers for a low friction angle material.

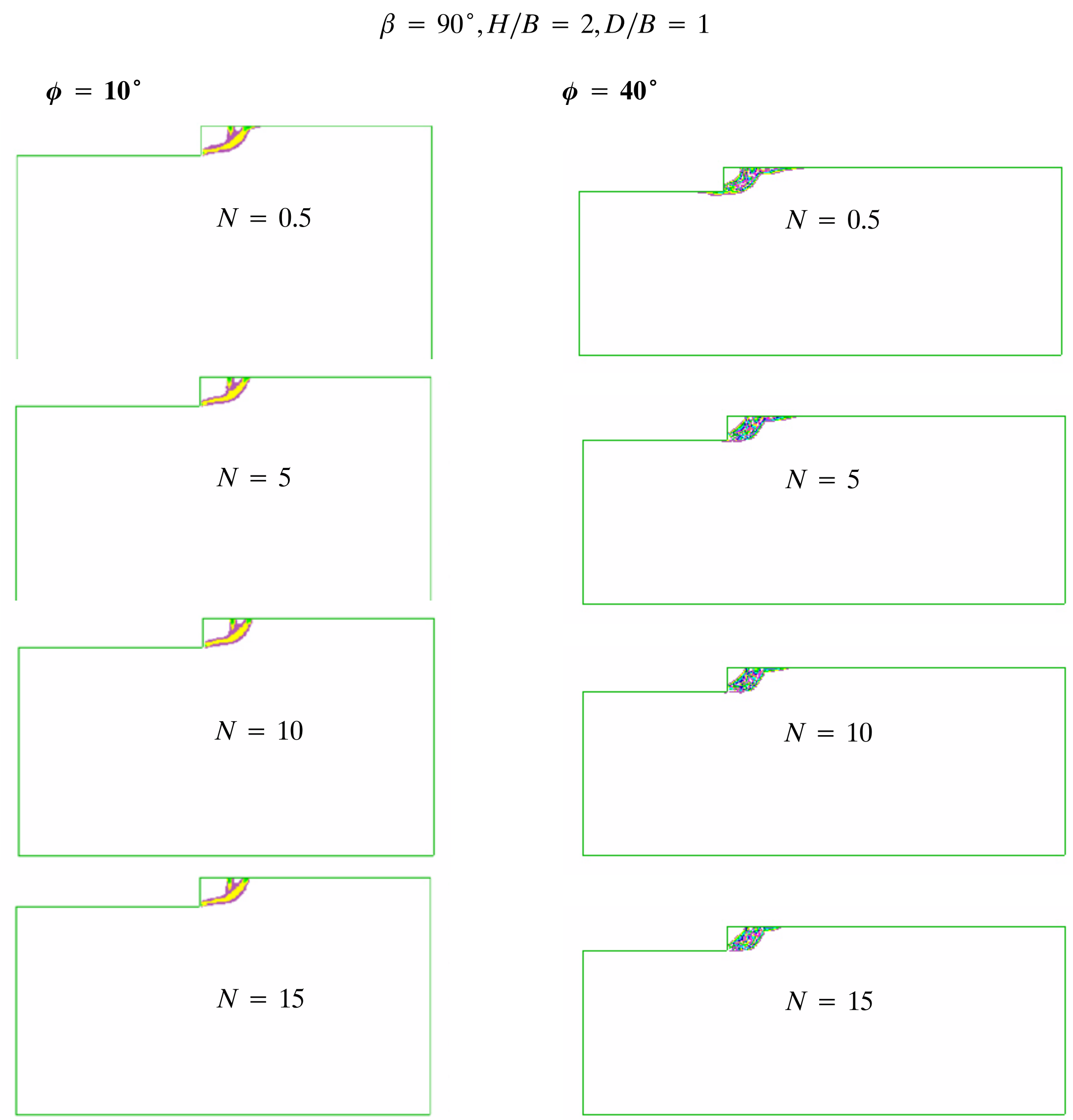

Figure 4.29: Contour plots for stability number with varied friction angle

In Figure 4.29 we see the same result as that obtained for dimensionless strength ratio with stability number not affecting the failure plane that occurs. In this figure we can see the difference between friction angles that has been stated before, with the higher stability number plots simply allowing a higher bearing capacity to take place.

4.6.3 Conclusion

The effects of stability number of bearing capacity were found to mirror that of the effects of dimensionless strength ratio. Due to the relationship of dimensionless strength ratio and slope height ratio on stability number only footing distance ratio and friction angle were able to be compared. As with strength ratio, the higher the stability number the greater the bearing capacity possible. The main idea behind including stability number was to allow interaction between people using different methods.

4.7 Conclusion

By examining each of the main parameters affecting bearing capacity of a slope- they being dimensionless strength ratio, friction angle, footing distance ratio, slope height ratio and stability number- it is hoped that a better understanding of footing on cohesive-granular material slopes could be obtained, enabling a better prediction of what could be expected of a slope given the dimensions and slope material properties.

Using the results that were gathered a set of design charts have been designed to show bearing capacities of different slopes with the main parameters varied. These charts were designed in a way that represented the best and easiest way to convey the information, so that the charts could be used in the geotechnical field by engineers wishing to gain an approximate value on what a particular slope in capable of supporting.

The design charts created include:

- Footing on Flat Ground or Slope Condition Charts
- Increased Bearing Capacity due to Increasing Strength Ratio Charts
- Increased Bearing Capacity due to Increasing Footing Distance Charts
- Decreased Bearing Capacity due to Increasing Slope Height Ratio Charts
- Increased Bearing Capacity due to Increasing Stability Number Charts

Example charts of each type are shown in the following sections with the complete set of each found in Appendix 8.2 - 8.6.

4.7.1 Footing on Flat Ground or Slope Condition Charts

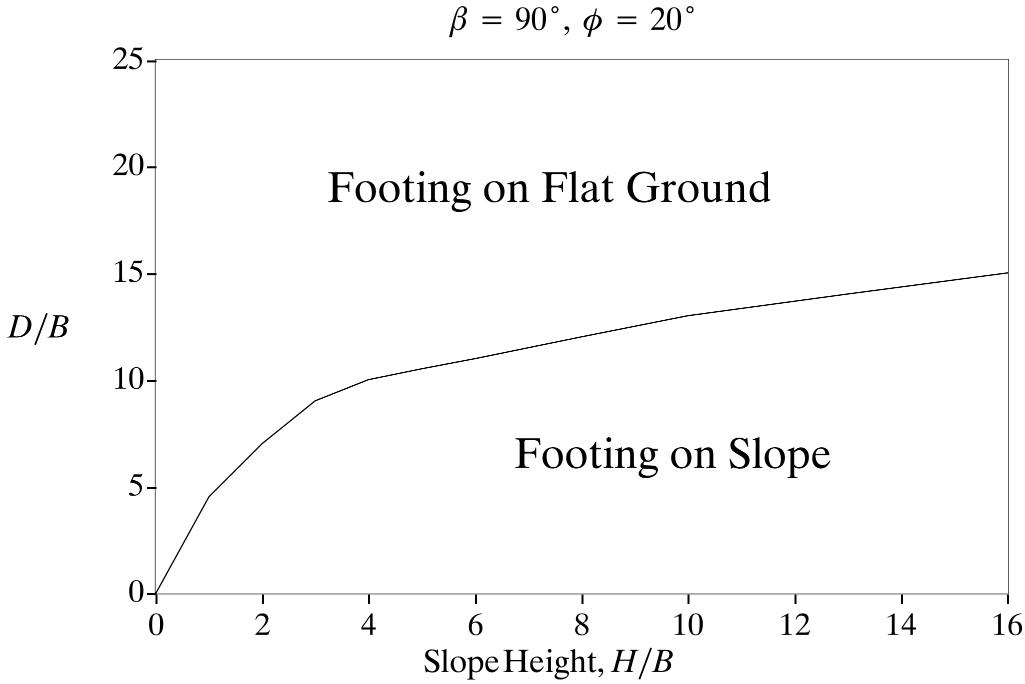

Figure 4.30: Footing on Flat Ground or Slope Condition Chart

Figure 4.30 demonstrates the first chart that would be used if using design charts to obtain an estimation on bearing capacity for a particular case. Using this chart at the first step will advise you if the footing you are designing is infact considered to bo a footing on slope or footing on flat ground problem.

Only 4 of these charts were created as it was found that flat ground behaviour was experienced at the same location for each strength ratio, which supports the findings in this chapter that dimensionless strength ratio effects only the bearing capacity of a slope and not the failure plane.

4.7.2 Increased Bearing Capacity with Increasing Strength Ratio Charts

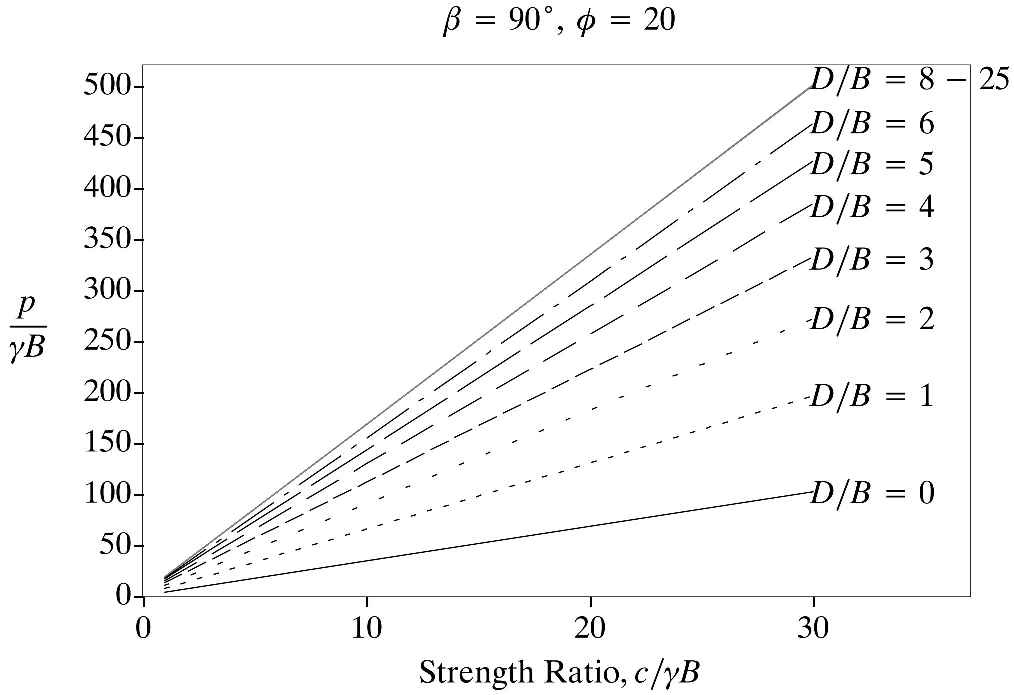

Figure 4.31: Increased Bearing Capacity with Increasing Strength Ratio Charts

Figure 4.31 shows a chart that would be used if the slope height ratio, soil strength ratio and friction angle are known along with the allowable bearing capacity of the slope. Using this information is can be determined at what footing distance a footing needs to be to ensure a slope failure will not occur.

4.7.3 Increased Bearing Capacity with Increasing Footing Distance Ratio Charts

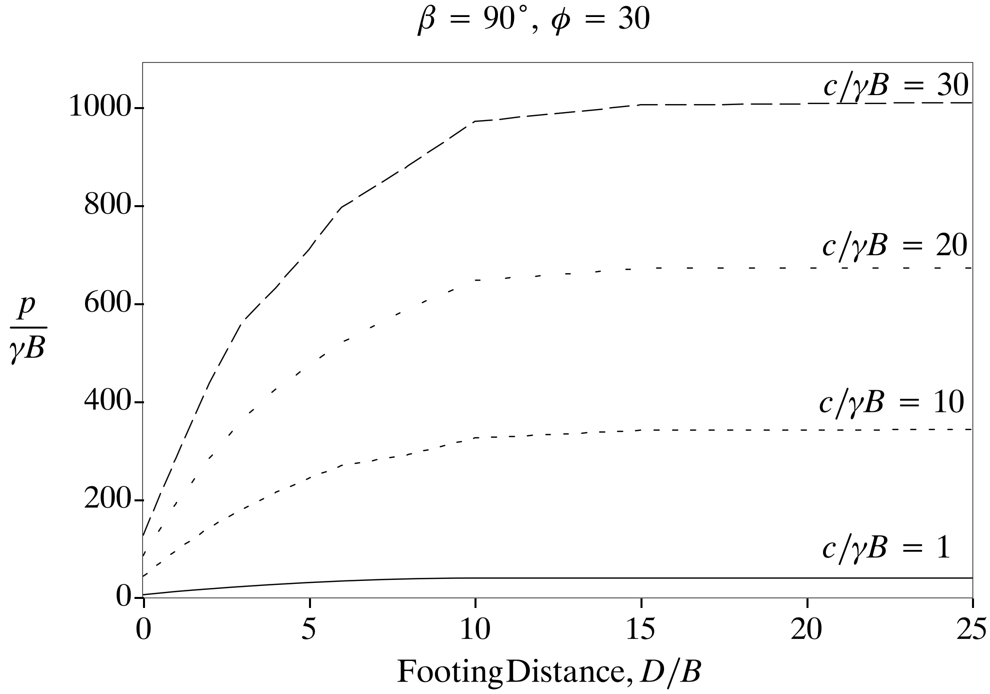

Figure 4.32: Increased Bearing Capacity with Increasing Footing Distance Ratio Charts

Figure 4.32 shows the type of chart that would be used if wanting to find an estimate on the capacity of a slope using footing distance, slope height, friction angle and strength ratio, or if creating an artificial slope then what strength ratio material should be used for a particular footing placement if the allowable bearing capacity is known.

4.7.4 Decreased Bearing Capacity with Increasing Slope Height Ratio Charts

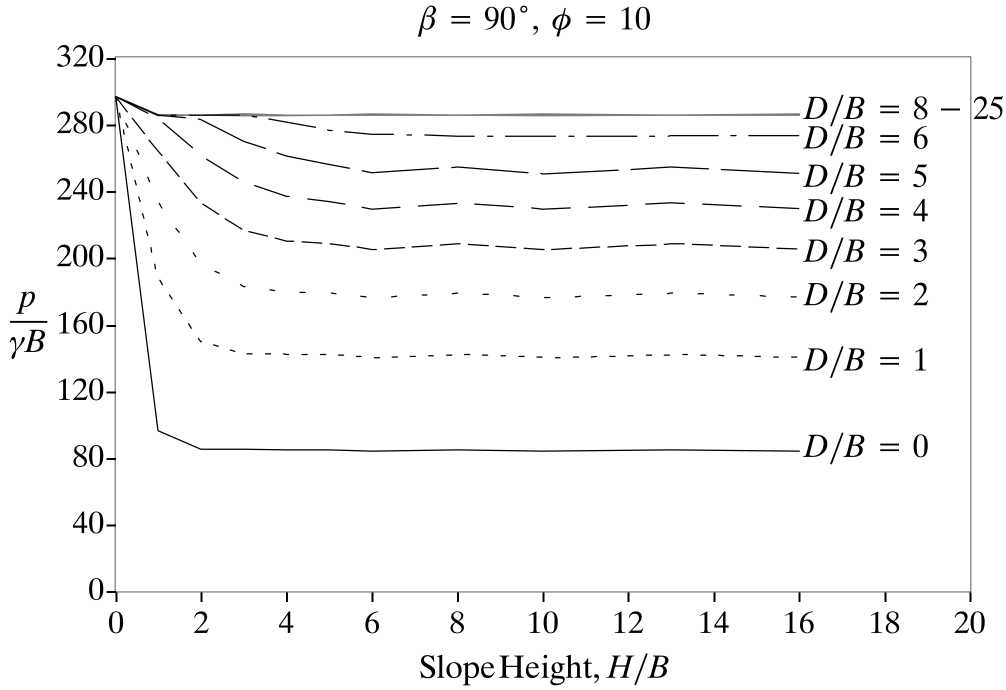

Figure 4.33: Decreased Bearing Capacity with Increasing Slope Height Ratio Charts

Figure 4.33 shows a chart that could be used if an excavation is occurring to see what decrease in bearing capacity there will be, or again if an artificial slope is to be created how high it can be built before it wont have sufficient strength to support the footing it is required to support.

4.7.5 Increased Bearing Capacity with Increasing Stability Number Charts

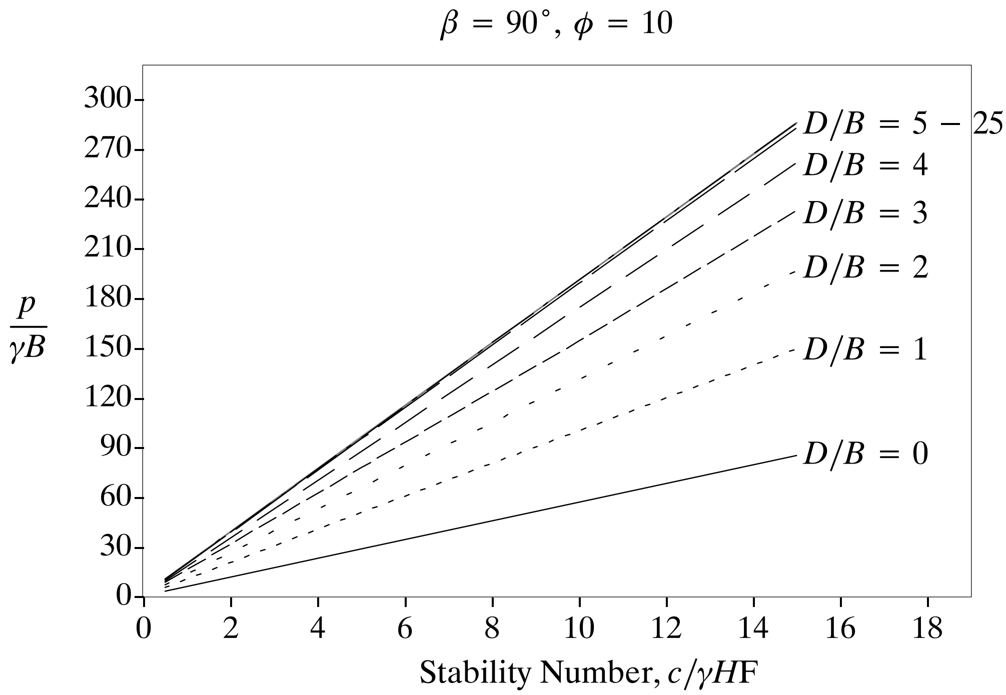

Figure 4.34: Increased Bearing Capacity with Increasing Stability Number Charts

The main purpose of the chart shown in Figure 4.34 is to allow correlation between different methods used within the geotechnical industry so that bearing capacity values can be compared or found if the stability number is found using another method. For the charts designed a safety factor (F) of one was used. For a larger safety factor it is simply necessary to divide the stability number found by the safety factor and use this new value with the chart.

4.8 Example of Chart Use

The following examples demonstrate how to use a design chart to find the bearing capacity of a particular slope.

4.8.1 Example 1

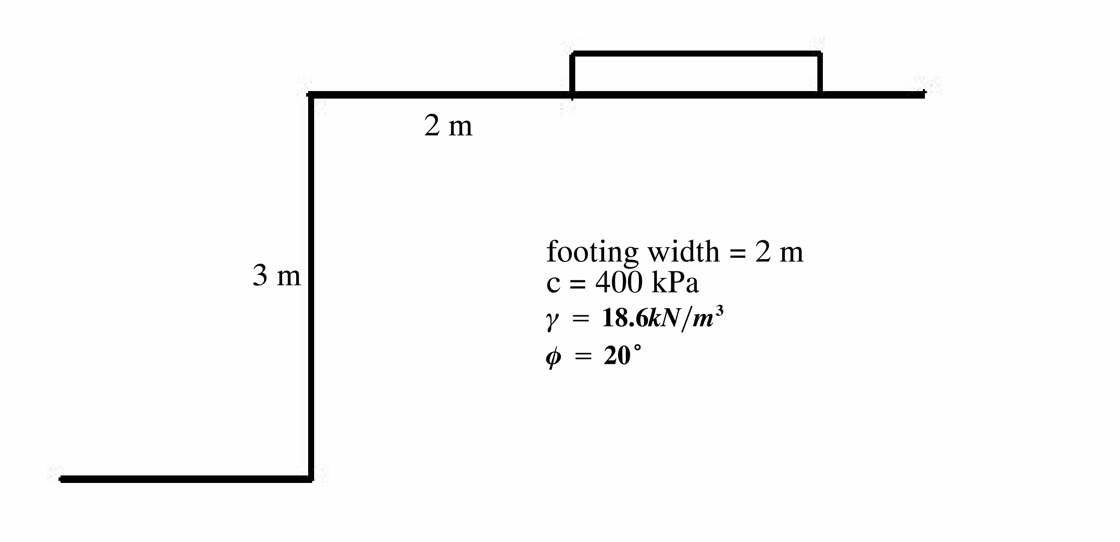

Figure 4.35: Example 1 slope scenario

We know that to find the bearing capacity of a slope using design charts we need the slope height ratio, footing distance ratio, dimensionless strength ratio and internal friction angle. From Figure 4.35 we know the friction angle is 20° and for the other parameters we obtain values for each of:

- H/B = 3/2 = 1.5
- D/B = 2/2 = 1
- $c/\gamma B$ = 400/(18.6 x 2) = 10.75

Using these parameters we can now choose an appropriate design chart to find the bearing capacity. As the slope height ratio was not a whole number interpolation will need to be used. The dimesnionless strength ratio of the slope material is close enough to ten for the purpose of this demonstartion so the design chart chosen for this case was a Decreased Bearing Capacity due to Increased Slope Height Ratio Chart and is shown in Figure 4.36. This chart relates to a soil with strength ratio equal to 10.

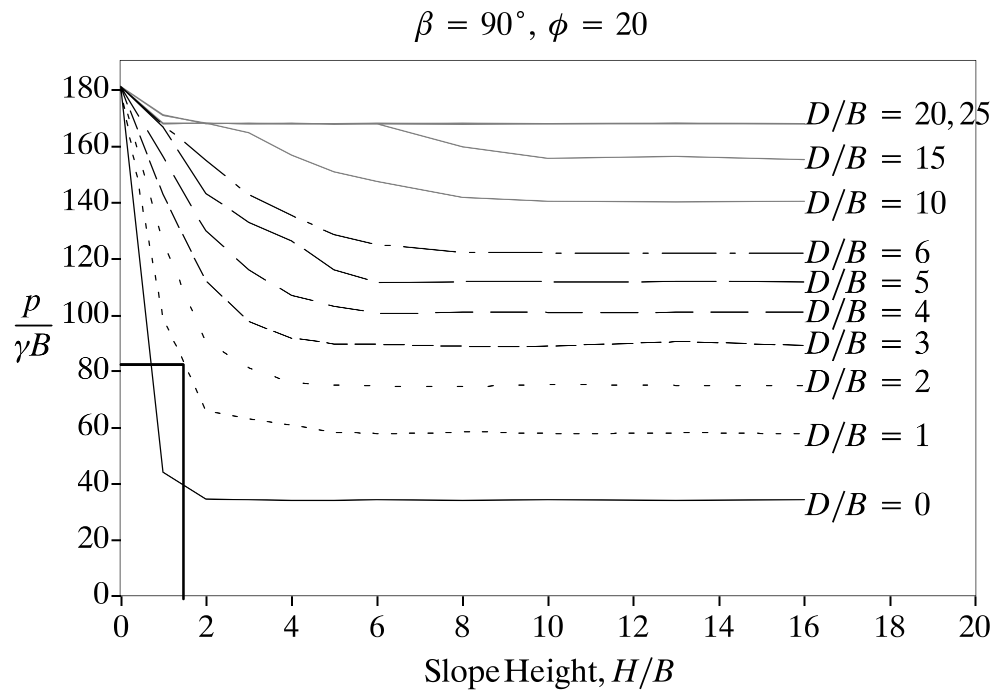

Figure E.6: Change in Normalised Bearing Capacity with Slope Height

Figure 4.36: Design chart chosen for Example 1

From the chart we see that we get a normalised bearing capacity of roughly 83. To get the bearing capacity in a force value we simply multiply this by the density of the soil and the footing width; $P = 83 \times 18.6\,kN/m^3 \times 2\,m = 3087.6\,kN/m^2$. This is the ultimate bearing capacity of the slope at which failure will occur, so to get an allowable bearing capacity simply divide this value by the safety factor required.

4.8.2 Example 2

The 2nd example will demonstrate how to use the stability number of a slope to obtain a bearing capacity.

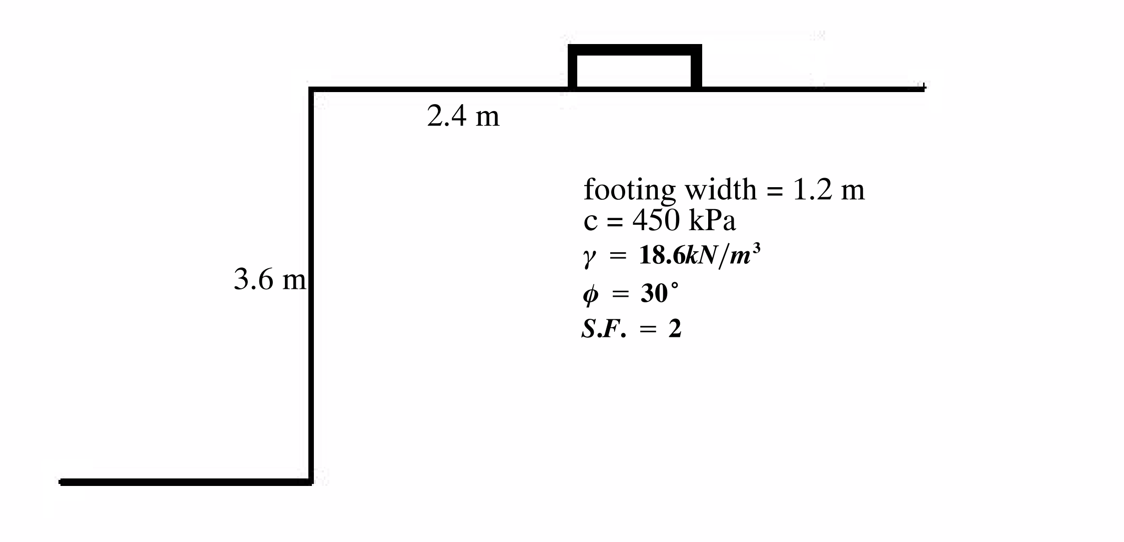

Figure 4.37: Example 2 slope scenario

We know that to find the bearing capacity of a slope using design charts we need the slope height ratio, footing distance ratio, internal friction angle and in this case the stability number of the slope which is derived using dimensionless strength ratio and slope height ratio. From Figure 4.37 we know the friction angle is 30° and for the other parameters we obtain values for each of:

- H/B = 3.6/2.4 = 3
- D/B = 2.4/1.2 = 2
- N = $c/\gamma HF$ = 450/(18.6 x 3.6 x 2) = 3.36

Using these parameters we can now choose an appropriate design chart to find the bearing capacity. Both the slope height ratio and footing distance ratio were whole numbers, so it is simply necessary to find an appropriate chart where an accurate reading for $\phi = 30^\circ$ and N = 3.36 can be taken. Of course since stability number is mentioned in this example we will use an Increased Bearing Capacity with Increasing Stability Number Chart shown in Figure 4.38.

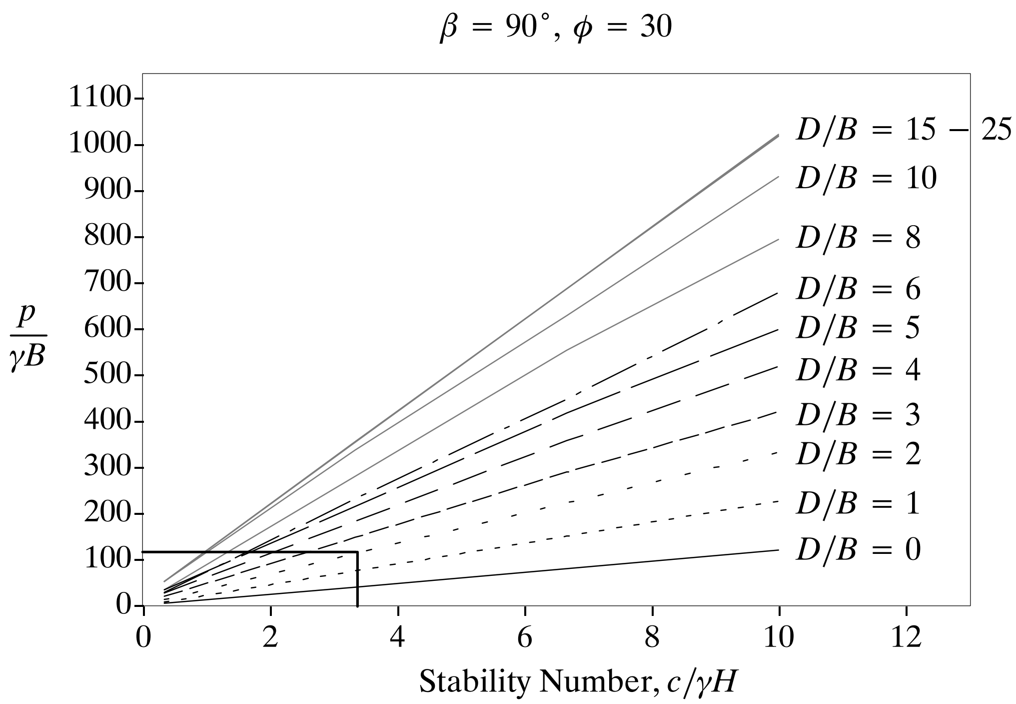

Figure F.11: Change in Normalised Bearing Capacity with Stability Number

Figure 4.38: Design chart chosen for Example 2

From the chart in Figure 4.38 we see that we get a normalised bearing capacity of roughly 112. To get the bearing capacity in a force value we simply multiply this by the density of the soil and the footing width as in Example 1; $P = 112 \times 18.6\, kN/m^3 \times 1.2\, m = 2499.84\, kN/m^2$. This is the allowable bearing capacity of the slope using the required safety factor that was given in the beginning of the problem. As the safety factor has already been considered in calculating the stability number there is no need to factor the bearing capacity any further. It would also be possible to use this chart if the required safety factor was unknown, such as during preliminary design work. In this case the safety factor would simply be assumed as 1 when calculating stability number and once an ultimate bearing capacity had been found this would then be divided by the safety factor as in Example 1.

Physical Modelling

5

5.1 Introduction

This chapter will explain the physical modelling aspect of my thesis project. In this chapter we will look at why and how the experiment was conducted, as well as the results and outcomes that eventuated after testing took place.

Only one set of parameters were used for the physical modelling due to both time and resource restraints. The parameters were chosen based on what numerical results were already available for clay and what was able to fit in with the size of the testing equipment used.

5.2 Modelling Objectives

While a number of studies have looked into the footing on slope problem based on numerical analysis, there has been very little work done on reproducing these results physically to determine how reliable the analytical results are. If we are able to reproduce these results using physical models and obtain bearing capacity values similar to that acquired from the numerical testing, then we can more confidently use the numerical analysis values for designing footings. Previously, Shiau et. al. (2006) and Boipuso Samuel (2005) have demonstrated a footing on slope situation using a physical model, however in these studies the capacity of the sample was not compared with numeric analytical results from FLAC of the same dimensioned slope.

As such, the objective of this chapter is to complete a physical modelling analysis of a clay soil based slope for a given set of parameters, then compare these results with numerical modelling results that have been previously derived using the FLAC software analysis program. It is hoped that by gaining bearing capacity values using the physical models and comparing these with the numerical results, we can verify that computer modelling can accurately depict what would happen with real world modelling. If the results appear to be accurate, then we will be able to conclude that FLAC software results are an acceptable output.

5.3 Methodology

Before any physical modelling could be completed the equipment needed had to be gathered and assembled. This included the testing load frame and associated equipment for simulating a footing force on a soil sample, the software to operate the equipment, and finally the test material with which the physical modelling will be based on.

The plans for the load frame were originally drawn up many years ago. Unfortunately, once these plans had been drawn up and the steel needed cut to size, the frame construction was postponed due to unknown events. This meant that when this project began at the beginning of 2009, the final touches needed to be made to the load frame elements and the whole frame needed to be assembled together. Once together, the equipment that would apply the load on the sample material, as well as the data acquisition units that would enable the footing force and displacement to be recorded, needed to be attached to the load frame. Figure 5.1 shows an overall picture of the load frame and associated equipment assembled together.

Figure 5.1: Overall view of Test Load Frame

A linear actuator was the device chosen to apply the load to the soil sample, which would replicate the force a footing would impose on a slope in a real world situation. The linear actuator consisted of an electric motor, able to be operated in both directions, which was connected through a series of gears to move a steel ram up and down. The actuator chosen was capable of applying a maximum force of 27kN as this is more then adequate when attempting to fail a soil slope sample, where the maximum envisioned forces are much less. Connected to the end of the steel ram was a load cell, which is used to detect the force that is being applied to the sample at any one time. To the other end of the load cell a piece of steel plate was attached which will simulate the footing of a building. Also attached to the actuator is a LVDT transducer. The purpose of the transducer is to measure the vertical movement of the ram. By knowing the vertical movement of the actuator we are able to work out an appropriate penetration speed when conducting the tests, and also know the penetration that has occurred to the slope before it has failed. Figure 5.2 shows how the linear actuator, LVDT transducer, load cell and the steel plate (footing) are assembled together.

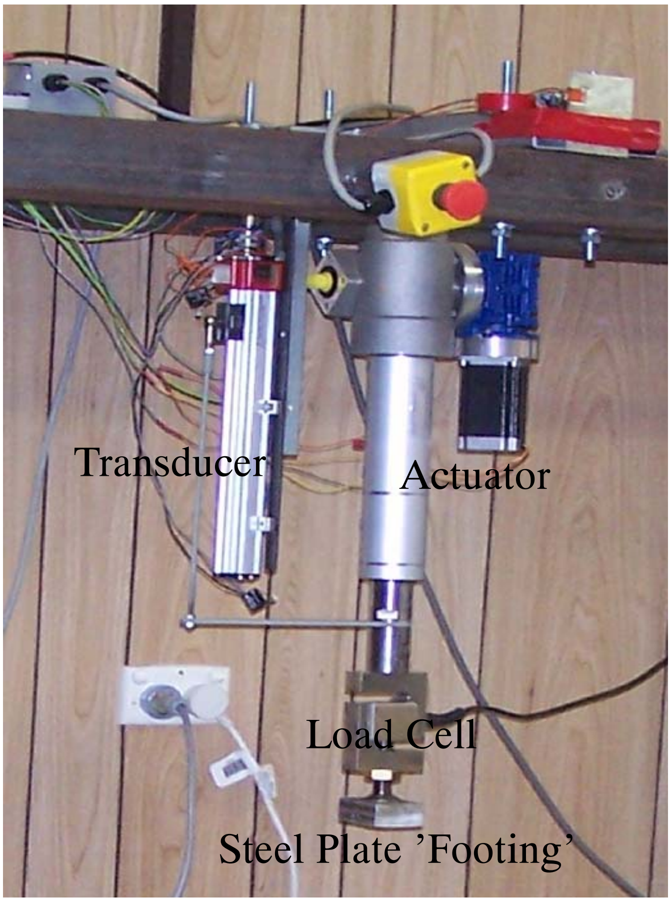

Figure 5.2: Linear actuator, transducer, load cell and steel plate configuration

In order to be able to record any data produced from conducting the physical modelling, a program needed to be created which would receive data signals from data acquisition units which received their signal from the actuator and the load cell. As this project is focussed on the footing on slope problem, which does not include being able to create software programs for performing any analysis, USQ computer technician Dean Beliveau was contacted and took on the responsibility of creating the software. What he created was a software program that was easy to use as it made setting up the actuator ready for testing and recording any output data very easy, and also had the conveniences of plotting the data and displaying it on-screen as it was recorded and being able to save the data in a multitude of formats. During the software creation stage, the actuator and load cell needed to be calibrated together to ensure force values were accurate. A loading ring was used to determine a factor, with this factor then used within the program to change the data signals received from the load cell into usable force values.

Now the testing equipment was ready, a material to test needed to be chosen. It was decided to use kaolin clay which is commercially available, and being a pure clay it has a high cohesion force but no internal friction which is perfect for comparing with numerical analysis results which were based on a material of these properties of high cohesion but zero friction.

Once the load frame and associated equipment had been created and assembled and the sample material chosen, it was necessary to manufacture some testing tanks which would be used to hold the sample material during testing. With the physical testing results being compared to 2D numerical results, the tanks were constructed so that the slope was only able to fail along one plane– resembling a 2D failure. With this in mind the tank dimensions chosen were 300mm high x 450mm wide x 70mm deep. As the kaolin clay was to be mixed with a high quantity of water it was decided to use marine ply and perspex in the tank construction. The marine ply was used for three of the four vertical sides and also the base, with perspex being used for one of the larger sides. The purpose of using the perspex was to allow visual assessment of the sample slope while testing was undertaken. This meant the slope could be observed to see how and when it failed, which meant it could be observed if the slope was failing as it theoretically should and also so it was known when the slope had failed so the testing could be stopped. The base piece of marine ply had holes drilled into in to allow excess water to drain out during consolidation (explained below). On top of this ply a piece of screen mesh lined the bottom of the tank, with a 30mm layer of sand applied on top of this mesh. The purpose of the mesh is to contain the sand within the tank, with the sand supporting and restricting the clay so only water is able to drain out through the mesh. Figure 5.3 shows what each constructed test tank looks like, including the sand and mesh screen.

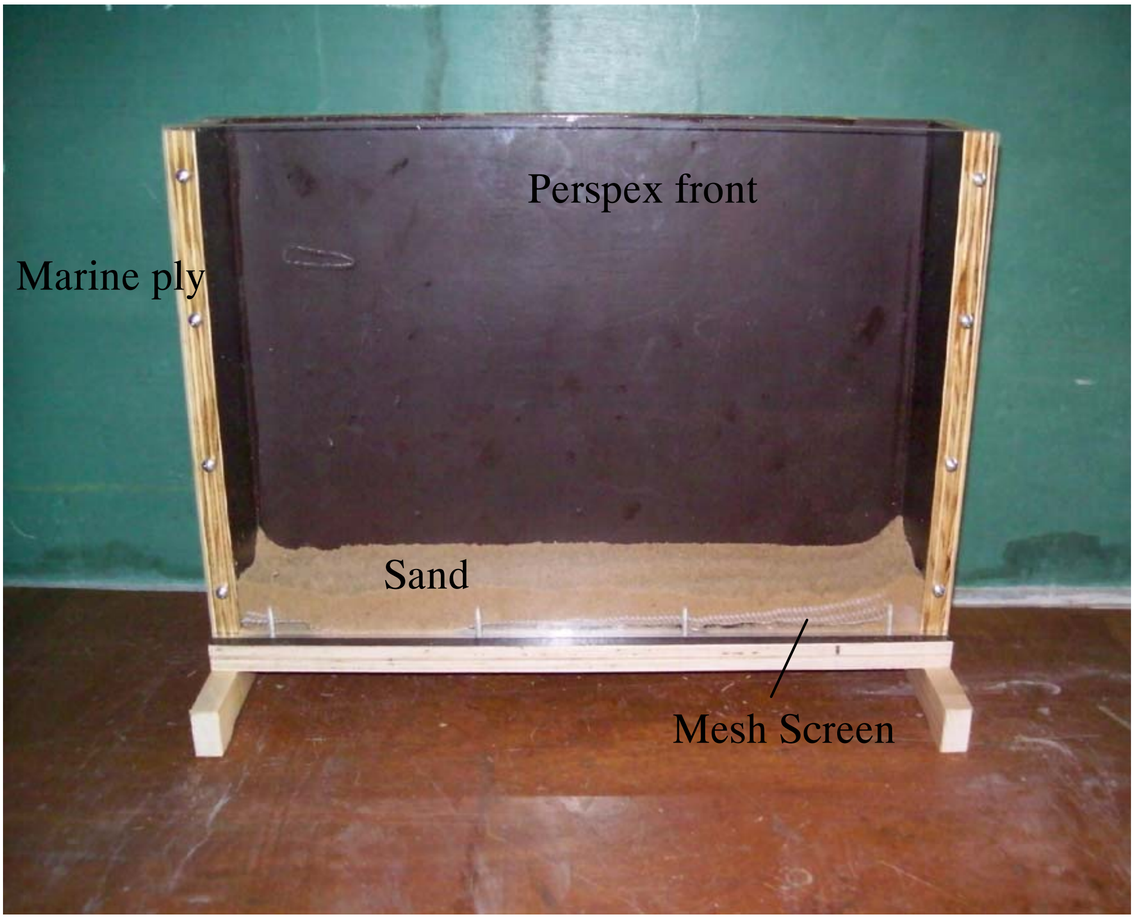

Figure 5.3: Test tank construction

With the test tanks created, the kaolin clay powder needed to be prepared. To do this a rubbish bin was used so that a reasonable amount of clay could be prepared which would save a lot of time as a large amount of mixing needed to be done. In this bin one 25kg bag of kaolin powder was mixed with water, with the amount of water being added equalling two 12L buckets. This gave the material a water content in the region of 90% and meant it was able to be mixed reasonably easy and allowed very good moisture consistency throughout each batch of material. Once it was deemed that the material was mixed enough, it was put into the testing tanks. Each tank was filled to the very top to allow for consolidation (explained in the next section) with 3 tanks able to be filled from each batch (a batch being one 25kg bag of clay and two 12L buckets of water). The clay and water was mixed together using an electric drill which had an attachment (shown in Figure 5.4) to enable mixing to be much quicker and easier then using simply only hands.

When mixing the clay and water, it was important to consider the safety precautions that were mentioned on the bag the clay came in. The information on the bag warned of possible cancer in the lungs due to the very fine crystalised silica and as such dust masks and eye protection were always worn when dealing with the dry clay.

Figure 5.4: Drill and attachment and bin used to mix material

With the tanks filled with the prepared material, a consolidation process was started. The purpose of this is to compact the clay material and squeeze excess water out increasing the strength of the material. When initially mixed, an excess of water is used to ensure the mixture is consistent throughout, as well as making sure there are minimal air voids within the material when placed in the tanks. This excess water needs to be removed to harden the material and provide it with some degree of strength. To do this, weight is applied to the top of the material which forces the water out the holes in the bottom of the test tanks as explained above. Immediately after the material was mixed only a light initial weight was applied. This weight was in the form of a concrete block of roughly 15kg that had dimensions the same as the inside of the testing tanks, which effectively meant a seal was formed between the block and the clay so the very soft material wasn't able to squeeze back past the concrete block. This weight was left for a period of one week before extra load was applied. The extra load was in the form a solid concrete building blocks weighing in at 30kg each with one block applied on top of two test tanks. Again this load was left for a week before the final application of weight was made. Two weeks had now passed since the clay was initially mixed, with the last load applied being 2 more solid concrete building blocks for each pair of tanks. This took the total load on each tank to 60kg. This weight remained in place for a period of 90 days, which from readings obtained was a time that allowed the material to reach acceptable moisture content and strength values (timeframe obtained from dissertation by Samuel, 2005). Figure 5.5, Figure 5.6 and Figure 5.7 show each weight that was applied.

Figure 5.5: Initial load applied to the clay

Figure 5.6: Load applied after 1 week

Figure 5.7: Load applied 2 weeks after mixing

Once the settlement (consolidation) period had elapsed the concrete block weights were removed, leaving a firm clay material. It was then necessary to select the slope parameters which would be used, ensuring numerical analysis results were available for a slope of the same parameters. The heights of each slope sample were measured and found to be roughly the same with a height equal to H/B = 4. Knowing this it was decided that a 90° slope with slope height ratio of H/B = 4 would be used with footing distance ratios of D/B = 0, 0.5, 1, 2, 3 and 4. Each clay sample was cut using a steel knife to the same size in an attempt to eliminate as many variables as possible. Once cut to size grid lines were drawn onto the side facing the perspex so the deformation that occurs during the testing can be easier seen during both the testing and when taking photos for documentation. When the clay was cut to the required size the perspex was also cleaned as it had become considerably dirty during the clay material preparation stage. Figure 5.8 shows the material cut to a 90° slope ready for testing.

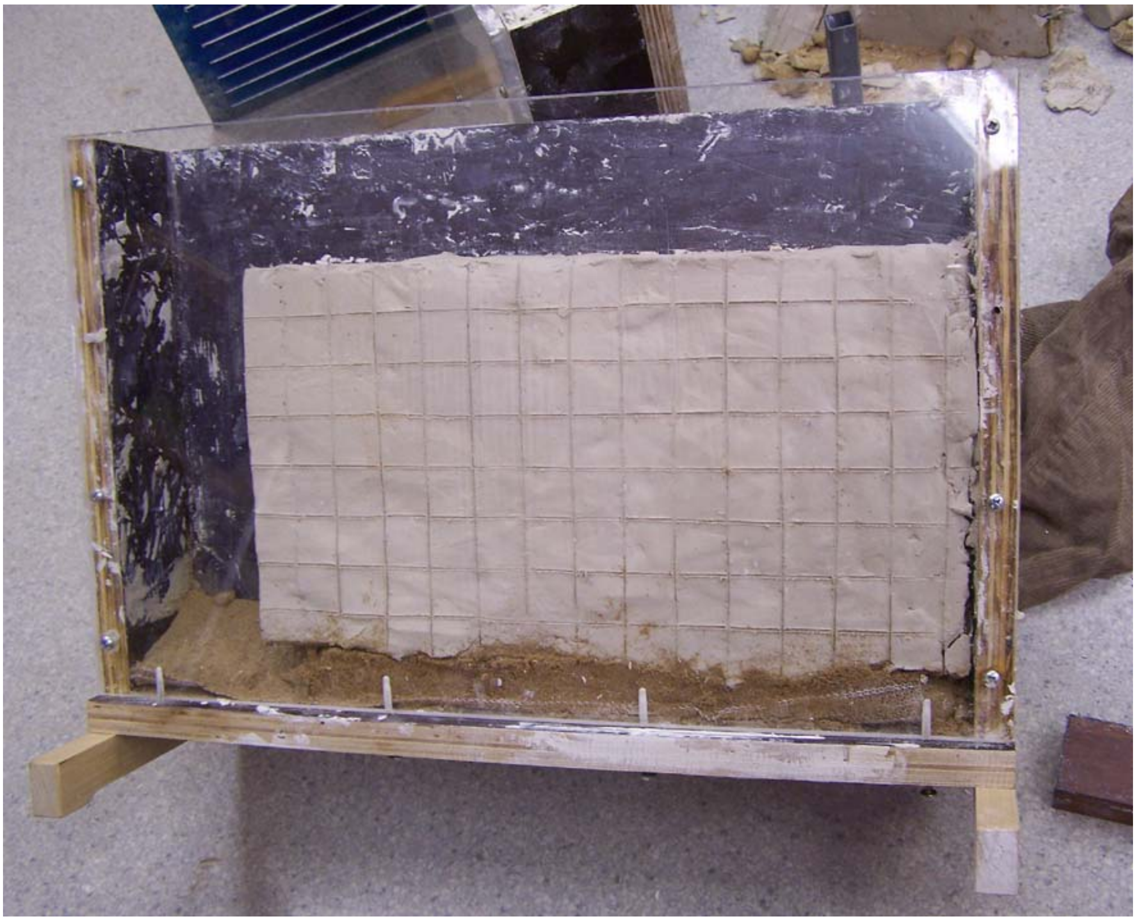

Figure 5.8: Consolidated material cut ready for testing

5.4 Testing Procedures

Before any testing could take place, it was necessary to determine the strength of the consolidated clay material. To do this a number of 100mm long, 50mm wide cylindrical samples were taken from the excess consolidated material that was cut out of each tank. On each of these samples unconfined triaxial tests were performed with an average then taken which was adopted as the soil strength. Figure 5.9 shows how the samples were obtained from the clay off-cuts, with Figure 5.10 showing a sample being subjected to the testing. It is important to note in this figure the failure plane within the example which is roughly close to 45° from the horizontal. This is the result expected from a clay material.

Figure 5.9: Clockwise from top left: obtaining triaxial test sample; trimming sample to required length; final sample ready for testing

Figure 5.10: Sample being subjected to triaxial test

From the triaxial tests, a soil cohesion of c = 100kPa was adopted. Using this value and the density of the clay (calculated by finding the weight of a known volume of soil, $\gamma = 18.6kN/m^2$), a dimensionless soil strength ratio of $c/\gamma B = 5.78$ was found. This ratio will be used for finding numerical analytical results to compare to the physical test results.

As each slope sample was cut to the same dimensions, altering the footing distance ratio simply involved placing the test tank so the steel plate was acting on an area of clay further away from the slope edge then the test previous. With footing distance ratios of D/B = 0, 0.5, 1, 2, 3 and 4, and a footing width of 2 inches, the first test situated the plate flush with the edge of the slope, the second test (D/B = 0.5) was 0.5×2 = 1 inch from the slope edge, the third test was (D/B = 1) 1×2 = 2 inches from the slope edge and so on. Figure 5.11 shows an example of the test setup before testing had begun.

Figure 5.11: Sample ready for testing to begin

If we observe Figure 5.11 we can notice a wooden block situated underneath the steel plate which is designed to simulate a building footing which is normally situated directly on top of the underlying material. This wooden block is designed to allow some horizontal displacement which could otherwise not occur due to the rigid mounting system used to secure the actuator to the load frame. This horizontal movement is cause by the tendency of the slope to slide horizontally towards the area where there is no soil and therefore no resistance. The use of the wooden block also simulates a 'smooth' interface between the footing and slope material as used by FLAC when obtaining numerical analysis data.

With everything now in place the speed in which the footing force will be applied to the slope needs to be decided before testing can commence. In a real world situation a slope failure may take years or even ten's of years to eventuate, which is an unfeasible time frame for any sort of replication testing that takes place. For this reason the force of the footing will be applied in a manner similar to that used in FLAC analysis. In FLAC analysis, y-velocity and stepping number parameters are used to determine the speed at which the footing force bears onto the slope and how many increments of this force occur, which combine to give a depth a penetration for the footing. In this physical test, the software that was used allowed the total depth of penetration that was allowed to occur to be set, as well as the time over which this penetration could occur. The combination of these two parameters determined the speed (or velocity) at which penetration occurred. With no previous physical testing procedures to work from, it was decided to use a maximum penetration depth of 50mm, which could occur over a 15 minute period. If during testing it was deemed that a slope had failed before the time had elapsed, the test would be stopped, as the force would still have been applied at a constant rate the same as that applied to all the other slope examples tested ensuring consistent testing conditions.

Even though the speed at which the tests were conducted is much faster then what would occur in a real life situation, and even faster then that used in FLAC analysis, it was judged that the testing procedure was adequate for obtaining indicative results.

5.5 Results

Results obtained from the physical testing were not quite what was expected. While the lower footing distance ratio value test slopes showed a failure plane that was consistent with that which was expected, the slopes with higher footing distance ratios did not behave as it was initially believed they would. As well as this, the bearing capacity values obtained did not replicate the numerical analysis results with maximum bearing capacities attained being much lower then expected. The test slope for each footing distance ratio used is discussed below. In the discussion of each test sample some problems that were noted during testing will be highlighted and the impact they may have possibly had on the final bearing capacity will be explained. Possible solutions to any problems identified will not be discussed in this section, rather, they will be commented on in section 5.6.

To find the bearing load of each footing, the maximum force value (in kN) was found for each test which was then divided by the area of the steel plate (footing) to give a value in MPa which was then changed to a value in kPa to allow better comparison with numerical results. This load (pressure, P) was then divided by γB ($\gamma = 18.6kN/m^2$, B=1) to give a dimensionless bearing capacity in the form of $P/\gamma B$.

5.5.1 D/B = 0

The first test conducted was for footing distance ratio of D/B = 0. With the footing being placed on the edge of the slope the bearing capacity of the slope was not expected to be large with a fairly quick failure predicted.

Figure 5.12: D/B = 0 test sample

The failure plane shown in Figure 5.12 for this test is a very good representation of what was expected. The failure (slip) plane is clearly visible, which has occurred from the inside edge of the footing as expected to approximately halfway down the slope face. There was no disturbance to the rest of the sample meaning the mass of material below the footing has simply sheared off as anticipated.

From the testing a maximum force of 0.63 kN was reached, which gave a pressure value of 180 kPa. When divided by γB this gave a dimensionless bearing capacity of 9.68.

5.5.2 D/B = 0.5

A footing distance ratio of D/B = 0.5 was selected for the second test to see how much difference in bearing capacity there was when the footing was only moved half of its width. While numerical results are not usually obtained for this particular footing distance ratio, interpolation will be used to gain an approximate value for comparison.

Figure 5.13: D/B = 0.5 test sample

In Figure 5.13 we can again see the expected failure plane which extends from the right hand side of the footing across to the slope face. It is also possible to see another failure plain (possible punching shear) extending vertically downwards from the left hand side of the footing to the expected failure plain. This may have been due to the sample possibly being too dry during testing which may have resulted in a crack in the material during the consolidation process. There is also another crack visible to the right of the footing, however this would have had minimal effect on the bearing capacity as there are no shear planes extending to or from this crack.

From the testing a maximum force of 0.697 kN was reached, which gave a pressure value of 199 kPa. When divided by γB this gave a dimensionless bearing capacity of 10.71.

5.5.3 D/B = 1

Figure 5.14: D/B = 1 test sample

In Figure 5.14 we can see that there has not been a failure plane formed, rather the slope has failed directly below the footing. With a footing distance ratio of D/B = 1 we still expect a failure plane similar to D/B = 0 or 0.5 in shape however we can see this has not occurred in this case. It would appear that during the consolidation stage a crack has formed in the clay material, which just happened to be below the footing. It is very likely that this will have had an effect on the bearing capacity of the slope, as rather then support the 'footing' the soil has simply moved as a mass in the direction of least resistance.

From the testing a maximum force of 0.442 kN was reached, which gave a pressure value of 126.29 kPa. When divided by γB this gave a dimensionless bearing capacity of 6.79.

5.5.4 D/B = 2

Figure 5.15: D/B = 2 test sample

With larger failures of footing distance, the slope will no longer fail and flat ground behaviour will be experienced. While flat ground behaviour was not expected for a footing distance of D/B = 2, at first glance Figure 5.15 tends to suggest the flat ground behaviour has occurred. If we look closer though, we can see a number of failure lines throughout the material. Of particular interest is the failure that has occurred on the left hand side of Figure 5.15. It can be seen that the soil on the immediate left of the footing has deformed with the load applied, while the mass of soil on the far left has remained at the same level as the original soil line. This tends to suggest that there may have again been a crack in the material which if this is the case, the bearing capacity is likely to be decreased as the footing acts as a wedge, pushing down and forcing the soil mass on the left to move.

From the testing a maximum force of 0.809 kN was reached, which gave a pressure value of 231.14 kPa. When divided by γB this gave a dimensionless bearing capacity of 12.43.

5.5.5 D/B = 3

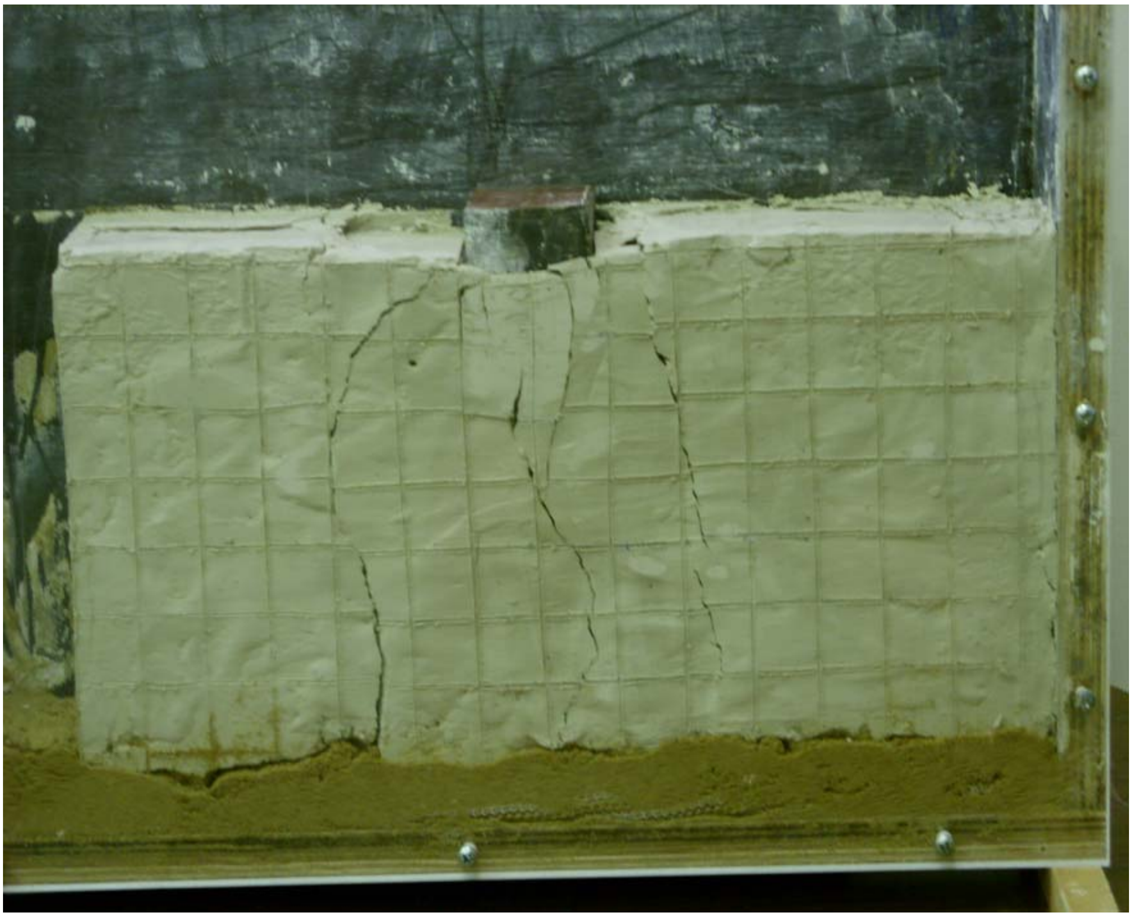

Figure 5.16: D/B = 3 test sample

For this particular slope height ratio of H/B = 4, flat ground could be expected with a footing distance ratio of D/B = 3. In Figure 5.16 we can see that the slope has not failed and that flat ground behaviour appears to have been attained. The failure lines within this particular sample suggest this as well with only narrow cracks forming which is simply due to the deformation that is occurring within the material. From this observation, it would appear as though this sample had consolidated correctly which should provide reasonably accurate results.

From the testing a maximum force of 1.45 kN was reached, which gave a pressure value of 414.29 kPa. When divided by γB this gave a dimensionless bearing capacity of 22.27.

5.5.6 D/B = 4

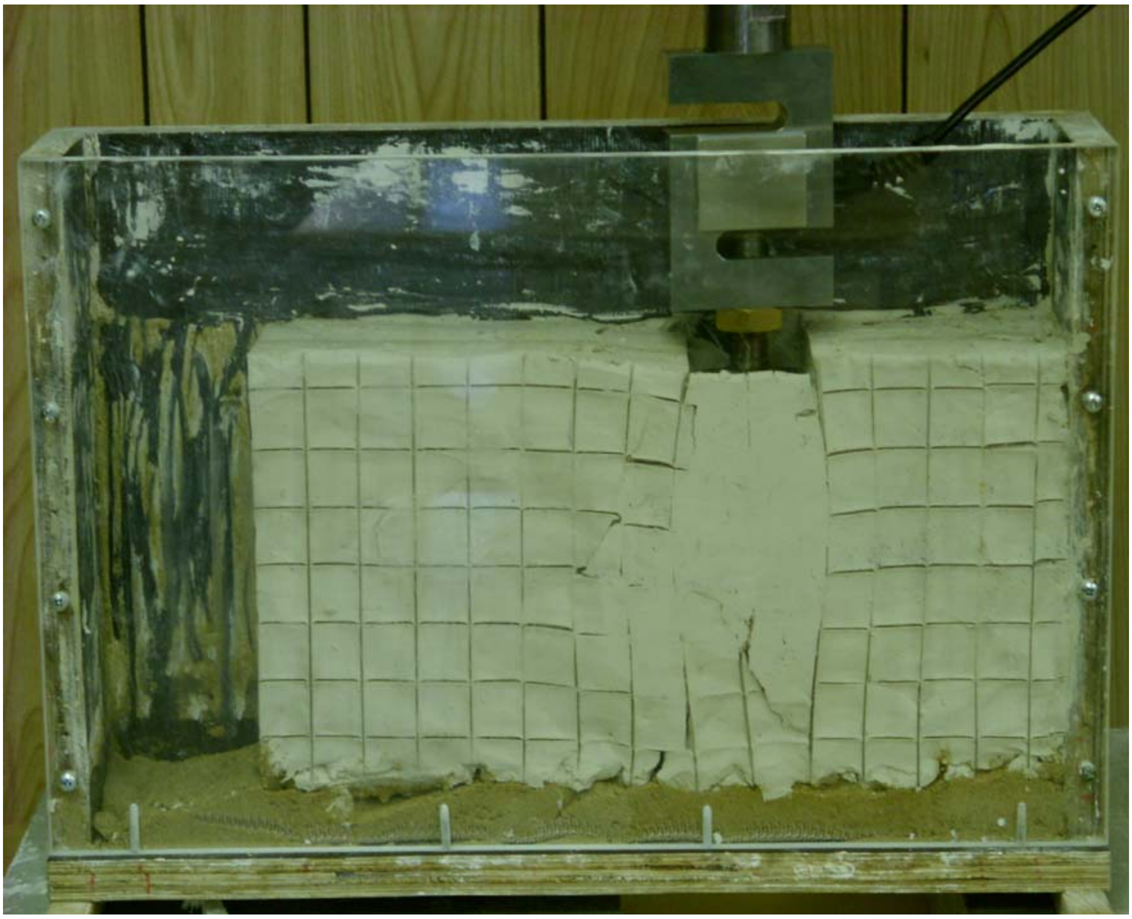

Figure 5.17: D/B = 4 test sample

The final footing distance chosen was D/B = 4. It was decided to use this ratio as the maximum as any larger footing distances may have had the bearing capacities affected by how close the footing was to the edge of the test tank. With a maximum of D/B = 4 it decided that there would be minimal effect of the tank edge on the soil if any at all. In Figure 5.17 we can see that flat ground behaviour has occurred as expected for a footing distance ratio of this size for this particular slope height. What is interesting to note is the depth of penetration that has occurred, and the fact that no failure planes have resulted from such a large deformation. Upon inspection it was found that even though this tank was subjected to exactly the same consolidation process, the material contained much more moisture then any of the other tanks that were subjected to testing. This is very likely to have had a significant effect on the bearing capacity of the slope due to the lower strength ratio of the soil.

From the testing a maximum force of 0.618 kN was reached, which gave a pressure value of 176.57 kPa. When divided by γB this gave a dimensionless bearing capacity of 9.49.

It should be noted that the maximum value for this test occurred at the last data point whereas for all the other tests the capacity peaked before decreasing once the slope had failed. This supports the conclusion that the water content for this sample was too high and that no failure planes occurred during testing.

5.5.7 Comparison with Numerical Results

To compare the physical results with numerical results, design charts based on clay material were used. The chart chosen for use was an increasing strength ratio chart, similar to that discussed in chapter 4 of this thesis except this time focussed on clayey soil, with the parameters of slope height ratio H/B = 4 and varying footing distance ratios. A chart was chosen for use as it was a quick method of finding values with acceptable accuracy which is the purpose for which the charts were created – to find bearing capacities of slopes quickly and easily. Figure 5.18 shows the chart that was used to find the numerical equivalent values.

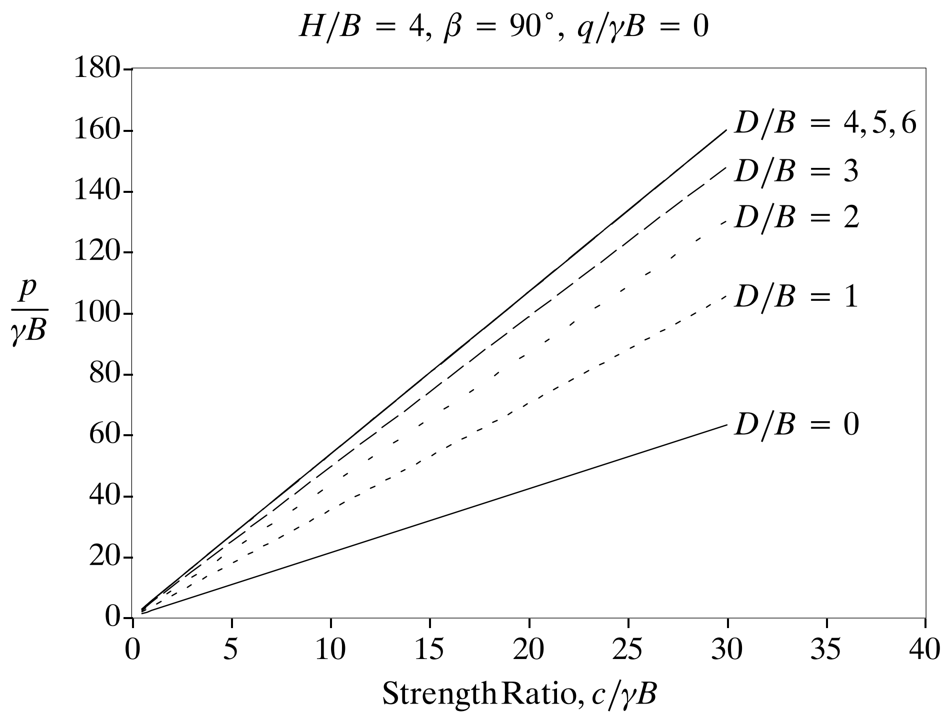

Figure 5.18: Design chart used for numerical comparison

To obtain more accurate results the chart in Figure 5.18 was zoomed in on, as the dimensionless strength ratio of the clay in the physical test was 5.78, so we only needed to know the bearing capacities relating to this soil strength. This produced a chart as seen in Figure 5.19.

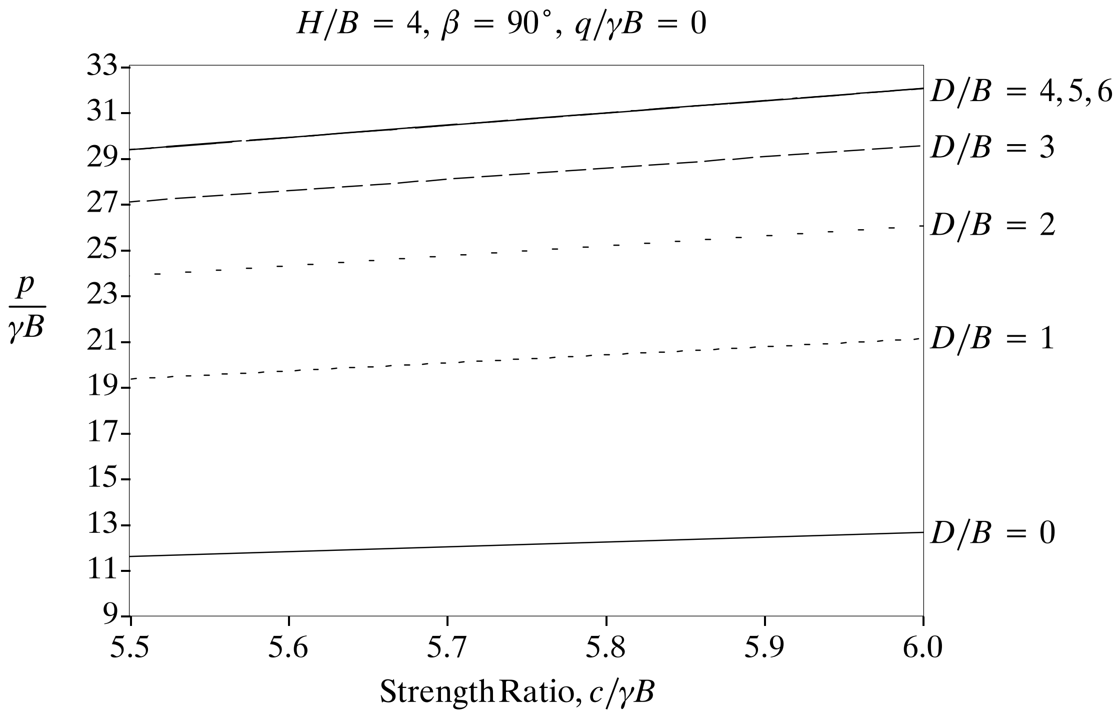

Figure 5.19: Zoomed in design chart

The values found by using the chart are compared with each physical test value in Table 5.1.

Table 5.1: Comparison of physical and numerical results

D/B	0	0.5	1	2	3	4
Physical Capacity	9.68	10.71	6.79	12.43	22.27	9.49
Numerical Capacity	12.2	16.4	20.3	25.1	28.6	29.9
Difference	-2.52	-5.69	-13.51	-12.67	-6.33	-20.41

We can see that the results for D/B = 0, 0.5 and 3 are within the vicinity of the numerical results, but perhaps still not close enough to be deemed accurate. The major positive of these 3 values is that they are all under the numerical results meaning the maximum bearing capacities are very conservative. The results for D/B = 1, 2 and 4 are 50% or less of the numerical value. These results cannot be considered accurate and support the belief that cracks within the test material affected the bearing capacity of the slopes.

5.6 Improvements for Future Physical Modelling

After conducting the physical tests and encountering some problems along the way, I believe there are some improvements/changes that could be made to the physical modelling methods and techniques.

The major problem experienced was cracking in the test samples which could be attributed to a number of things. The first is that the samples were left for too long after mixing and became too dry. As there has been very little work done on the physical modelling aspect of footing on slope analysis, there was not a lot of information available to aid in the timing of critical events. For future physical tests it would be recommended that the samples not be left for quite as long, thus creating a sample with a larger moisture content. The end moisture content is also dependent on the moisture content during the mixing stage, so this also needs to be taken into consideration. While the samples being too dry isn't believed to be the major cause of cracking, there is definitely the chance that it contributed to the problem.

The second theory for the cracking of the samples was the amount of weight applied, and cohesion occurring between the clay and the test tests. The clay used is naturally very cohesive, and this combined with the amount of weight acting on the soil during the consolidation phase is believed to have forced the clay against the test tanks sides effectively sticking it the the plywood and perspex. As the clay dried out, rather then shrink as a whole mass, it remained stuck the the tanks sides due to the weight of the concrete blocks which meant the internal clay had to move to the outside clay, resulting in cracks in the middle of each clay block. To solve this problem there could be a number of solutions. One would be to reduce the amount of weight applied which would hopefully reduce the force pushing the clay against the tank sides and creating less of a bond between the tank and clay, allowing the clay to shrink as a whole mass and eliminate any cracking. The second solution could be to coat the inside of the tanks with a thin layer of oil or grease. This could act as a type of frictionless barrier which would not allow the clay to stick to the tank sides, and should not affect the strength of the clay when it comes time for testing as only the outside surfaces of the clay would be contaminated with the grease.

The final consideration would be to reduce the consolidation time. This was a major factor in the amount of testing that could be completed as it was unfeasible to have a 100 test tanks available all filled with clay at the same time. It is because of this that only a small amount of tanks and samples could be prepared.

5.7 Conclusion

The testing procedure appeared to work well for obtaining the results. The software created for recording the data works well and is easy to use, and enables the speed at which the testing will occur to be set. Combined with the actuator and transducer used, I believe this testing system works well and does not need any changing.

As for the preparation of the test materials, it is recommended that a combination of less weight and grease be used during the consolidation phase. Applying a thin film of grease before the clay/water mixture is poured into the tanks will allow the clay to move independently of the tank sides as it dries out, and a reduction in the amount of weight that is applied will reduce the force pushing the clay against the tank walls. This should hopefully reduce the amount of cracking occurring and make the physical test results much more accurate and reliable.

It is also recommended that the consolidation time be reduced as mentioned previously so that more testing can take place. During the timeframe of this thesis, it was not possible to repeat any of the physical tests as there was not enough time available to prepare new samples due to the long consolidation time. During the physical modelling work performed for this thesis, a delay in the availability of materials was experienced which postponed the preparation of the clay which meant the consolidation phase was not started as early as originally planned. With materials ready and available, and a shorter consolidation time it could be expected that a second round of testing could take place for a different set of parameters, or as a repeat of the parameters already used to support and validate the results initially obtained.

Conclusion

6

6.1 Results Summary

After completing the analytical sections of this project there are a number of conclusions we can draw on and now accept as fact when studying the footing on slope problem.

From the numerical analysis we identified that the internal friction angle of the soil could be considered to have the largest effect on bearing capacity of a slope. We observed that for a small friction angle the results converged when compared against all other parameters indicating that there was little change in bearing capacity for a soil that could be considered as being close to a clay nature. However with a large friction angle we could see that as friction angle increased the bearing capacity of the slope increased exponentially as the material approached a sandy nature. The increase in bearing capacity with an increase in friction angle we found was due to the larger interaction that occurred between the particles which meant a larger mass of material became involved in supporting the footing load and therefore a larger load could be supported before failure would occur. A larger friction angle however also meant that it was possible at large slope height ratios for a footing to change from being classified as footing on flat ground back to a footing on slope problem.

Obviously the dimensionless strength ratio plays an important role in the maximum bearing capacity of a slope, with a higher strength ratio giving a larger bearing capacity. The interesting observation made during the study of the effects of dimensionless strength ratio was that it had no effect of the failure surface that eventuated. We were able to see that for each of the strength ratios used in this project that the differences in failure surfaces were negligible.

Finally, footing distance ratio and slope height ratio could be taken as having the least effect on the bearing capacity of a slope, with each ratio affecting equally as much as the other.

While internal friction angle and strength ratio of the slope material controlled the stability of the slope under its own weight whilst also providing support for the footing load, the slope height ratio and footing distance ratio simply determined the height of the slope and the location the footing was at which affected whether the failure plane was below toe or above toe. Whilst it was noted that slope height did have an effect on the stability of a slope, its effect was not as dramatic as that of friction angle or strength ratio.

From the physical analysis that was conducted, the results varied greatly between each test and when compared with numerical results for a slope with the same parameters a large difference in most results could be seen.

The smallest difference in results for some of the physical models tested was found to be roughly 20% and while this may be on the limit of acceptability for a physical test it isn't the reliable results that were wanted or expected. For the worst physical models, a difference in bearing capacity of around 100% was obtained meaning these results can safely be considered unsatisfactory. From the results that were gathered it is not appropriate to attempt to perform an analysis on them and say whether the numerical analysis results can be replicated with scale models and therefore further validate the results output by FLAC.

The problems experienced during the physical modelling occurred due to this section of study having not been previously attempted by another person. These problems have been recognised and possible solutions identified in an attempt to make the results of any further testing in this area more reliable. The physical modelling would need to be performed again to be able to make a proper comparison with numerical results. These problems and solutions are recapped in the following sections.

6.2 Problems Encountered

This section will explain problems that were encountered in both the numerical and physical modelling sections of this project.

6.2.1 Numerical Modelling

In the numerical analysis there were a few problems that were encountered along the way. The first very simple problem was in setting up the folders of script files which keeps the data in an understandable and organised fashion. The problem was due to there being many levels of folders within folders which created a very long pathname that FLAC needed to write the output results to. The problem was that with slope height and footing distance ratios that were double figures (i.e. > 10) the pathnames were becoming too long and FLAC was unable to write to the required area. This initially took a while to figure out the problem as it had not been encountered before but once discovered it was a simple fix by simply reducing the amount of characters in the pathname.

The second problem met was due to the length of time it took to run each slope case. If any cases were accidently missed when setting up the script files, they had to be found and run at a later time, which delayed the analysis of the data which in turn delayed the completion of the design charts. These delays would accumulate and meant of lot of time was spent waiting for run cases to finish.

Another problem encountered was the amount of script files that needed to be created. The shear volume of files sometimes created confusion even using the thoughtout and organised method of folders developed. This confusion is what led to the missing of cases mentioned before.

The final problem that was met was very rare but also very strange and seemed to be internal within the FLAC software. The problem was that for a couple of cases that were run (out of the thousands that were done) the results output would be for a different slope case. When the script file was examined everything appeared as it should and the source of the problem could not be found so the case was simply run again which returned the proper data. It was decided that this problem may have been due to the temper-mentality of computers and computer software.

6.2.2 Physical Modelling

The physical modelling component of this project contained a few critical problems which affected how well the output data would be. The first problem was the amount of cracking that occurred in the clay samples that were to be tested. These cracks created zones of zero cohesion and meant that the separated masses of soil were able to move independently of each other as they effectively had no ties between each section to resist movement. This effected the results that were obtained severely in some cases and reduced the bearing capacity considerably making comparison with numerical results very difficult.

The second problem was how long the consolidation process and overall initial setup concerning the clay material that was to be used took. When the clay had been ordered there was a slight delay in its delivery which delayed the rest of the work on the physical modelling as it was needed so a start could be made. When finally received and prepared a very long period of waiting followed before the samples were able to be tested. While this waiting period did allow work to be completed on the numerical modelling it meant that only one set of samples could be made and tested in the time available.

6.3 Procedure Improvements

Whilst completing this project and having encountered some problems along the way some possible improvements in the procedures used were thought of that would make life easier if someone else continued on with the work on each area of this project.

6.3.1 Numerical Modelling

In the numerical modelling not a great deal can be done to improve the procedure as a lot of it is simply waiting for FLAC to finish running each case. The problem of pathnames being too long should not occur due to it now being known that there is a limit on the number of characters being used. The number of script files that need to be run will always be large due to the need to have an individual file for each individual slope case, when the temper-mentality of computers is not something that can really be fixed as it is a very rare and random occurrence in technology.

6.3.2 Physical Modelling

In the physical modelling there are a number of suggestions already been made to improve this aspect of the project. The combination of high cohesion between the testing tanks and the clay and the amount of weight that was applied during the consolidation process is believed to have caused the cracks that were observed in a majority of samples. It would be recommended that the amount of weight be reduced to lower the amount of force pushing the clay against the test tanks edges and therefore reducing the bond between the tanks and the clay so that it is able to consolidate and shrink as a total mass and not develop cracks through its centre.

The second improvement that could be made would be to reduce the amount of time the samples were left to consolidate, as the current time requirements means it is very hard to get a second set of testing completed. Reducing the consolidation time would allow two or even three sets of samples to be tested and provide more results to gain greater accuracy.

6.4 Future Work

In completing this project a number of areas have been observed where future testing may be possible. These recommended areas are described below.

6.4.1 Numerical Modelling

In the numerical area of this project there is much more research to be done on cohesive-granular materials. The results produced here are only for a 90° slope, which immediately raises concerns about the load it can support as it is basically a cliff face. It would be recommended that results for slope angles of 30° and 60° be obtained first as this will give a good spread between flat ground and a vertical soil wall. Once this has been completed other angles such as 15°, 45° and 75° could be obtained making the overall results collection very comprehensive. This would give the results more reliability and make them more appealing for use within the geotechnical industry.

The next research that could be included would be on the effect of dilation angle of a soil. Dilation angle refers to the shearing of a soil when a load is a applied, such as a footing, and is concerned with the plastic energy that this causes. In this study a dilation angle equal to the friction angle was used which means there would be no physical energy dissipation in the material which in unrealistic, however if a dilation angle of 0° was used it means plastic deformation occurs at a constant rate which means there would be no change in soil volume when subjected to loading which is also unrealistic. A study of dilation angles between zero and the friction angle would provide a further research area.

Another area that could be looked into would be the bearing capacities of slopes that are subjected to surcharge loading. Some work in the area has been performed on slopes based on pure clay but as yet nothing has been done in the cohesive-granular soil area. This study could prove interesting to see whether similar trends are displayed by $c - \phi$ soils as seen by clay soils.

The final area that could be researched would be computer analysis of 3 dimensional slopes. Some work in this area has been completed for clay based slopes but as yet nothing has been done for $c - \phi$ materials.

6.4.2 Physical Modelling

As the physical modelling aspect of footing on slope analysis is a new area there is a great deal of work that can be done.

Performing tests on a larger range of samples and gathering more reliable results would be the first step to ensure the procedure being used was correct and produced acceptable results. This could be done by varying slope dimensions such as slope height or slope angle, or moving the location of the footing. The material properties could also be varied which would allow comparison with results for $c - \phi$ soils such as what was used in the numerical section of this project.

Another possible area of research could be to develop a procedure specifically for physical modelling such as what was done here. By using a range of masses during the consolidation process, as well as varying the time over which consolidation took place, the optimum weight and time periods could be determined which will produce the best results most closely resembling those obtained from numerical analysis. The optimum moisture content for testing could also be found to allow future testers some guidelines to aim for.

Utilising the design of the load frame that was created research into the effect of an angled load force could be studied. It would be expected that bearing capacity of a slope would decrease when the footing force is angled toward the slope face however it could be interesting to see the effects of the force angled away from the slope face.

Further research work is also possible in the geotechnical area that does not relate to the shallow footing on slope problem. It may be possible to create scaled versions of piles to determine the bearing capacity of a slope with these acting on the soil and see what effect they have. It is also possible to run the linear actuator in reverse to create a tensile force which could be used to model anchorage either at the top of a slope or through the slope face.

The final area that could be investigated would be to perform modelling of 3 dimensional slopes and use pad and/or strip footings. These results could also be compared with numerical analysis results that have been obtained by Joshua Watson or if the sample material that was used was changed to a cohesive granular material, could be compared with results obtained from any 3D research into cohesive granular materials as recommended above.

References

7

Cheng, Y.M. & Au S.K. 2003, 'Solution of the bearing capacity problem by the slip line method', *Canadian Geotechnical Journal*, NRC Research Press, Canada

Craig, R.F. 1997, *Soil Mechanics*, 6th Edition, Spon Press, London, England

Das, B.M. 1999, *Shallow Foundations: Bearing Capacity and Settlement*, CRC Press, USA

GeotechnicalInfo.com, 2007, 'Bearing Capacity Factors', *Career Development and Resources for Geotechnical Engineers*, Last viewed 30/08/2009, <http://www.geotechnicalinfo.com/>

Itasca Consulting Group, 2002, 'Getting Started', *FLAC Manual - Chapter 2*, Minnesota, USA

Itasca Consulting Group, 2002, 'Problem Solving With FLAC', *FLAC Manual - Chapter 3*, Minnesota, USA

Kusakabe, O., Kimura, T., & Yamaguchi, H. 1981, 'Bearing capacity of slopes under strip loads on the top surfaces', *Soils and Foundations, Japanese Society of Soil Mechanics and Foundation Engineering*, Volume 21, No. 4, pp. 29–40

Ministry of Science and Technology, 'Chapter 5 – Bearing Capacity', *Effects of Angle of Incidence of Earthquake Excitation on Tall Building with Flexible Mat Foundation Founded on Soft Soil*, Last updated 17/03/2009, Last Viewed 13/10/2009, <http://www.most.gov.mm/techuni/media/CE_04015_PII_5.pdf>

Shiau, J.S. Lyamin, A.V. & Sloan, S.W. 2003, 'Bearing Capacity of a Sand Layer on clay by Finite Element limit Analysis', *Canadian Geotechnical Journal*, NRC Research Press, Canada

Spigolon, J. 2001, ’Chapter 8 : Shallow Foundations - Footings and Rafts’, *Geotechnical Engineering - The McGraw Hill Civil Enginnering PE Exam Depth Guide*, New York, New York

U.S Army Corps of Engineers, 1992, ’Engineering and Design - Bearing Capacity of Soils’, *Engineer Manual 1110-1-1905*, Washington, DC

Various sources, *Civil Engineering References*, website, Last viewed 16/06/2009, <http://www.ce-ref.com/>

Zhu, M. 2004, ’Bearing Capacity of strip Footings on Two-Layer Clay Soil by Finite ElementMethod’, *2004 ABAQUS Users Conference*, Univeristy of Michigan, Ann Arbor

Appendix

8

8.1 Appendix A – Project Specification

University of Southern Queensland

Faculty of Engineering and surveying

ENG 4111/2 Research Project

PROJECT SPECIFICATION

FOR: **ANDREW COLE**

TOPIC: A comprehensive study of footing on c-ϕ soil slopes - numerical and physical modelling.

SUPERVISOR: Dr. Jim Shiau

SPONSORSHIP: Faculty of Engineering and Surveying

PROJECT AIM: To perform physical tests on clay soil slopes and compare with theoretical analyses, as well as providing a more comprehensive numerical analysis of c-ϕ soils.

PROGRAMME: **Issue A, 24 March 2009**

1. Research the background information relating to the footing on slope problem.
2. Review studies on footing on slope concepts and previous studies.
3. Perform physical model tests for footing on clay slope and compare results with the relevant numerical analysis results.
4. Perform numerical analysis of footing on c-ϕ soil slopes using FLAC to study the effect of H/B, D/B, c/.B and ϕ.
5. Create charts for c-ϕ soils to display numerical modelling results.

As time permits

6. Analyse dilation angle effect on slope.
7. Investigate two-way failure mechanism.
8. Investigate combination shear failure.

AGREED: ________________(student) ________________(supervisor)

Date____/____/2009 Date____/____/2009

Examiner/Co-examiner:______________________________

8.2 Appendix B

Footing on Flat Ground or Slope Condition Charts

The purpose of this first type of chart is to allow the decision to be made on whether the footing should be considered as a footing on slope problem or footing on flat ground problem. By obtaining the values for the height of the slope, the width of the footing, the distance of the footing from the edge of the slope and the internal friction angle of the slope material we can determine the required relationship ratios of slope height ratio and footing distance ratio and therefore determine the classification of the footing. If the footing lies in the flat ground area of the chart then simple flat ground calculations can be performed however, if the footing is found to be classed as on slope then the charts displayed later can be used to gain an approximate ultimate bearing capacity for a slope. For each value of soil friction angle there is a different chart, with interpolation used for values in between.

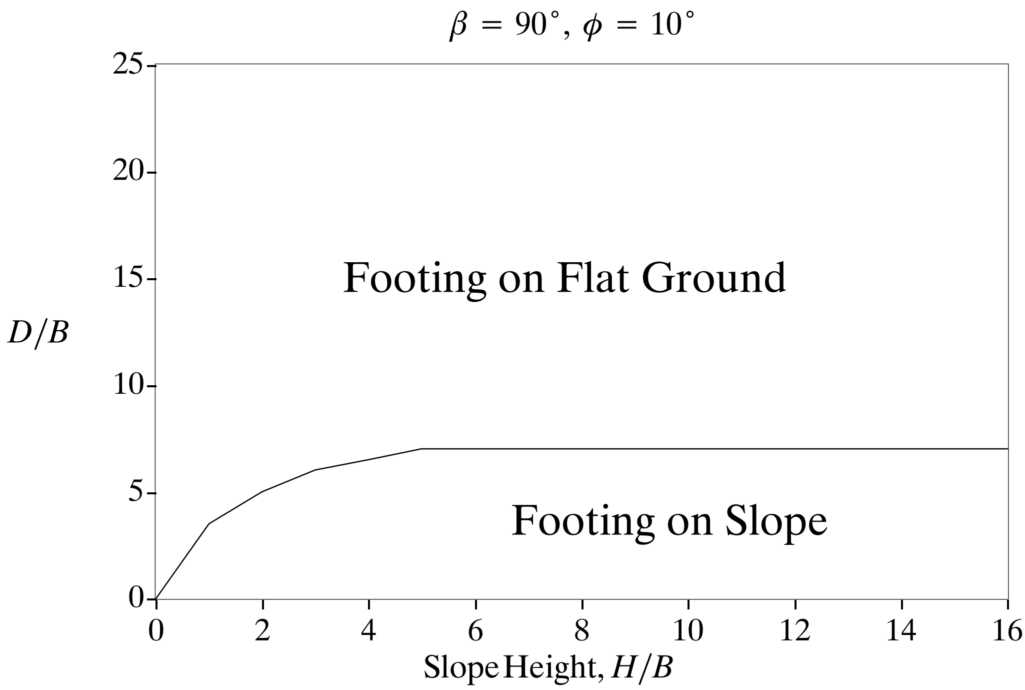

Figure B.1: Footing on Flat Ground or Slope Condition

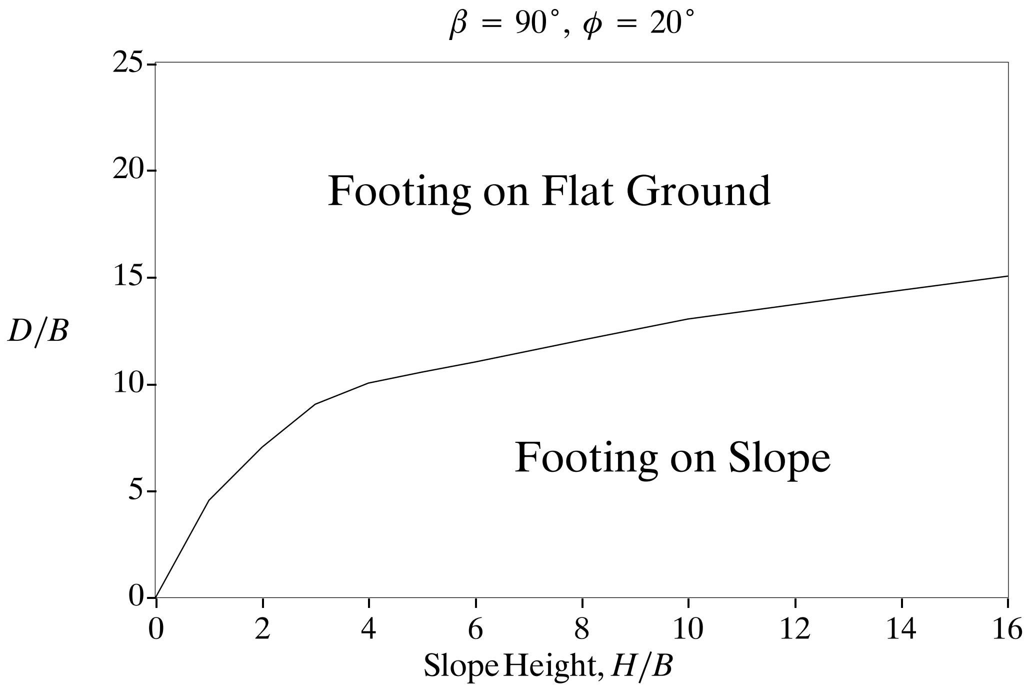

Figure B.2: Footing on Flat Ground or Slope Condition

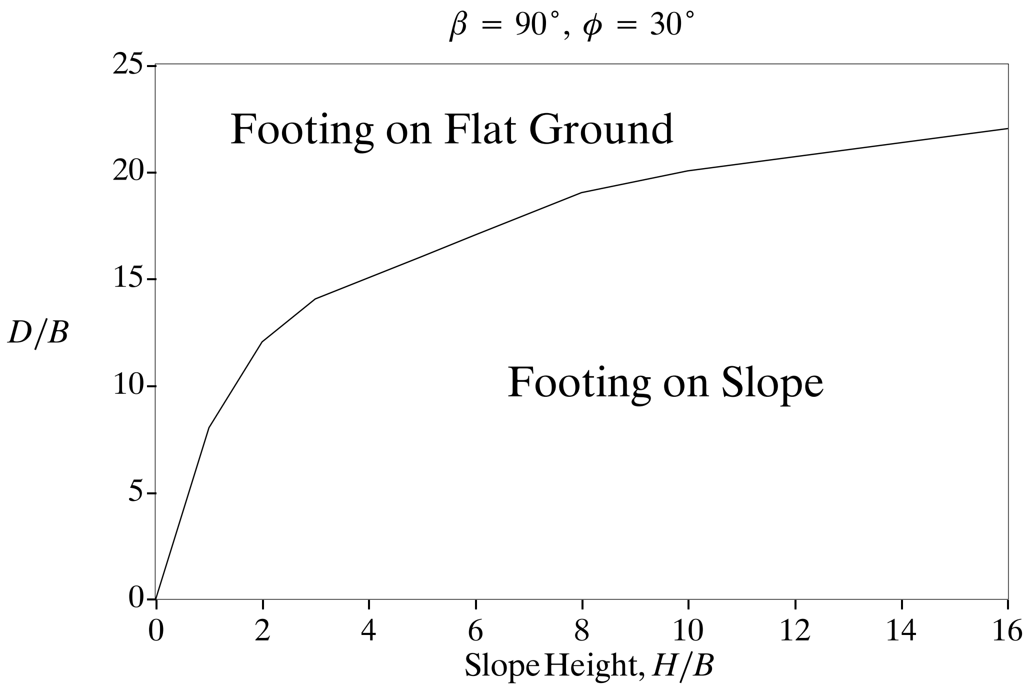

Figure B.3: Footing on Flat Ground or Slope Condition

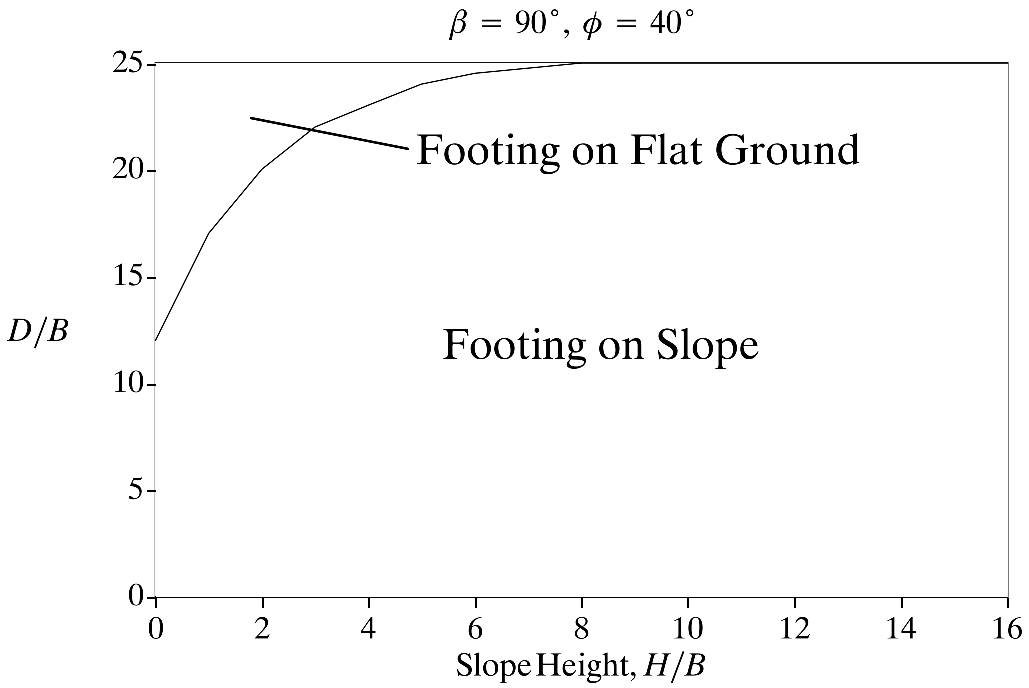

Figure B.4: Footing on Flat Ground or Slope Condition

8.3 Appendix C

Increased Bearing Capacity due to Increased Strength Ratio Charts

The charts shown in this section (8.3) enable it to be seen what difference soil strength has on the bearing capacity then can be achieved for a particular slope. This may be handy particularly when constructing a man-made slope for a height advantage. If the size of the building and the load it will apply to the soil are known, then the ratios of slope height and footing distance can be determined for a given strength of soil, or if these ratios are set then the appropriate soil strength to use can be determined.

This type of chart consists of a number of groups which is set by the slope height ratio. Within each slope height group there are 4 charts for the varying friction angles that were studied.

H/B = 0

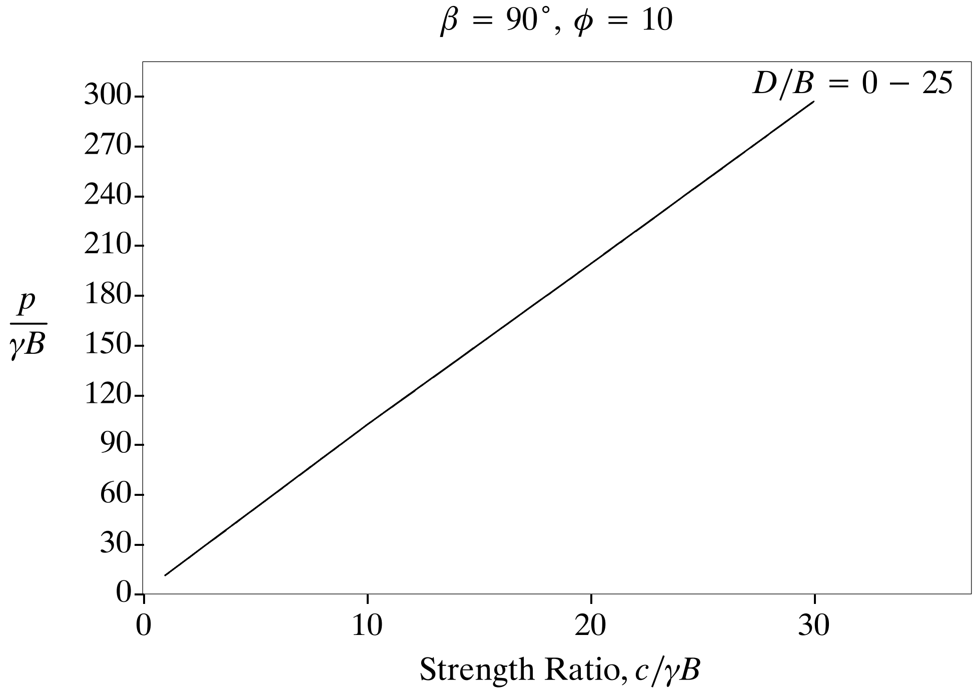

Figure C. 1: Change in Normalised Bearing Capacity with Strength Ratio

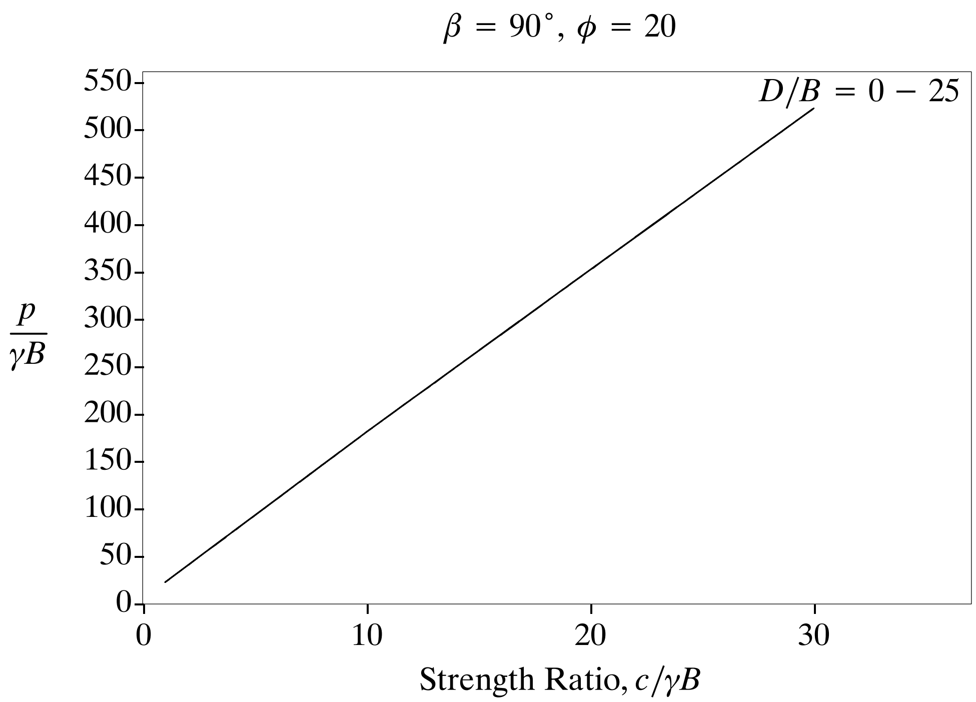

Figure C. 2: Change in Normalised Bearing Capacity with Strength Ratio

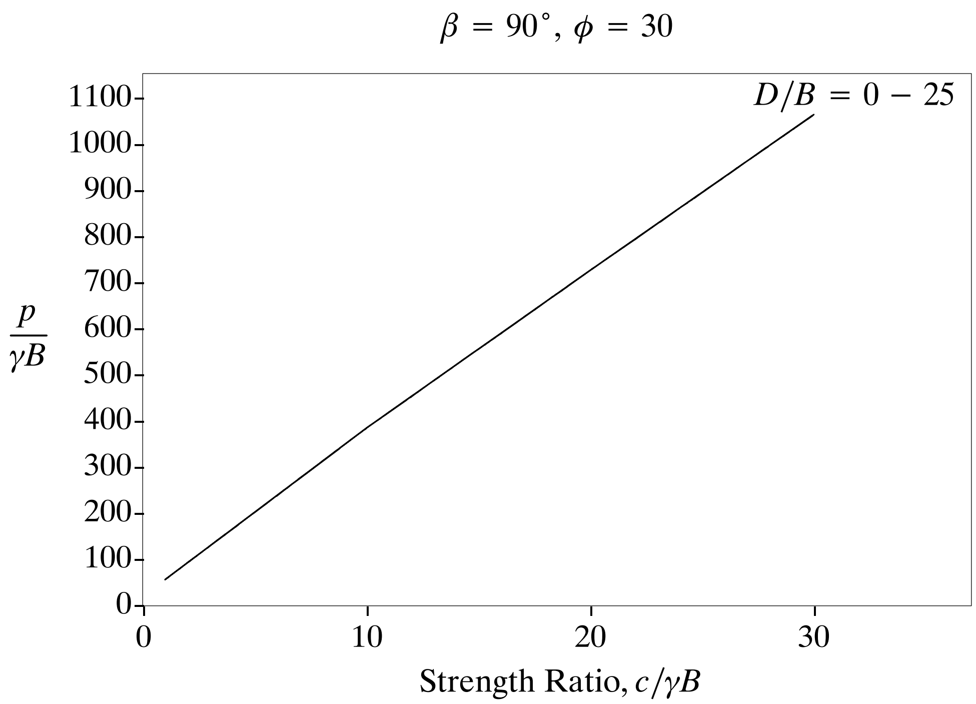

Figure C. 3: Change in Normalised Bearing Capacity with Strength Ratio

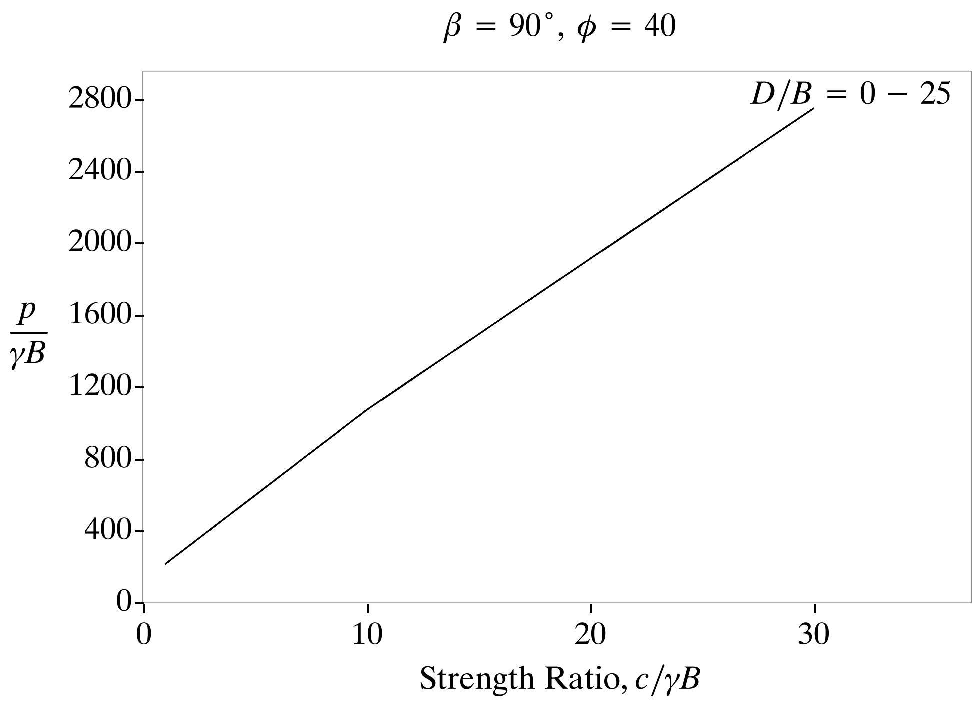

Figure C. 4: Change in Normalised Bearing Capacity with Strength Ratio

H/B = 1

$\beta = 90^\circ, \phi = 10$

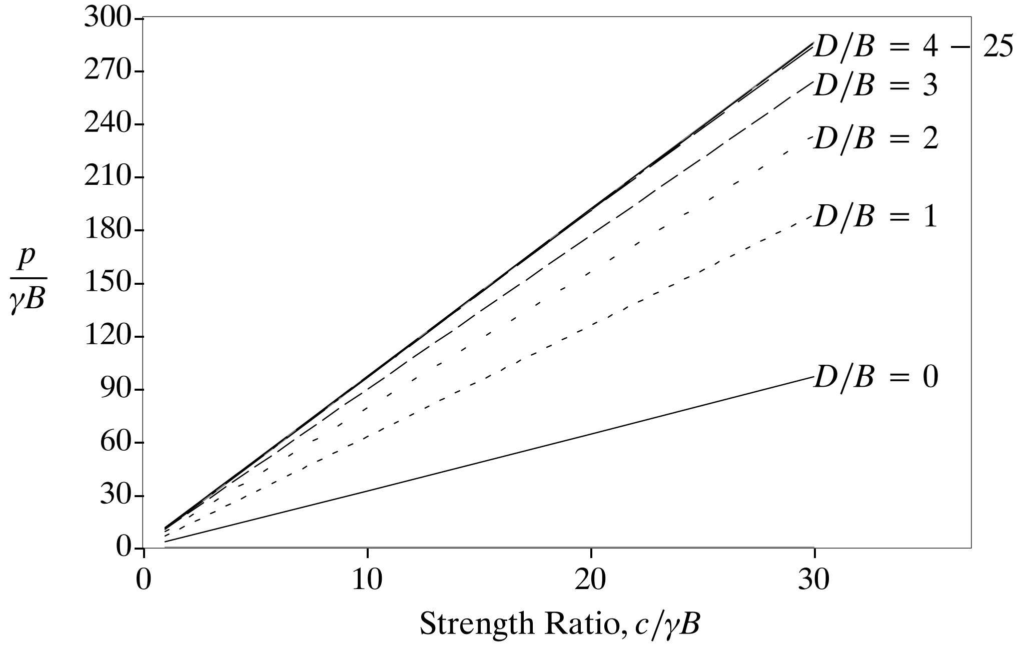

Figure C. 5: Change in Normalised Bearing Capacity with Strength Ratio

$\beta = 90^\circ, \phi = 20$

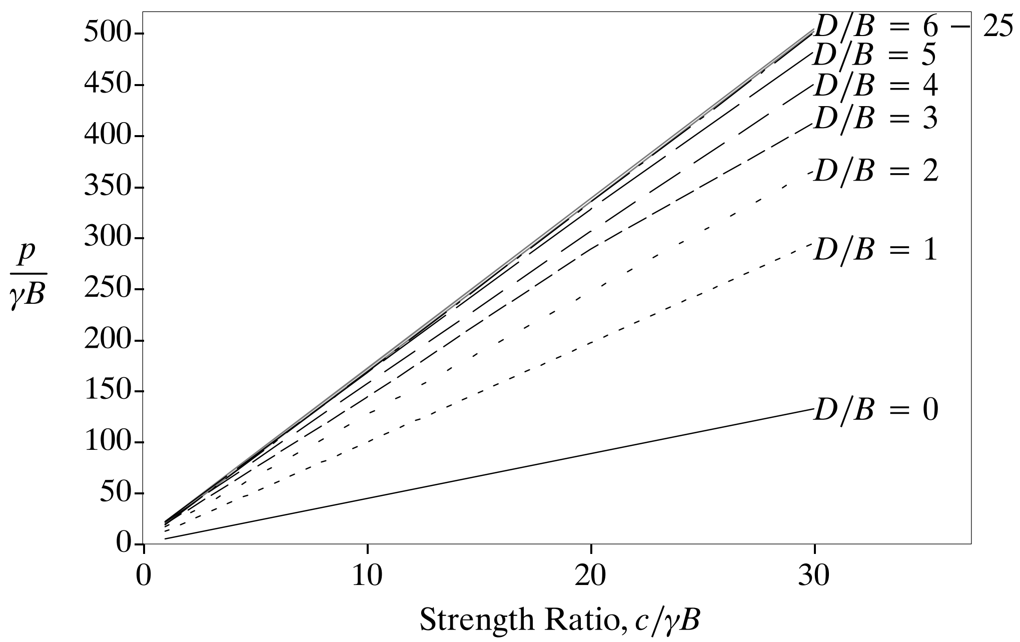

Figure C. 6: Change in Normalised Bearing Capacity with Strength Ratio

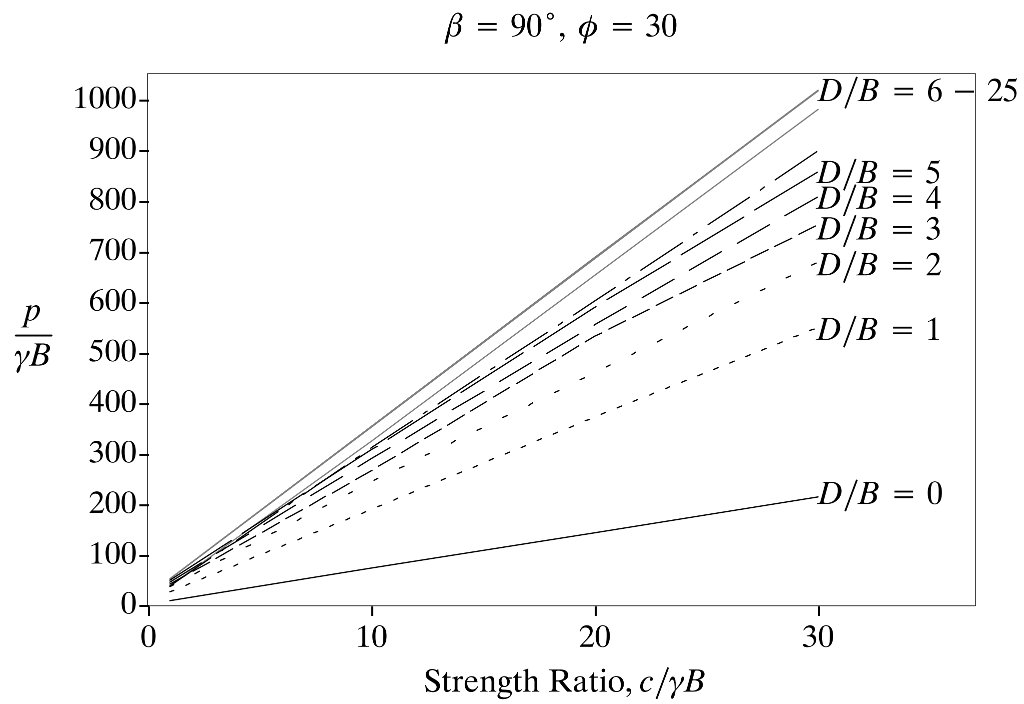

Figure C. 7: Change in Normalised Bearing Capacity with Strength Ratio

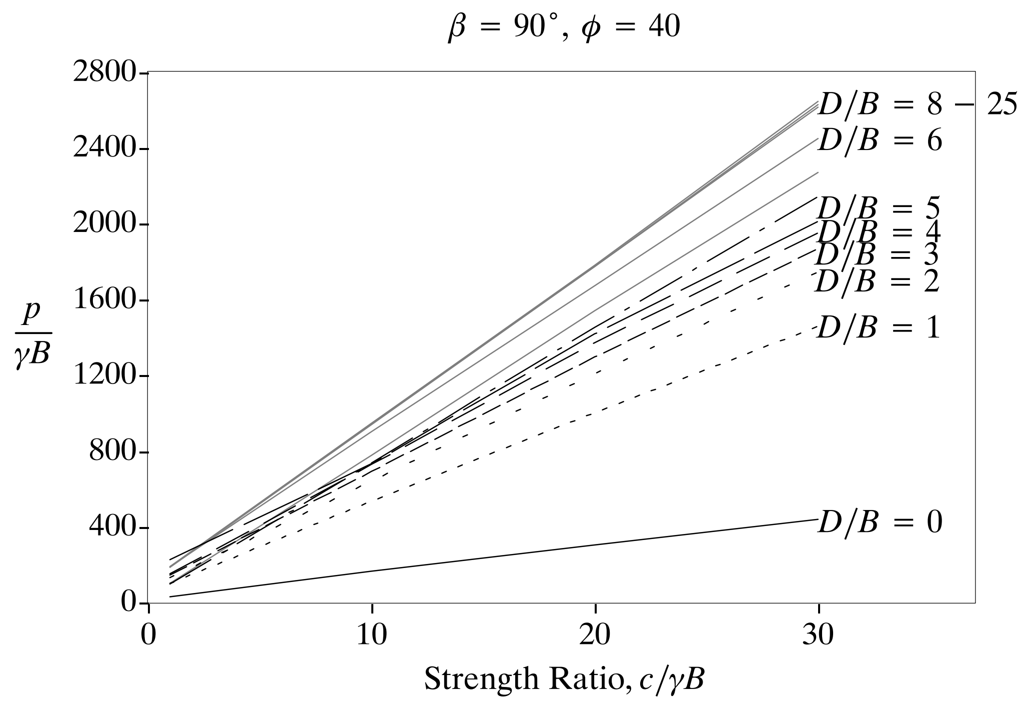

Figure C. 8: Change in Normalised Bearing Capacity with Strength Ratio

H/B = 2

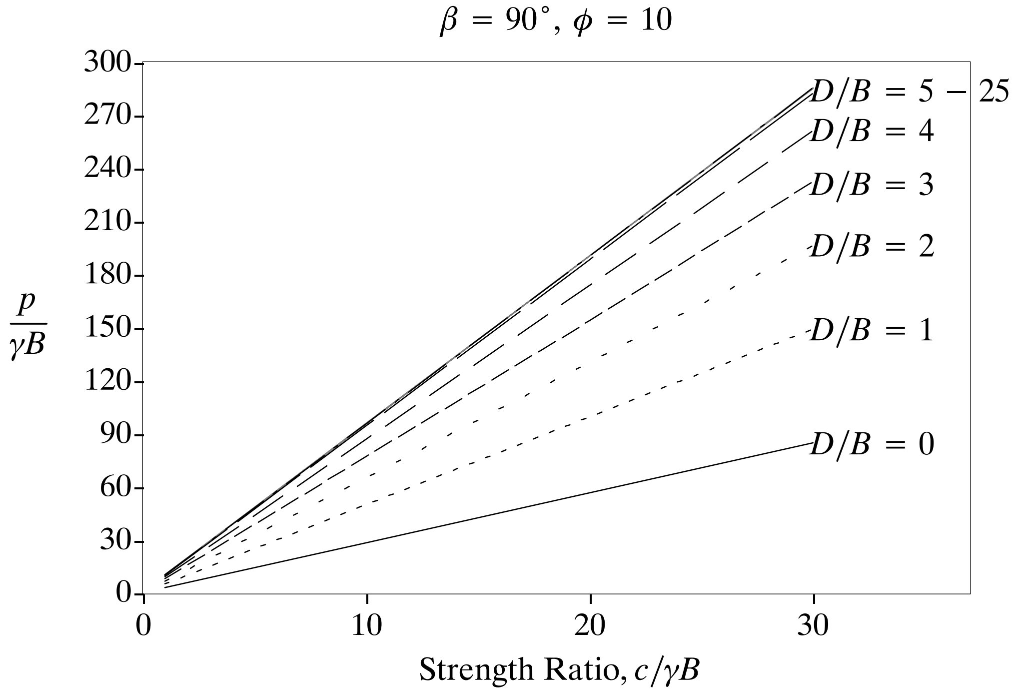

Figure C. 9: Change in Normalised Bearing Capacity with Strength Ratio

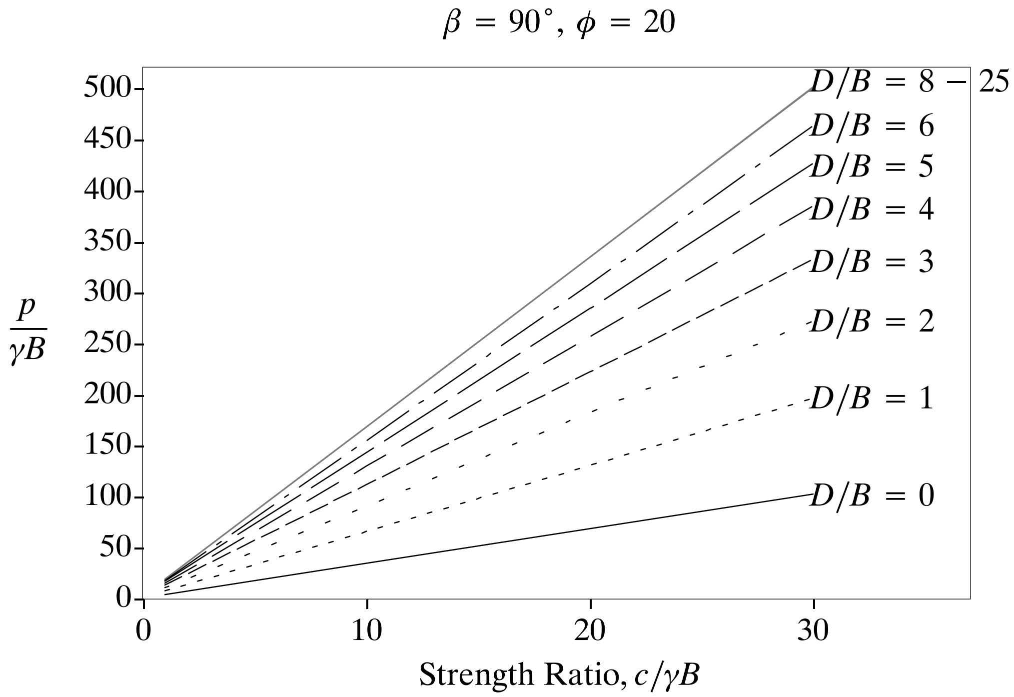

Figure C. 10: Change in Normalised Bearing Capacity with Strength Ratio

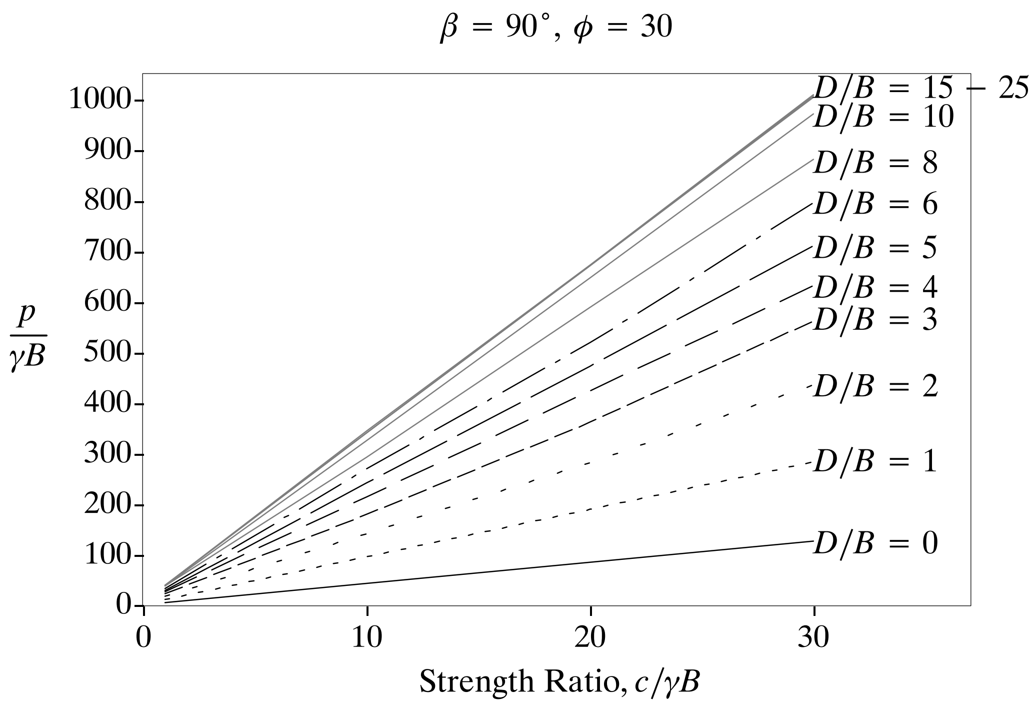

Figure C. 11: Change in Normalised Bearing Capacity with Strength Ratio

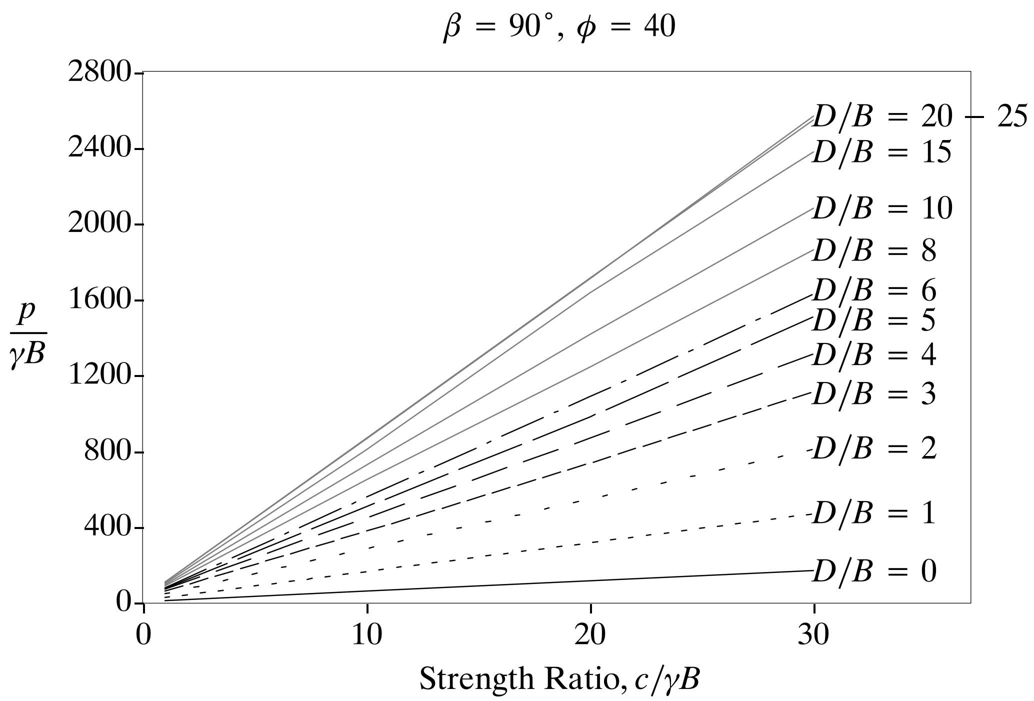

Figure C. 12: Change in Normalised Bearing Capacity with Strength Ratio

H/B = 3

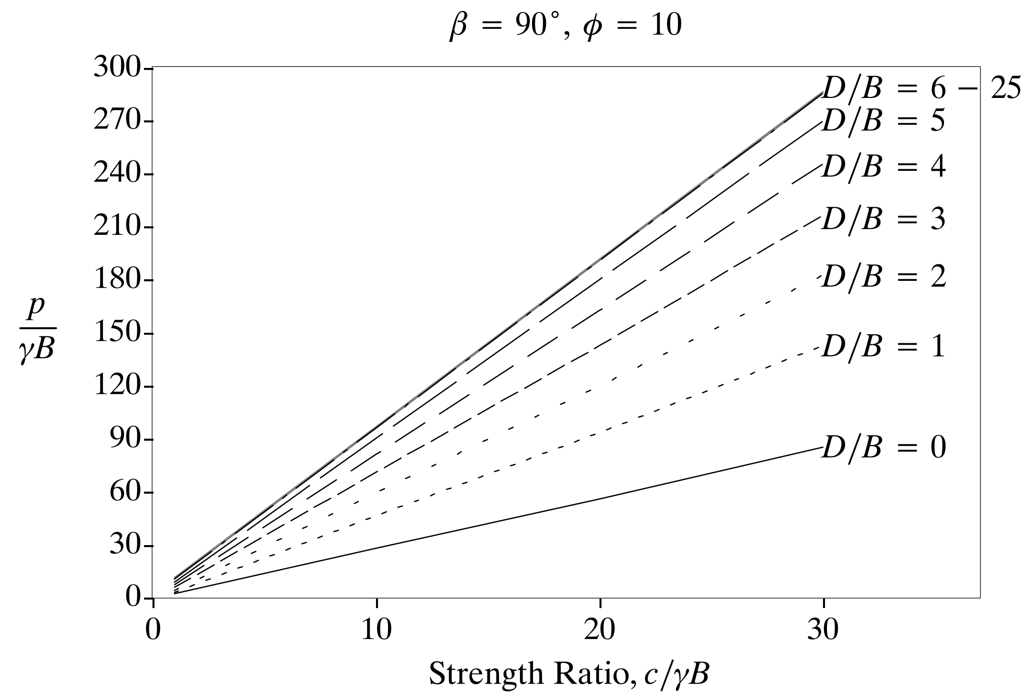

Figure C. 13: Change in Normalised Bearing Capacity with Strength Ratio

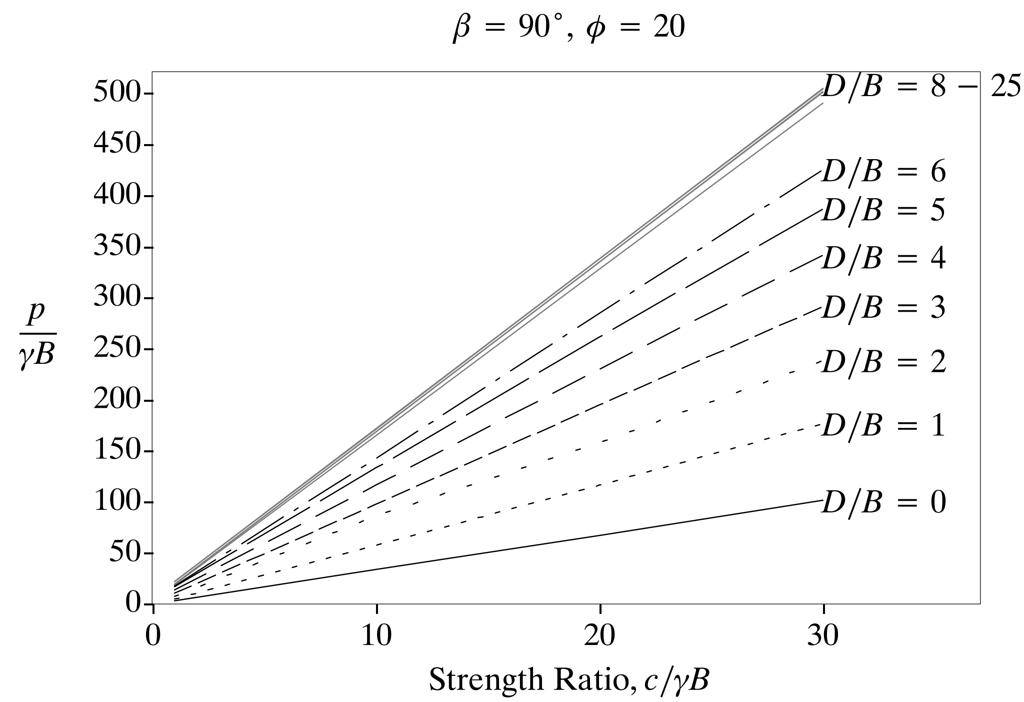

Figure C. 14: Change in Normalised Bearing Capacity with Strength Ratio

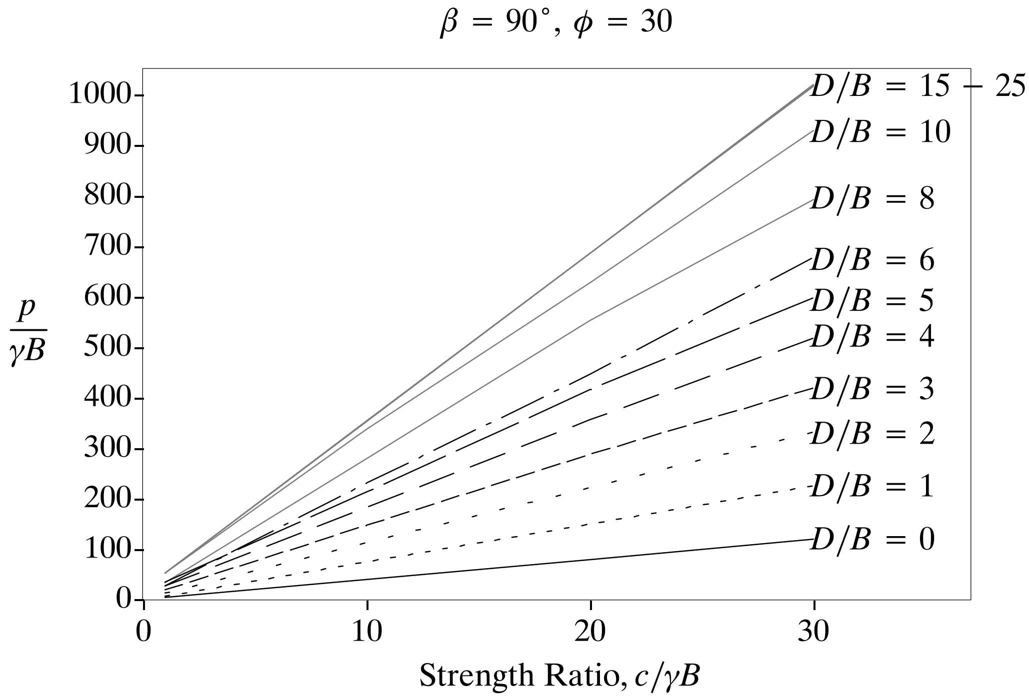

Figure C. 15: Change in Normalised Bearing Capacity with Strength Ratio

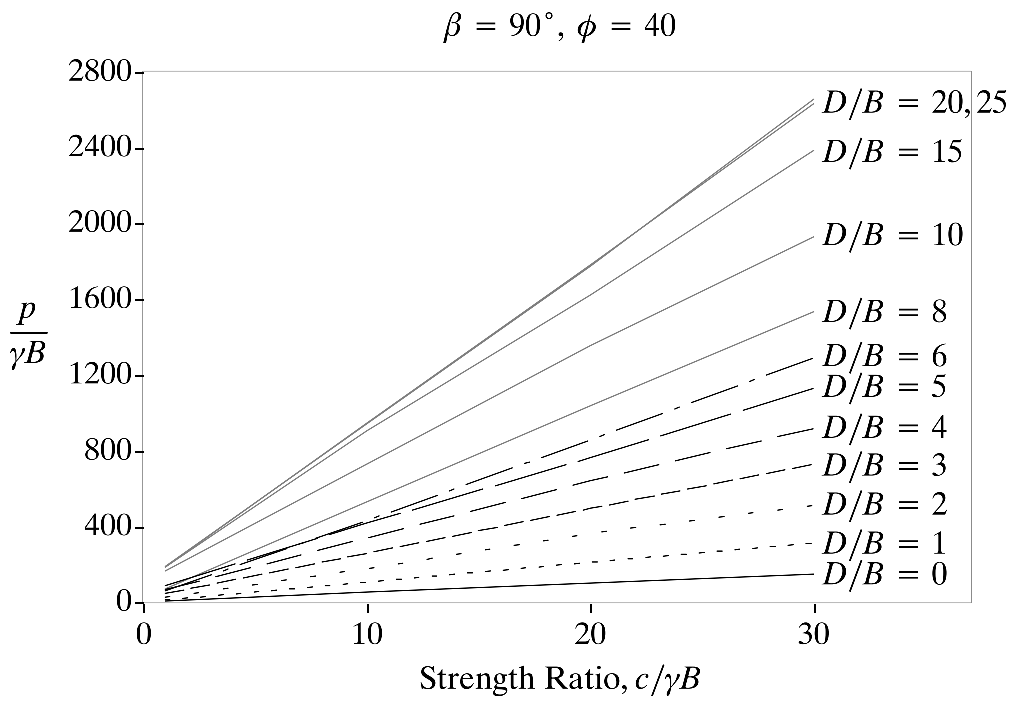

Figure C. 16: Change in Normalised Bearing Capacity with Strength Ratio

H/B = 4

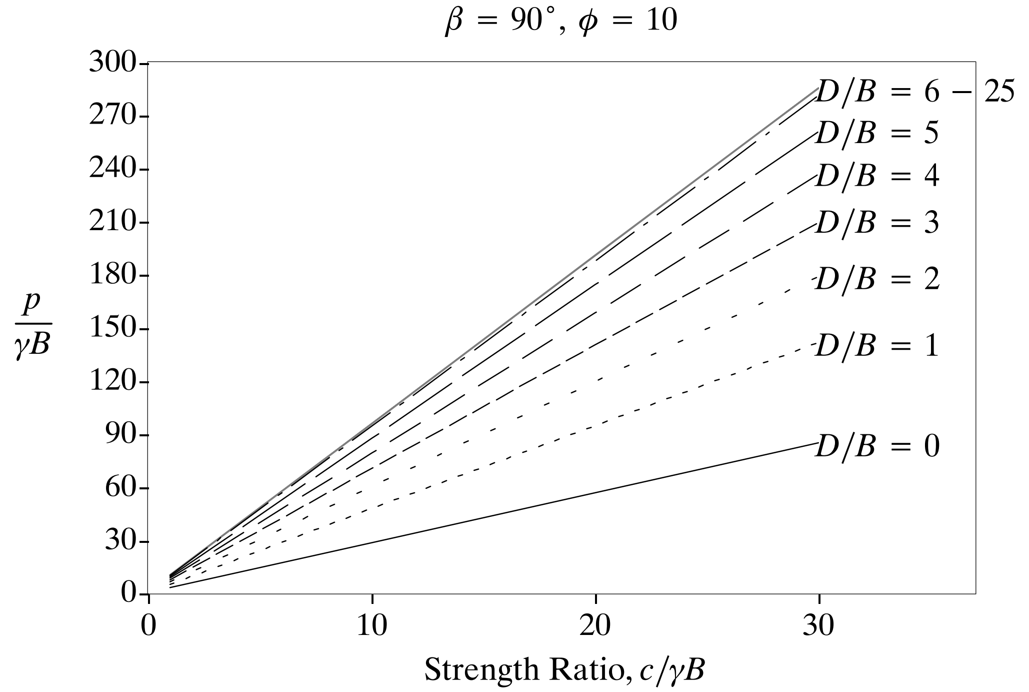

Figure C. 17: Change in Normalised Bearing Capacity with Strength Ratio

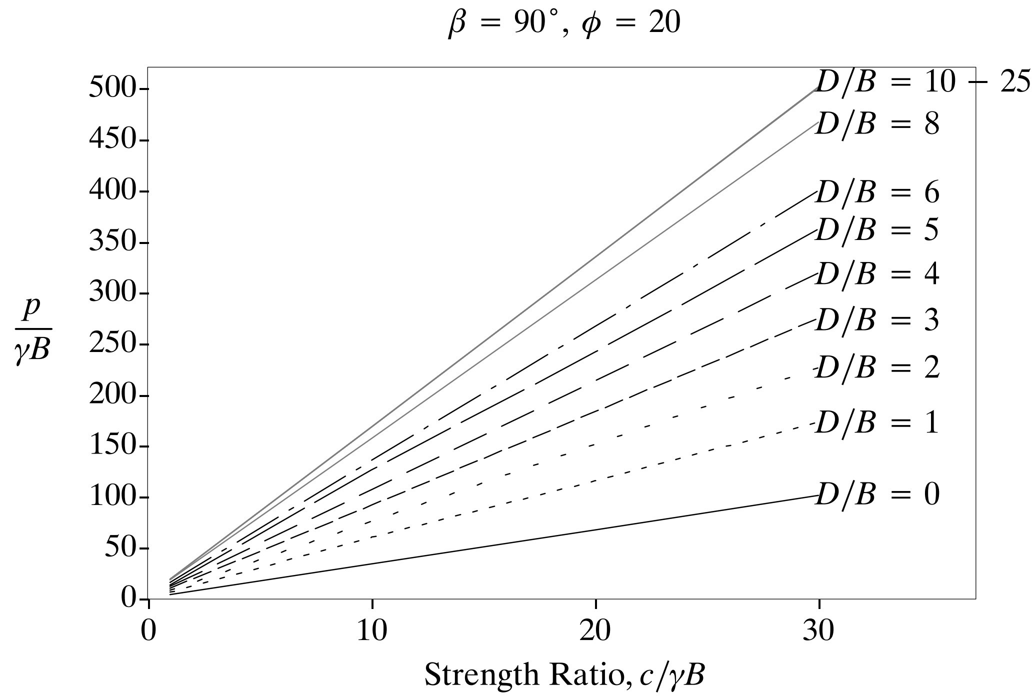

Figure C. 18: Change in Normalised Bearing Capacity with Strength Ratio

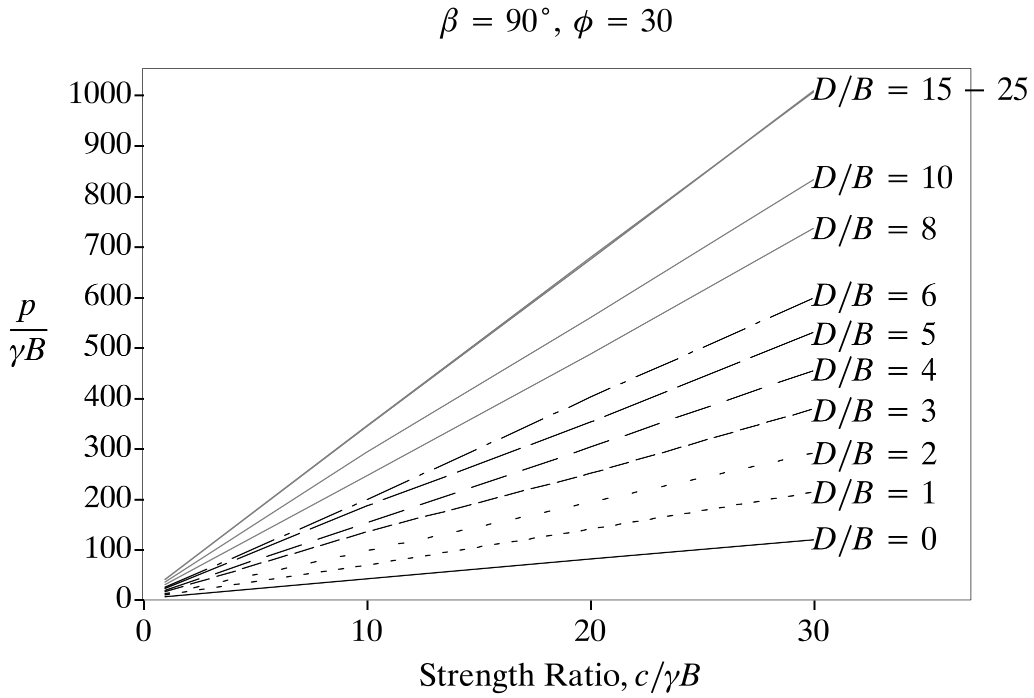

Figure C. 19: Change in Normalised Bearing Capacity with Strength Ratio

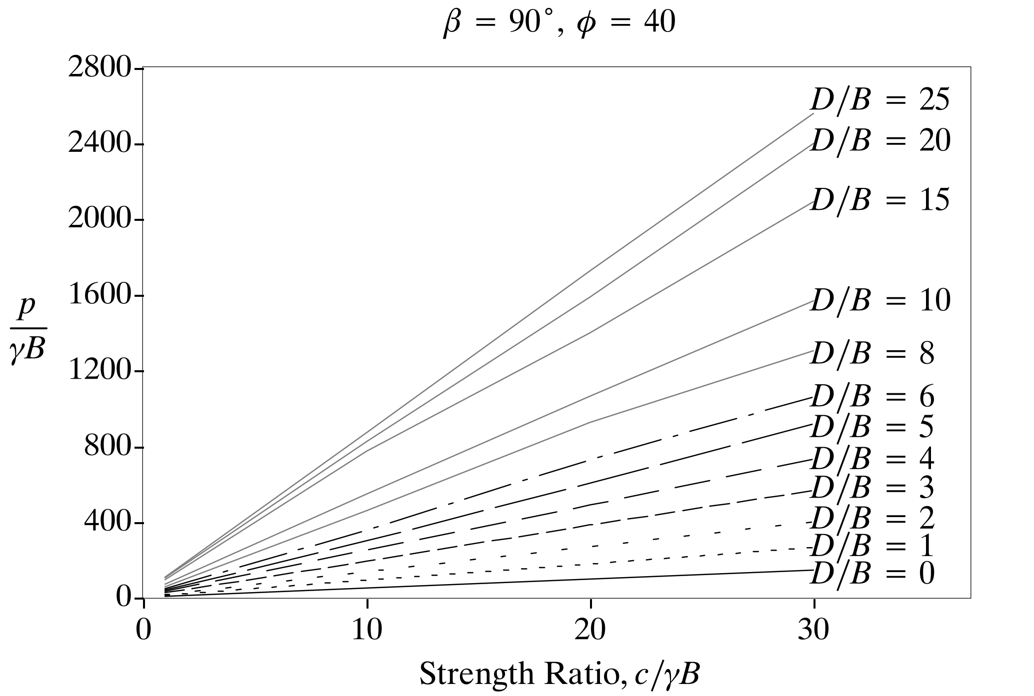

Figure C. 20: Change in Normalised Bearing Capacity with Strength Ratio

H/B = 5

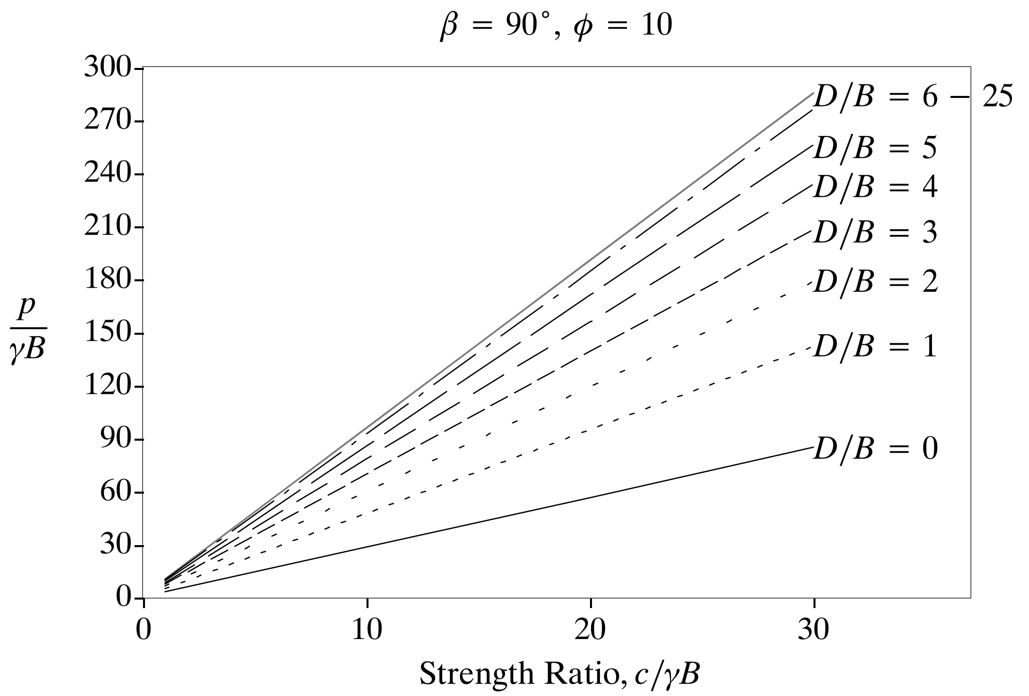

Figure C. 21: Change in Normalised Bearing Capacity with Strength Ratio

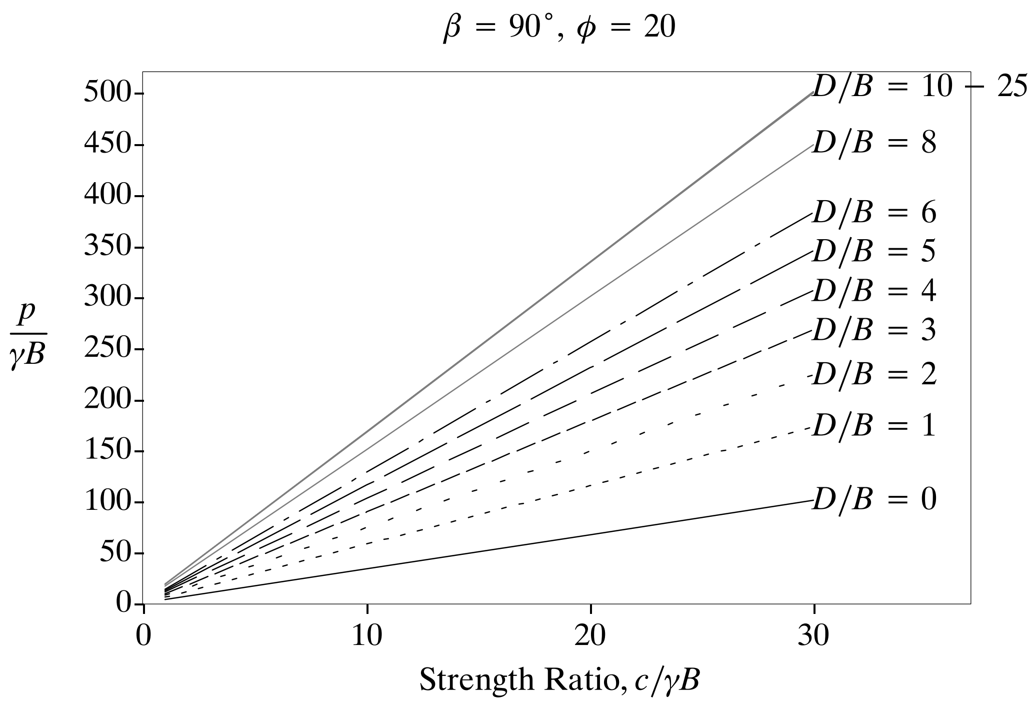

Figure C. 22: Change in Normalised Bearing Capacity with Strength Ratio

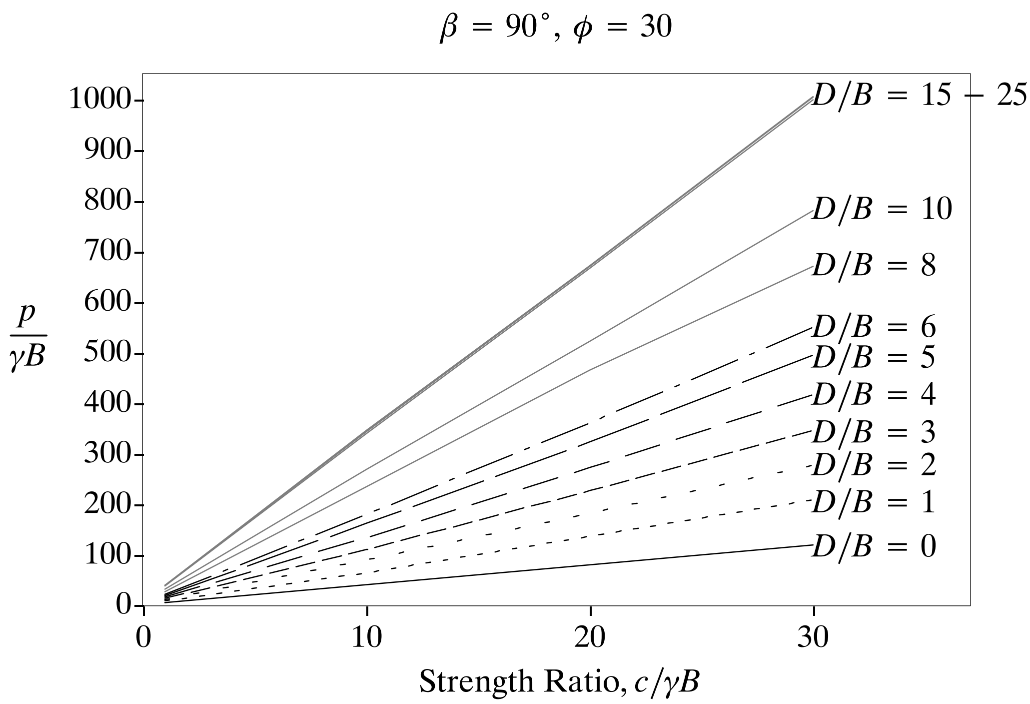

Figure C. 23: Change in Normalised Bearing Capacity with Strength Ratio

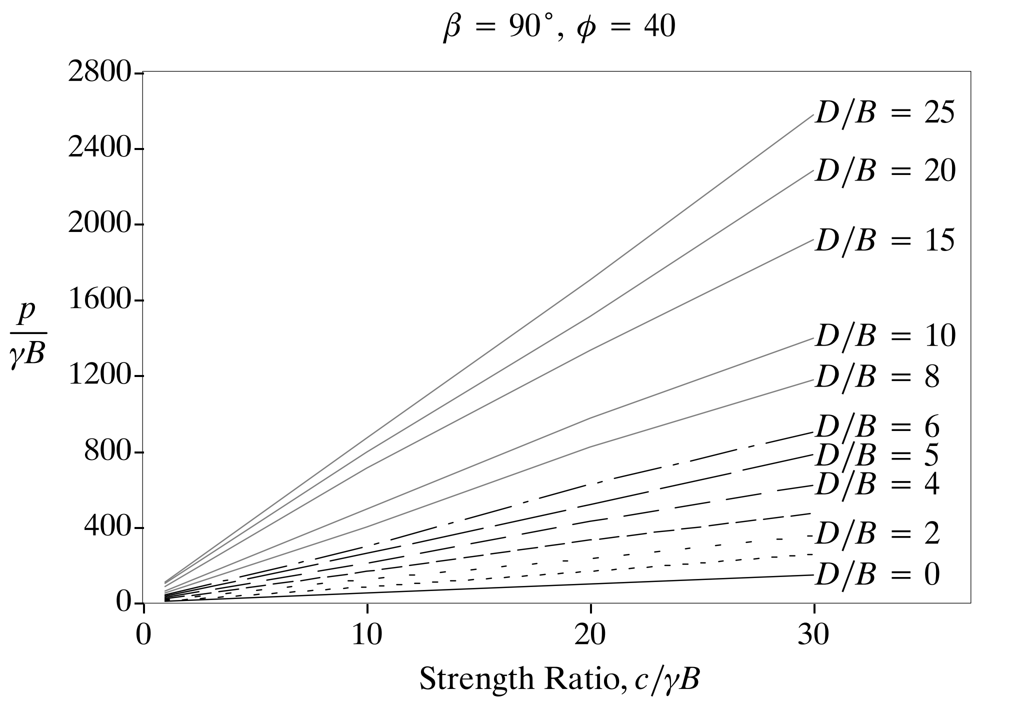

Figure C. 24: Change in Normalised Bearing Capacity with Strength Ratio

H/B = 6

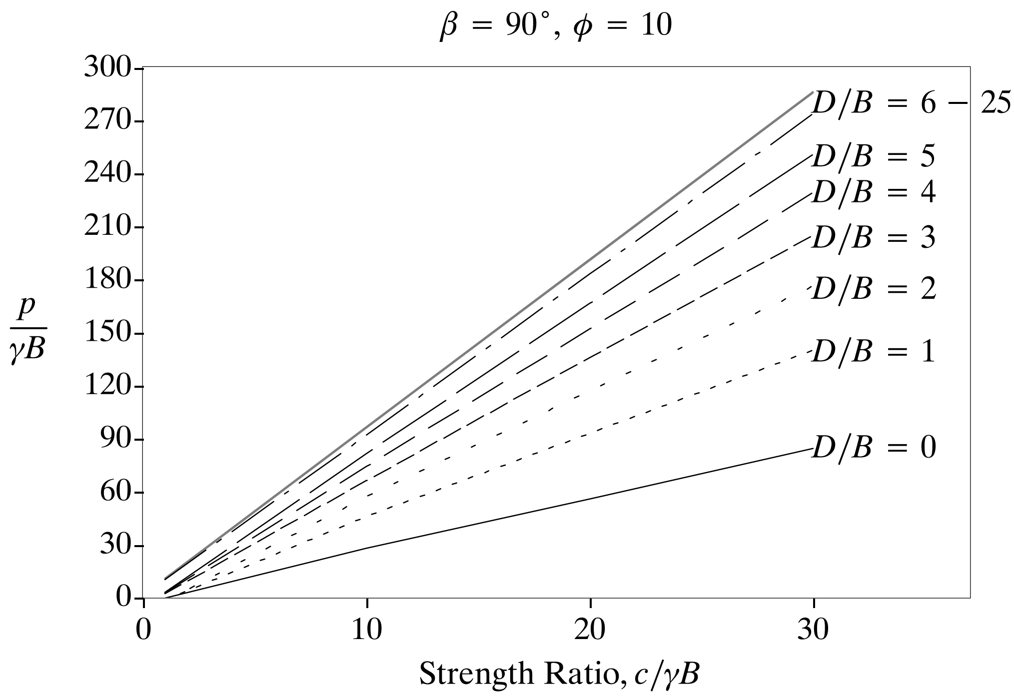

Figure C. 25: Change in Normalised Bearing Capacity with Strength Ratio

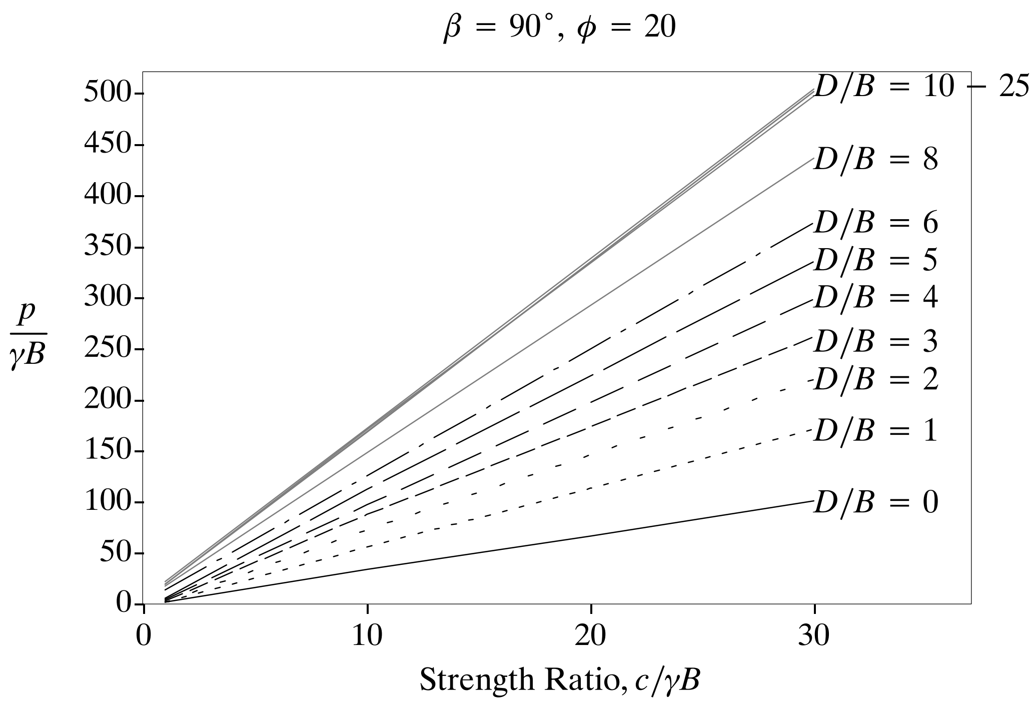

Figure C. 26: Change in Normalised Bearing Capacity with Strength Ratio

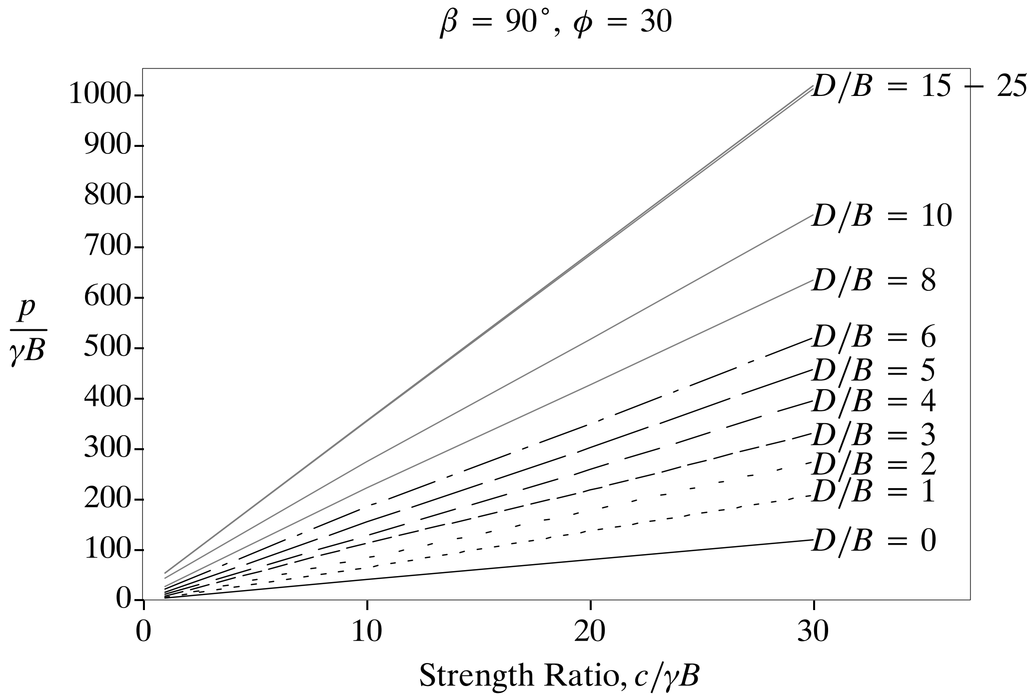

Figure C. 27: Change in Normalised Bearing Capacity with Strength Ratio

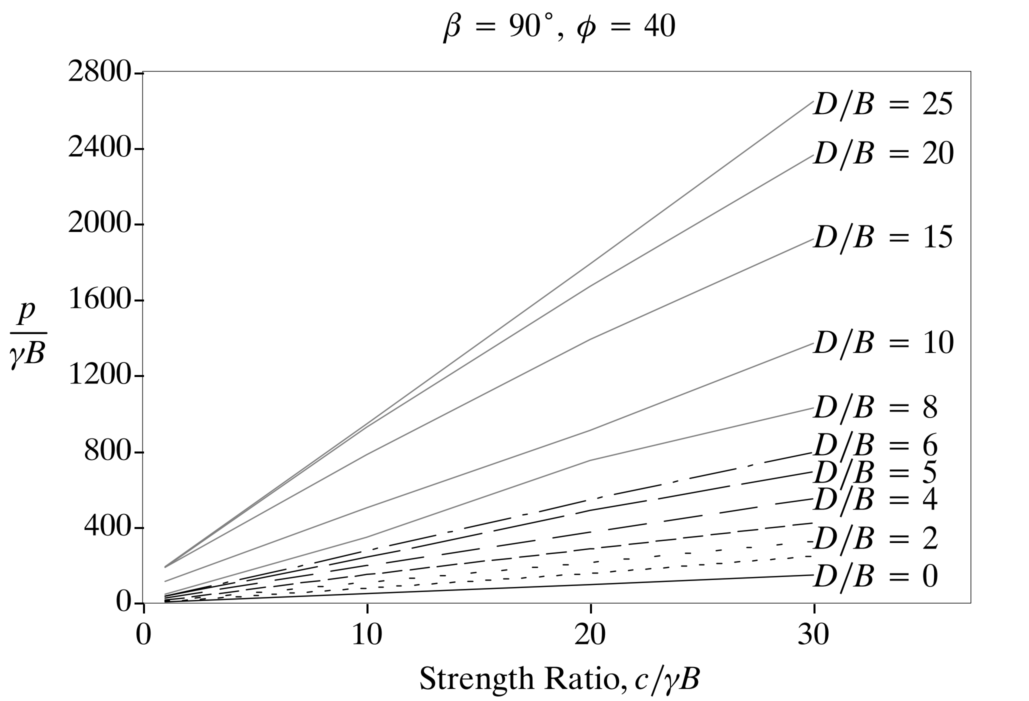

Figure C. 28: Change in Normalised Bearing Capacity with Strength Ratio

H/B = 8

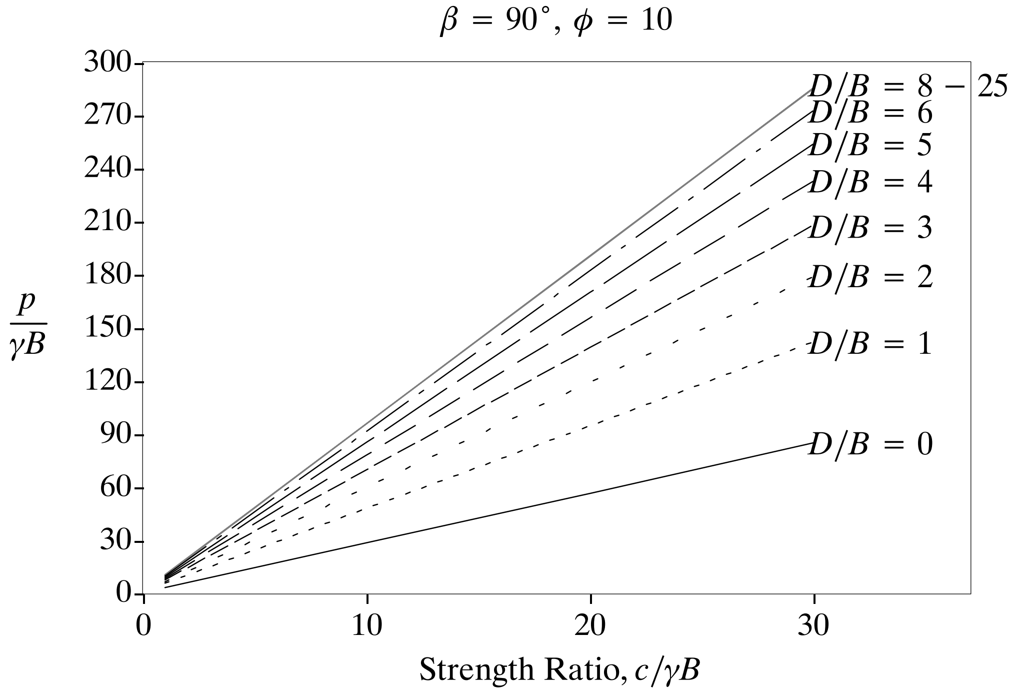

Figure C. 29: Change in Normalised Bearing Capacity with Strength Ratio

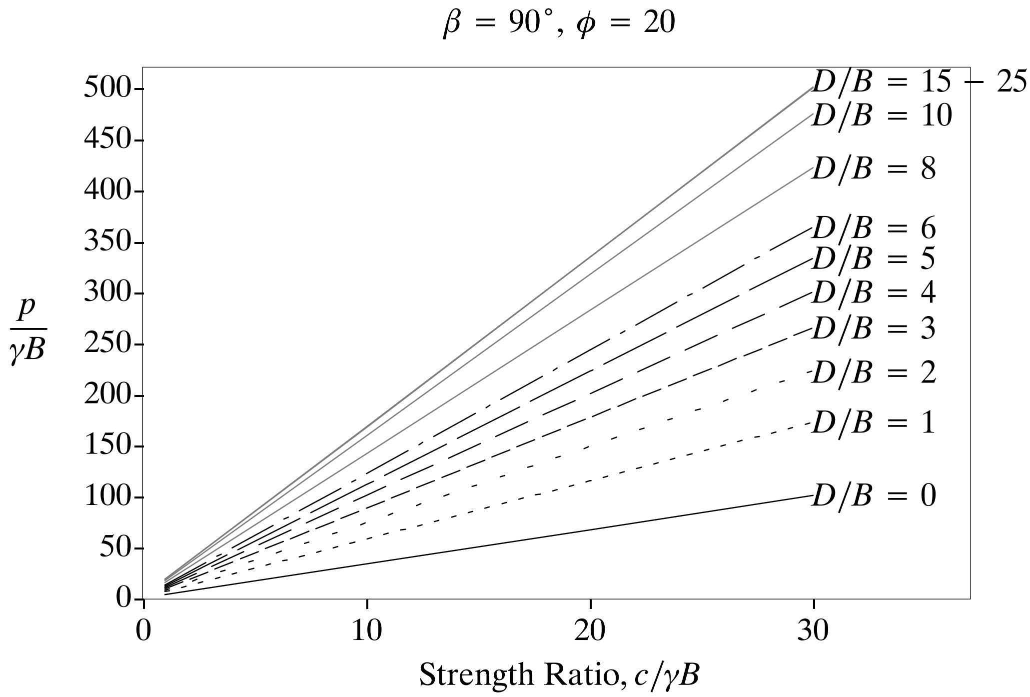

Figure C. 30: Change in Normalised Bearing Capacity with Strength Ratio

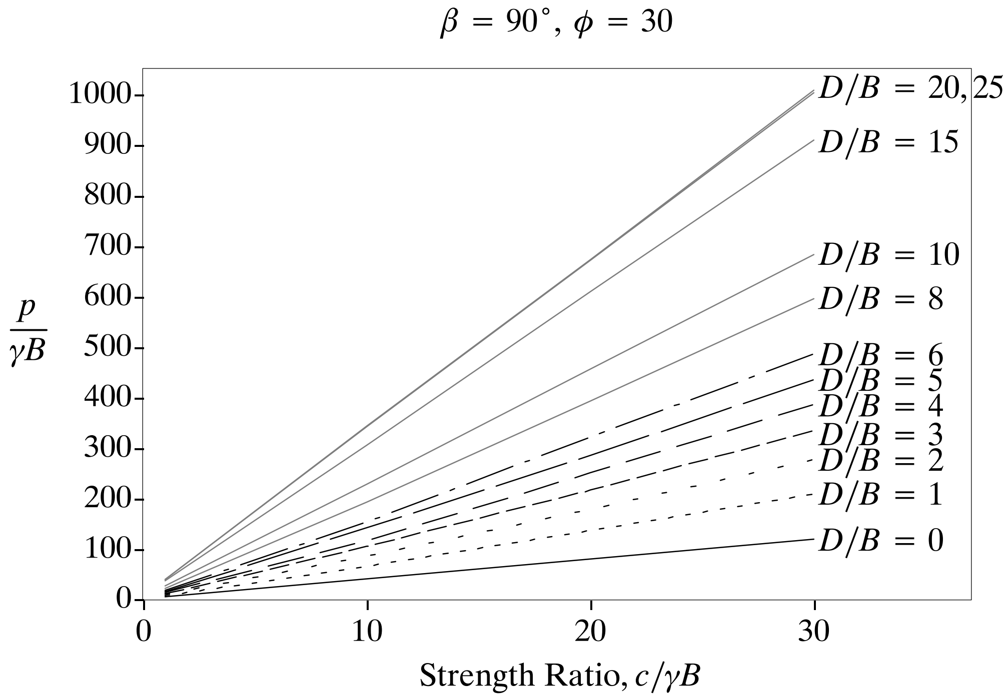

Figure C. 31: Change in Normalised Bearing Capacity with Strength Ratio

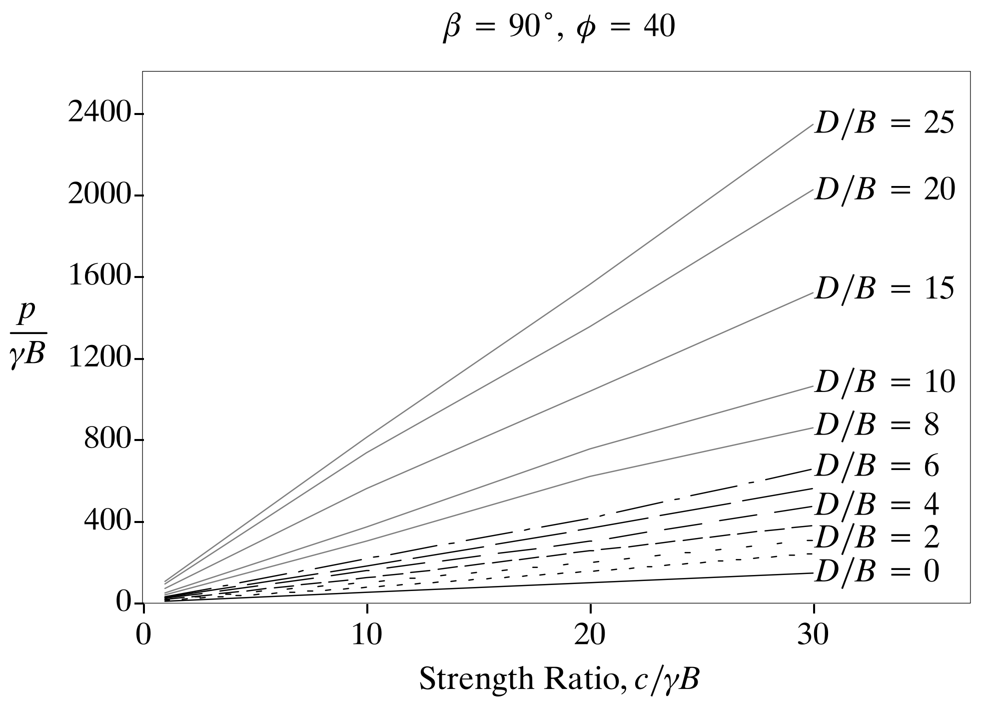

Figure C. 32: Change in Normalised Bearing Capacity with Strength Ratio

H/B = 10

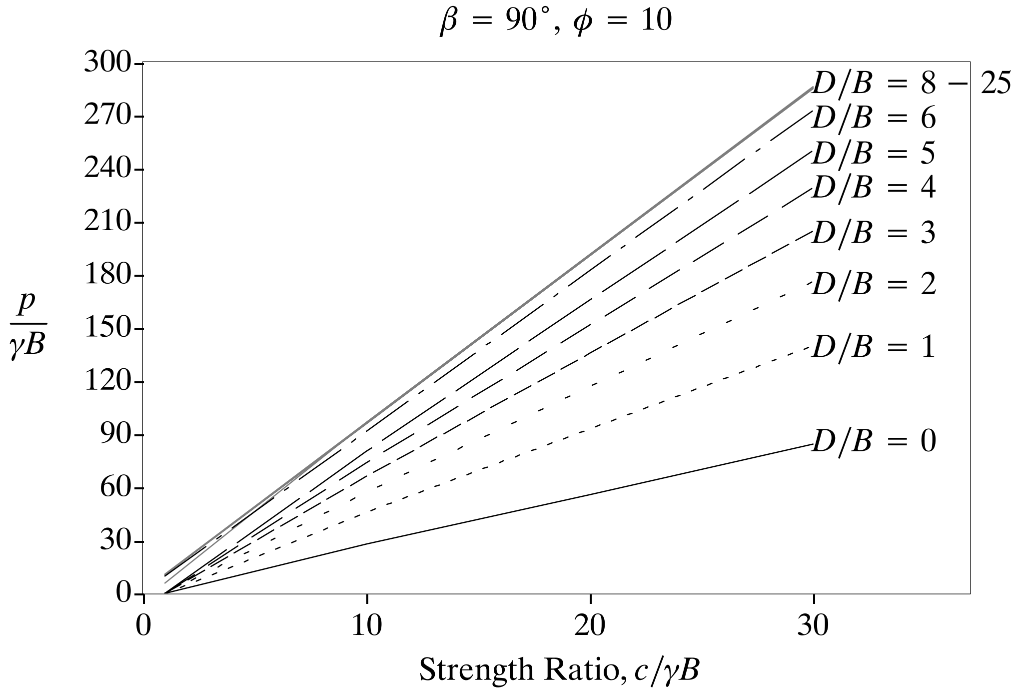

Figure C. 33: Change in Normalised Bearing Capacity with Strength Ratio

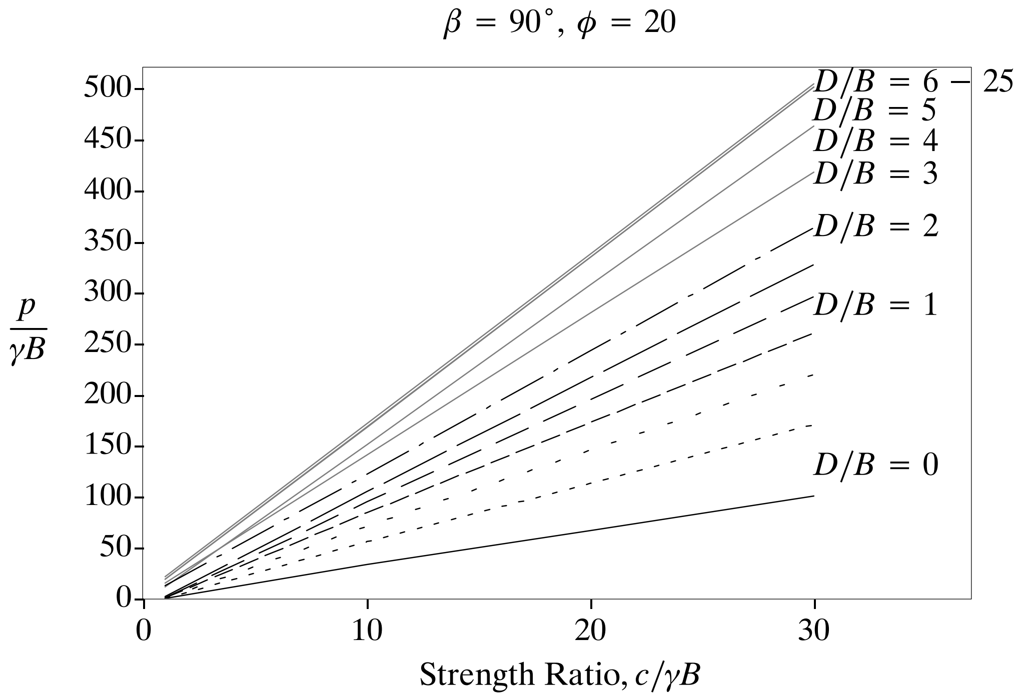

Figure C. 34: Change in Normalised Bearing Capacity with Strength Ratio

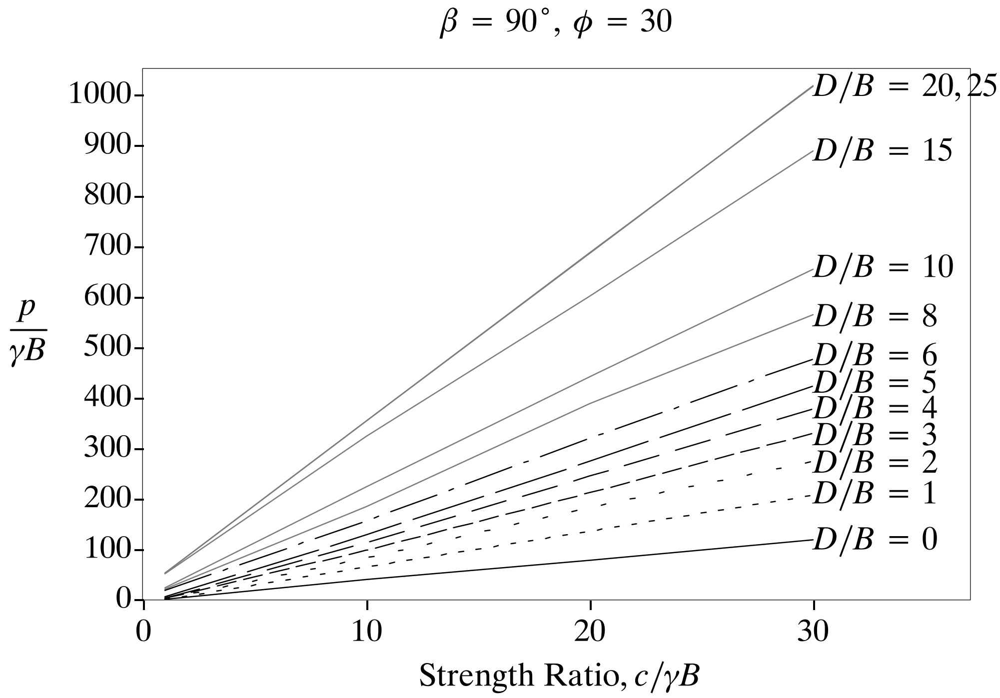

Figure C. 35: Change in Normalised Bearing Capacity with Strength Ratio

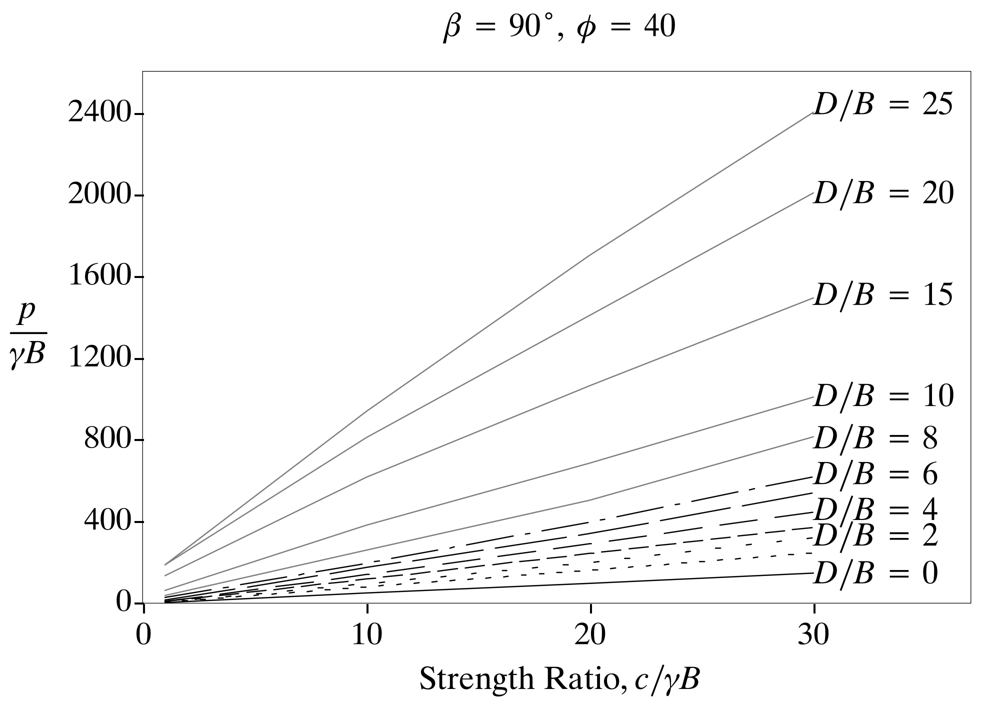

Figure C. 36: Change in Normalised Bearing Capacity with Strength Ratio

H/B = 13

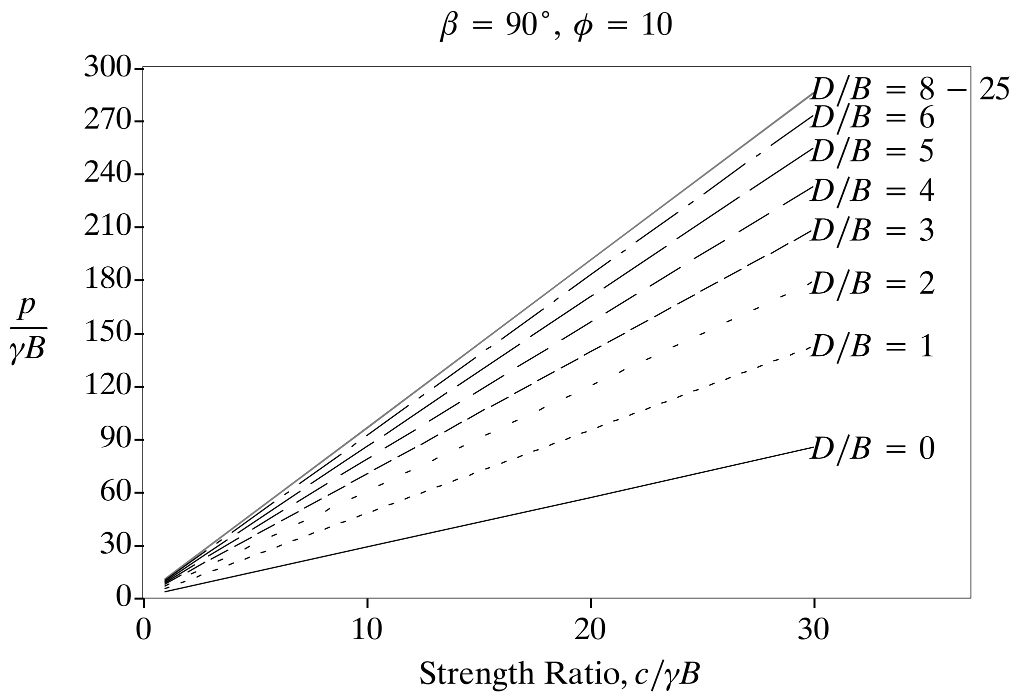

Figure C. 37: Change in Normalised Bearing Capacity with Strength Ratio

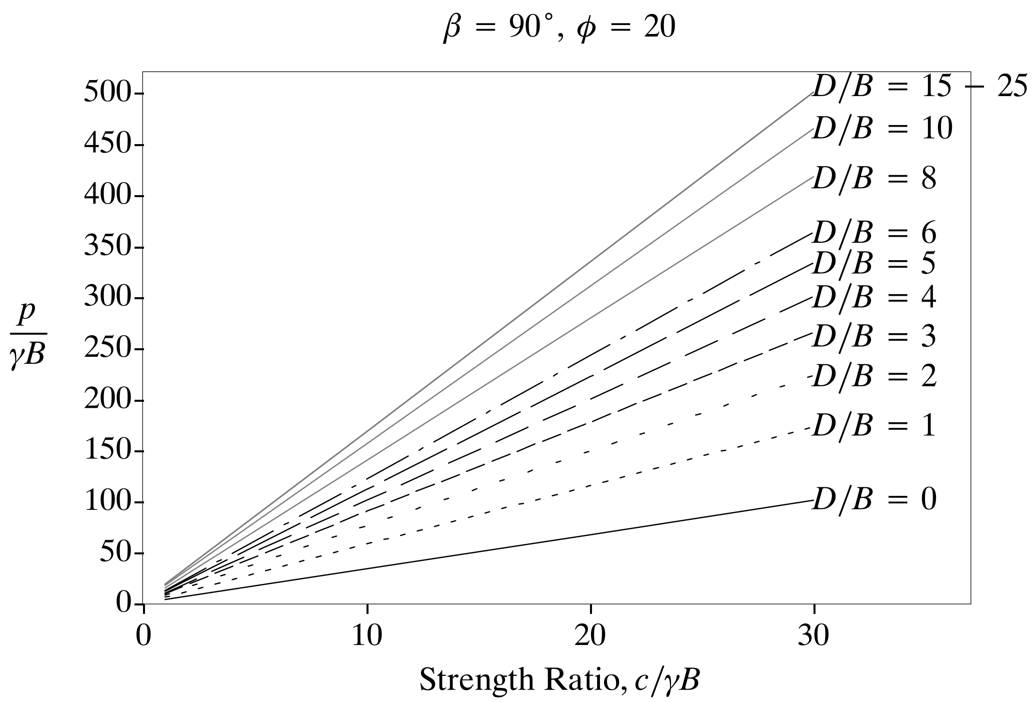

Figure C. 38: Change in Normalised Bearing Capacity with Strength Ratio

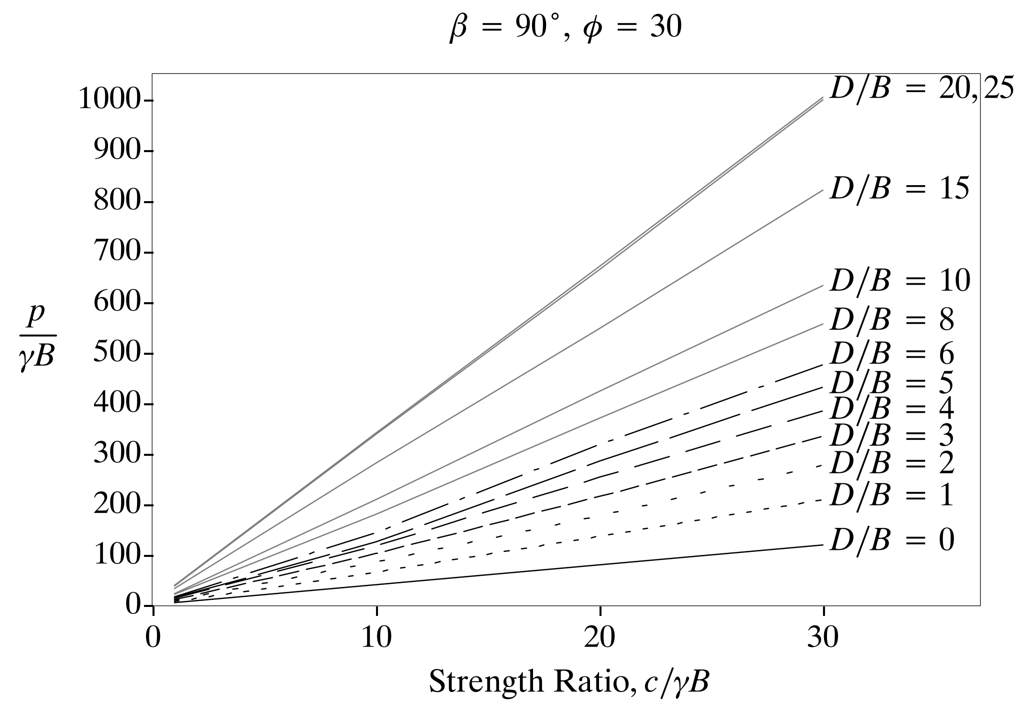

Figure C. 39: Change in Normalised Bearing Capacity with Strength Ratio

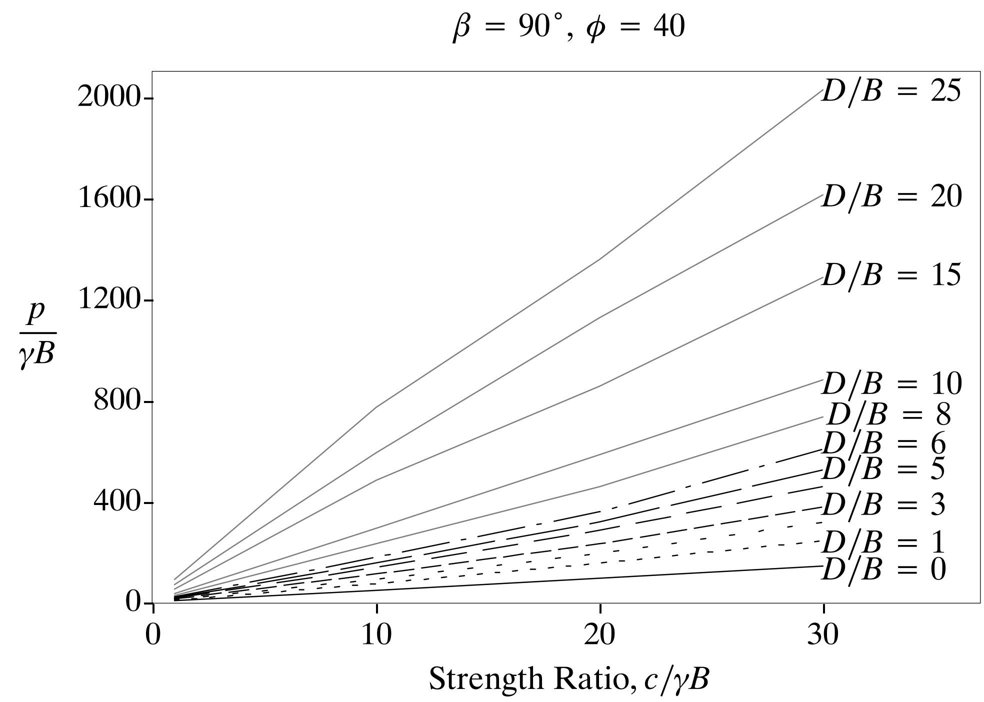

Figure C. 40: Change in Normalised Bearing Capacity with Strength Ratio

H/B = 16

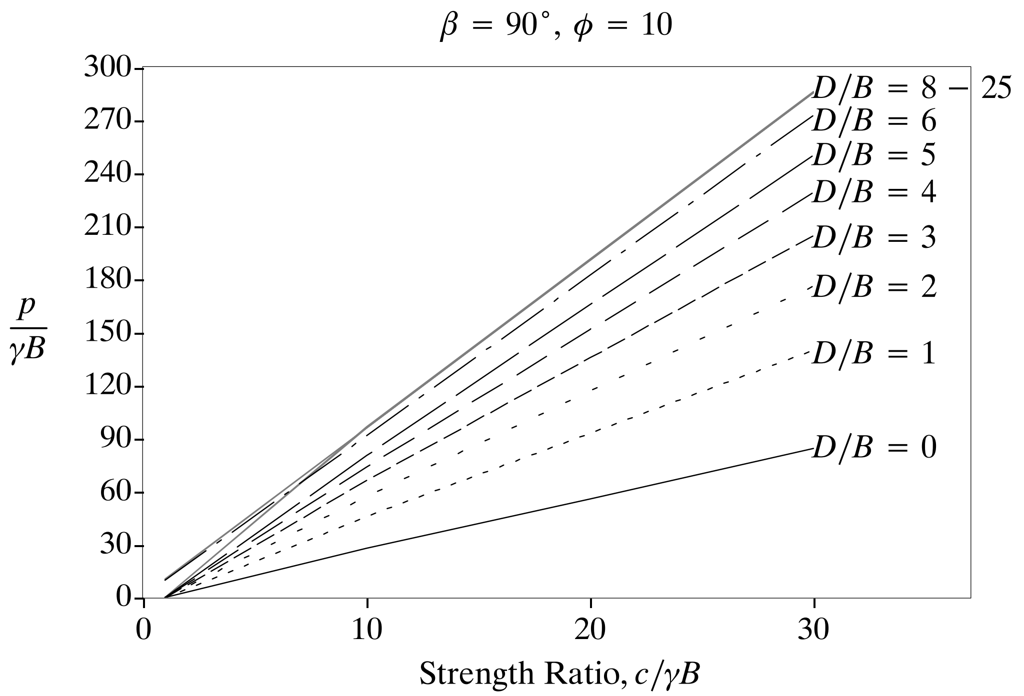

Figure C. 41: Change in Normalised Bearing Capacity with Strength Ratio

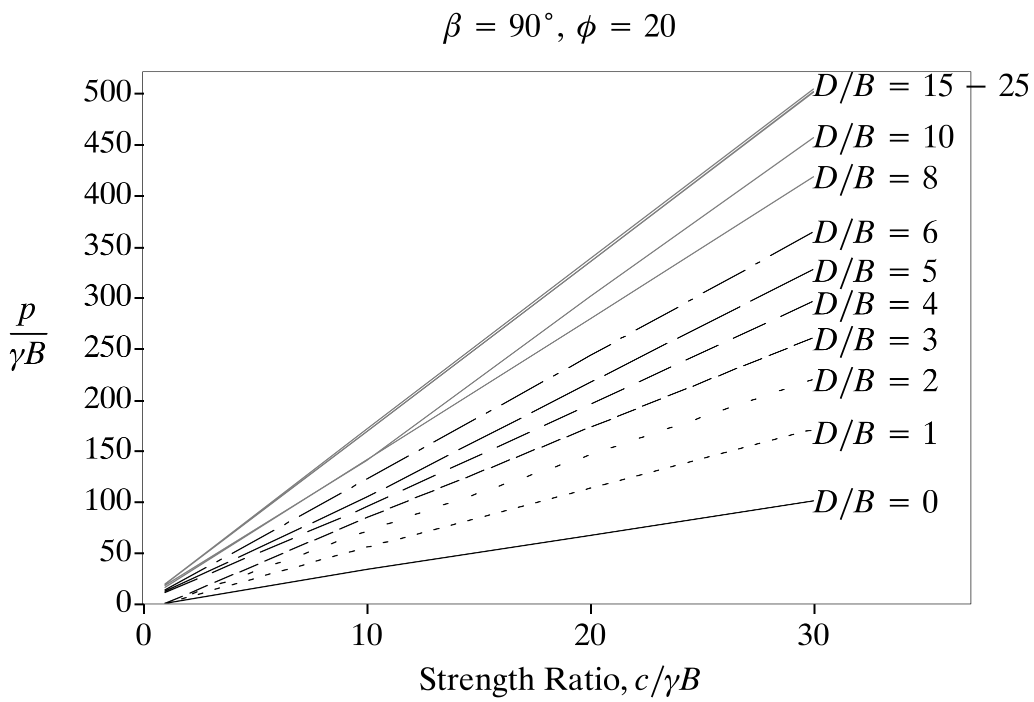

Figure C. 42: Change in Normalised Bearing Capacity with Strength Ratio

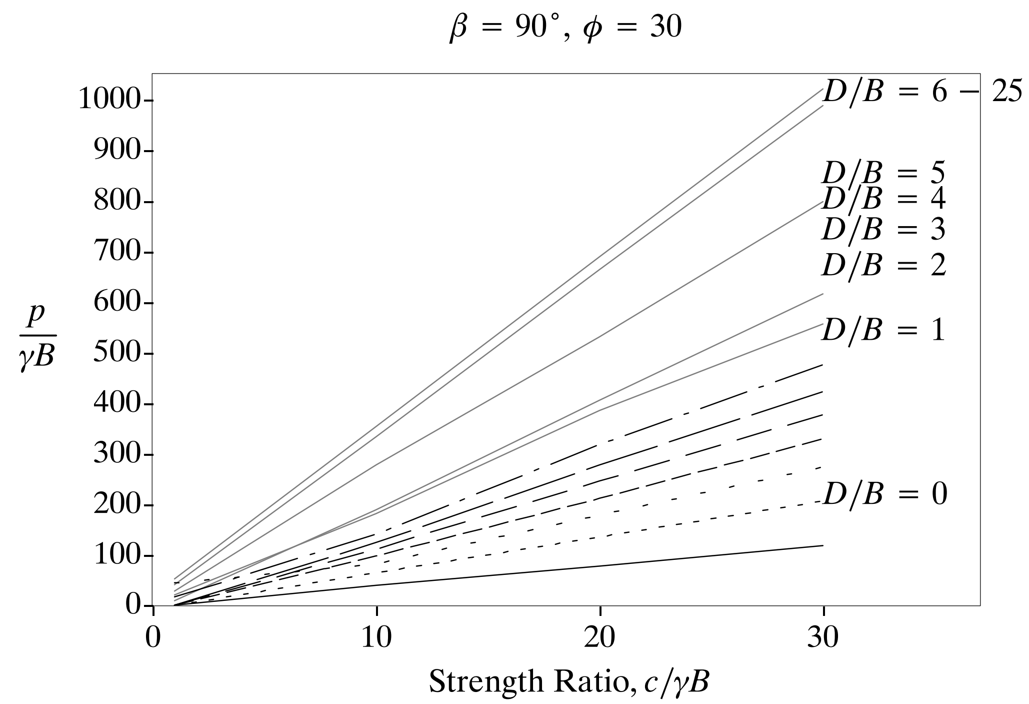

Figure C. 43: Change in Normalised Bearing Capacity with Strength Ratio

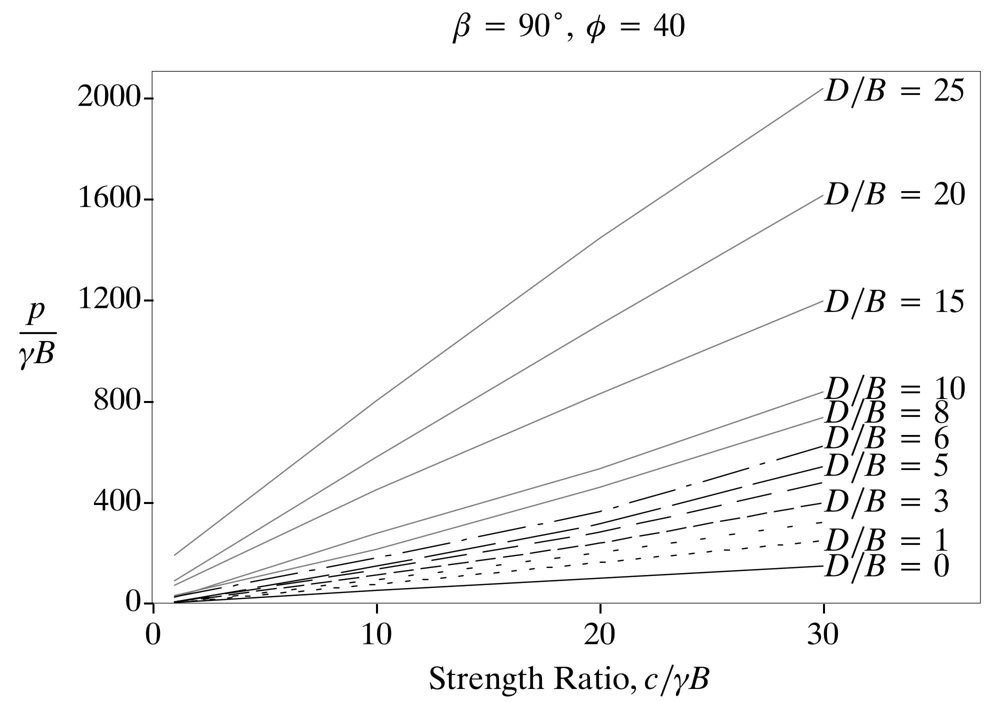

Figure C. 44: Change in Normalised Bearing Capacity with Strength Ratio

8.4 Appendix D

Increased Bearing Capacity due to Increasing Footing Distance Ratio Charts

The charts in this section best demonstrate the effect changing the distance of a footing from the edge of a slope has on the bearing capacity of a slope. This is particularly useful if a set slope is available to build on, and how close to the slope edge the structure is able to be placed needs to be determined. If the load of the footing is known, it is a simple matter of selecting the chart corresponding to the correct slope height ratio then choosing the footing distance that can provide adequate bearing capacity.

Again this chart type is divided into groups according to the slope height ratio with a chart for each friction angle for each slope height.

H/B = 0

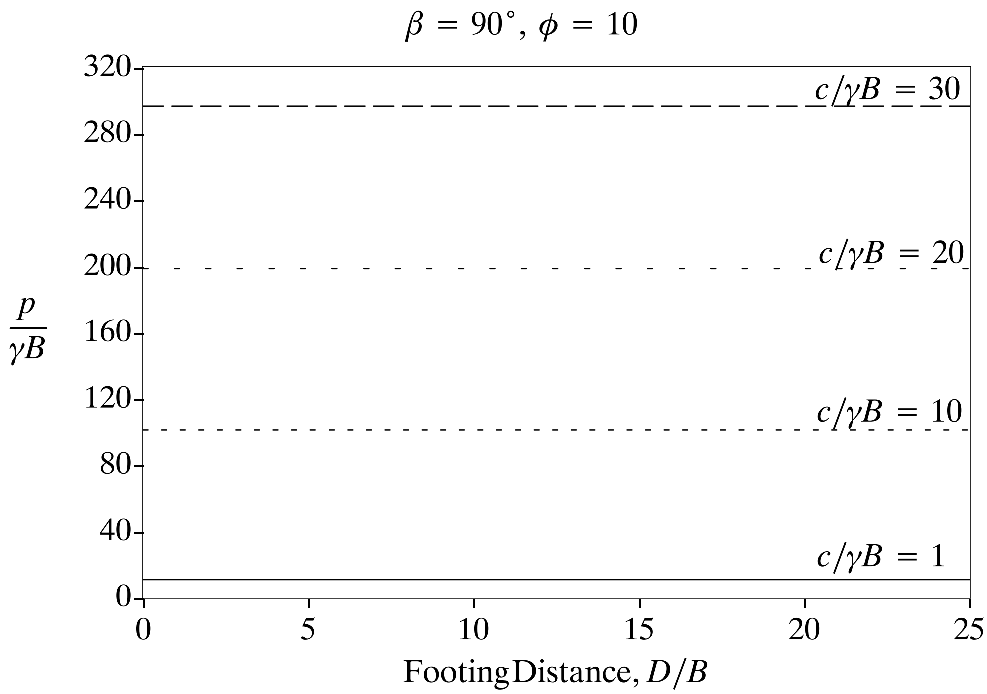

Figure D.1.: Change in Normalised Bearing Capacity with Footing Distance

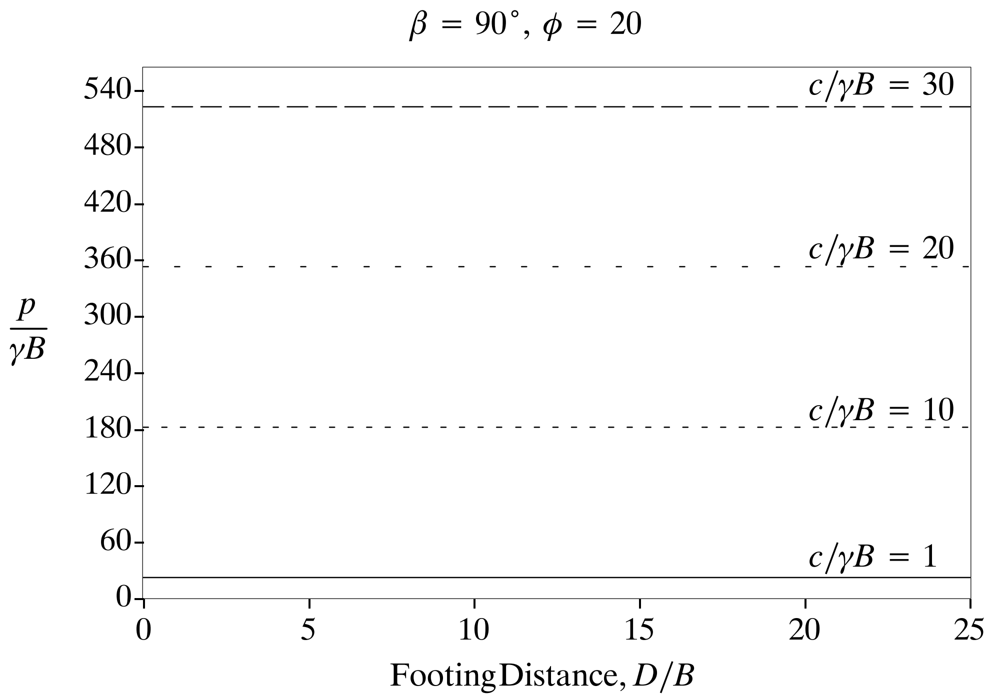

Figure D.2.: Change in Normalised Bearing Capacity with Footing Distance

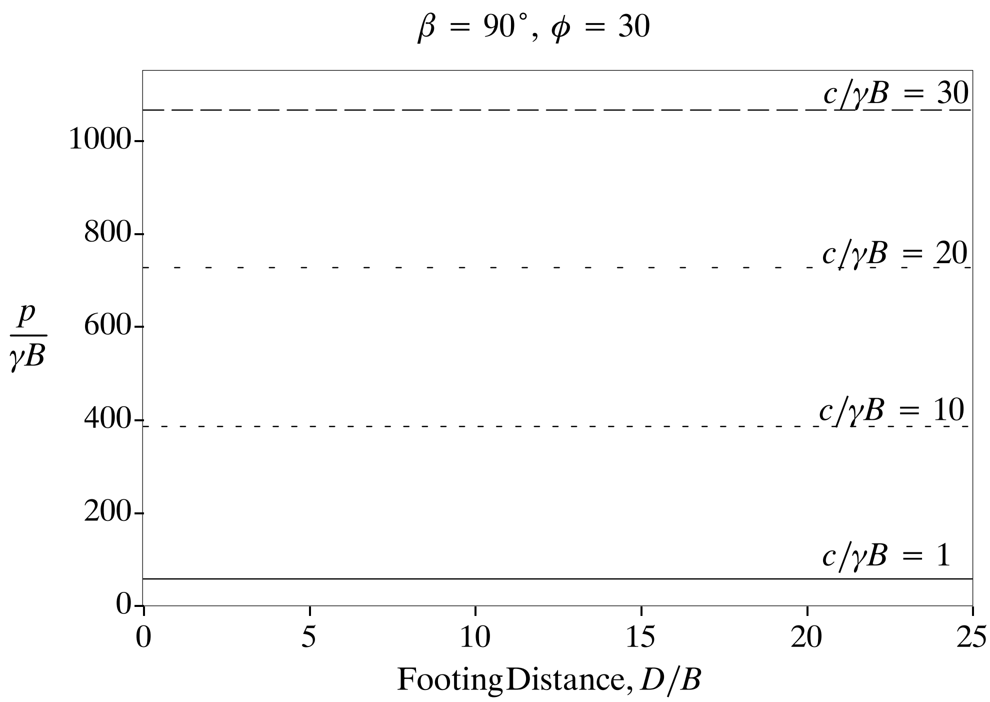

Figure D.3.: Change in Normalised Bearing Capacity with Footing Distance

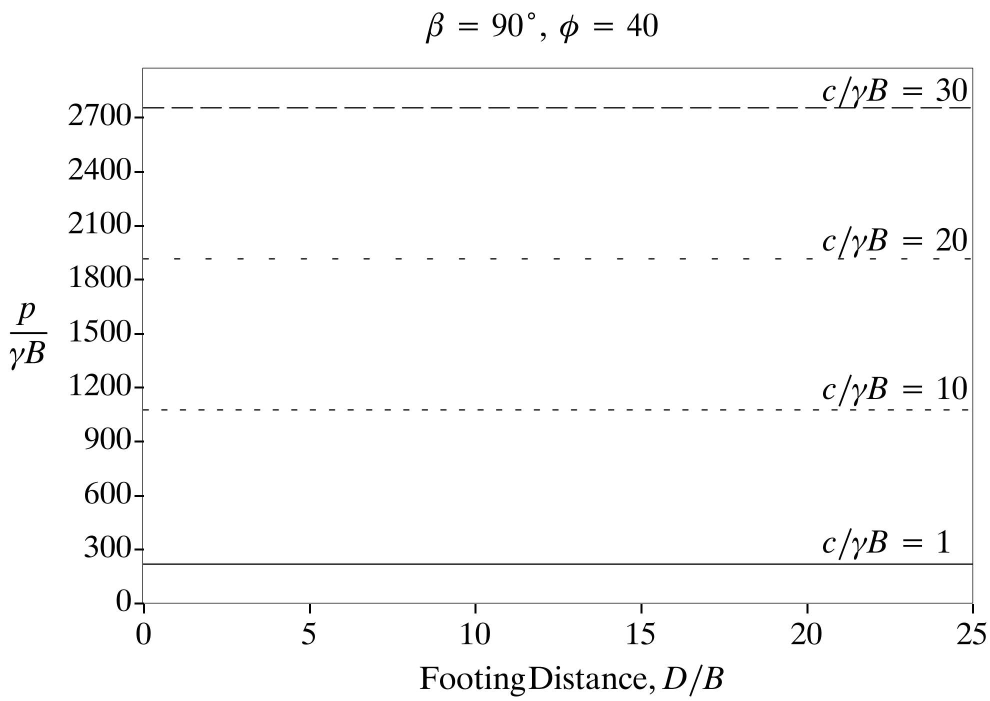

Figure D.4.: Change in Normalised Bearing Capacity with Footing Distance

H/B = 1

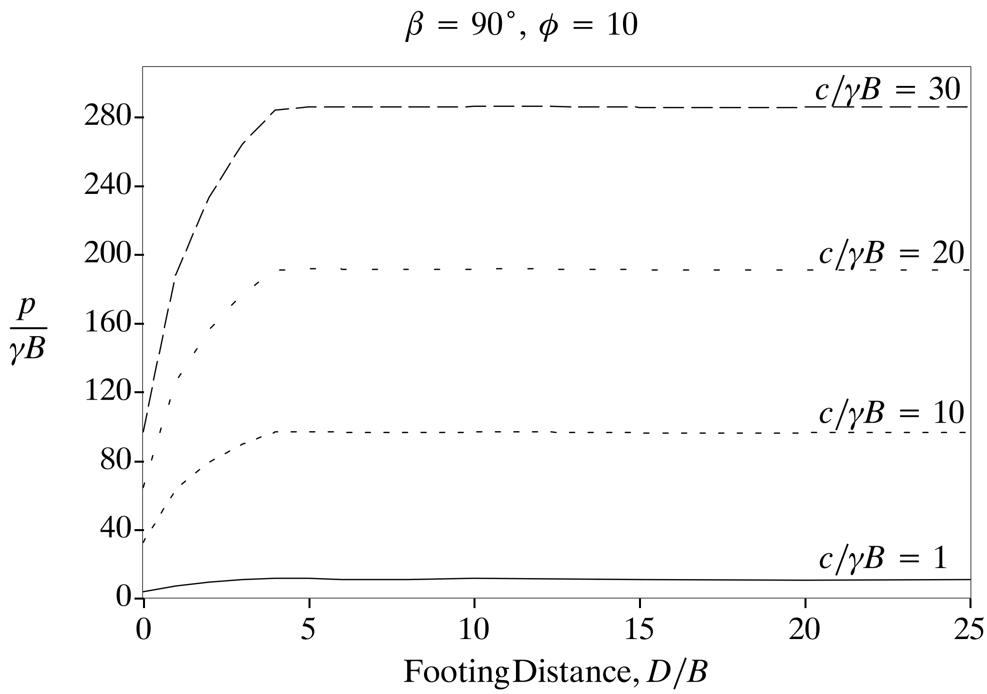

Figure D.5.: Change in Normalised Bearing Capacity with Footing Distance

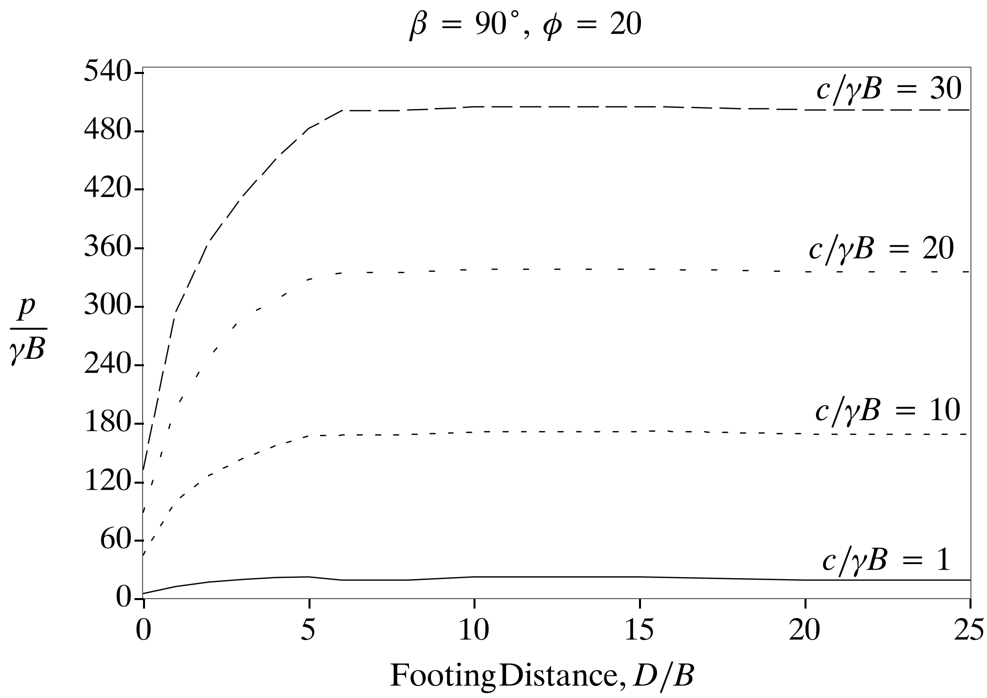

Figure D.6.: Change in Normalised Bearing Capacity with Footing Distance

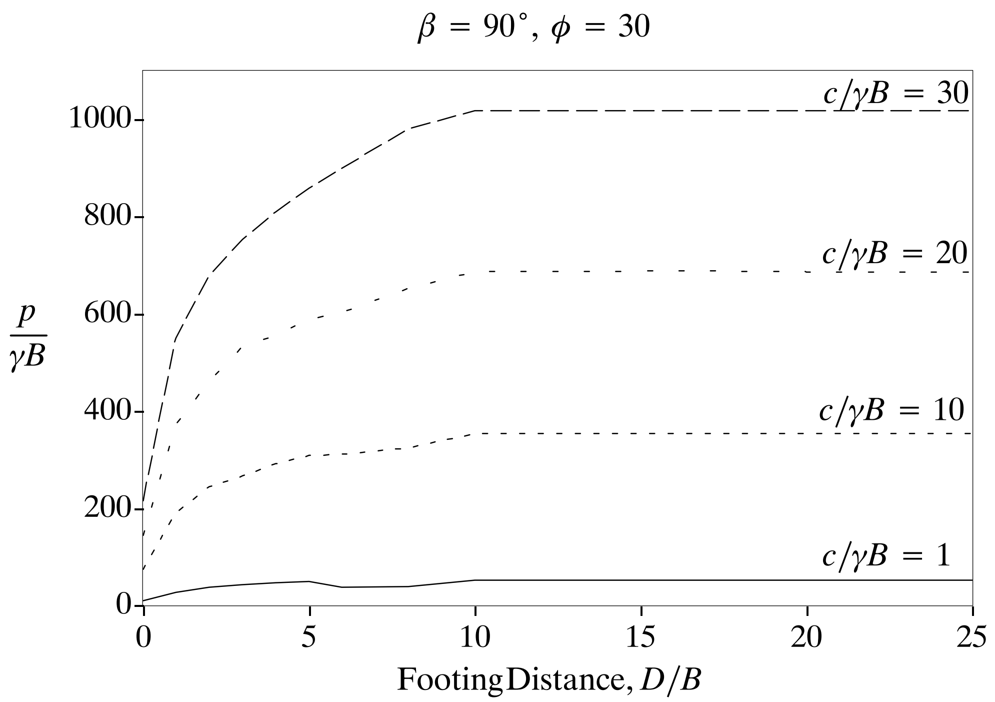

Figure D.7.: Change in Normalised Bearing Capacity with Footing Distance

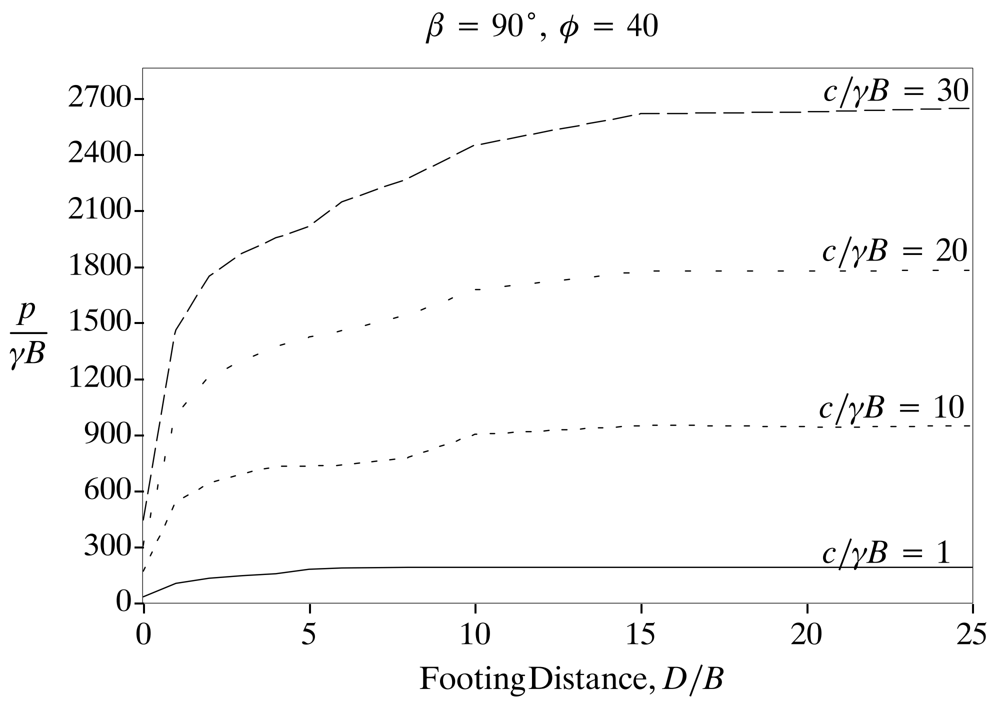

Figure D.8.: Change in Normalised Bearing Capacity with Footing Distance

H/B = 2

$\beta = 90^\circ,\ \phi = 10$

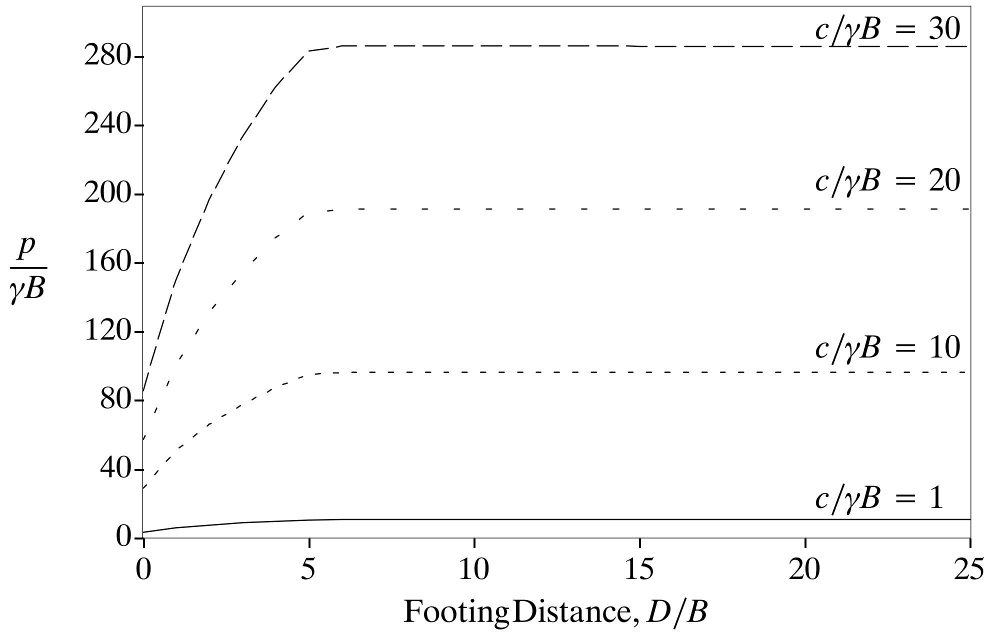

Figure D.9.: Change in Normalised Bearing Capacity with Footing Distance

$\beta = 90^\circ,\ \phi = 20$

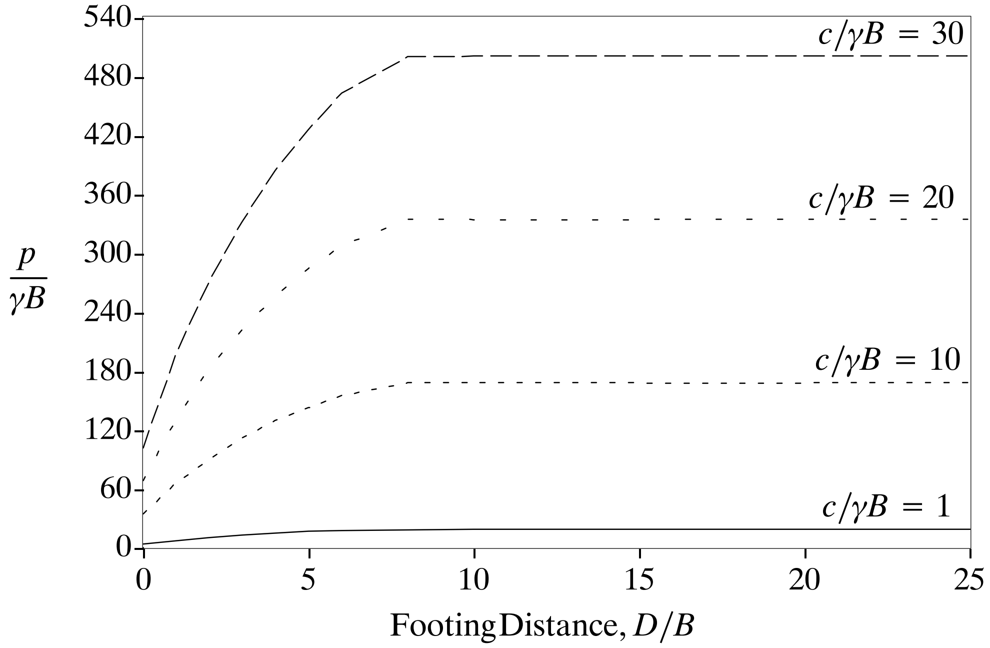

Figure D.10.: Change in Normalised Bearing Capacity with Footing Distance

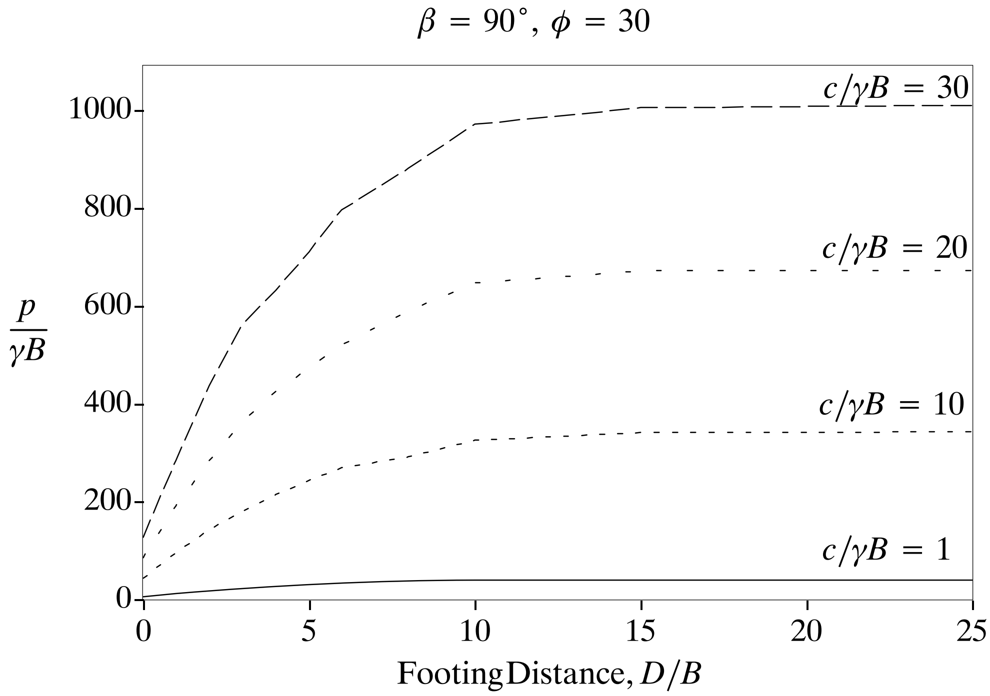

Figure D.11.: Change in Normalised Bearing Capacity with Footing Distance

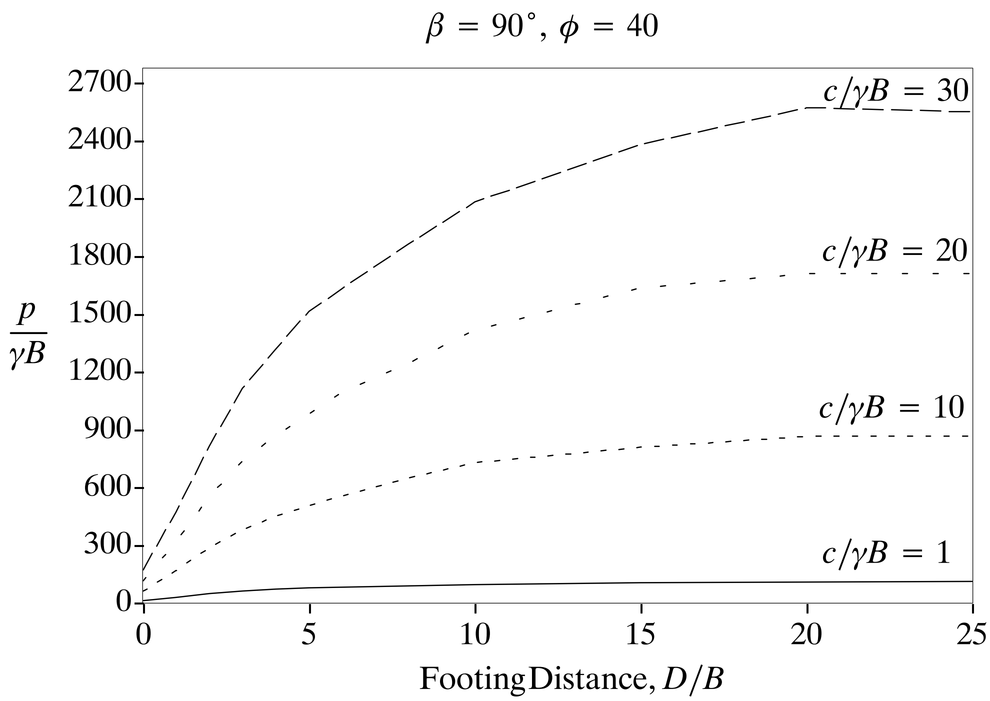

Figure D.12.: Change in Normalised Bearing Capacity with Footing Distance

H/B = 3

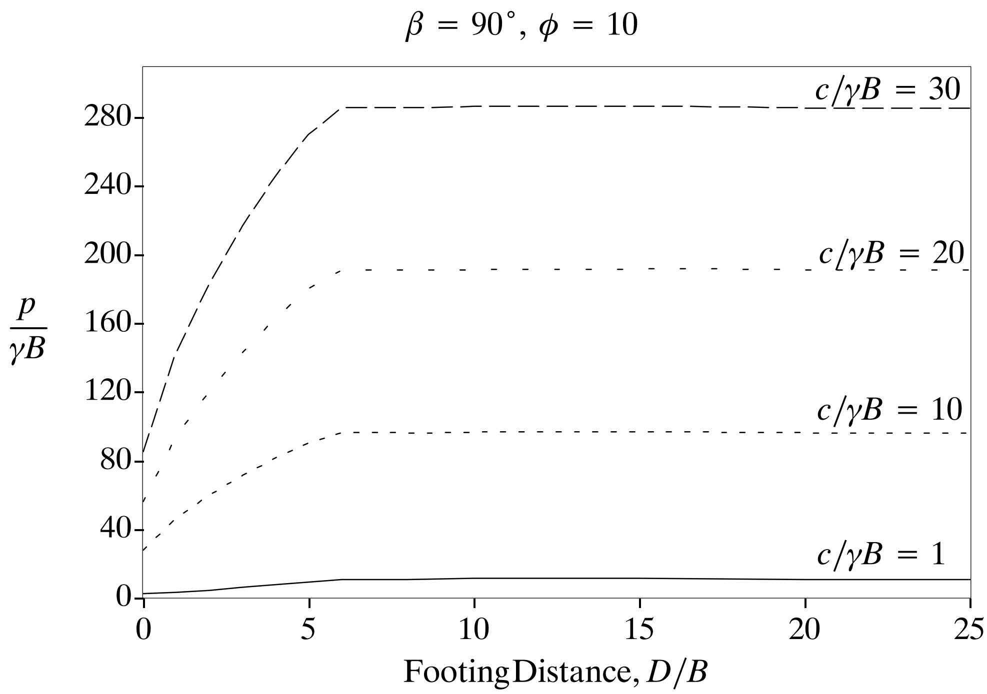

Figure D.13.: Change in Normalised Bearing Capacity with Footing Distance

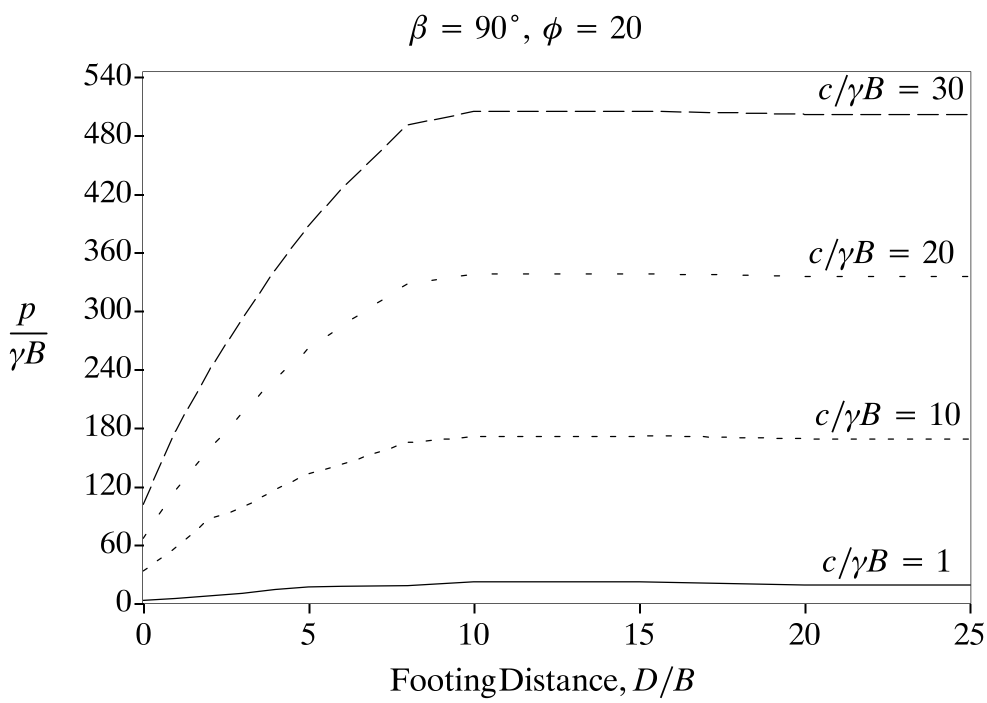

Figure D.14.: Change in Normalised Bearing Capacity with Footing Distance

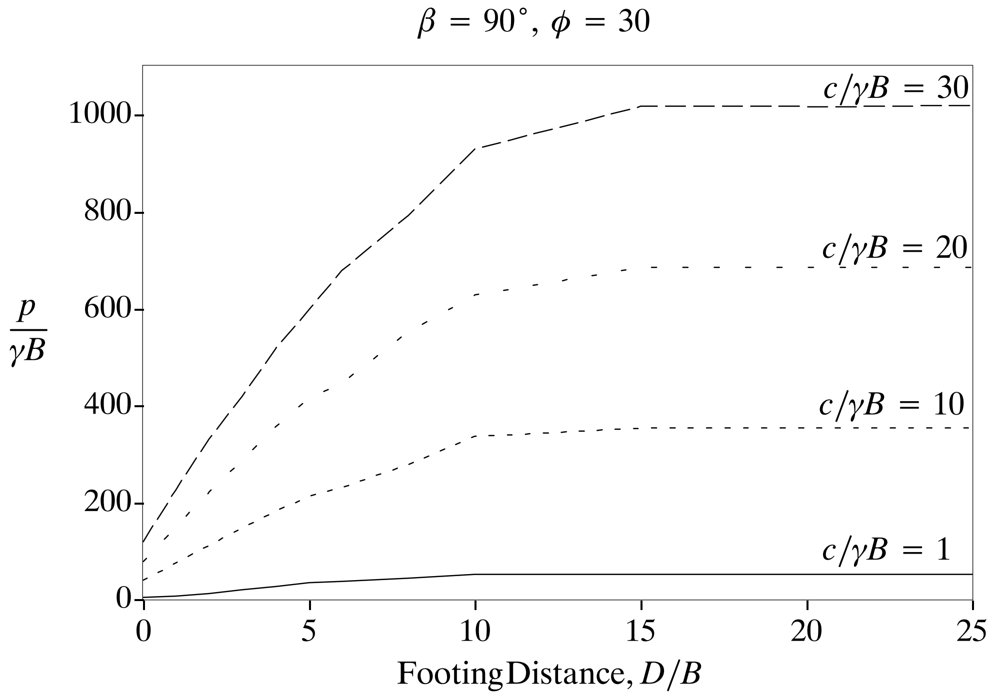

Figure D.15.: Change in Normalised Bearing Capacity with Footing Distance

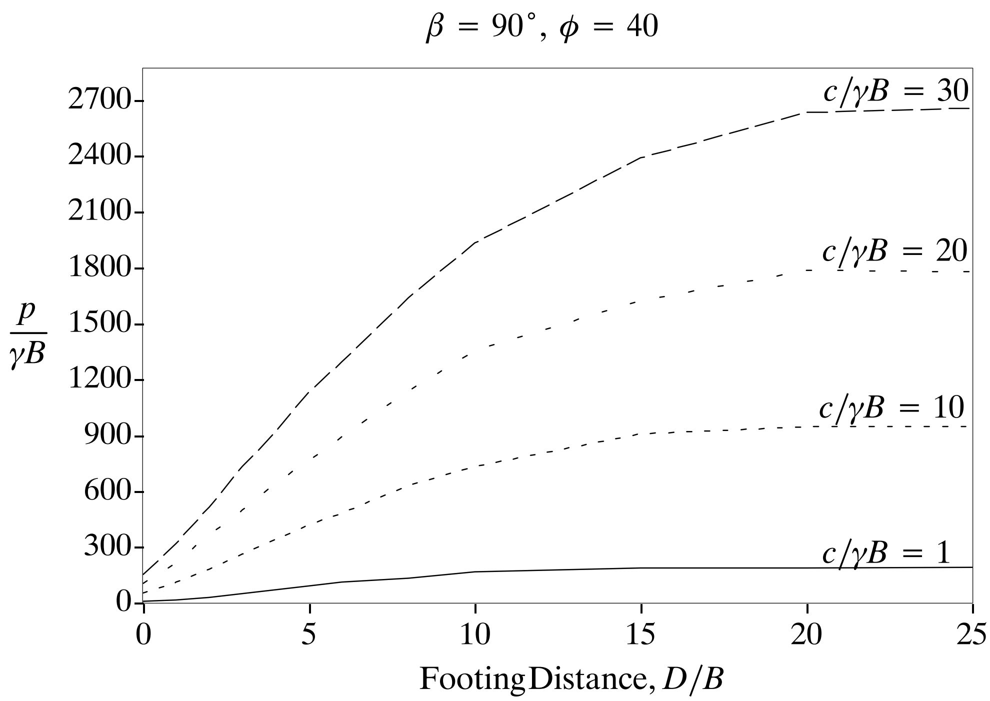

Figure D.16.: Change in Normalised Bearing Capacity with Footing Distance

H/B = 4

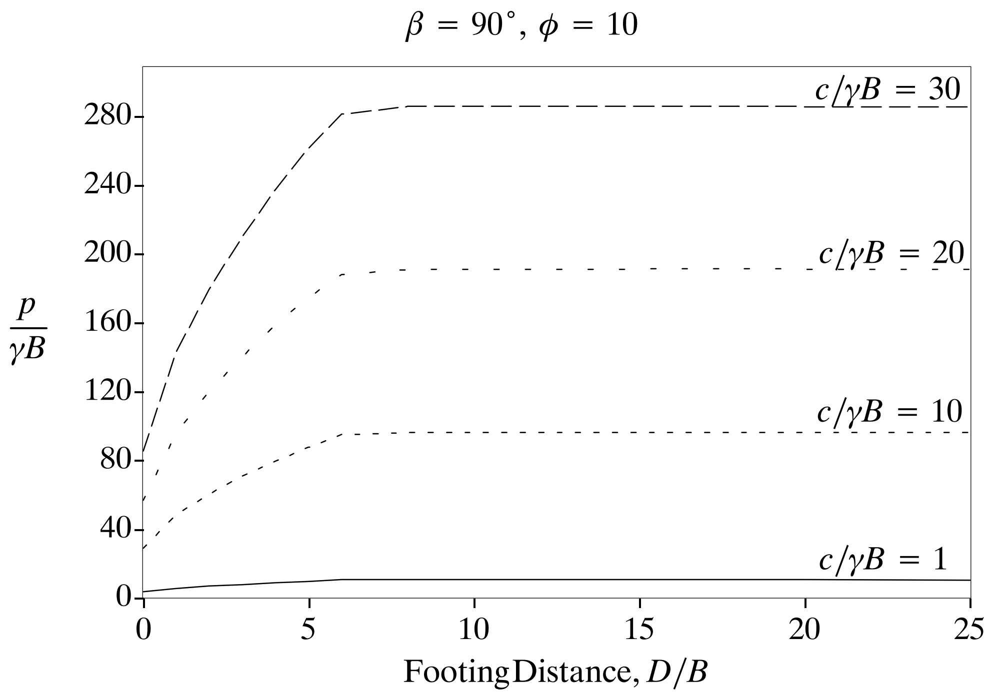

Figure D.17.: Change in Normalised Bearing Capacity with Footing Distance

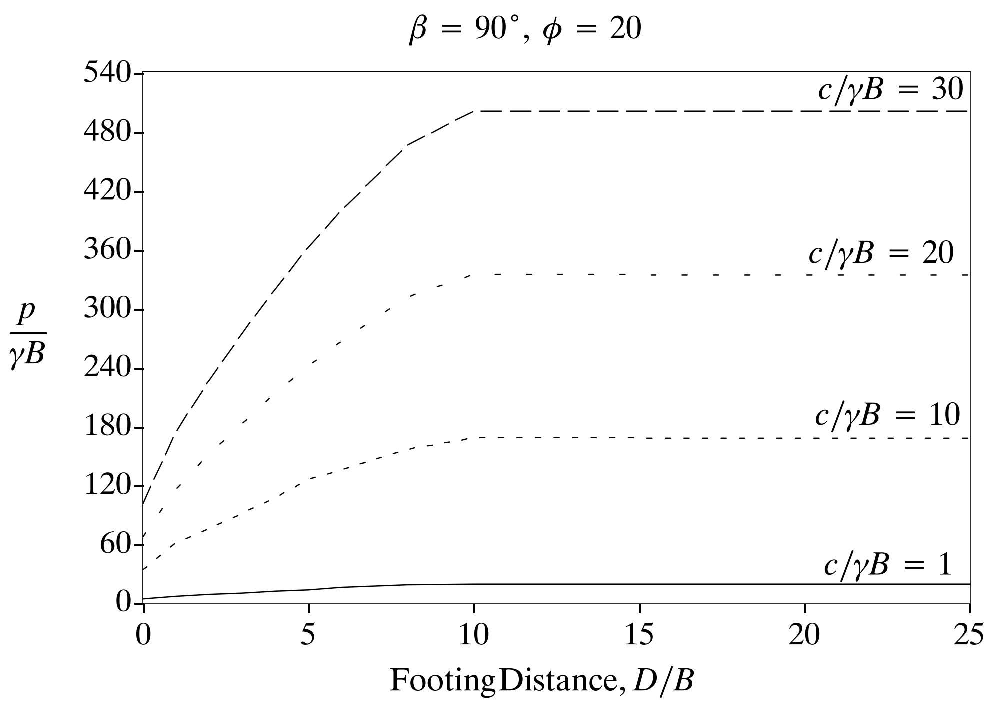

Figure D.18.: Change in Normalised Bearing Capacity with Footing Distance

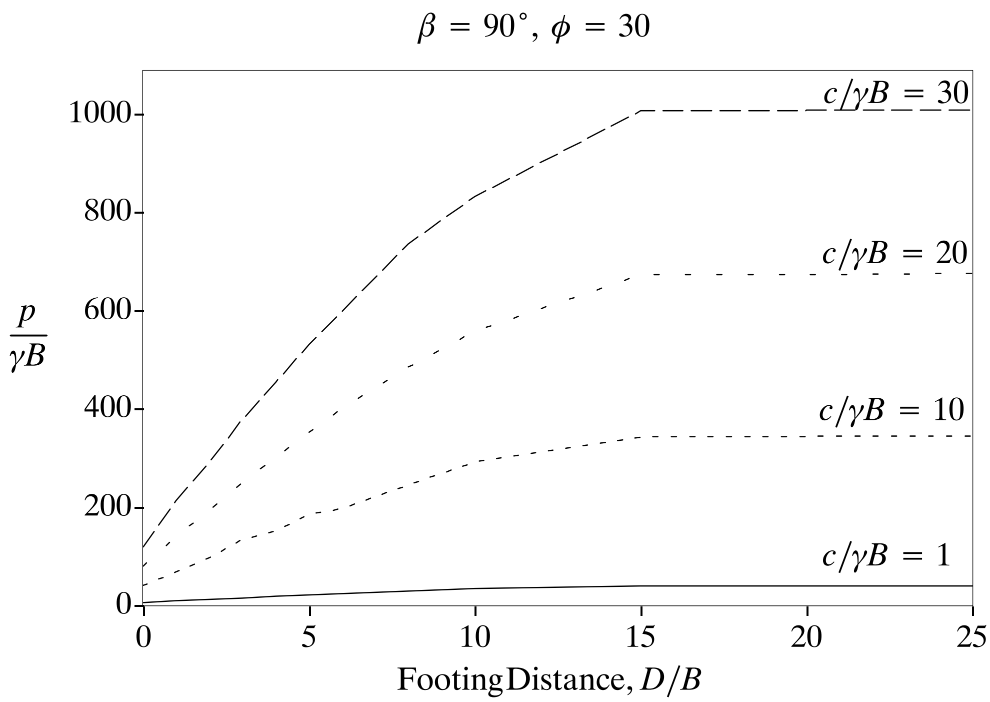

Figure D.19.: Change in Normalised Bearing Capacity with Footing Distance

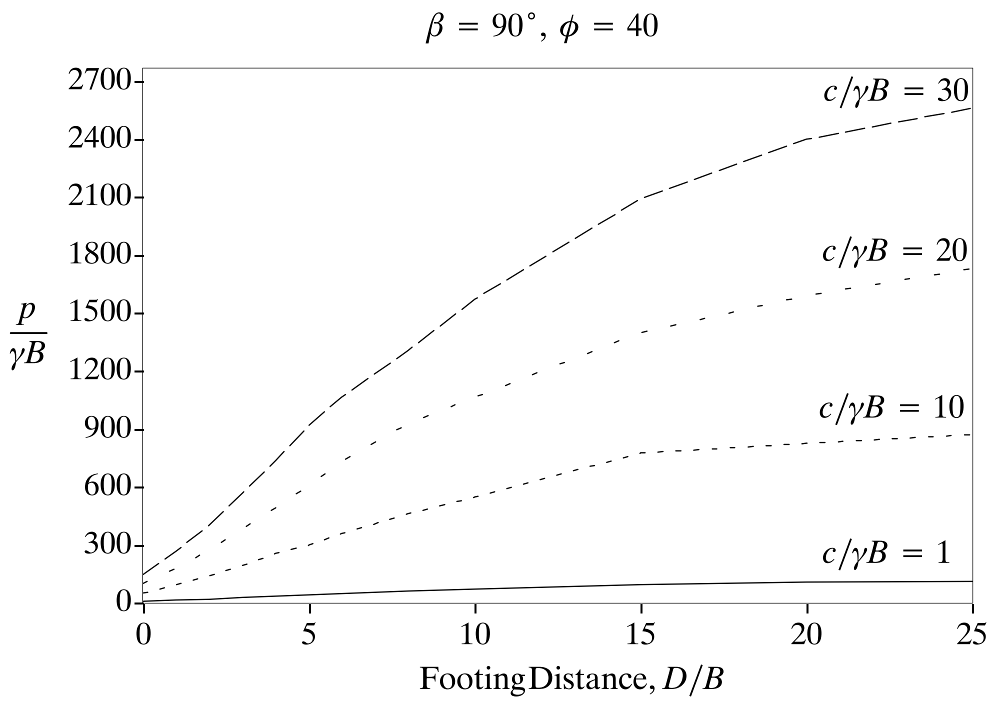

Figure D.20.: Change in Normalised Bearing Capacity with Footing Distance

H/B = 5

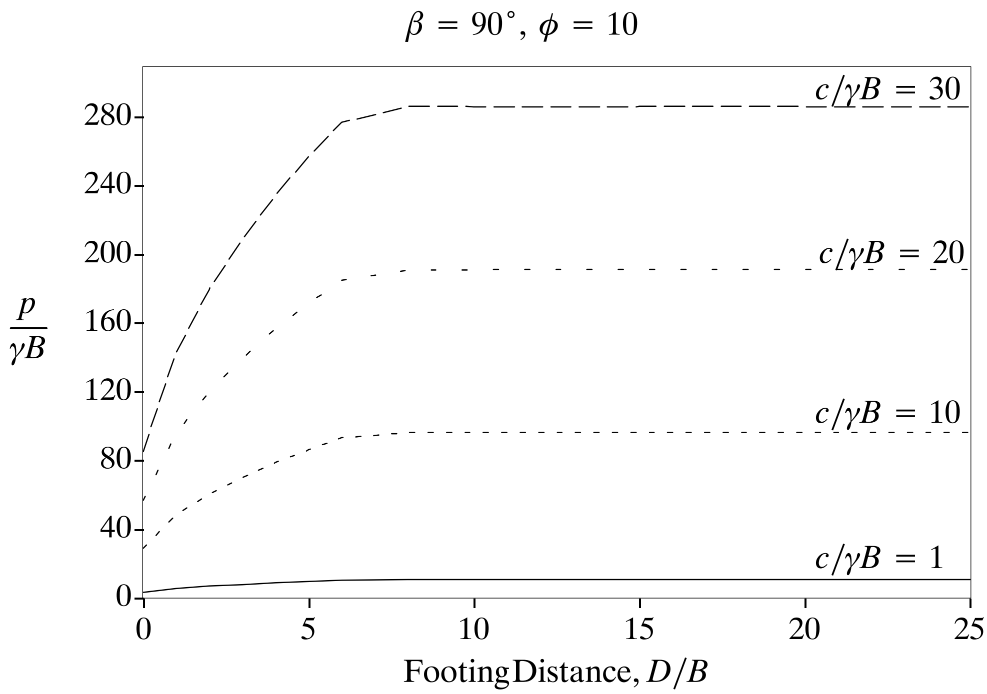

Figure D.21.: Change in Normalised Bearing Capacity with Footing Distance

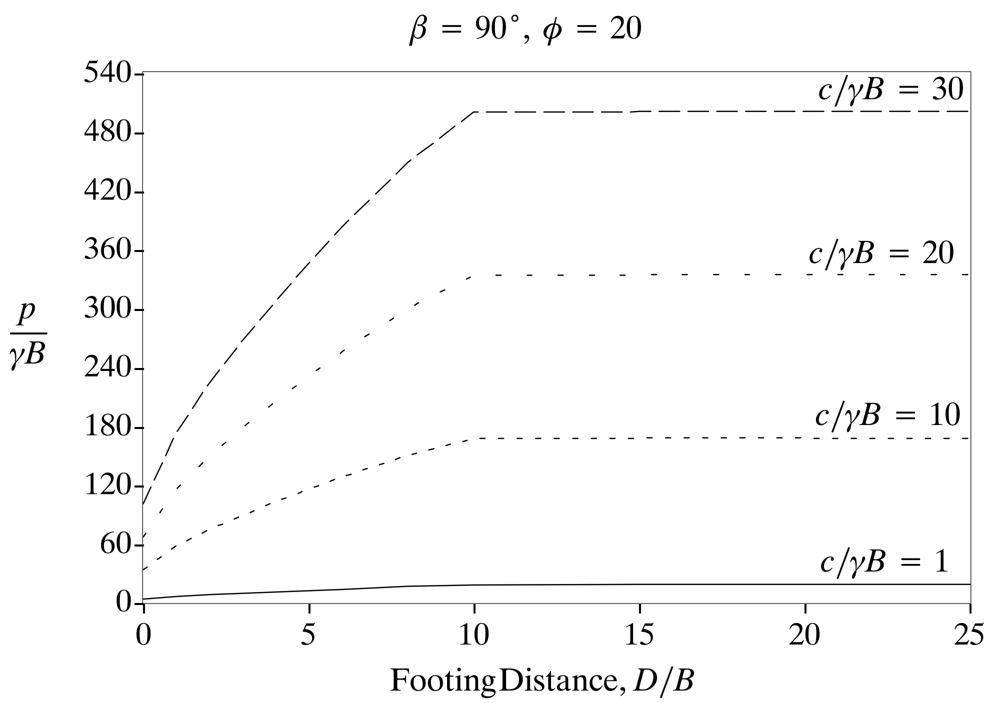

Figure D.22.: Change in Normalised Bearing Capacity with Footing Distance

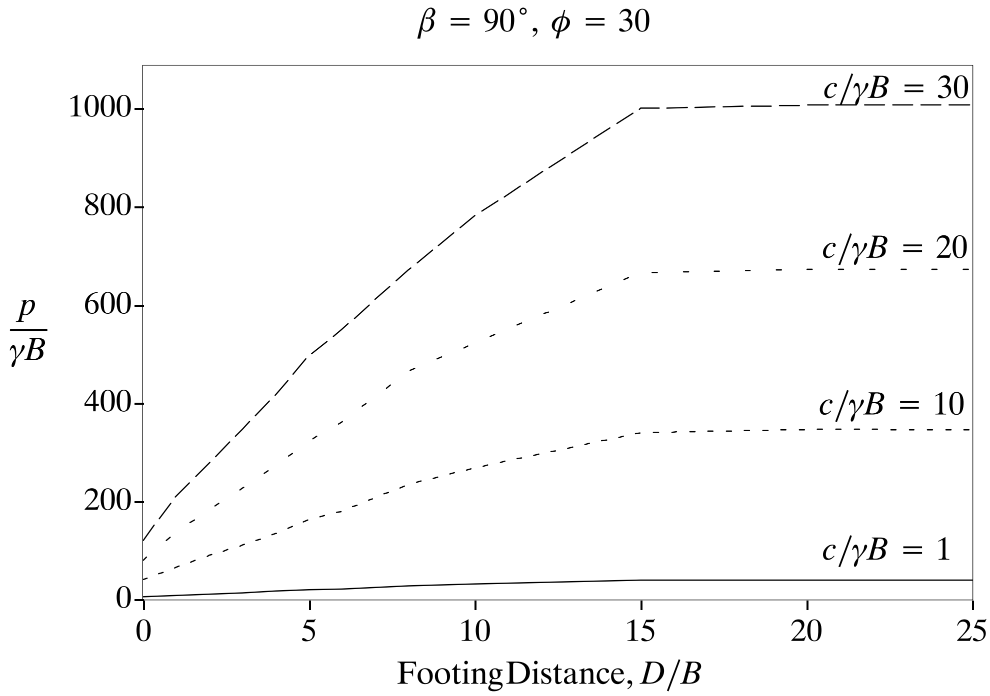

Figure D.23.: Change in Normalised Bearing Capacity with Footing Distance

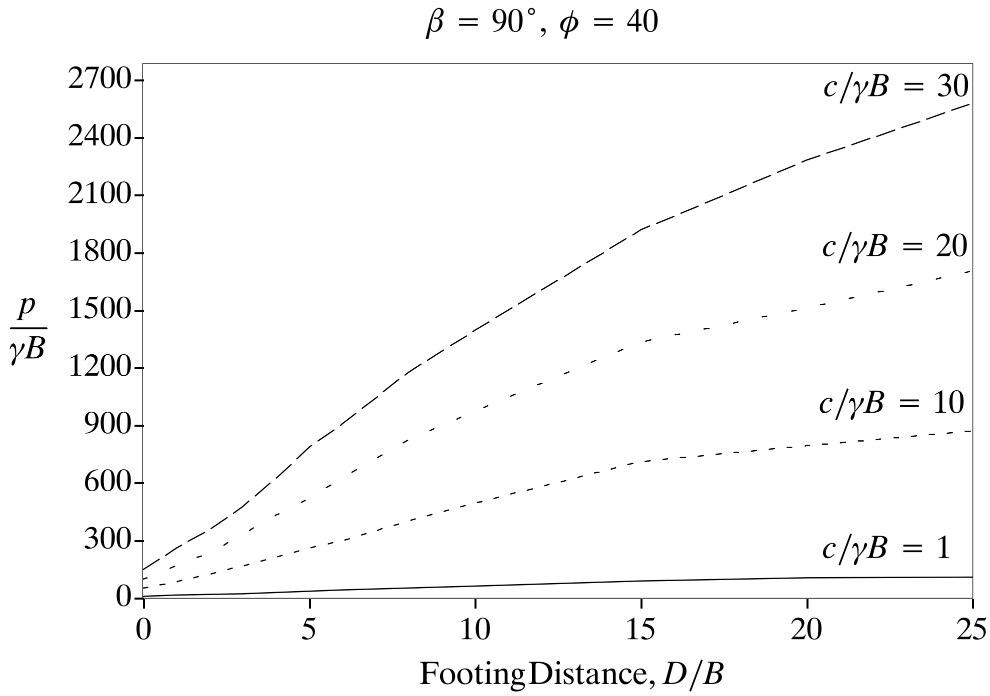

Figure D.24.: Change in Normalised Bearing Capacity with Footing Distance

H/B = 6

$\beta = 90^\circ$, $\phi = 10$

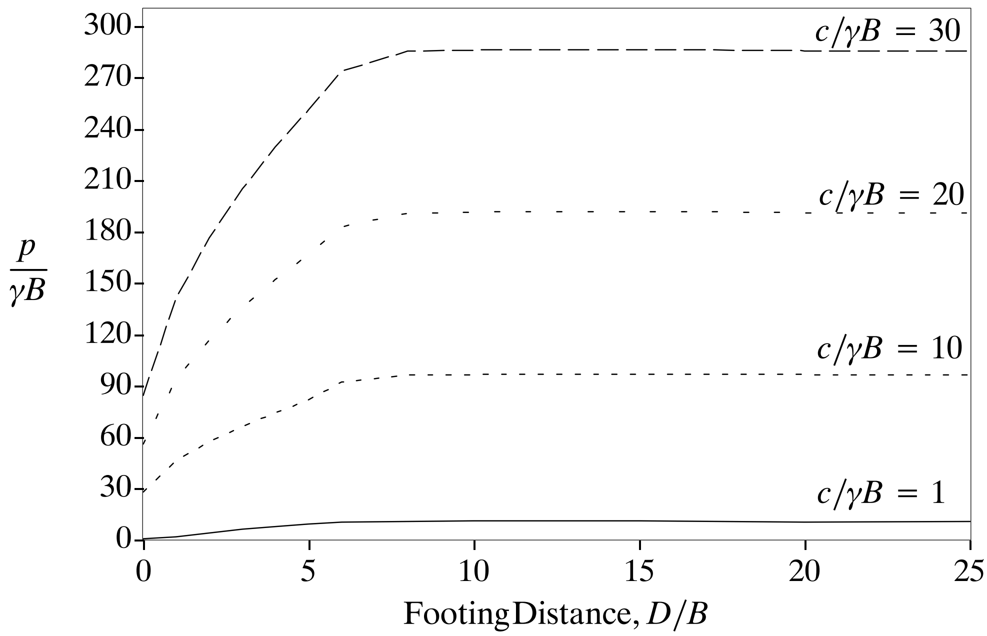

Figure D.25.: Change in Normalised Bearing Capacity with Footing Distance

$\beta = 90^\circ$, $\phi = 20$

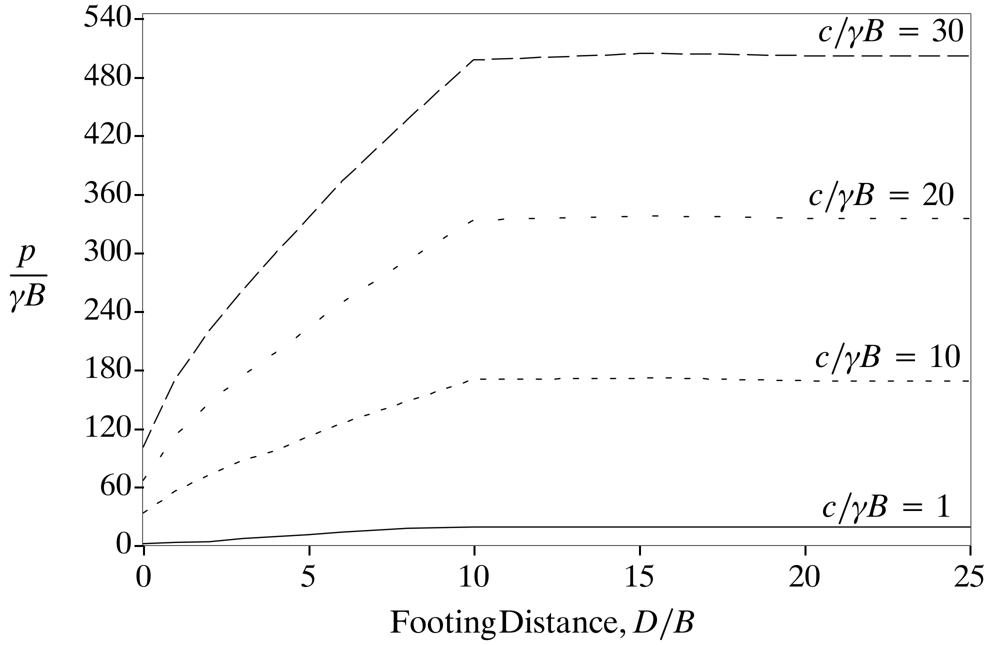

Figure D.26.: Change in Normalised Bearing Capacity with Footing Distance

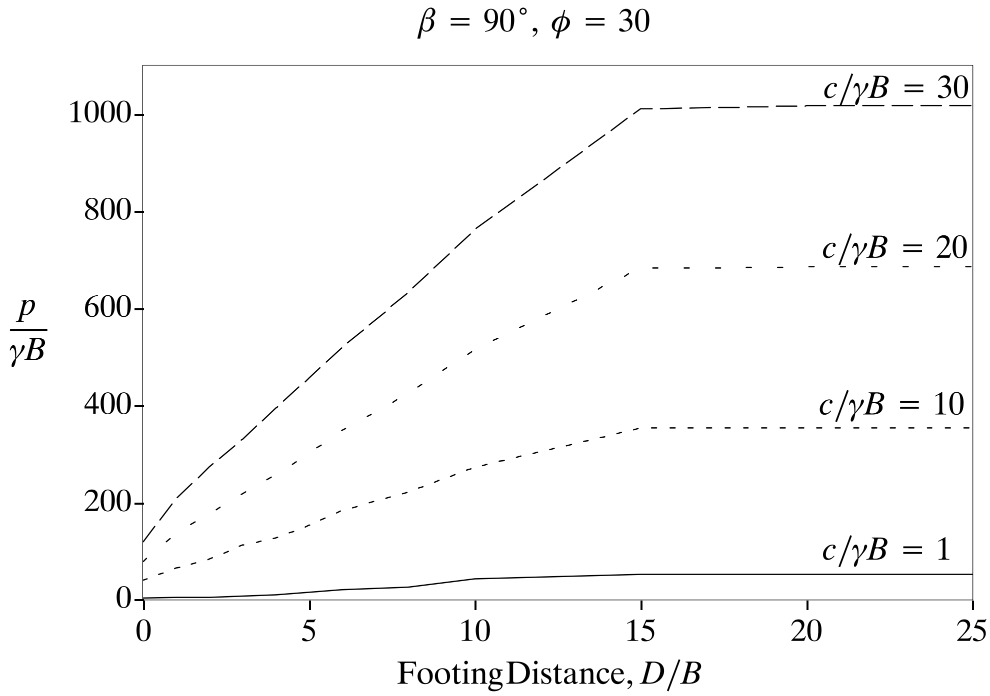

Figure D.27.: Change in Normalised Bearing Capacity with Footing Distance

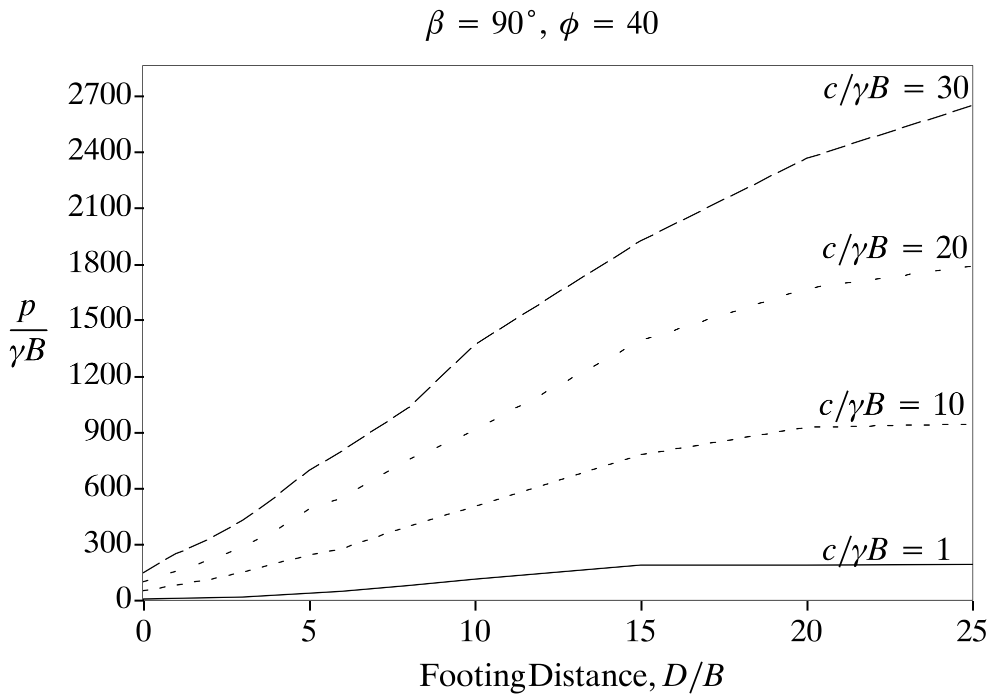

Figure D.28.: Change in Normalised Bearing Capacity with Footing Distance

H/B = 8

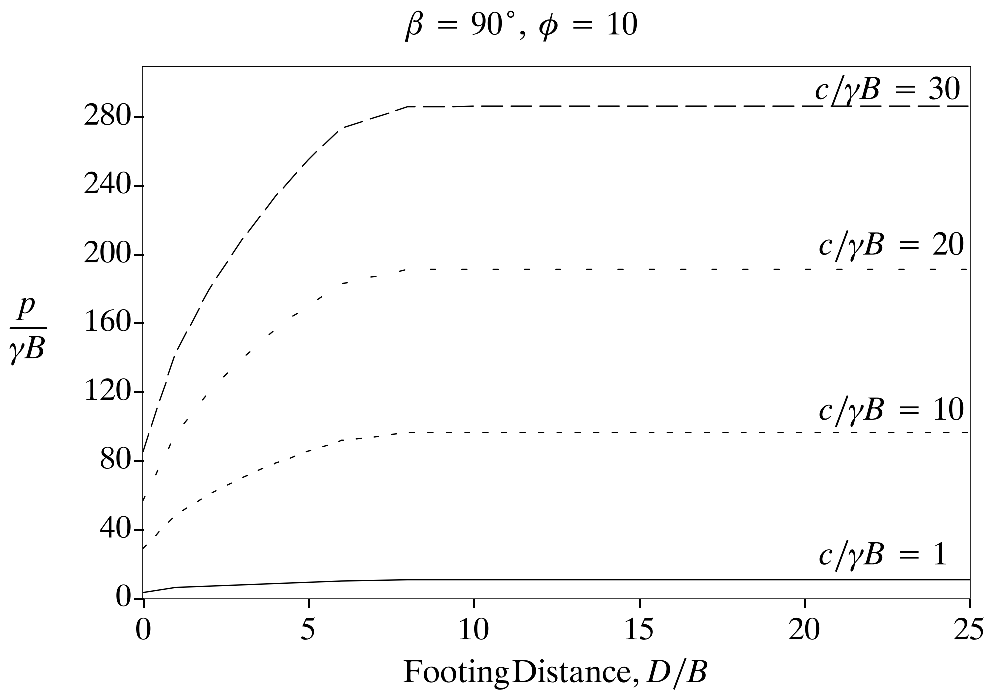

Figure D.29.: Change in Normalised Bearing Capacity with Footing Distance

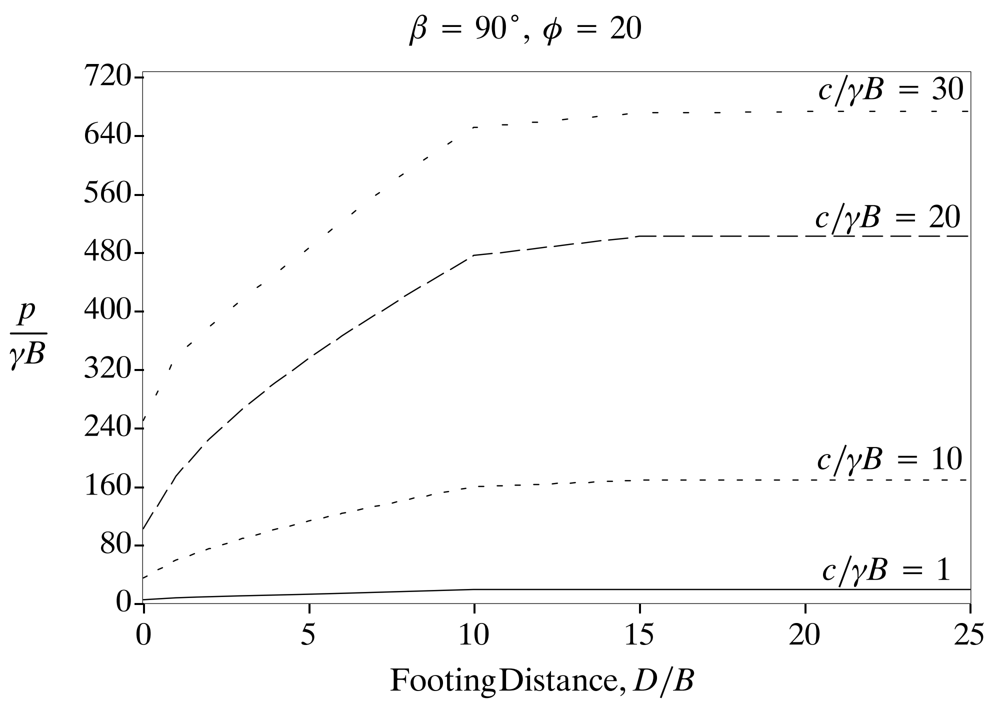

Figure D.30.: Change in Normalised Bearing Capacity with Footing Distance

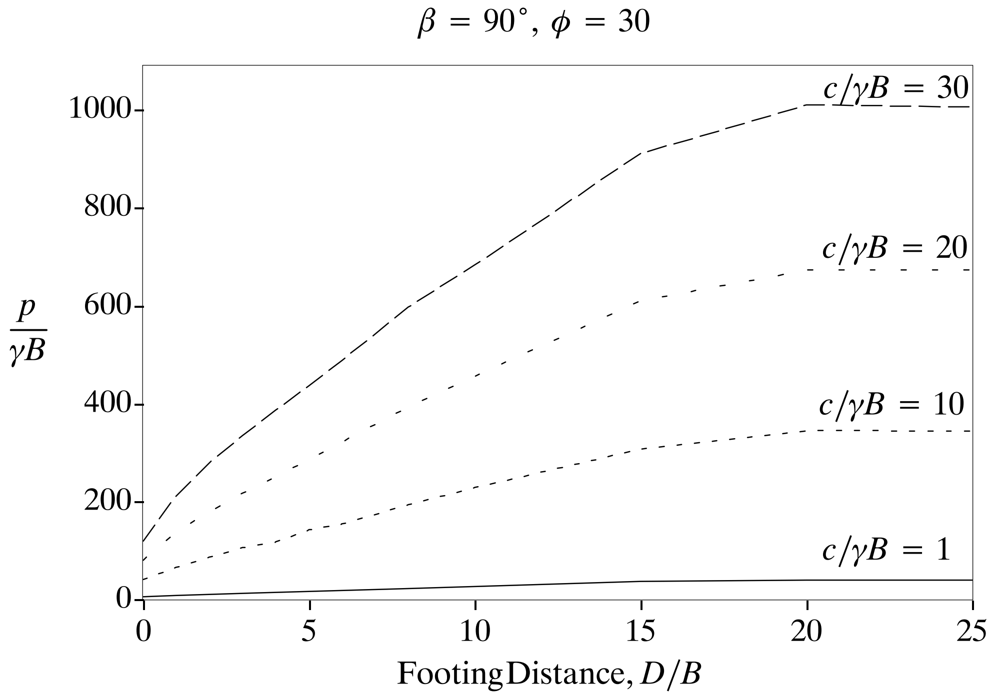

Figure D.31.: Change in Normalised Bearing Capacity with Footing Distance

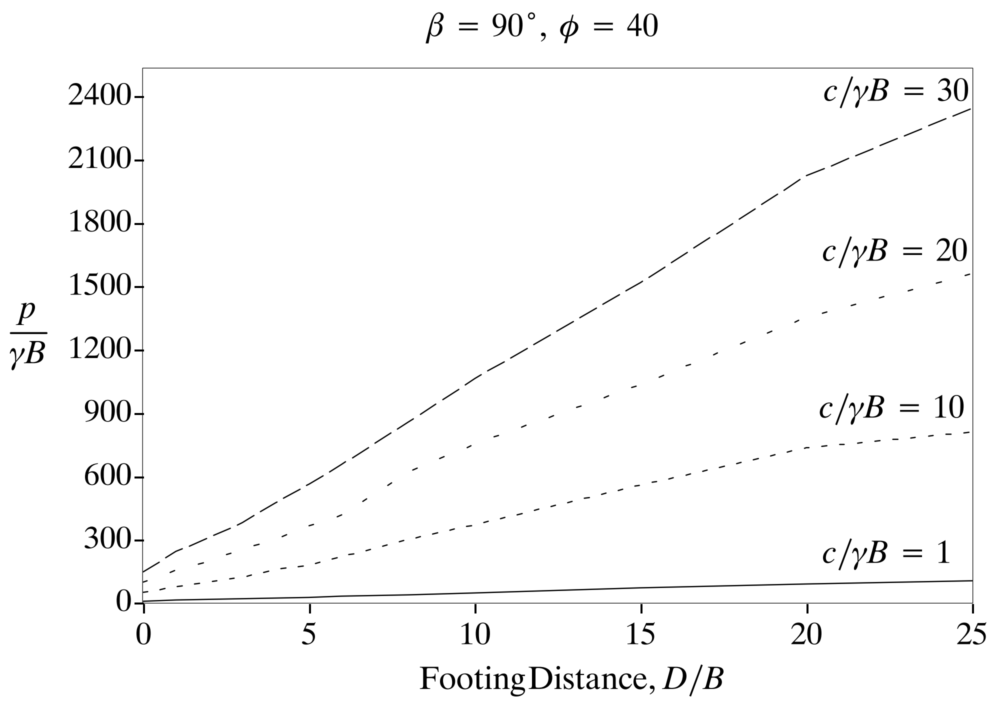

Figure D.32.: Change in Normalised Bearing Capacity with Footing Distance

H/B = 10

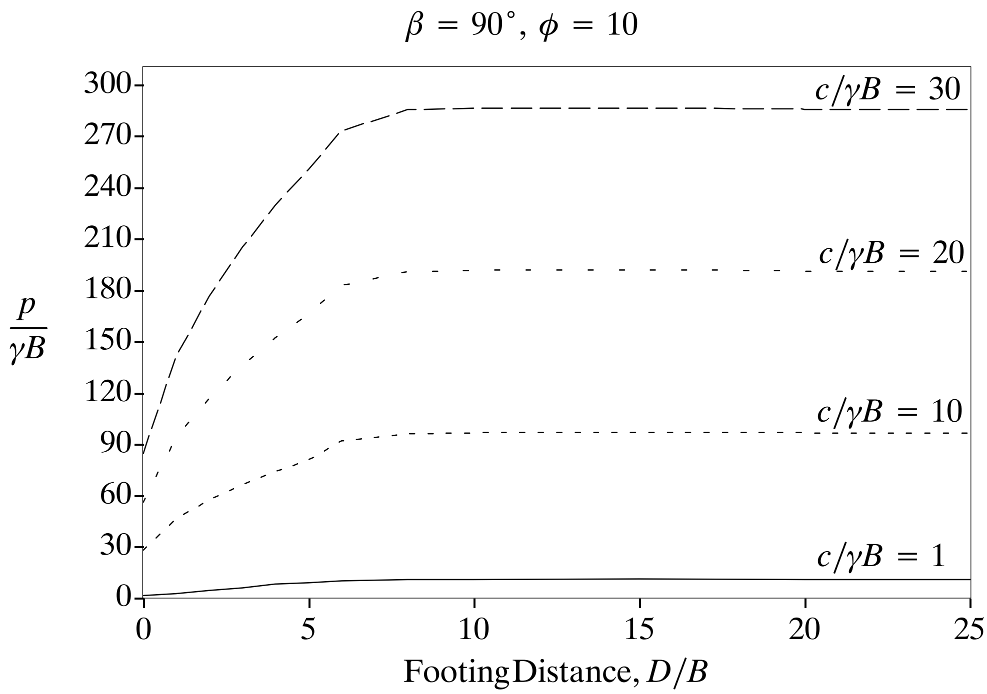

Figure D.33.: Change in Normalised Bearing Capacity with Footing Distance

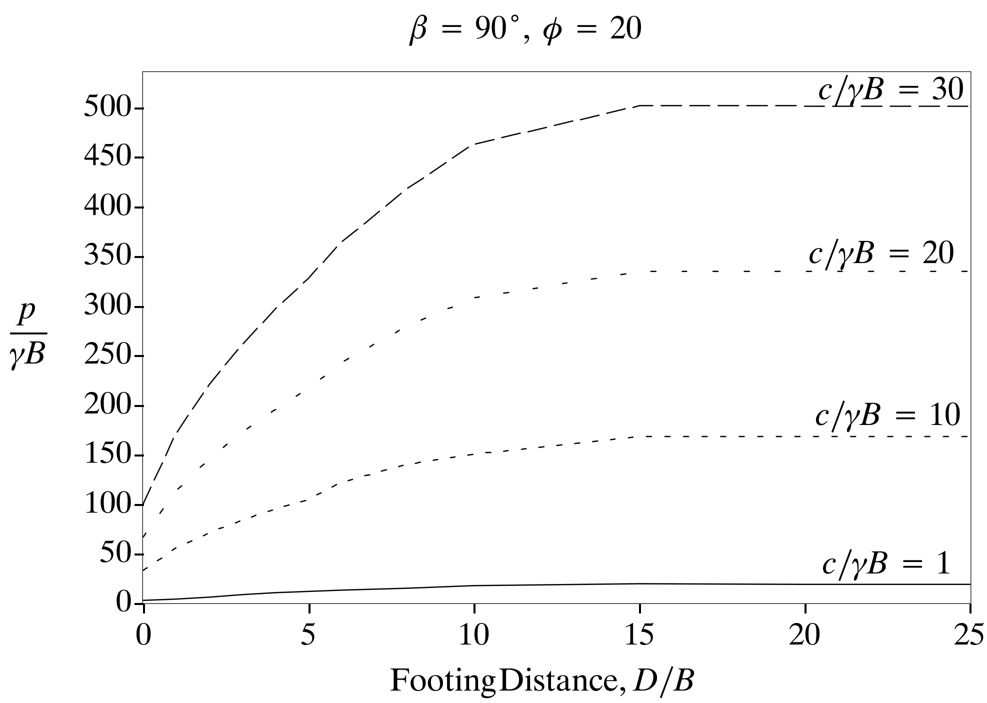

Figure D.34.: Change in Normalised Bearing Capacity with Footing Distance

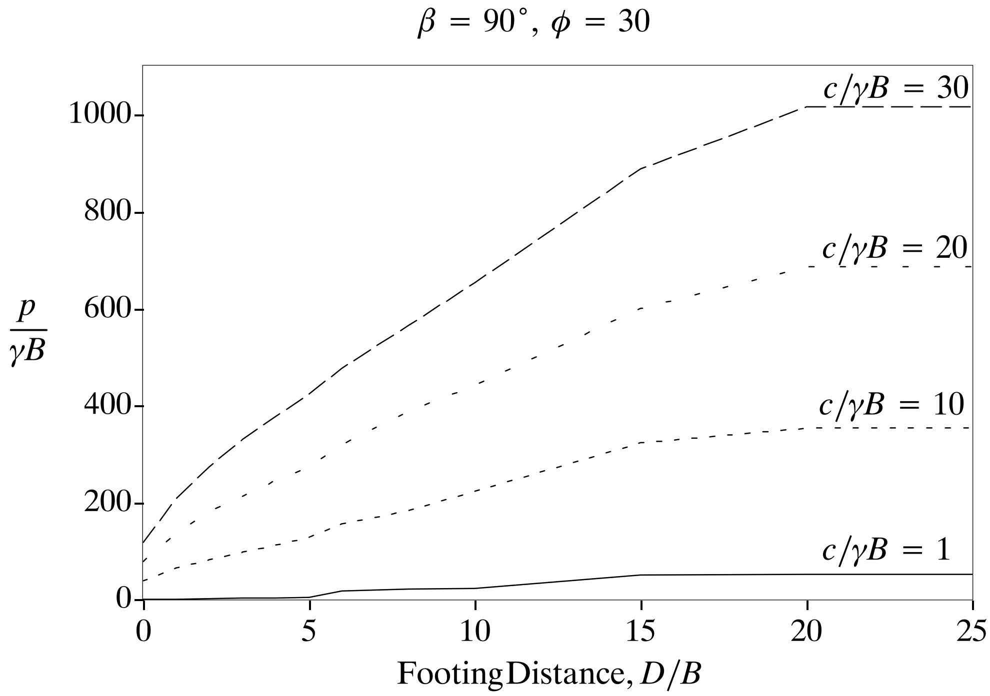

Figure D.35.: Change in Normalised Bearing Capacity with Footing Distance

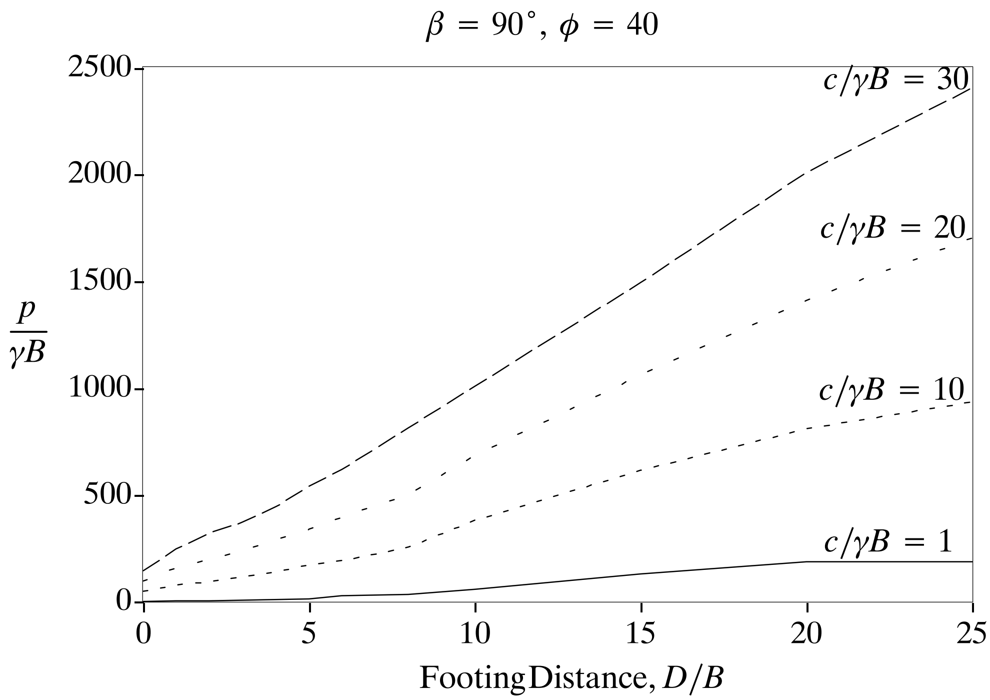

Figure D.36.: Change in Normalised Bearing Capacity with Footing Distance

H/B = 13

$\beta = 90^\circ,\ \phi = 10$

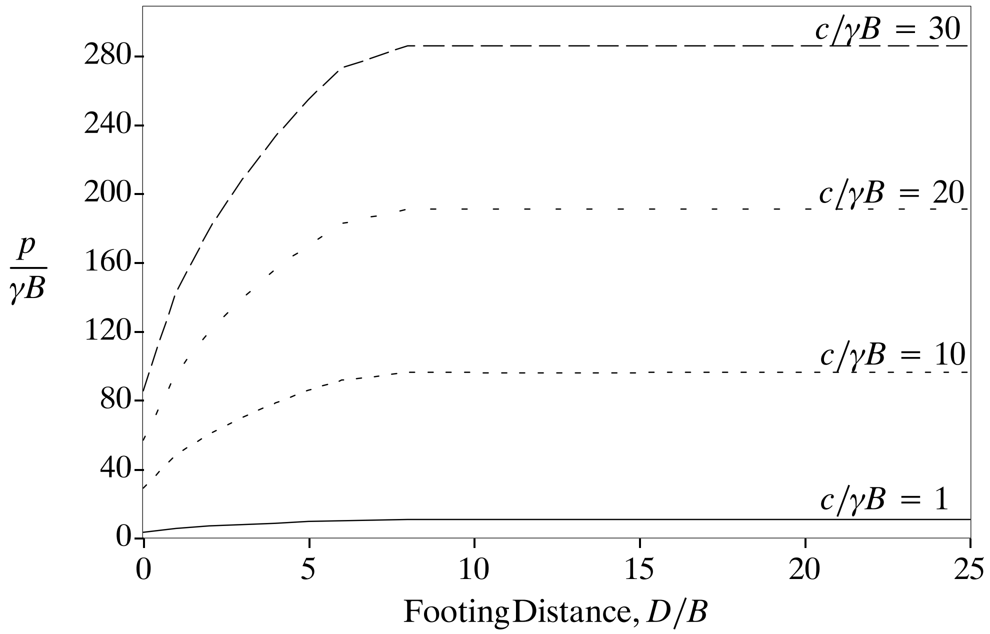

Figure D.37.: Change in Normalised Bearing Capacity with Footing Distance

$\beta = 90^\circ,\ \phi = 20$

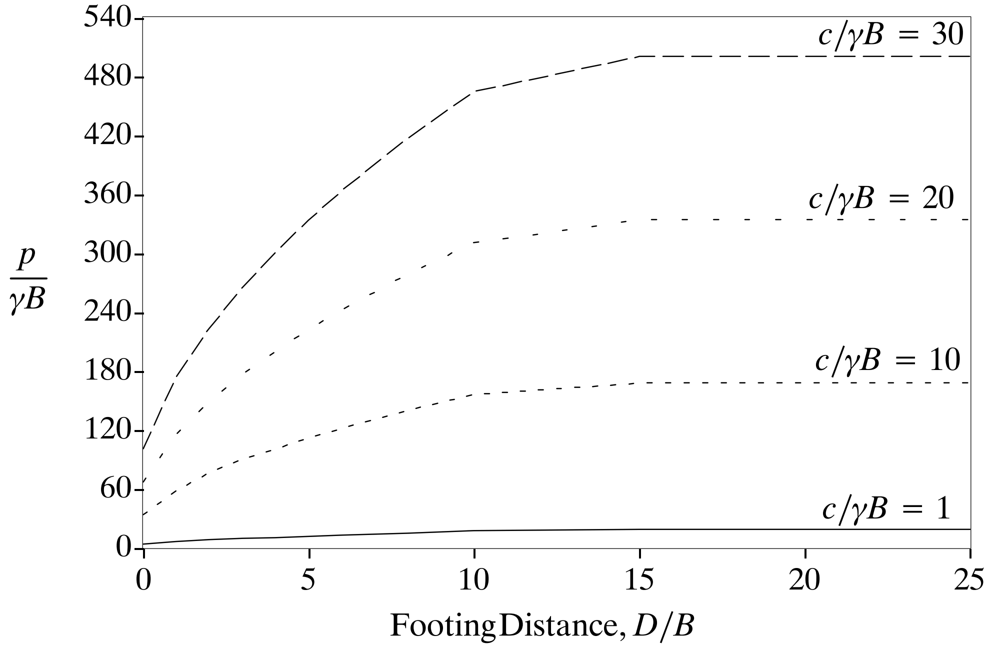

Figure D.38.: Change in Normalised Bearing Capacity with Footing Distance

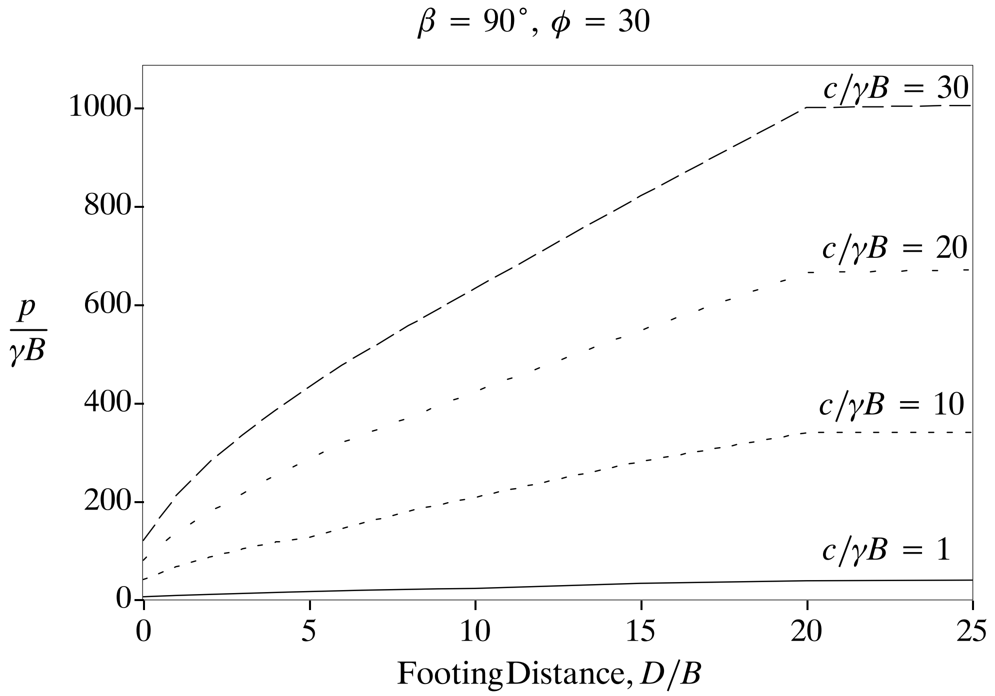

Figure D.39.: Change in Normalised Bearing Capacity with Footing Distance

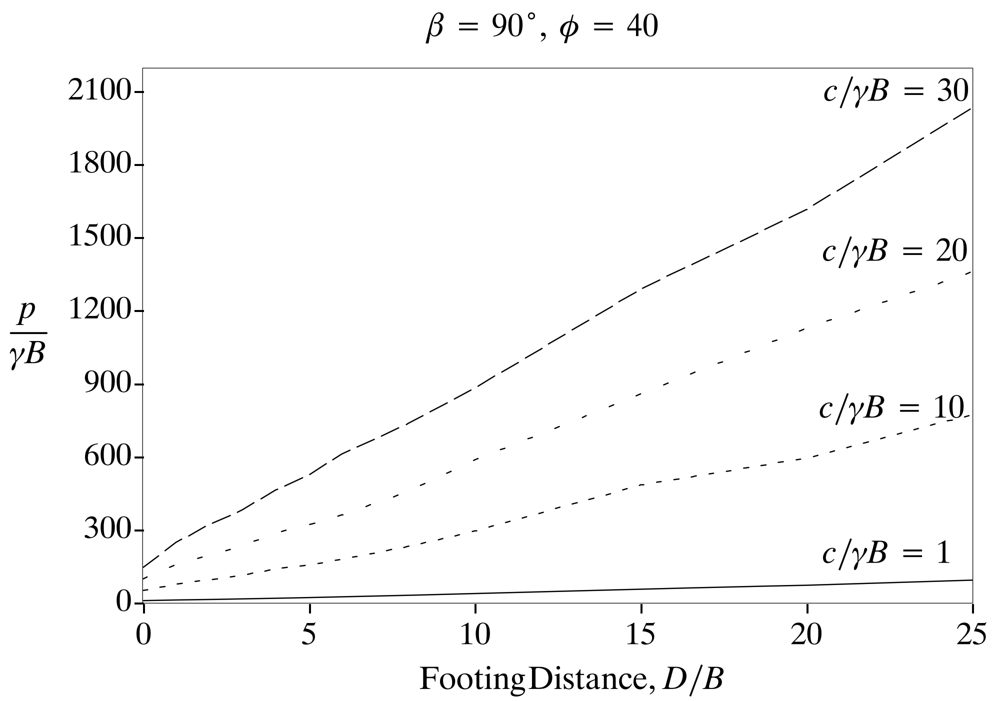

Figure D.40.: Change in Normalised Bearing Capacity with Footing Distance

H/B = 16

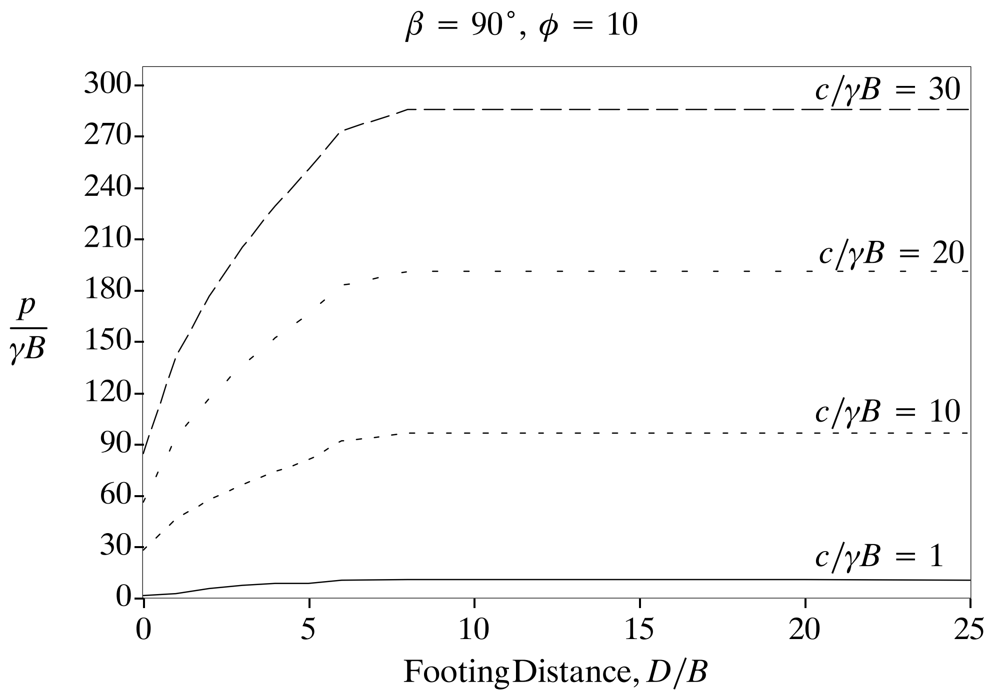

Figure D.41.: Change in Normalised Bearing Capacity with Footing Distance

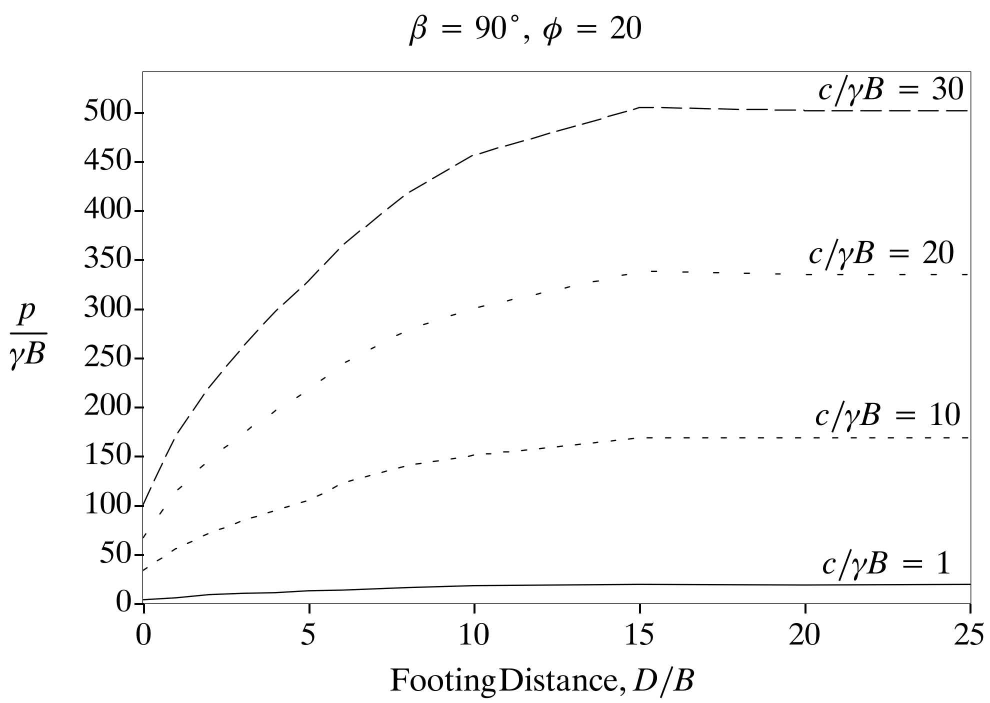

Figure D.42.: Change in Normalised Bearing Capacity with Footing Distance

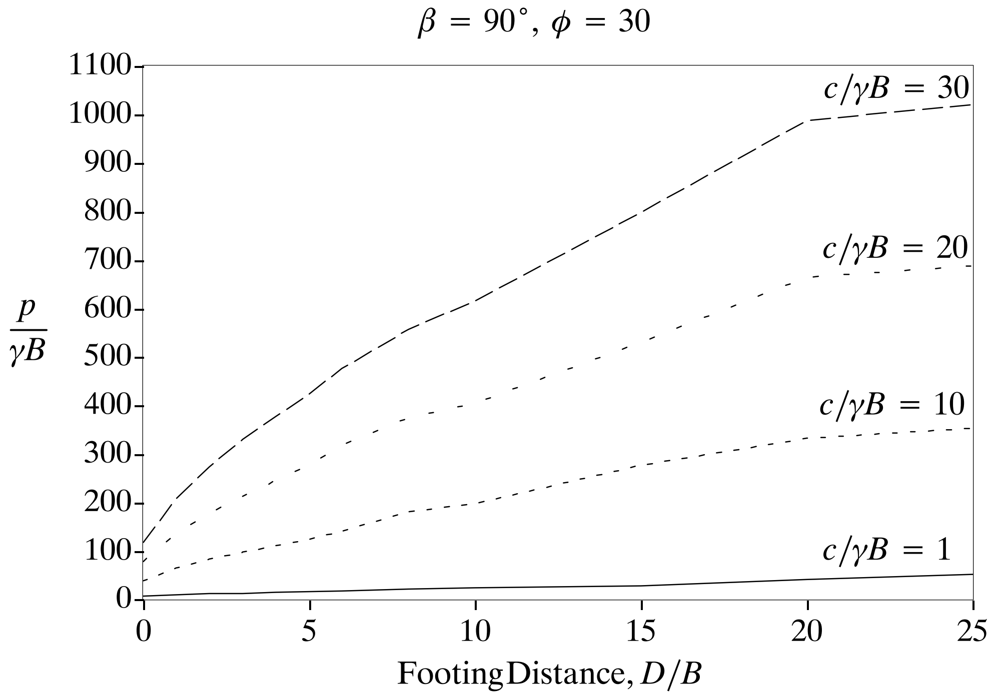

Figure D.43.: Change in Normalised Bearing Capacity with Footing Distance

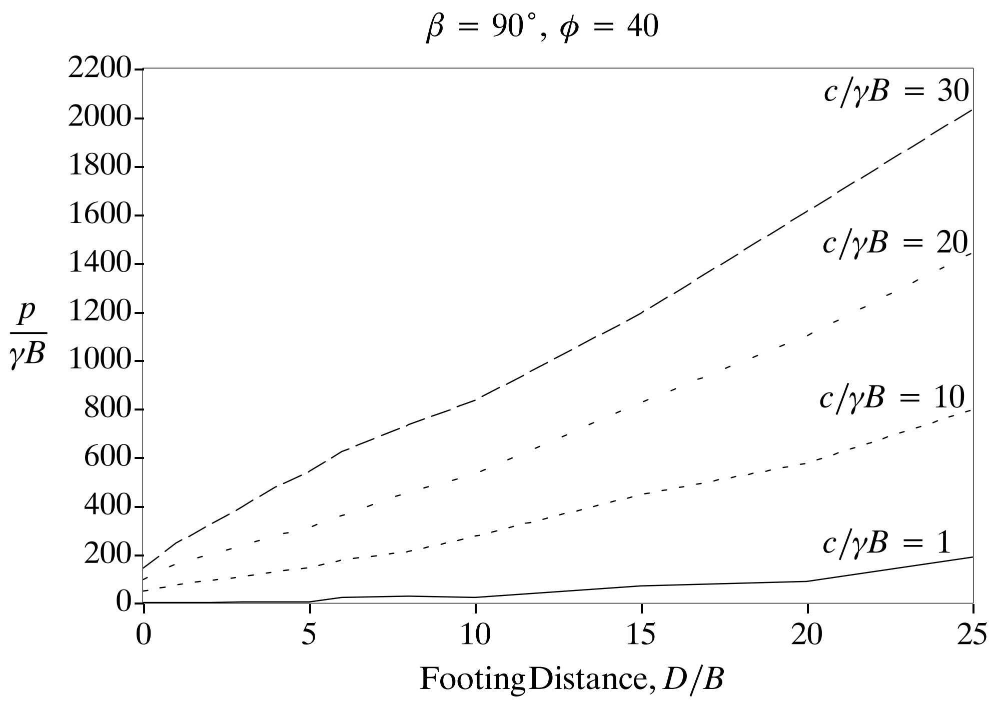

Figure D.44.: Change in Normalised Bearing Capacity with Footing Distance

8.5 Appendix E

Decreased Bearing Capacity due to Increasing Slope Height Ratio Charts

These charts demonstrate the lowering of bearing capacity as the height of a slope increases. This is most applicable for the scenario where excavation occurs lowering the height of the area to be built upon rather then raising it. Situations such as this occur when soil is excavated for the construction of an underground carpark which is surrounded by existing structures. Using these charts will allow the depth to which excavation can occur be determined before the slope will be unable to support to the footing load of the existing structures.

This chart type is organised once again in groups, which are this time based on the strength ratio of the soil.

$c/\gamma B = 1$

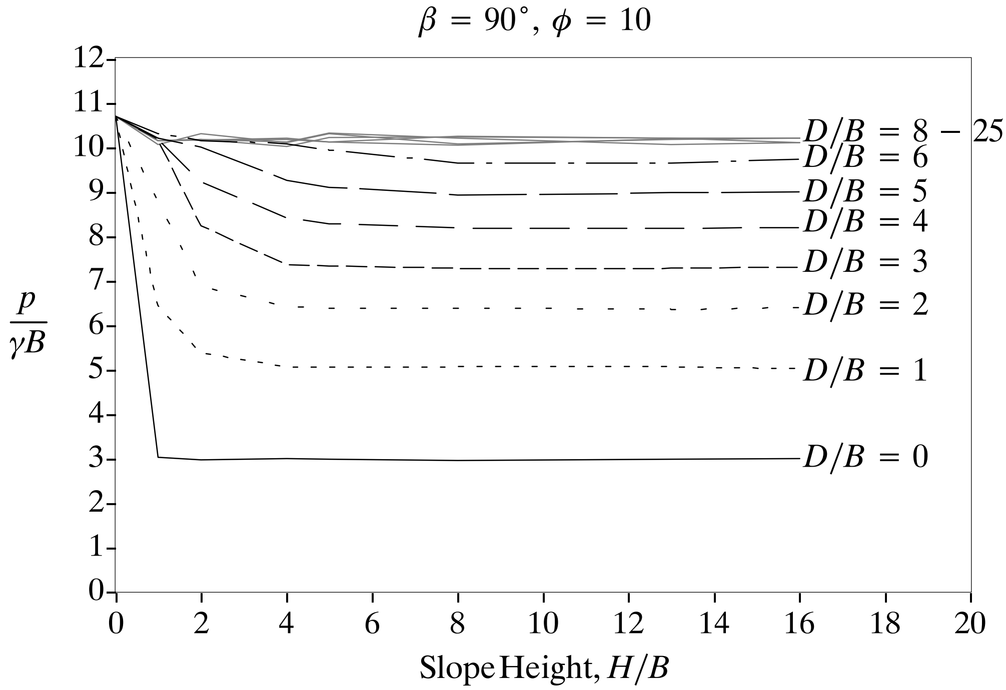

Figure E.1.: Change in Normalised Bearing Capacity with Slope Height

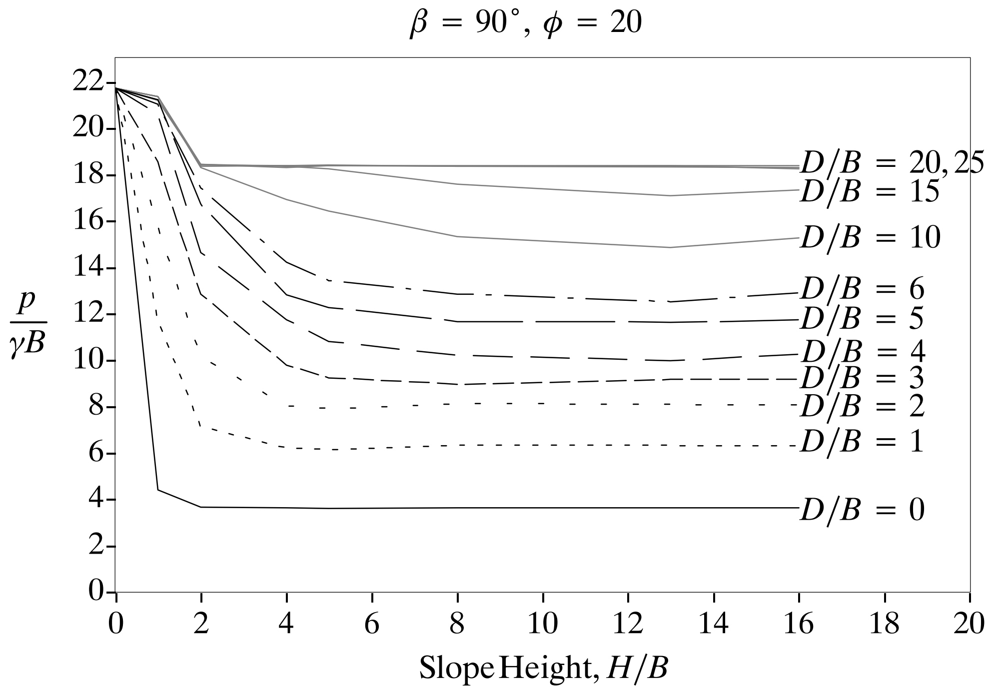

Figure E.2.: Change in Normalised Bearing Capacity with Slope Height

$\beta = 90^{\circ}$, $\phi = 30$

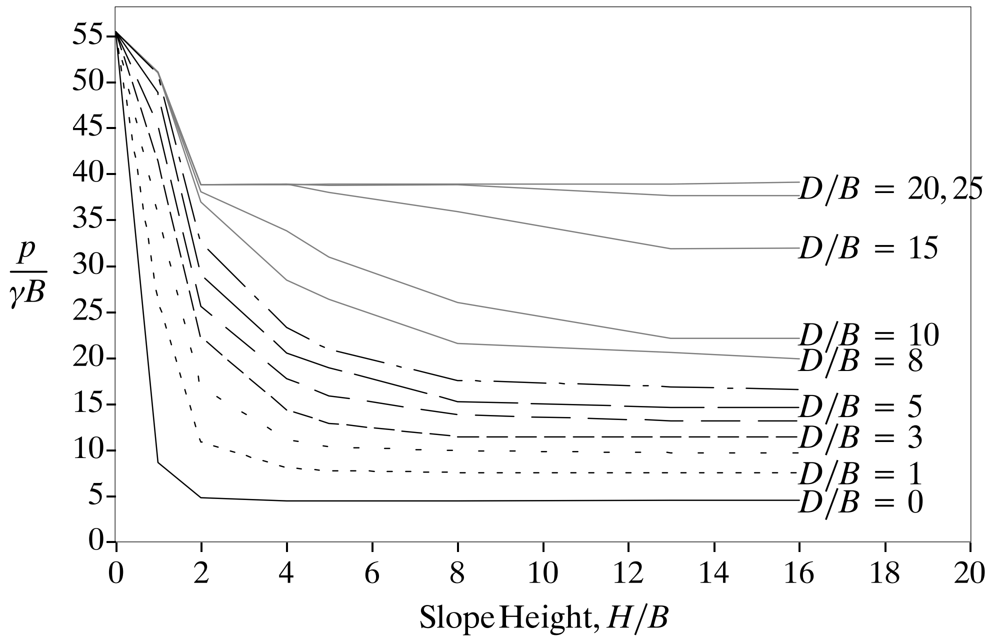

Figure E.3.: Change in Normalised Bearing Capacity with Slope Height

$\beta = 90^{\circ}$, $\phi = 40$

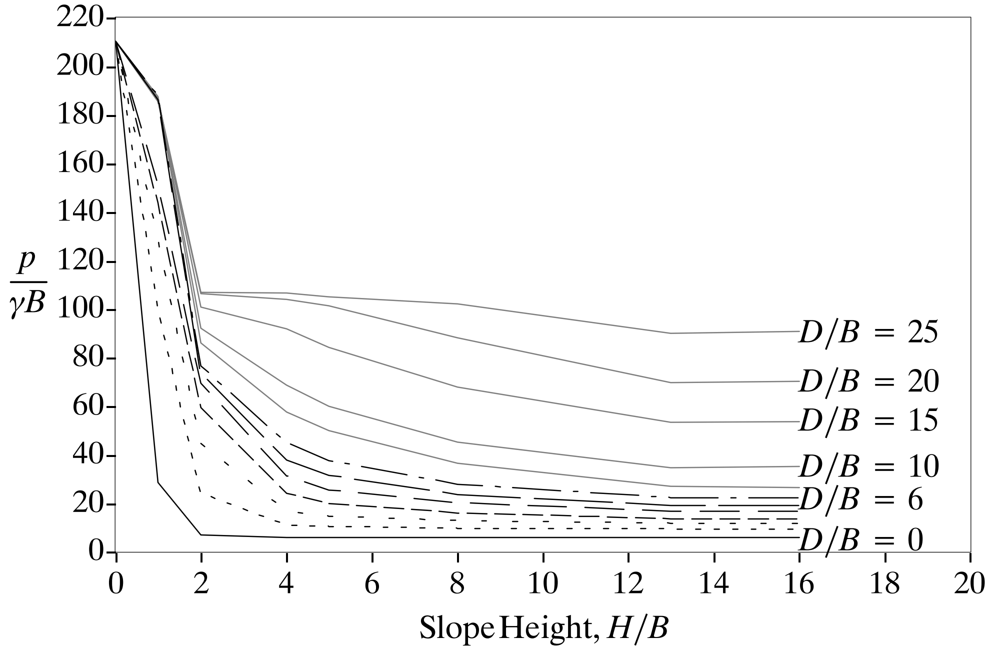

Figure E.4.: Change in Normalised Bearing Capacity with Slope Height

$c/\gamma B = 10$

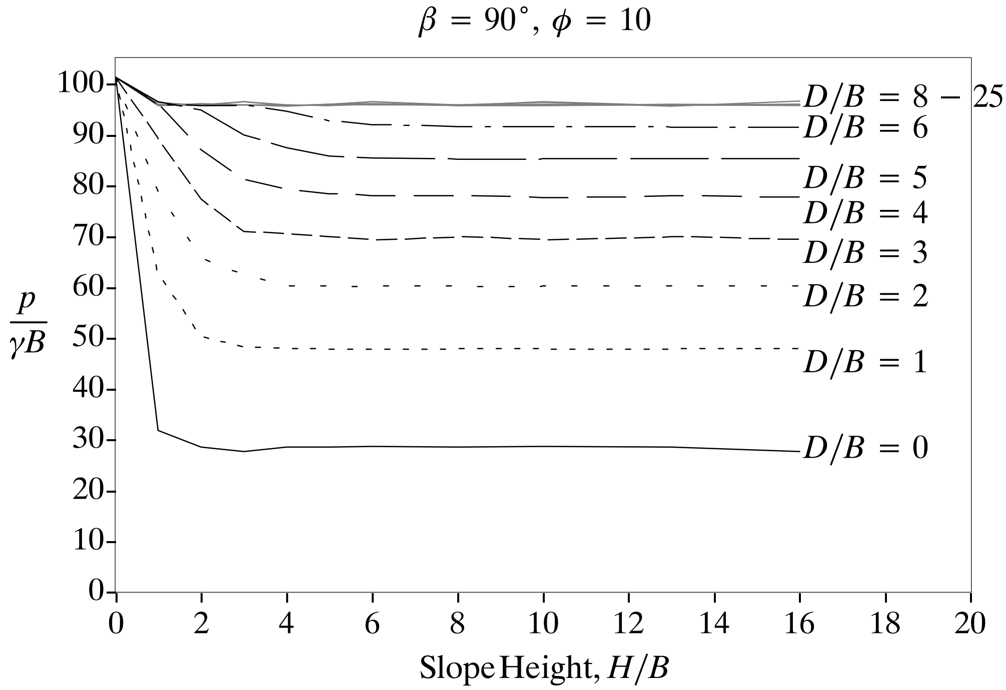

Figure E.5.: Change in Normalised Bearing Capacity with Slope Height

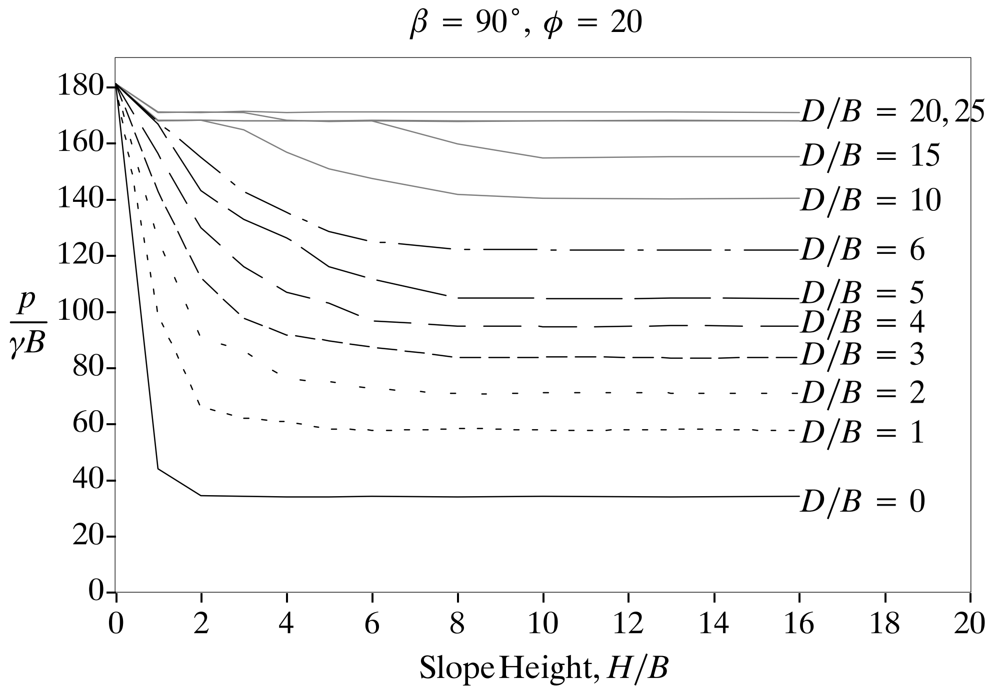

Figure E.6.: Change in Normalised Bearing Capacity with Slope Height

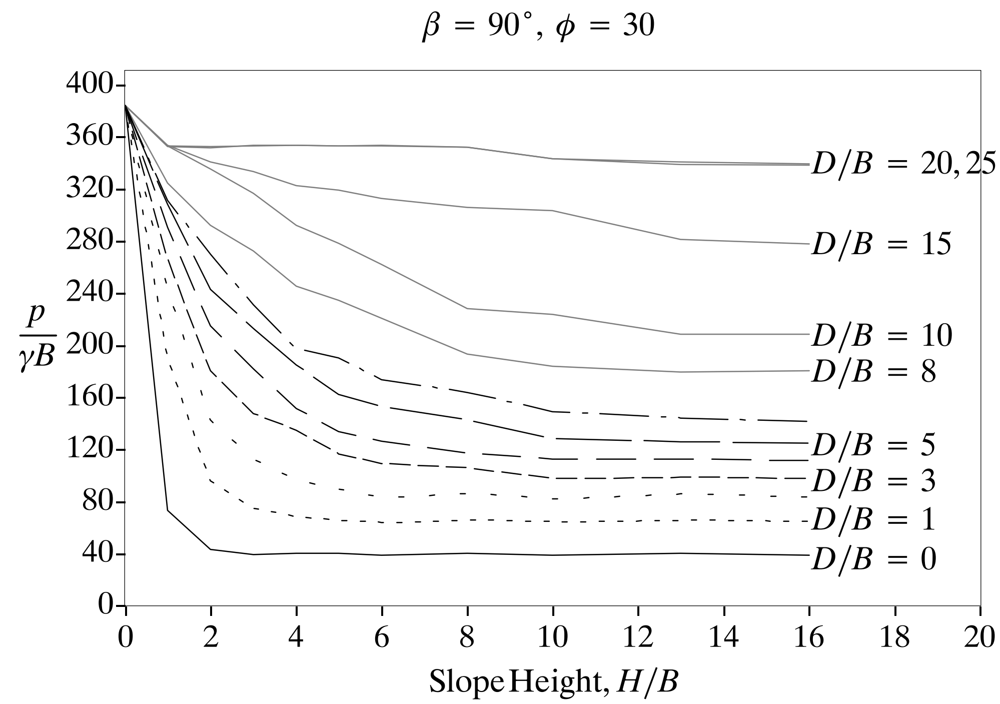

Figure E.7.: Change in Normalised Bearing Capacity with Slope Height

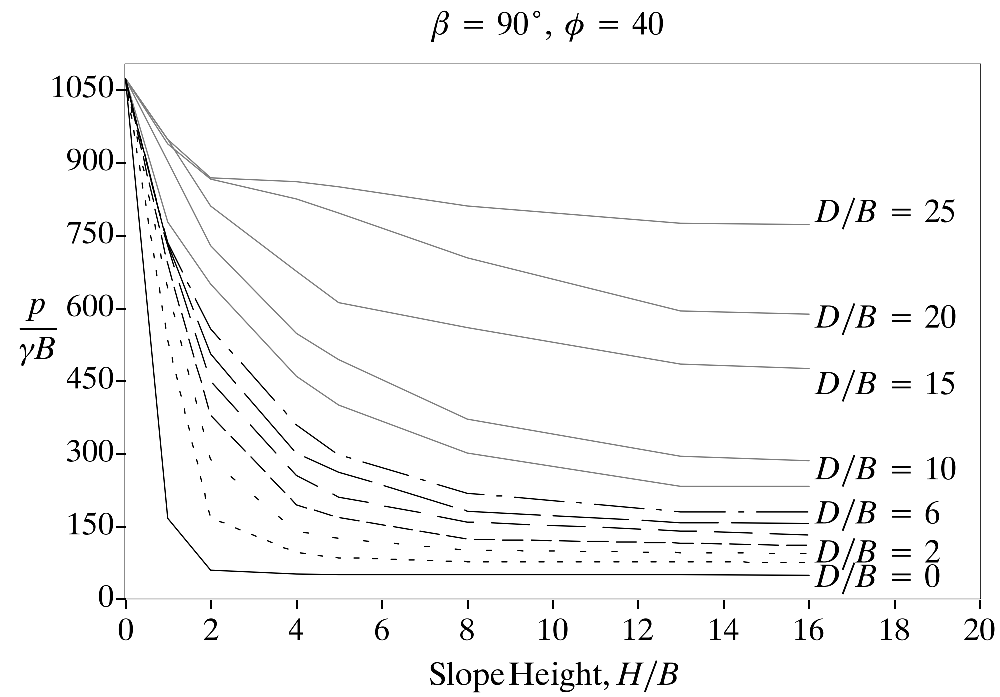

Figure E.8.: Change in Normalised Bearing Capacity with Slope Height

$c/\gamma B = 20$

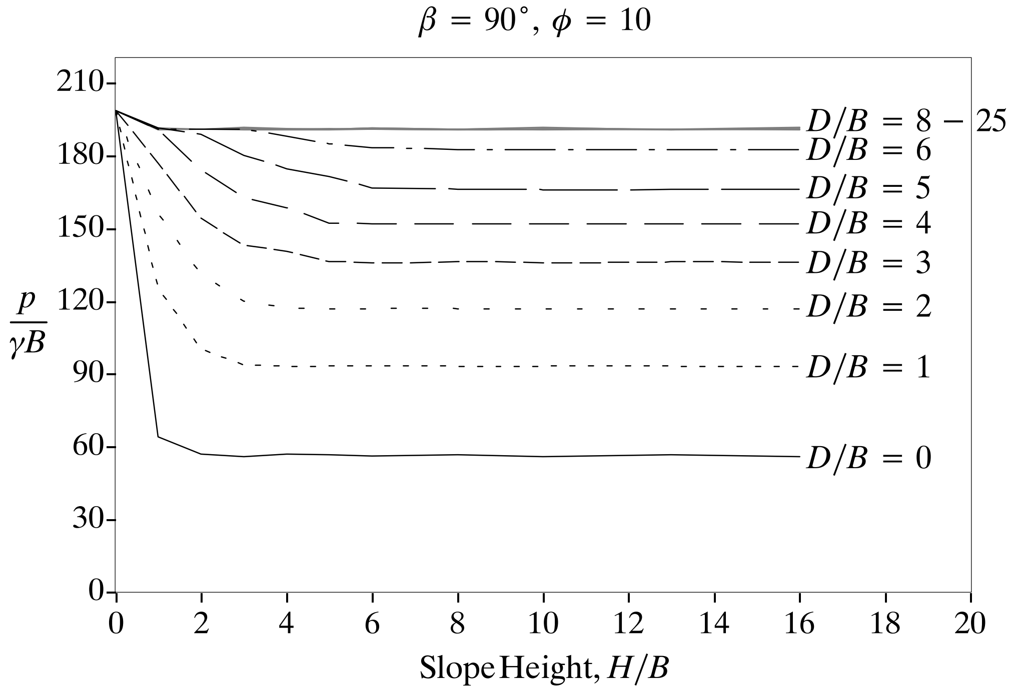

Figure E.9.: Change in Normalised Bearing Capacity with Slope Height

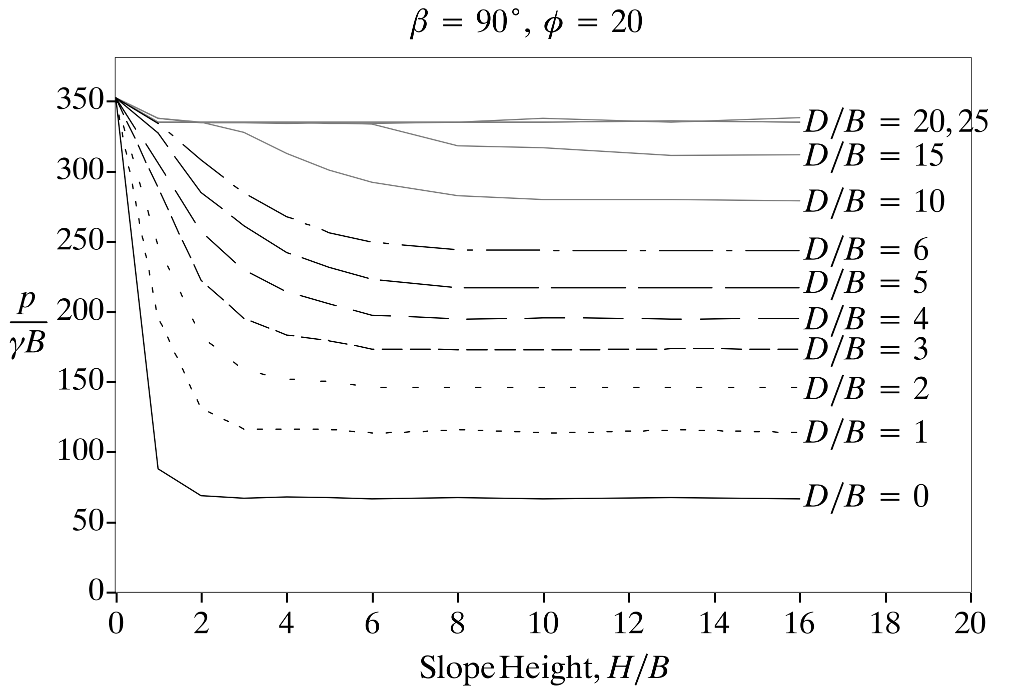

Figure E.10.: Change in Normalised Bearing Capacity with Slope Height

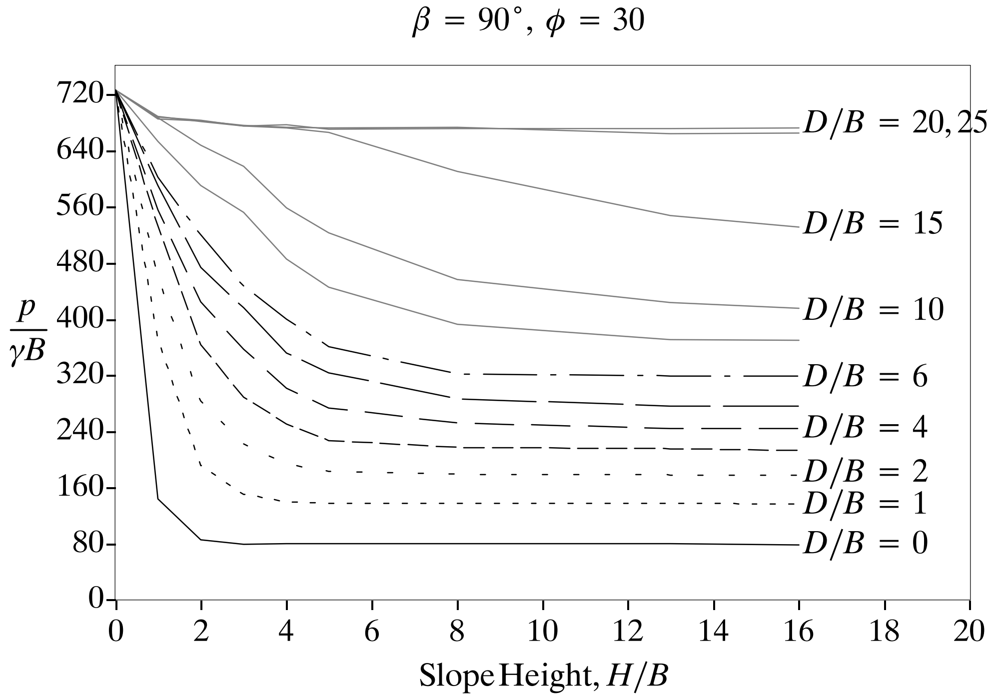

Figure E.11.: Change in Normalised Bearing Capacity with Slope Height

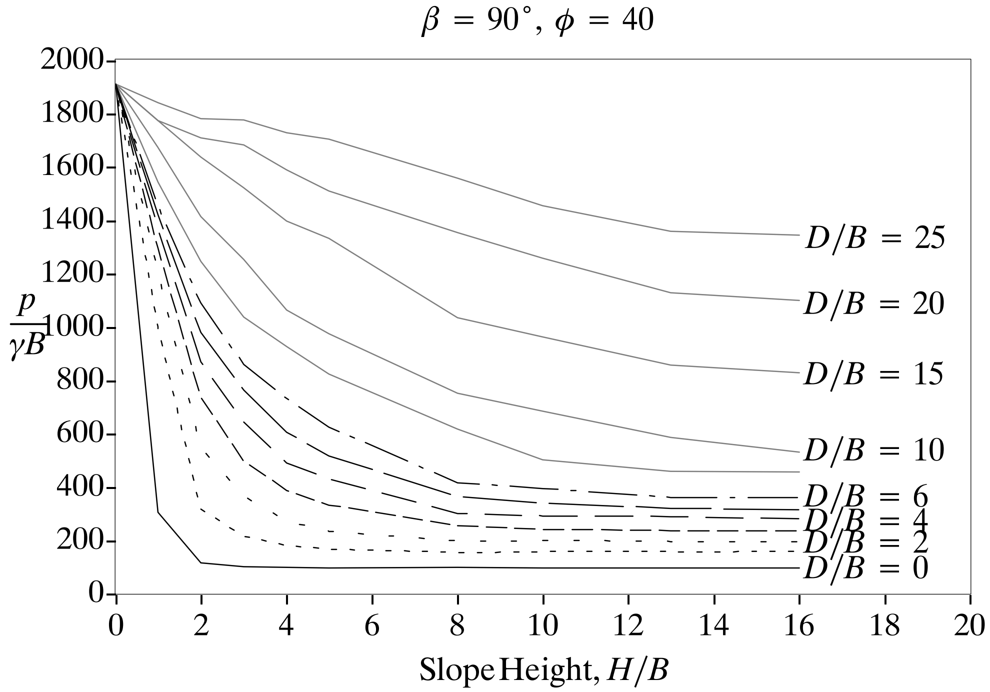

Figure E.12.: Change in Normalised Bearing Capacity with Slope Height

$c/\gamma B = 30$

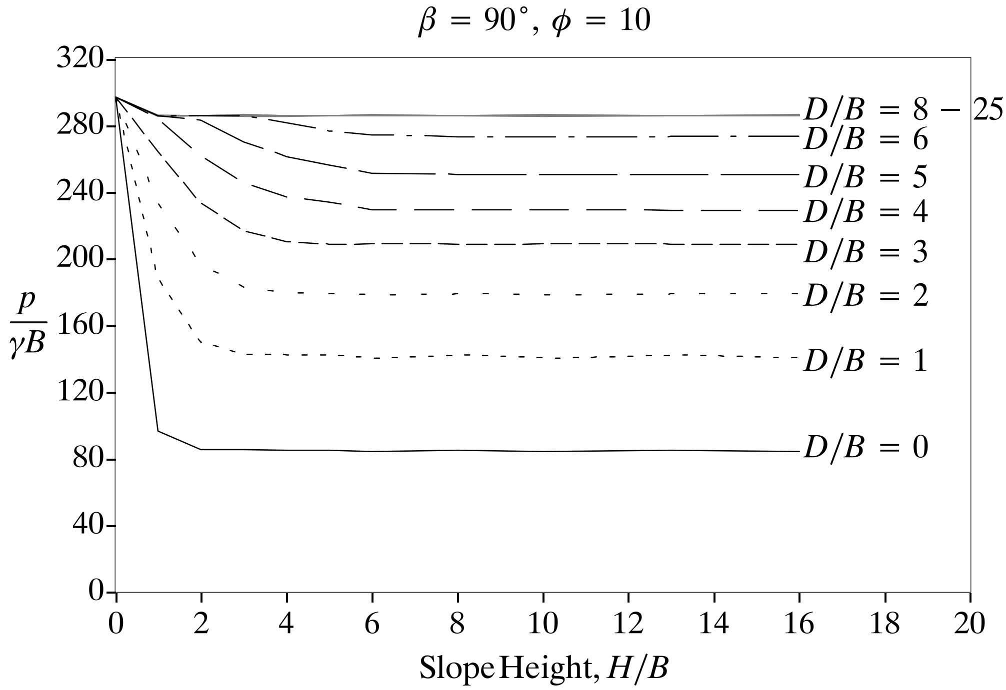

Figure E.13.: Change in Normalised Bearing Capacity with Slope Height

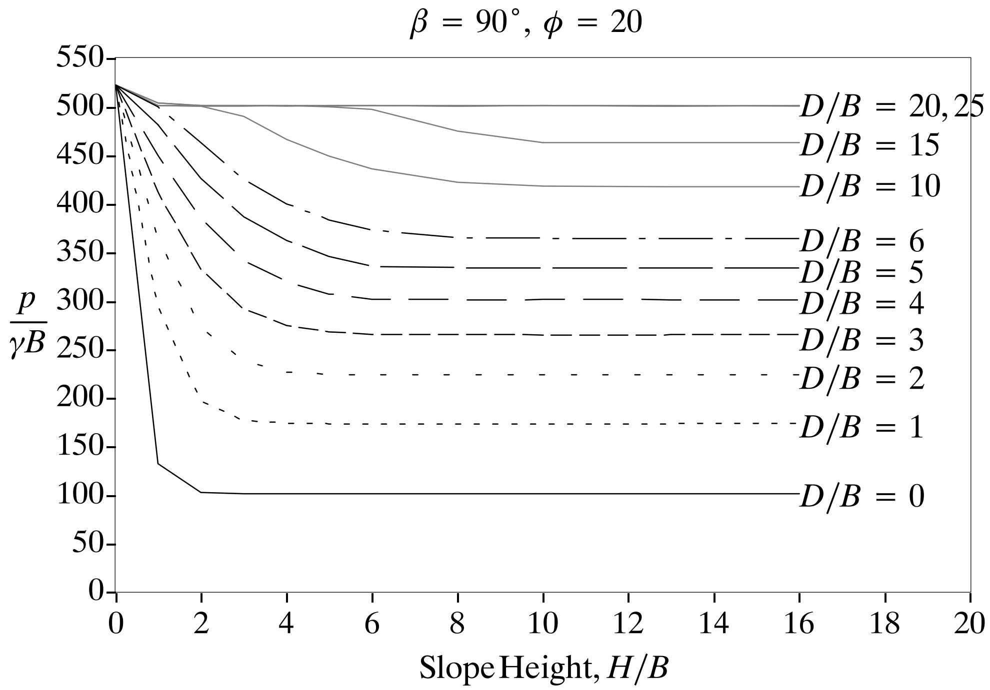

Figure E.14.: Change in Normalised Bearing Capacity with Slope Height

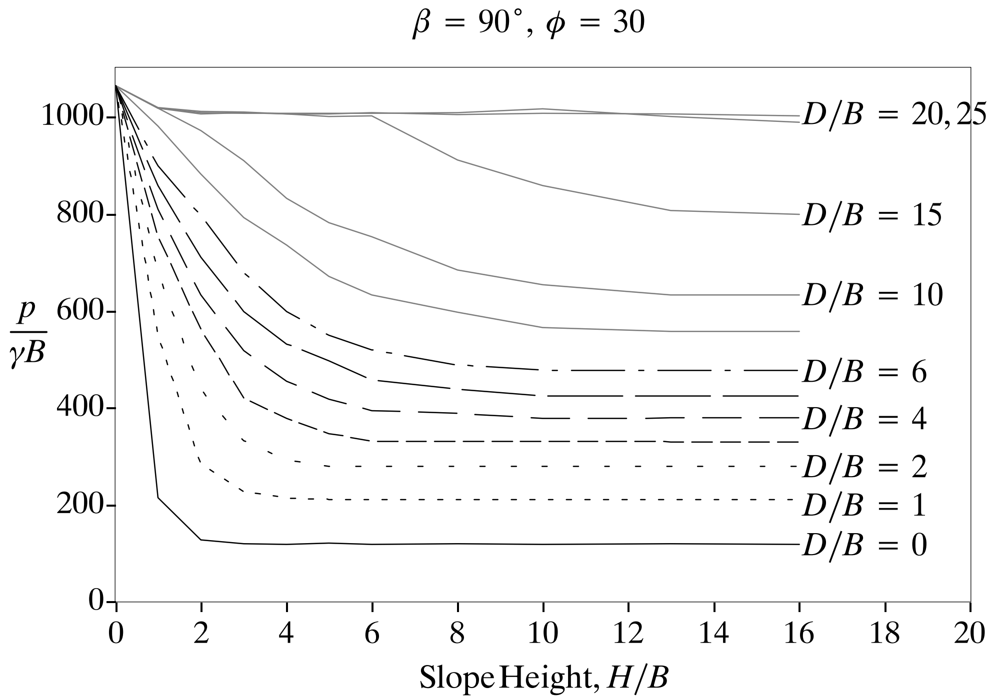

Figure E.15.: Change in Normalised Bearing Capacity with Slope Height

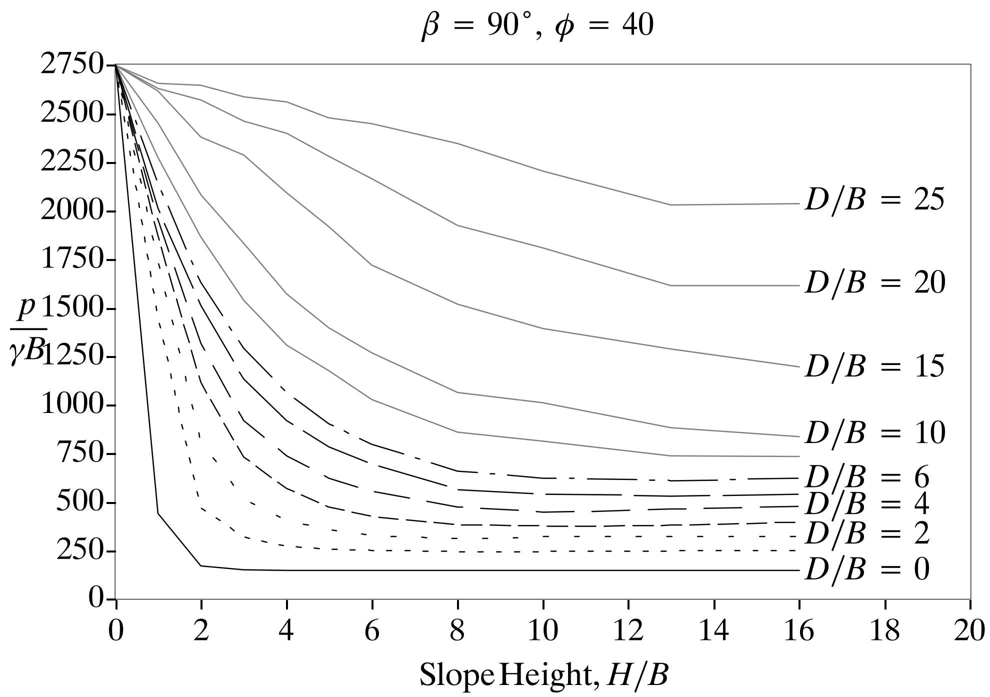

Figure E.16.: Change in Normalised Bearing Capacity with Slope Height

8.6 Appendix F

Increased Bearing Capacity due to Increased Stability Number Charts

The final chart type is concerned with the stability of the slope when a load is applied. These charts are most effective when the safety factor of a slope has been determined by another method (these charts are based on stability safety factor of 1 giving the ultimate capacity) which can then be used in conjunction with the soil cohesion and density to determine a stability number. These charts provide a good correlation with existing solutions to the footing on slope problem and are another option when wishing to determine the bearing capacity of a slope.

As the stability of a slope is a relationship between the strength ratio and slope height ratio, the chart is divided into groups based on slope height with a separate chart for each friction angle at each slope height.

H/B = 1

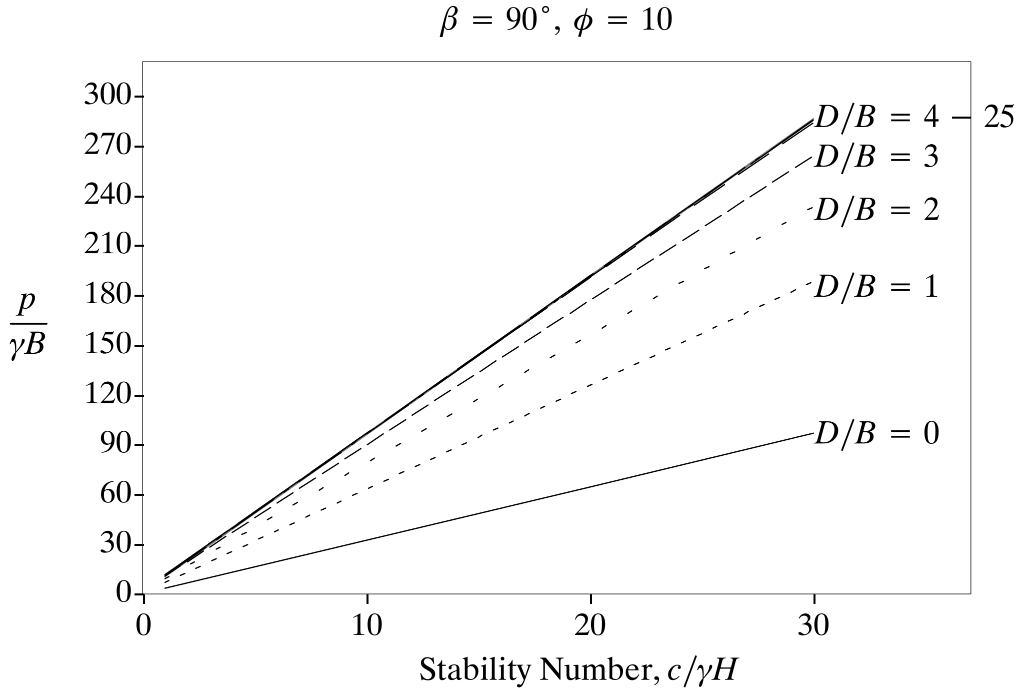

Figure F.1: Change in Normalised Bearing Capacity with Stability Number

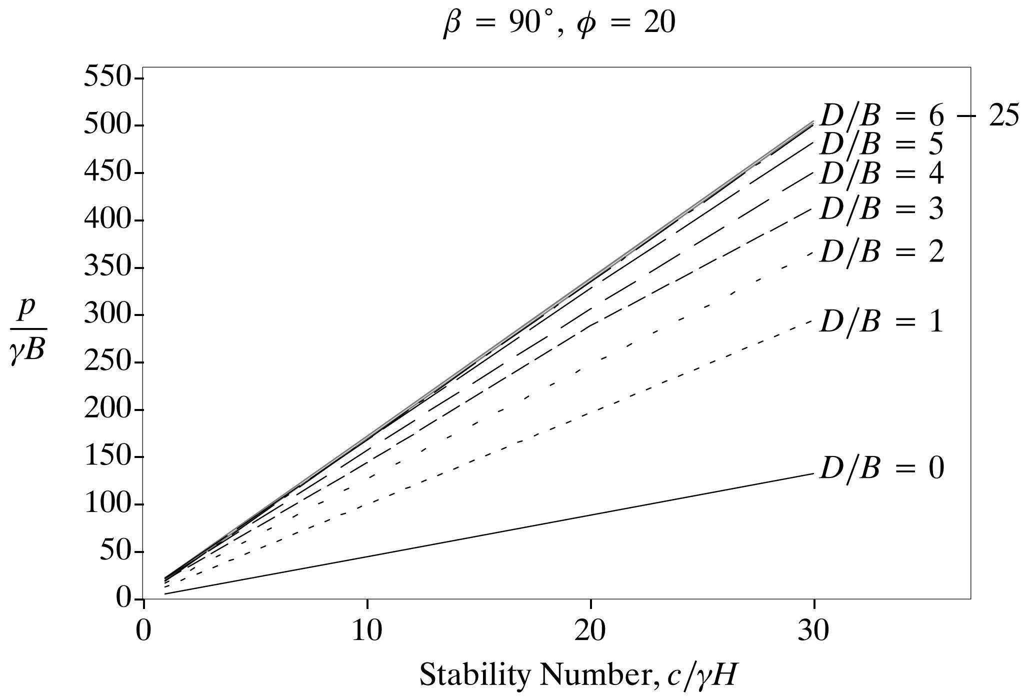

Figure F.2: Change in Normalised Bearing Capacity with Stability Number

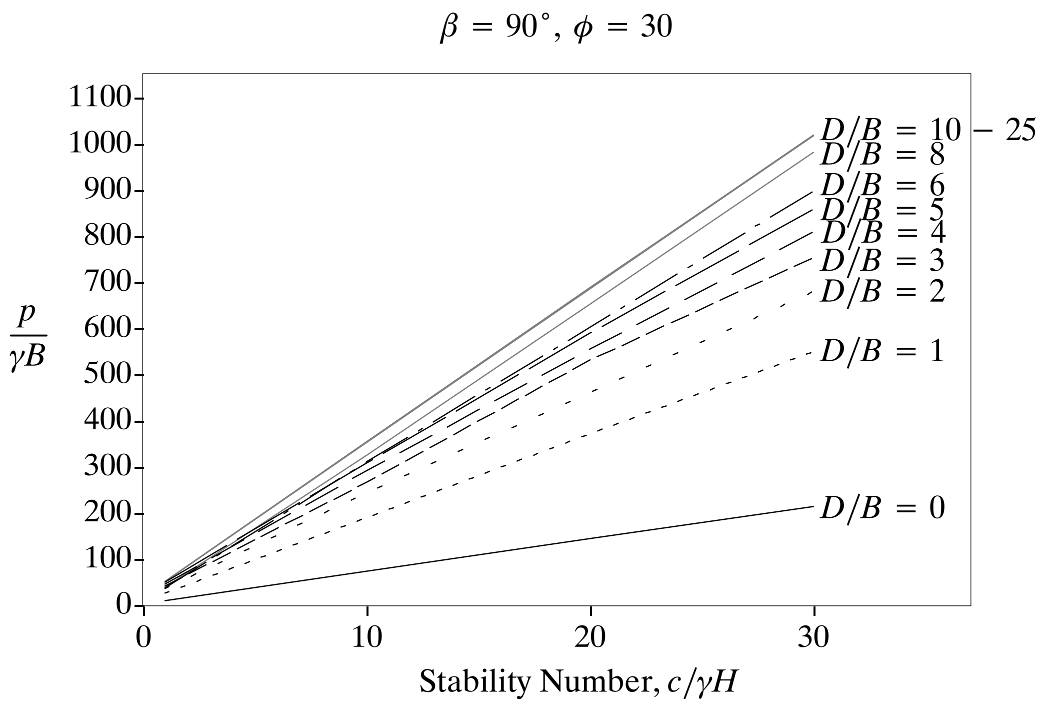

Figure F.3: Change in Normalised Bearing Capacity with Stability Number

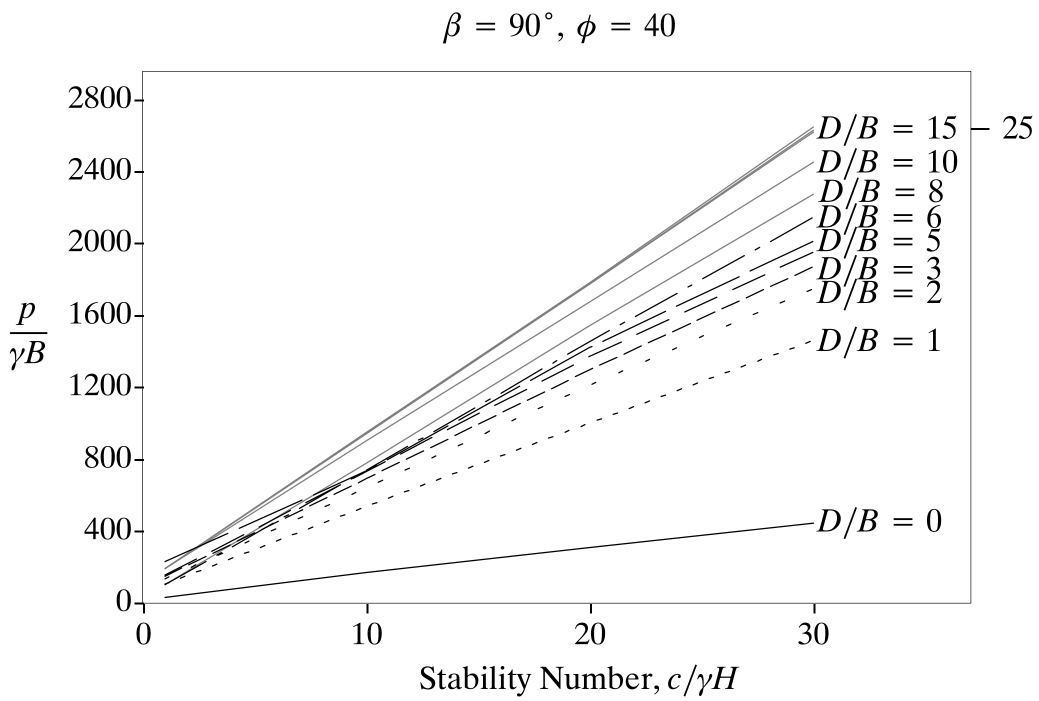

Figure F.4: Change in Normalised Bearing Capacity with Stability Number

H/B = 2

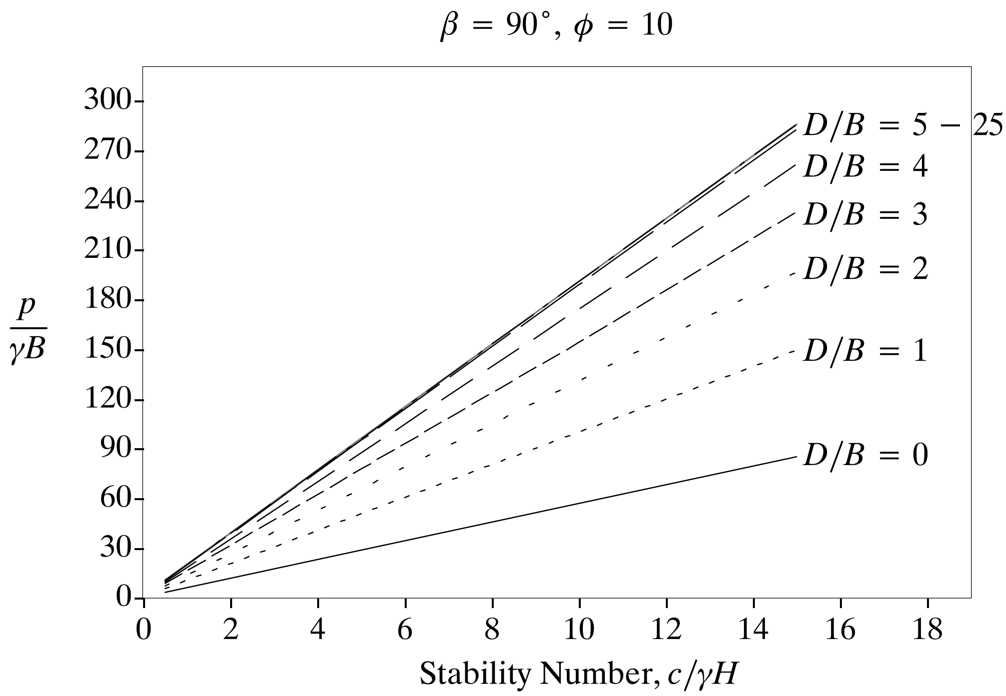

Figure F.5: Change in Normalised Bearing Capacity with Stability Number

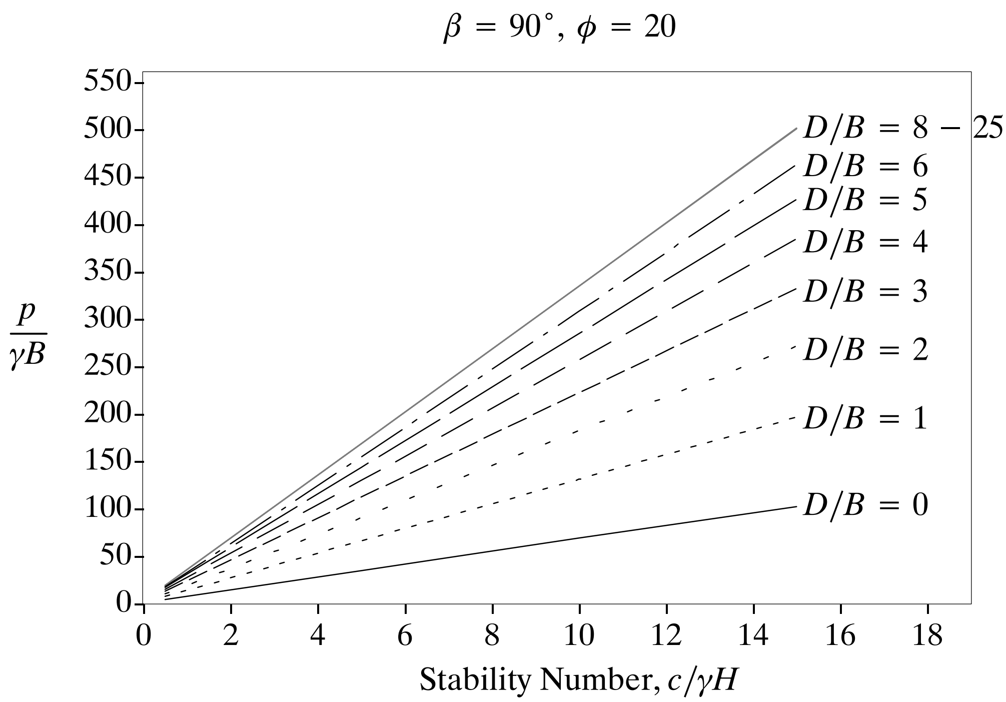

Figure F.6: Change in Normalised Bearing Capacity with Stability Number

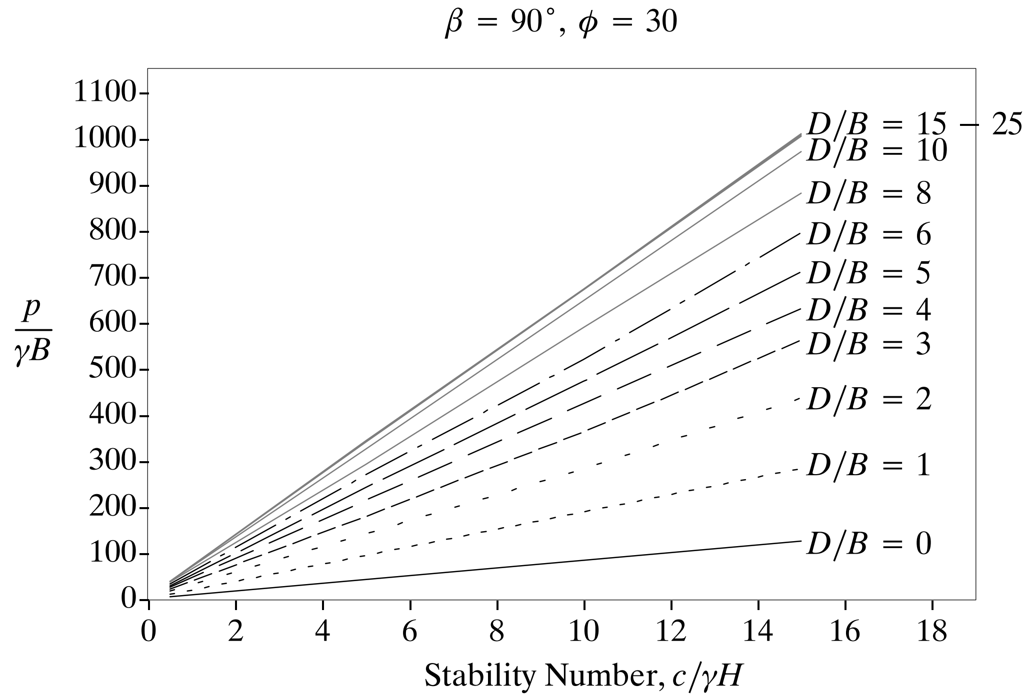

Figure F.7: Change in Normalised Bearing Capacity with Stability Number

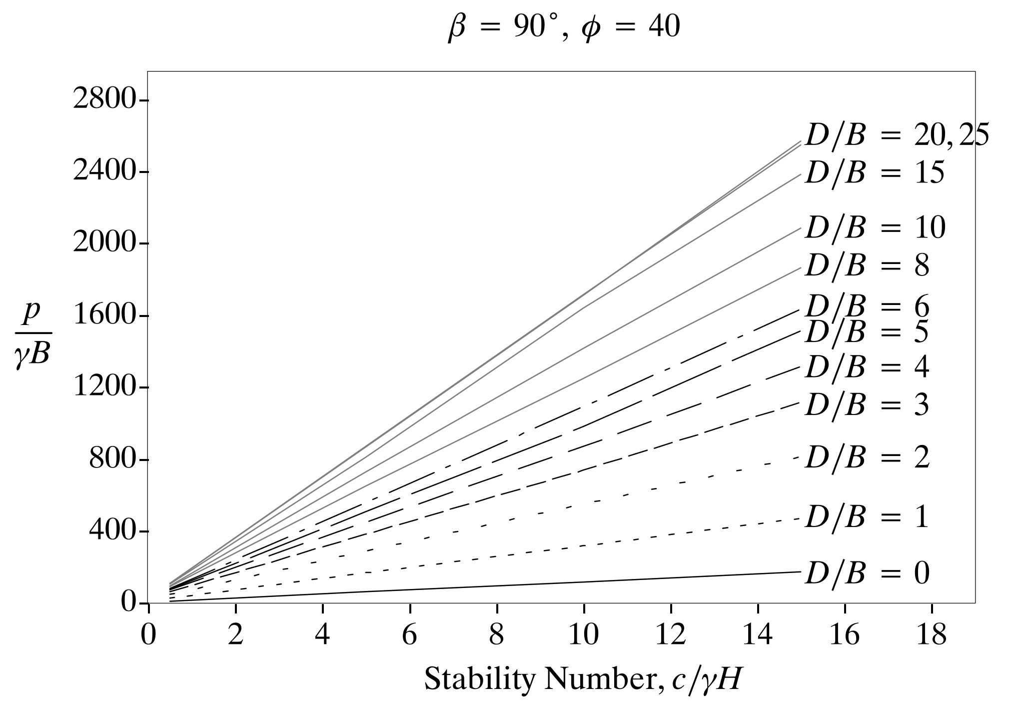

Figure F.8: Change in Normalised Bearing Capacity with Stability Number

H/B = 3

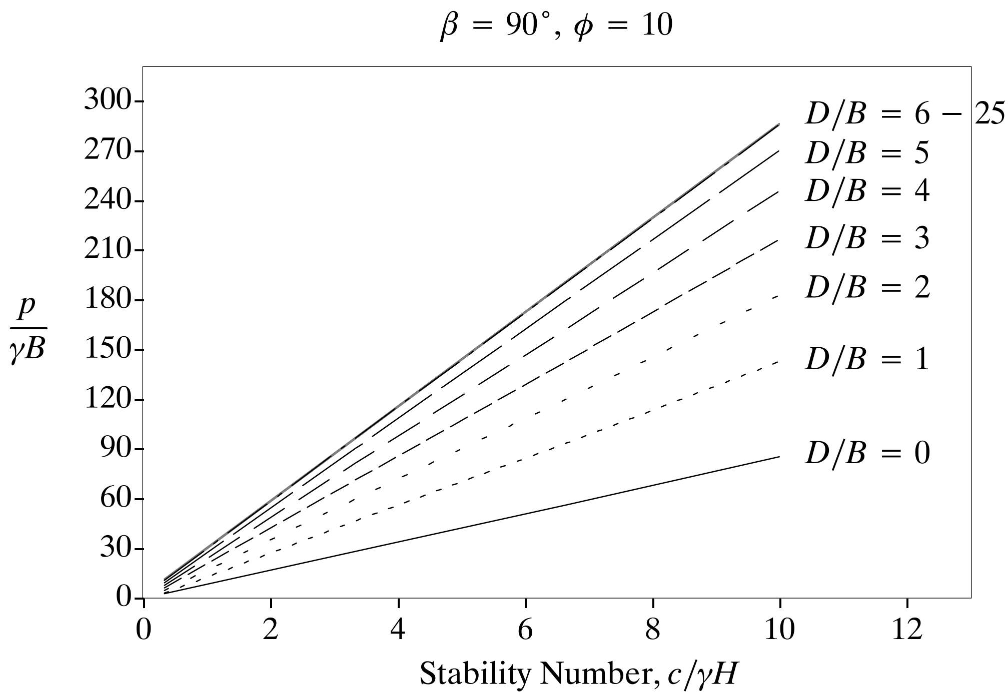

Figure F.9: Change in Normalised Bearing Capacity with Stability Number

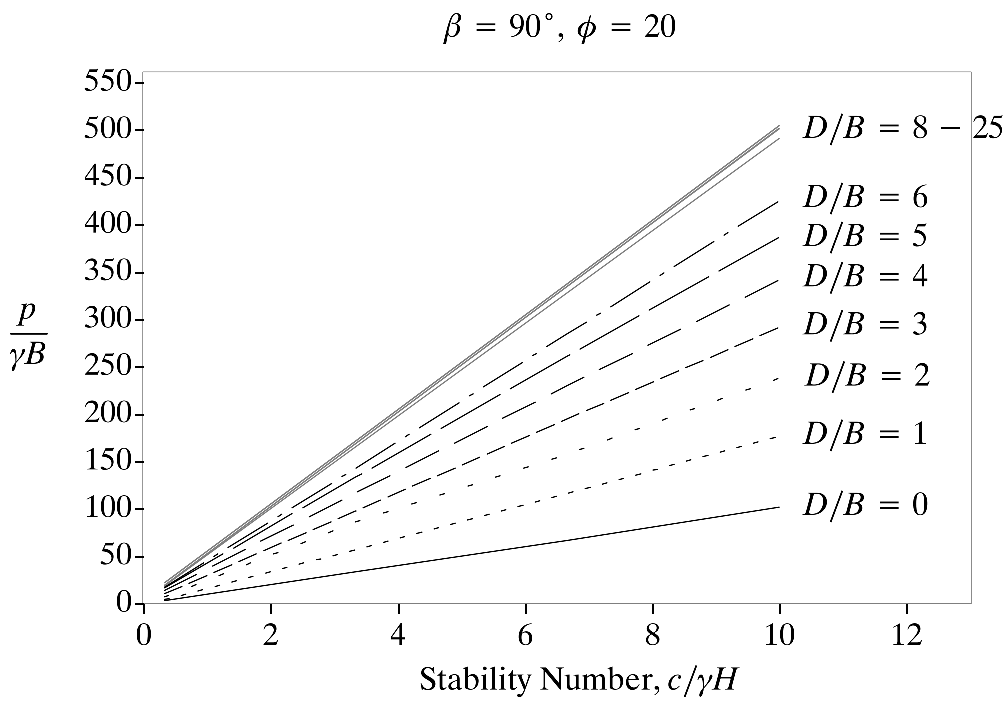

Figure F.10: Change in Normalised Bearing Capacity with Stability Number

$\beta = 90^\circ,\ \phi = 30$

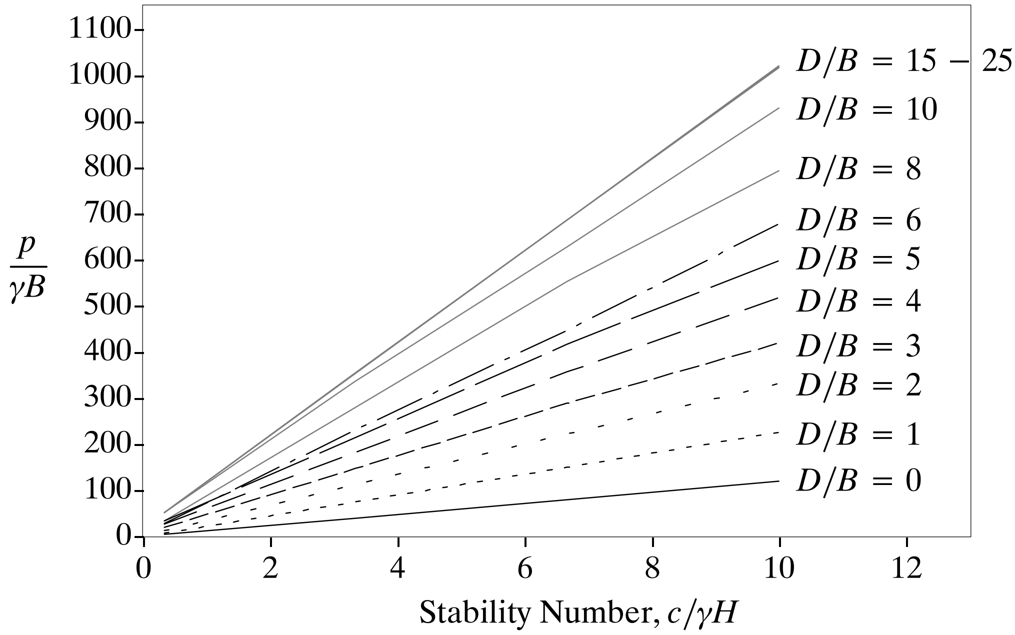

Figure F.11: Change in Normalised Bearing Capacity with Stability Number

$\beta = 90^\circ,\ \phi = 40$

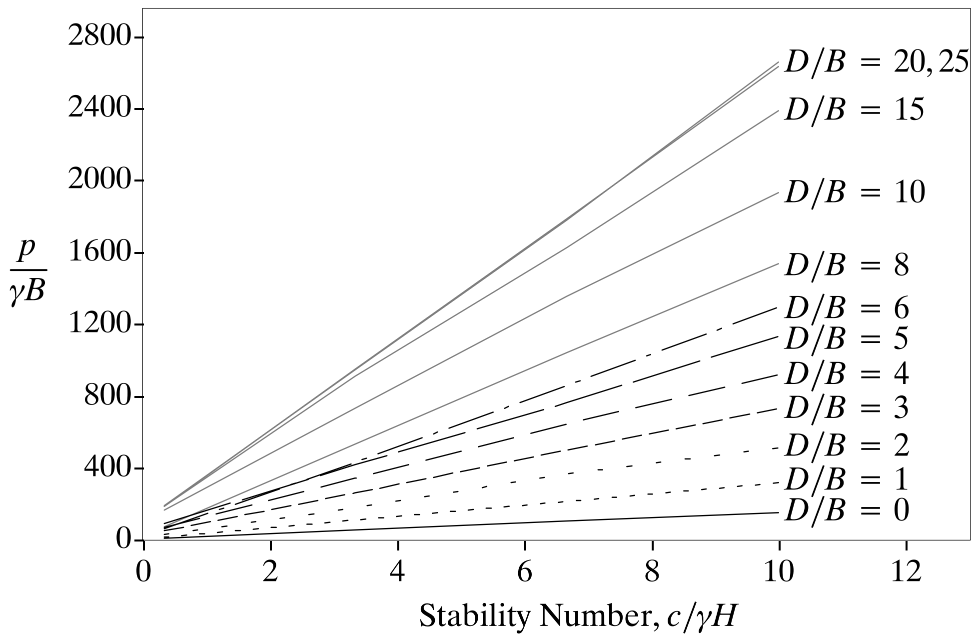

Figure F.12: Change in Normalised Bearing Capacity with Stability Number

H/B = 4

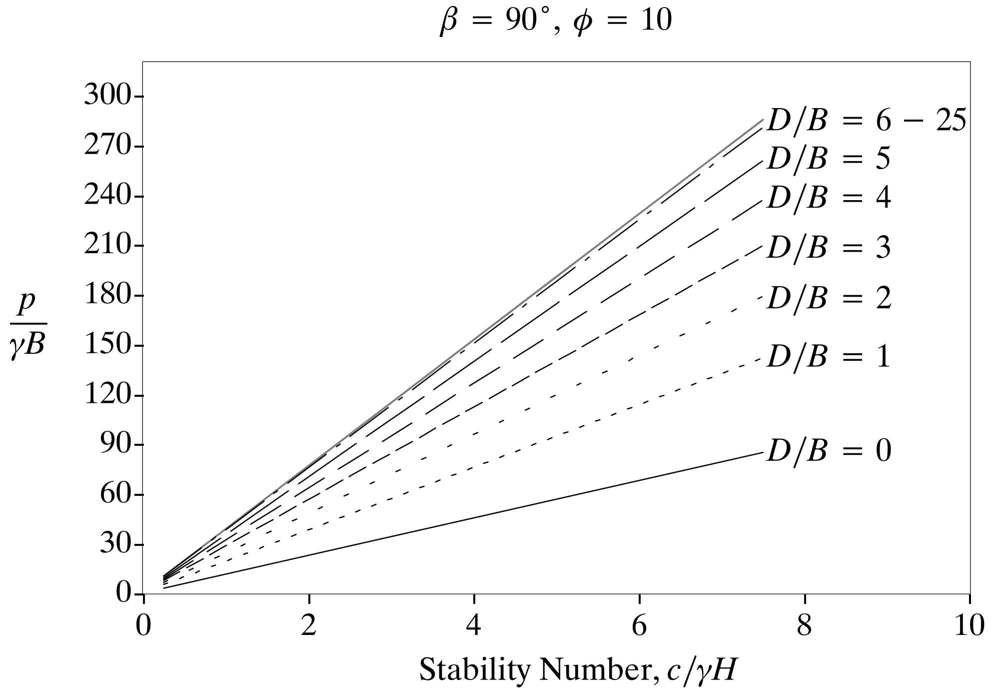

Figure F.13: Change in Normalised Bearing Capacity with Stability Number

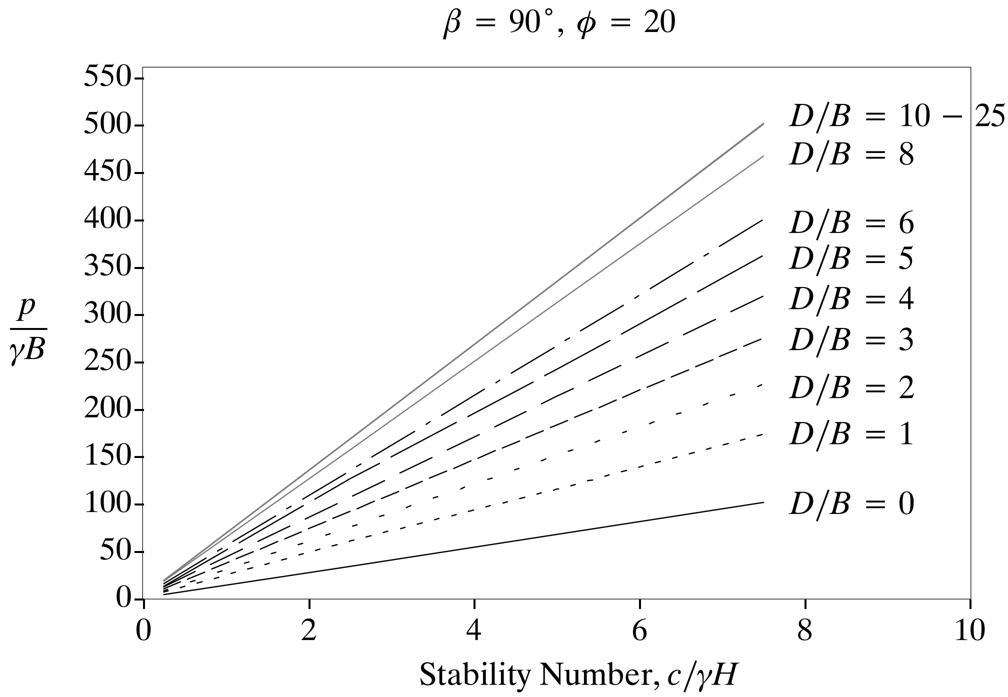

Figure F.14: Change in Normalised Bearing Capacity with Stability Number

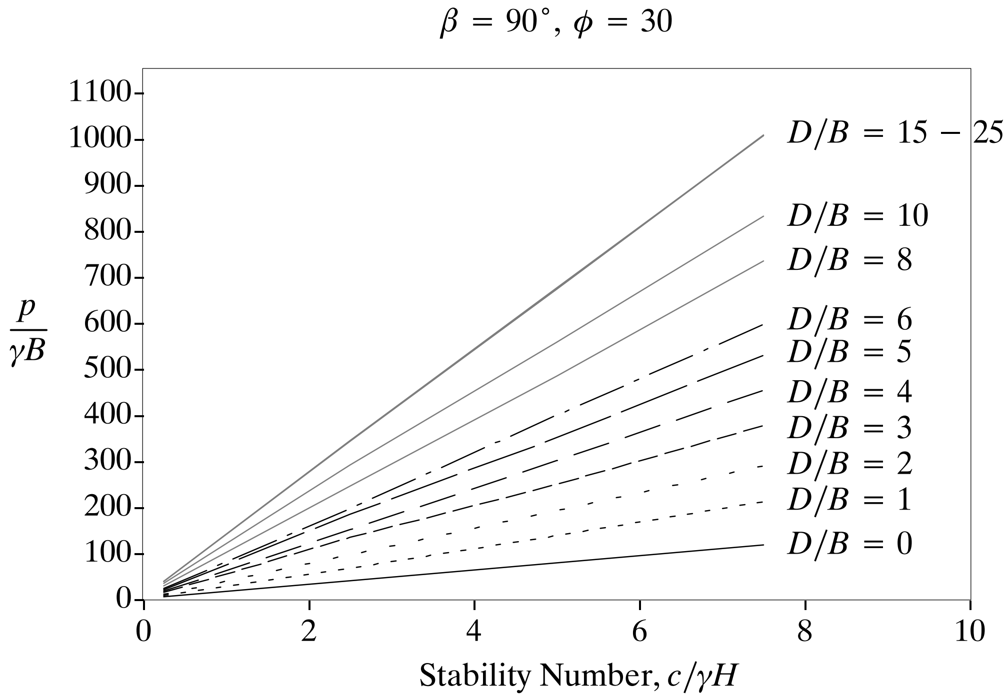

Figure F.15: Change in Normalised Bearing Capacity with Stability Number

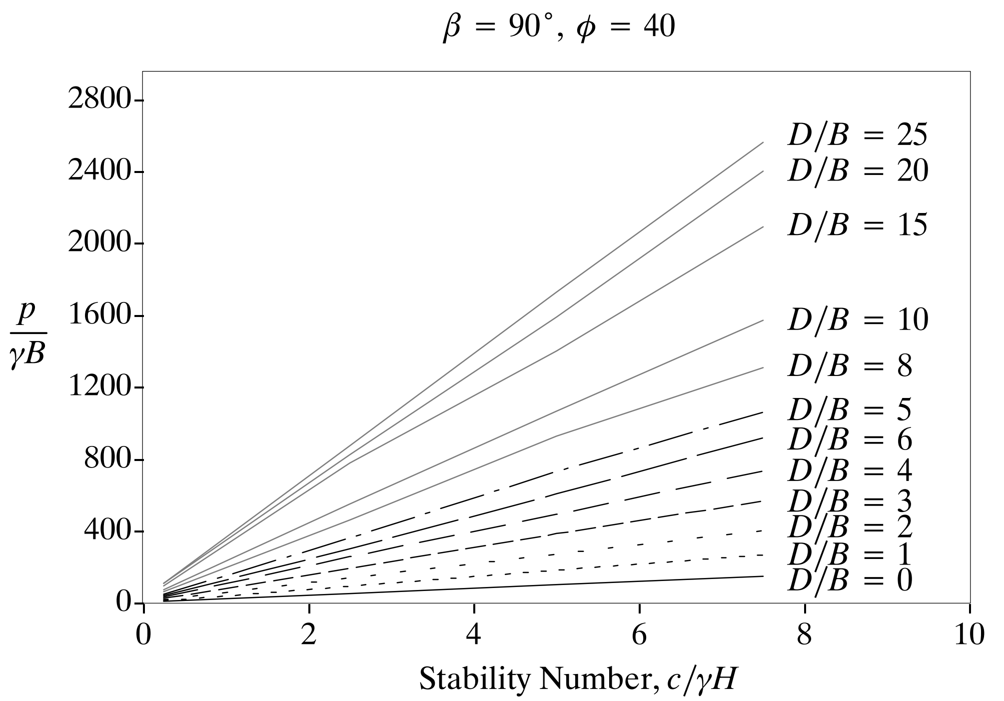

Figure F.16: Change in Normalised Bearing Capacity with Stability Number

H/B = 5

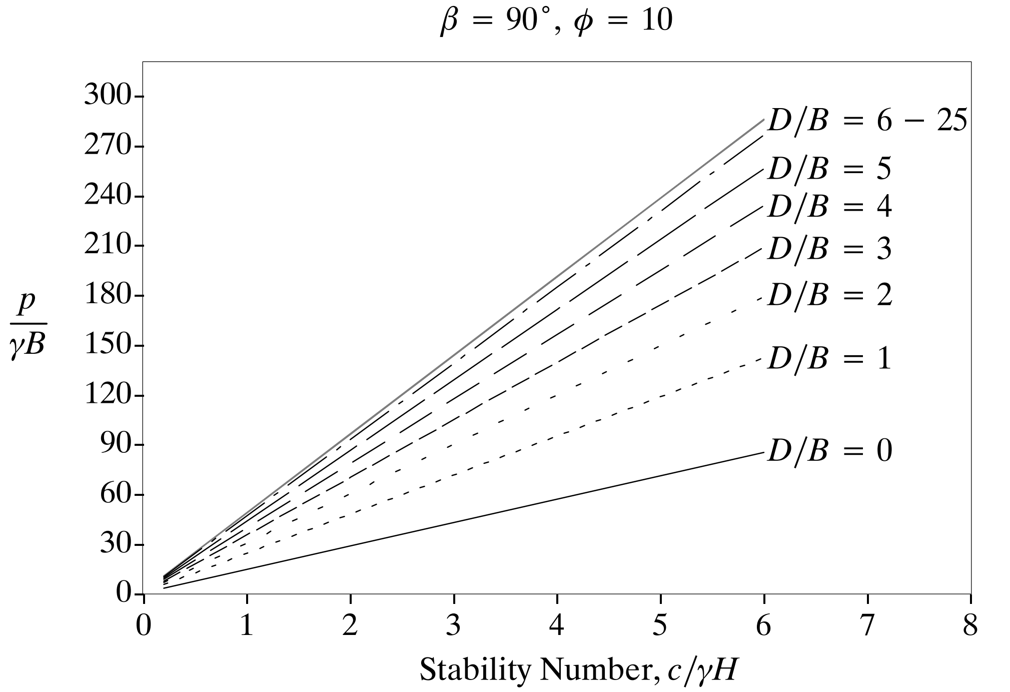

Figure F.17: Change in Normalised Bearing Capacity with Stability Number

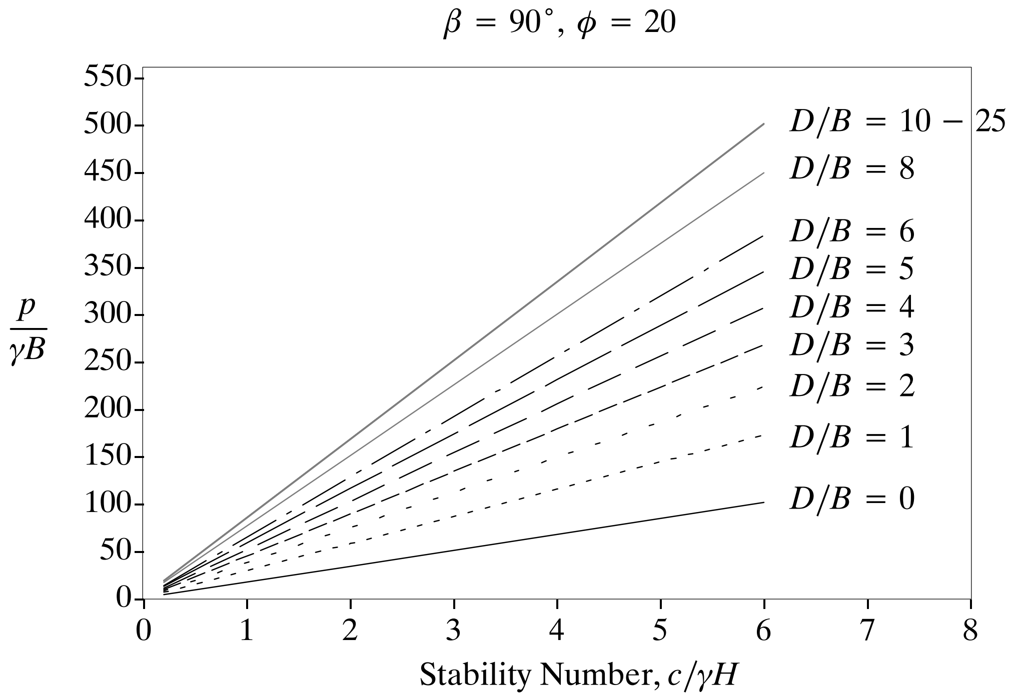

Figure F.18: Change in Normalised Bearing Capacity with Stability Number

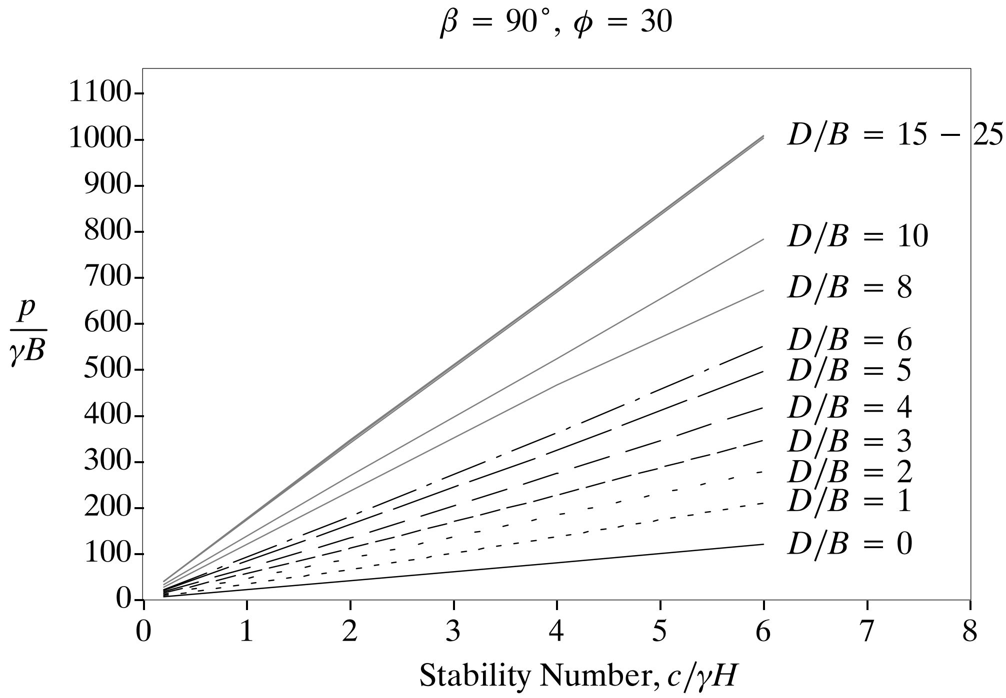

Figure F.19: Change in Normalised Bearing Capacity with Stability Number

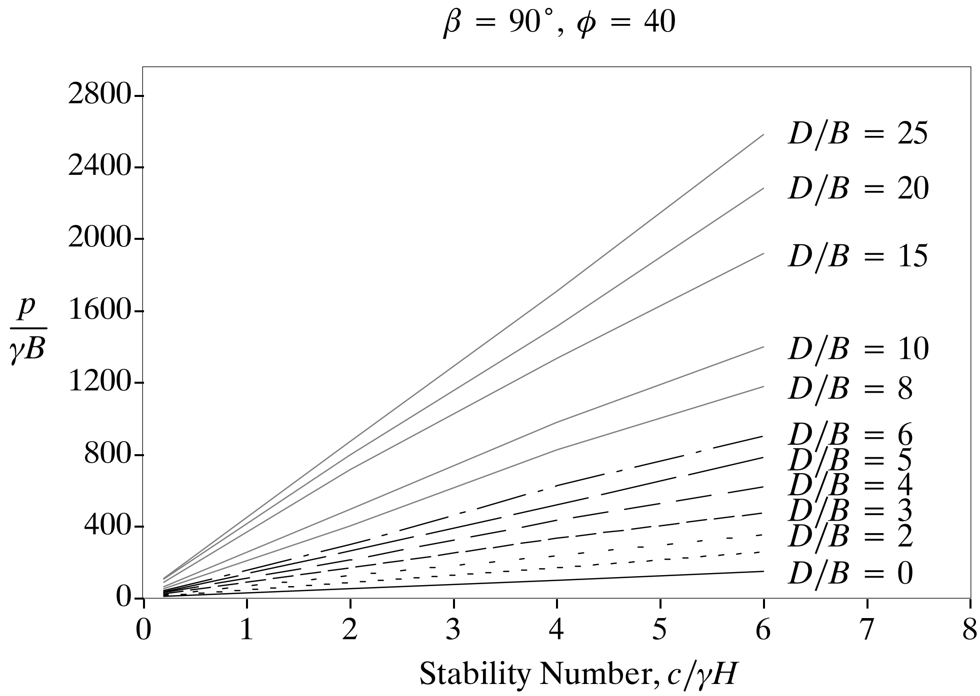

Figure F.20: Change in Normalised Bearing Capacity with Stability Number

H/B = 6

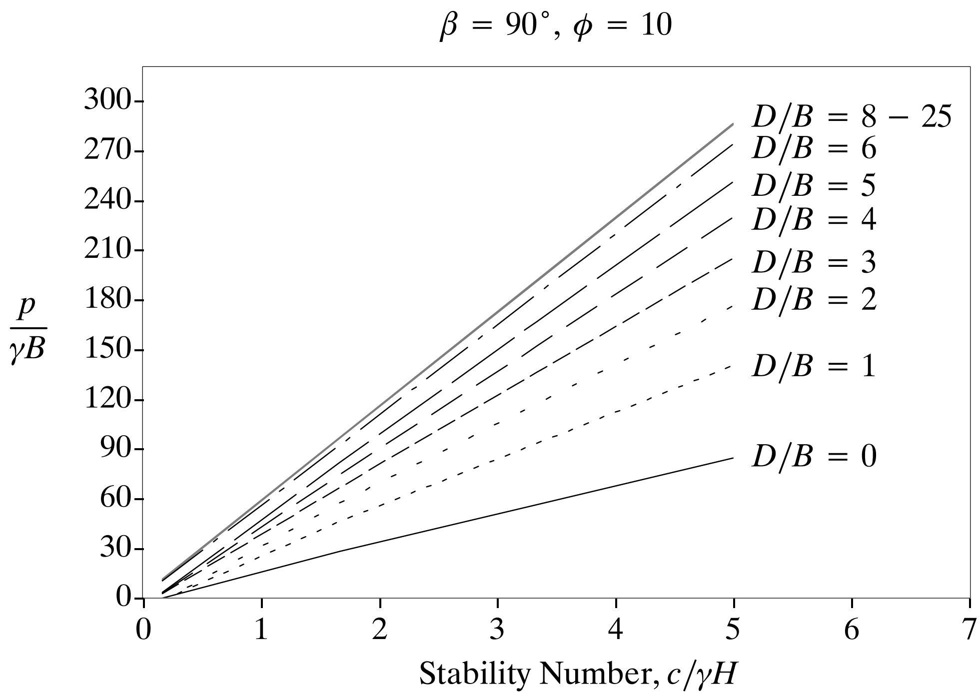

Figure F.21: Change in Normalised Bearing Capacity with Stability Number

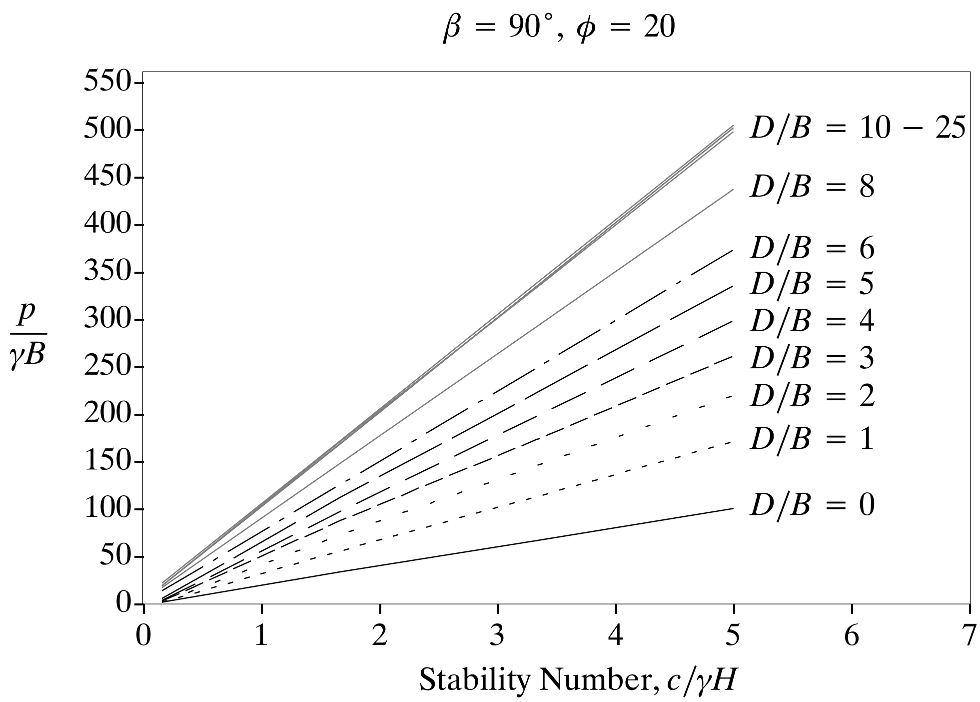

Figure F.22: Change in Normalised Bearing Capacity with Stability Number

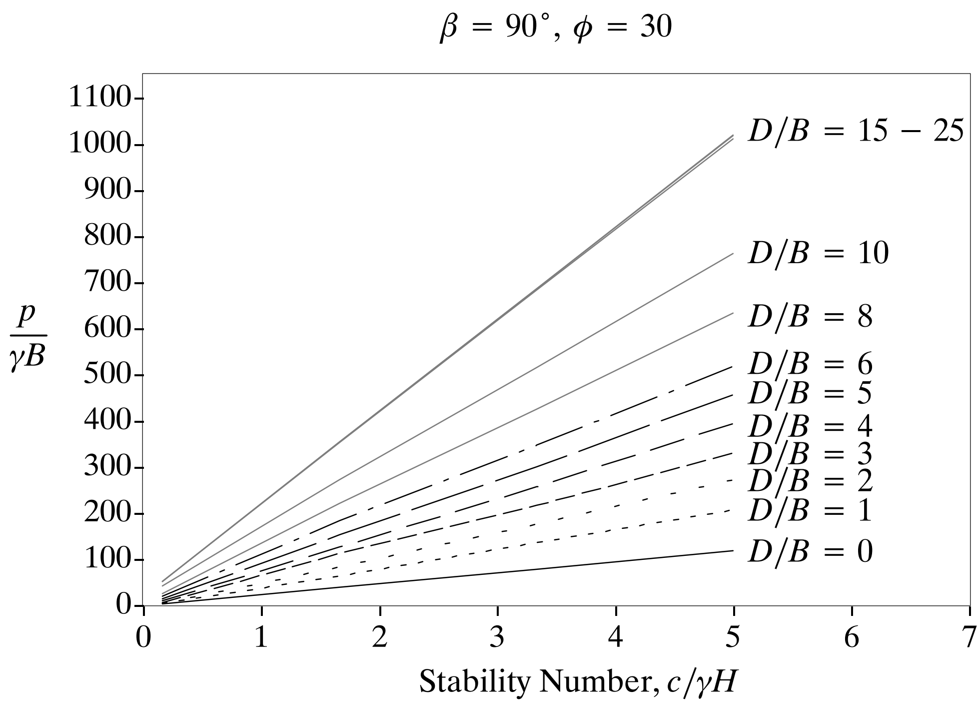

Figure F.23: Change in Normalised Bearing Capacity with Stability Number

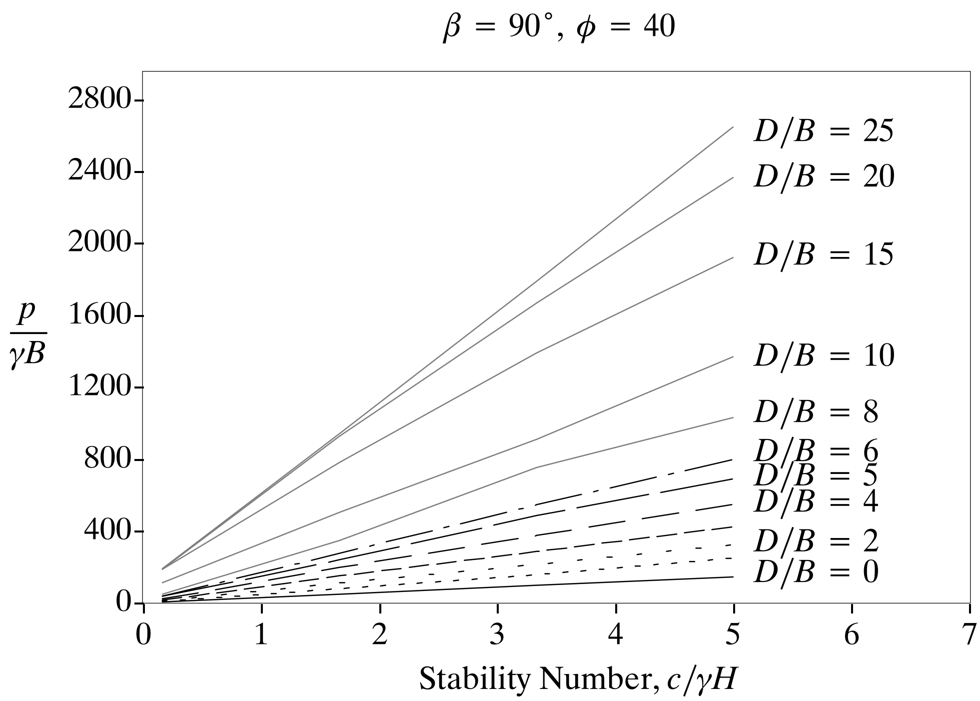

Figure F.24: Change in Normalised Bearing Capacity with Stability Number

H/B = 8

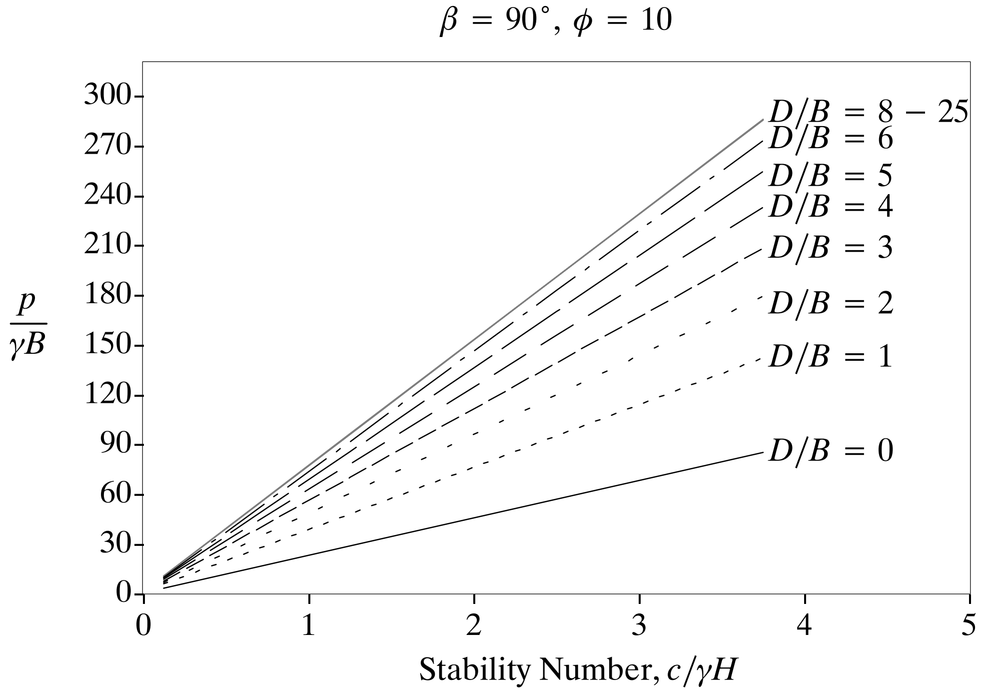

Figure F.25: Change in Normalised Bearing Capacity with Stability Number

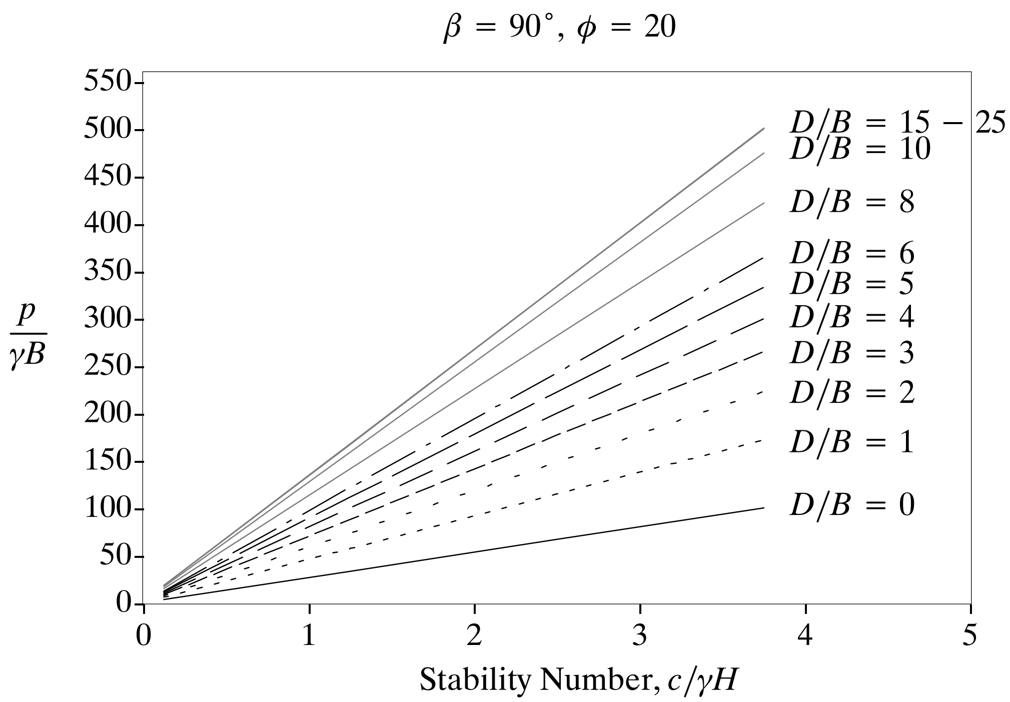

Figure F.26: Change in Normalised Bearing Capacity with Stability Number

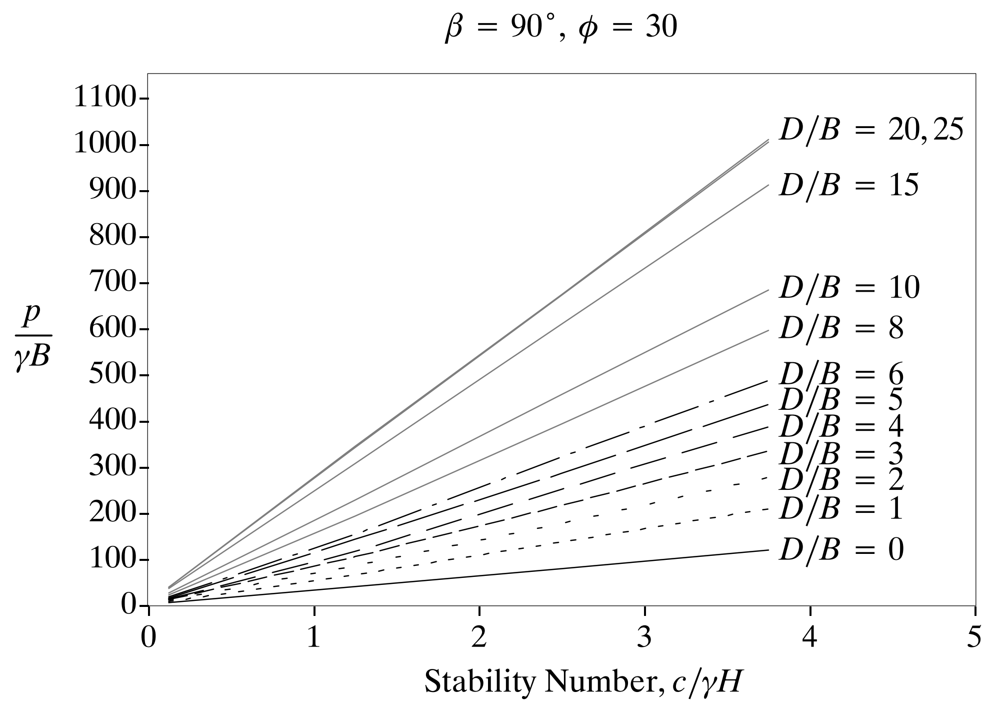

Figure F.27: Change in Normalised Bearing Capacity with Stability Number

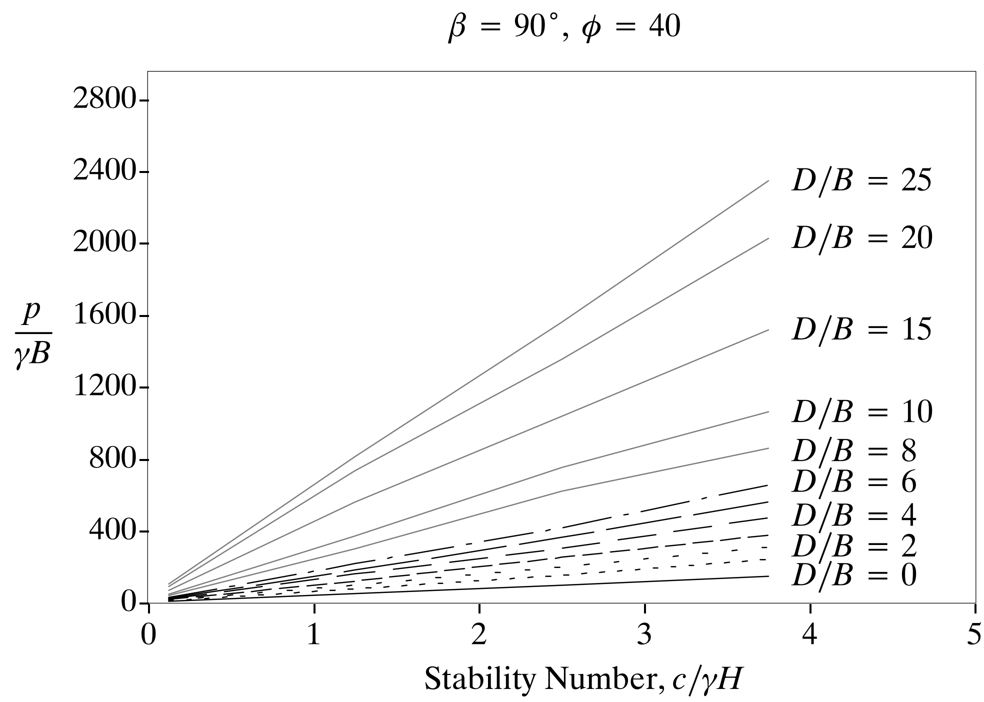

Figure F.28: Change in Normalised Bearing Capacity with Stability Number

H/B = 10

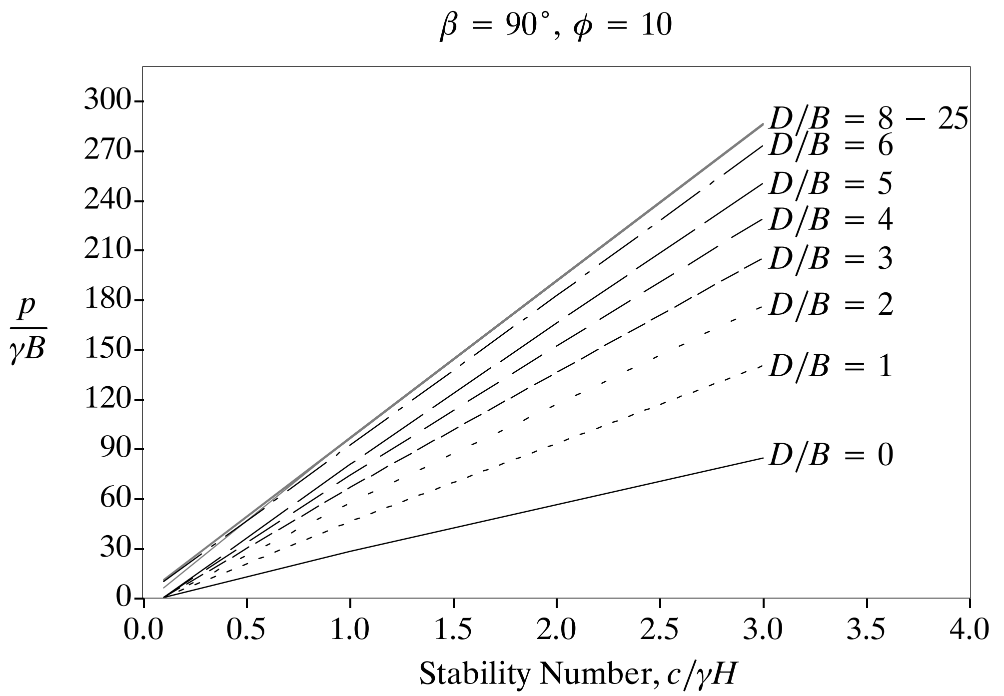

Figure F.29: Change in Normalised Bearing Capacity with Stability Number

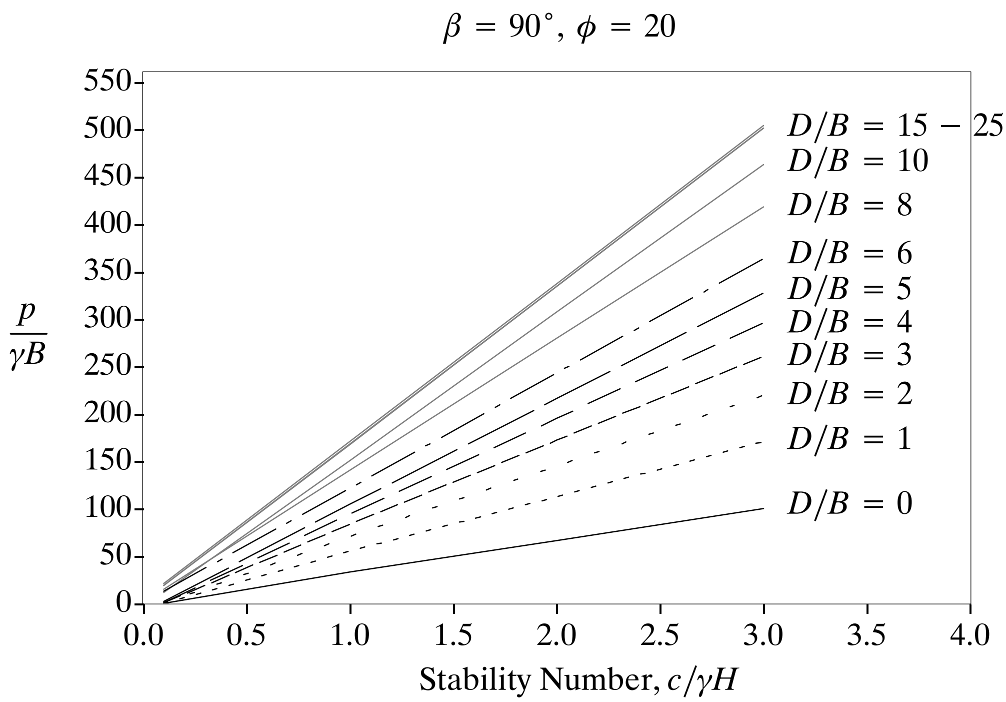

Figure F.30: Change in Normalised Bearing Capacity with Stability Number

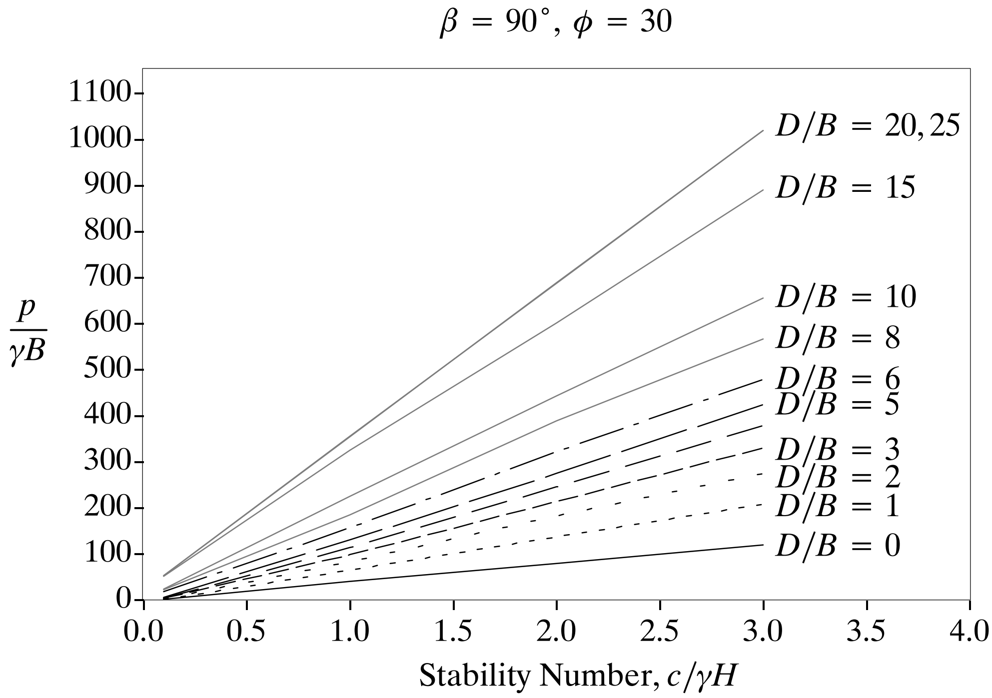

Figure F.31: Change in Normalised Bearing Capacity with Stability Number

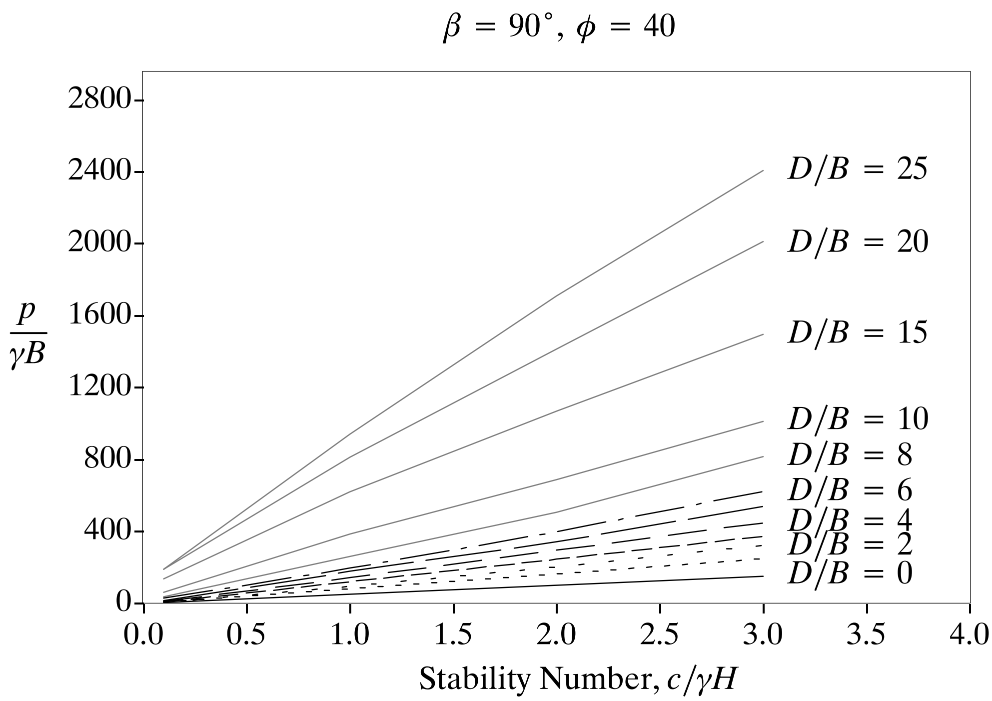

Figure F.32: Change in Normalised Bearing Capacity with Stability Number

H/B = 13

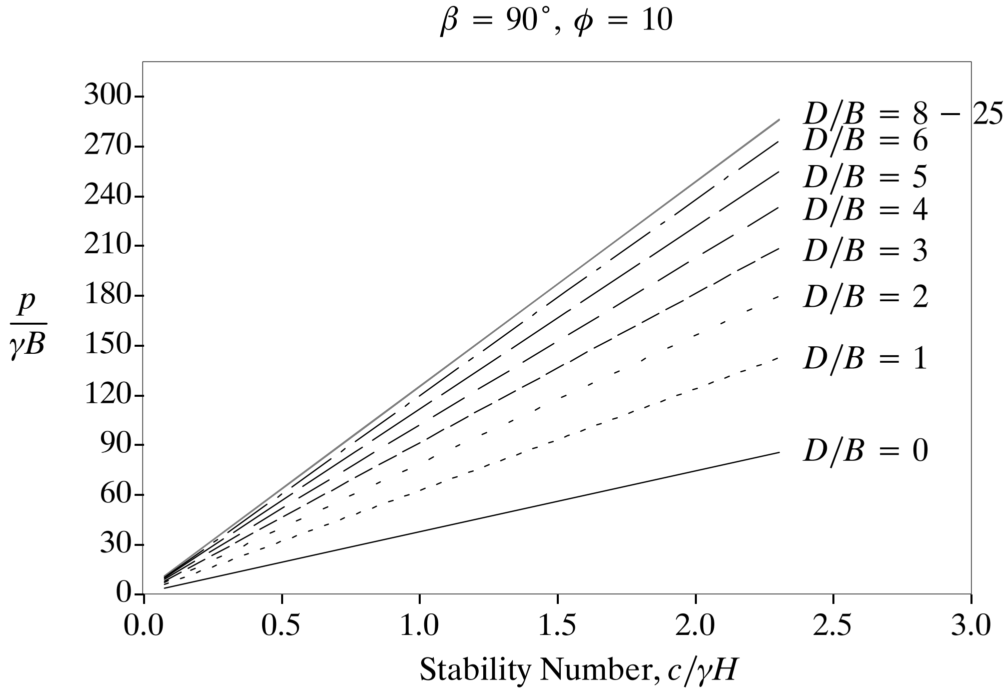

Figure F.33: Change in Normalised Bearing Capacity with Stability Number

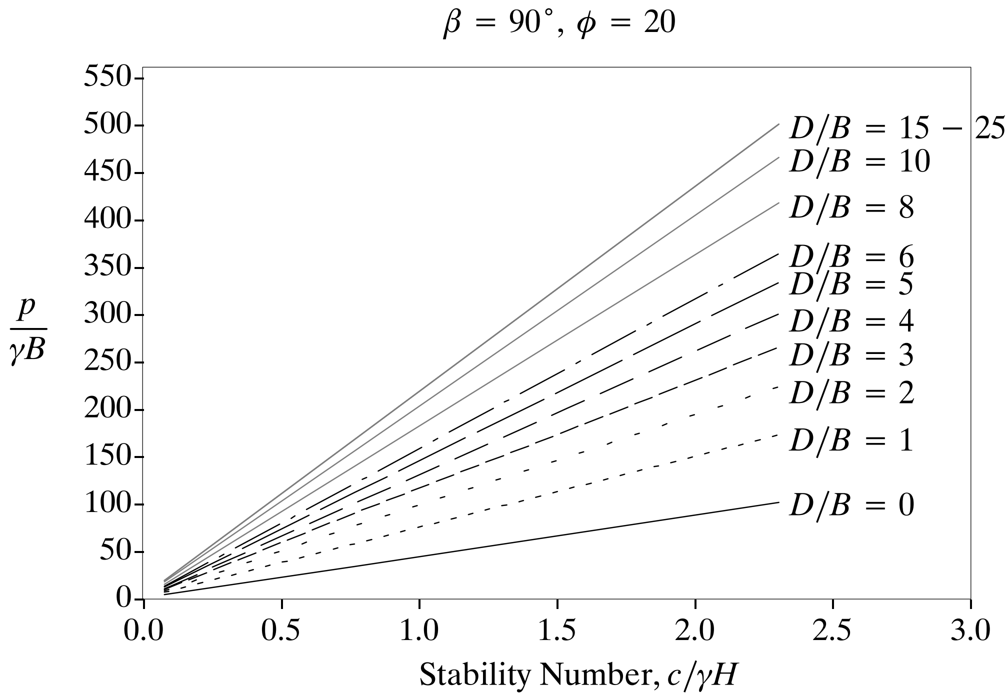

Figure F.34: Change in Normalised Bearing Capacity with Stability Number

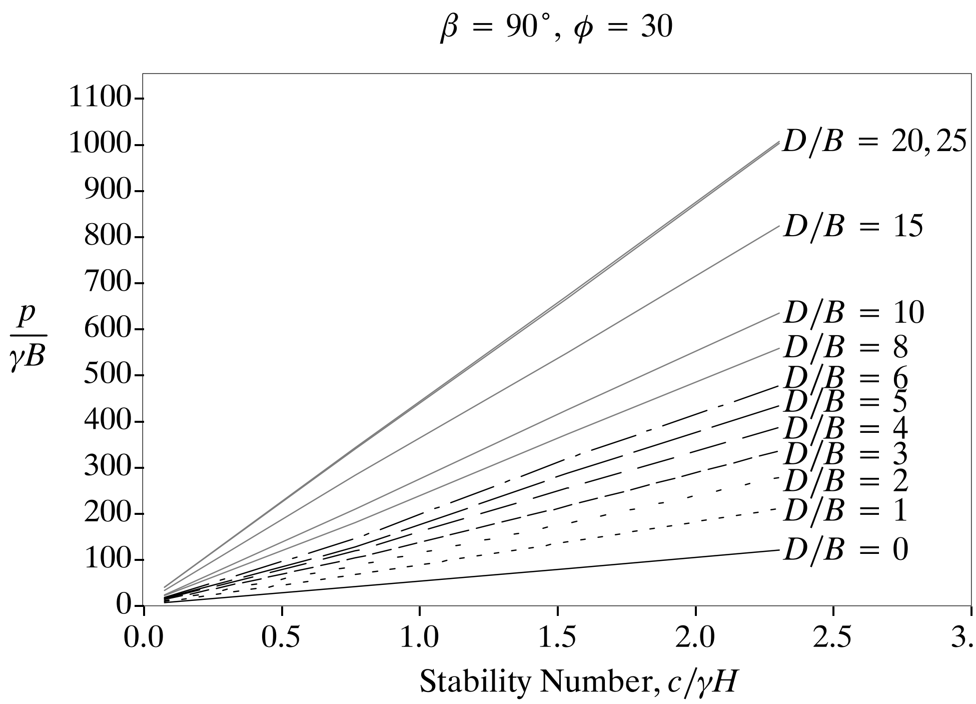

Figure F.35: Change in Normalised Bearing Capacity with Stability Number

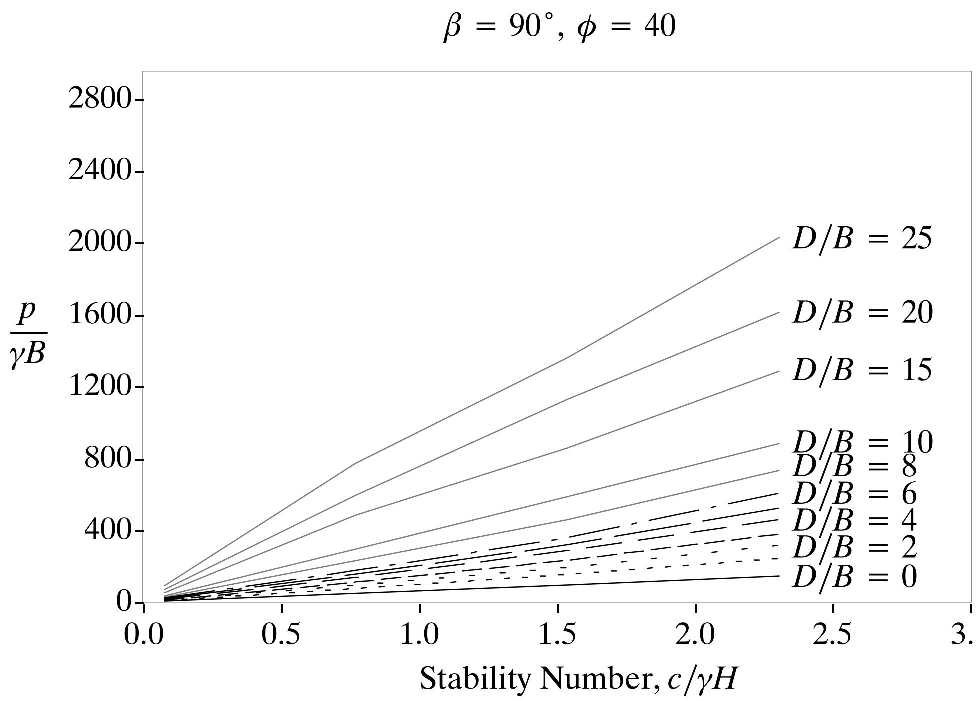

Figure F.36: Change in Normalised Bearing Capacity with Stability Number

H/B = 16

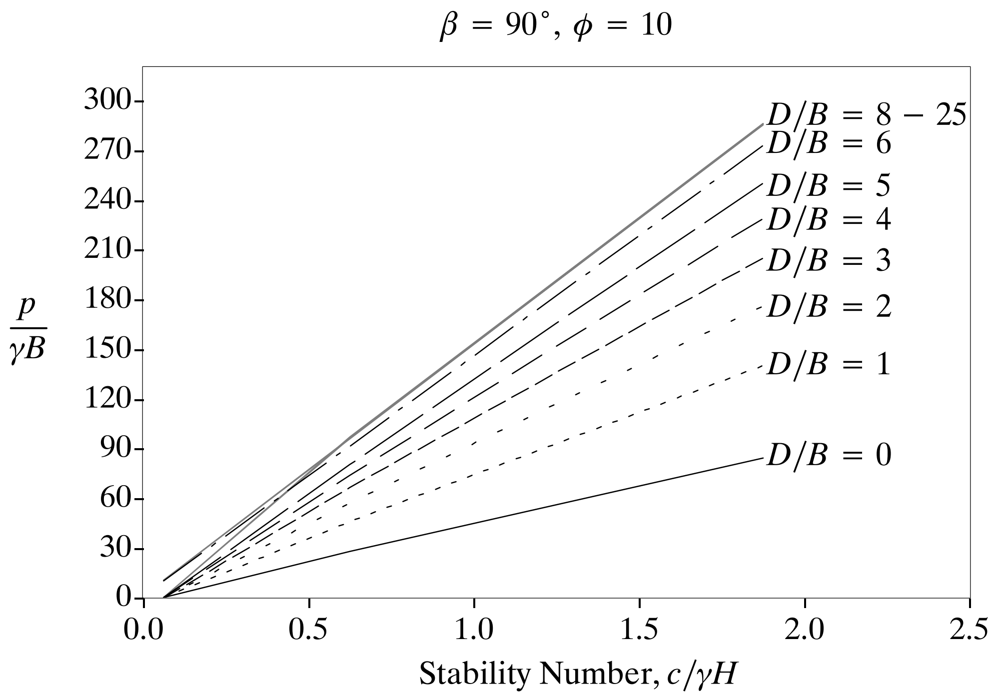

Figure F.37: Change in Normalised Bearing Capacity with Stability Number

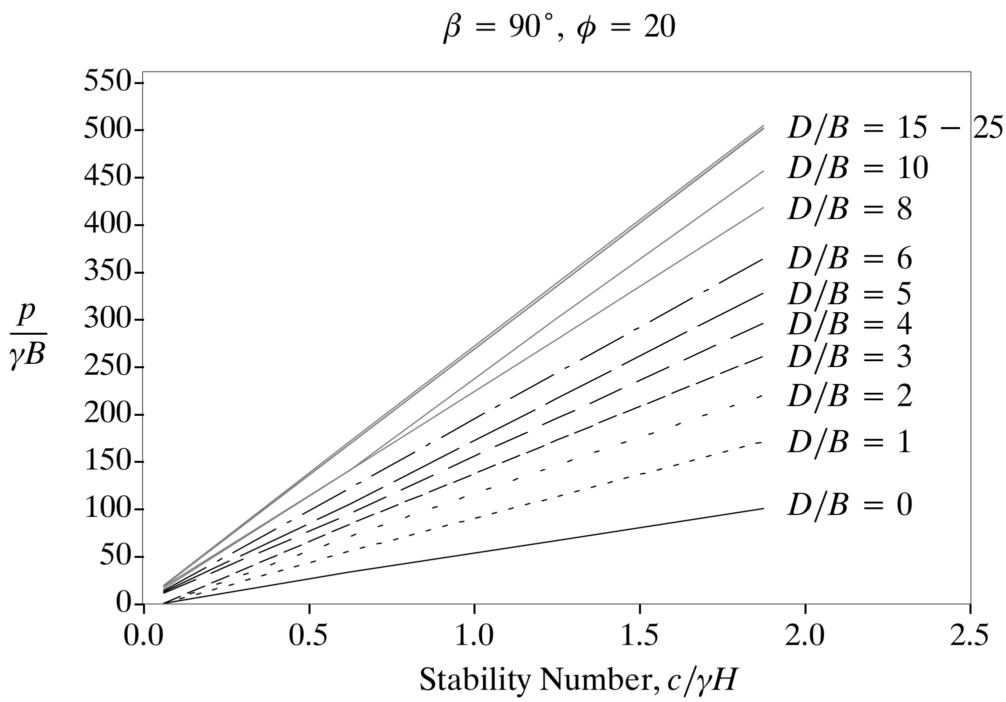

Figure F.38: Change in Normalised Bearing Capacity with Stability Number

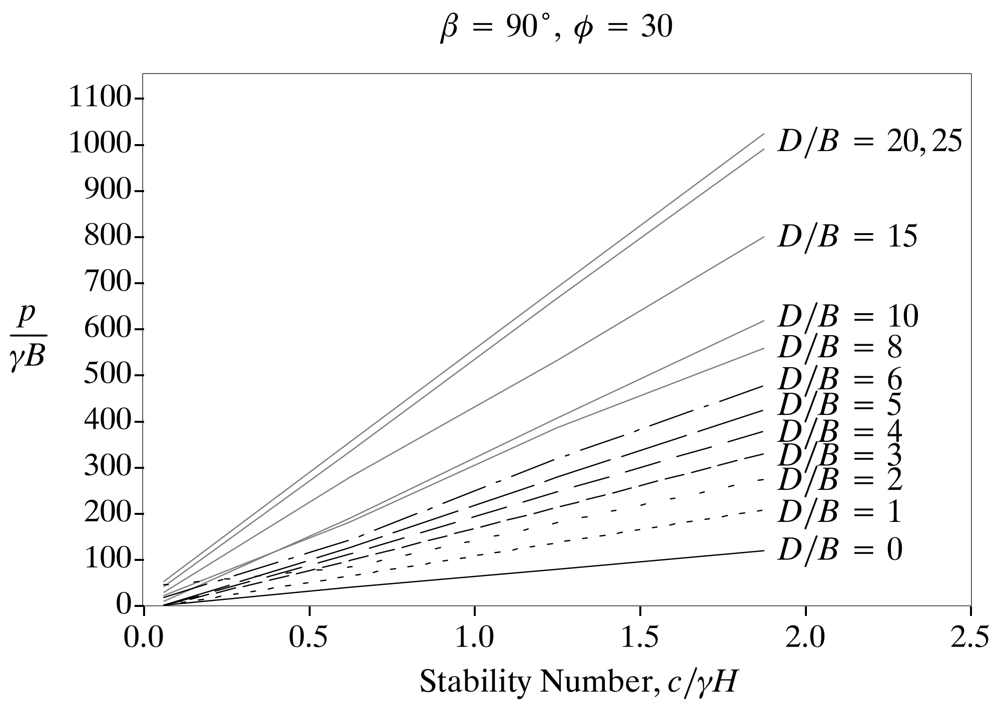

Figure F.39: Change in Normalised Bearing Capacity with Stability Number

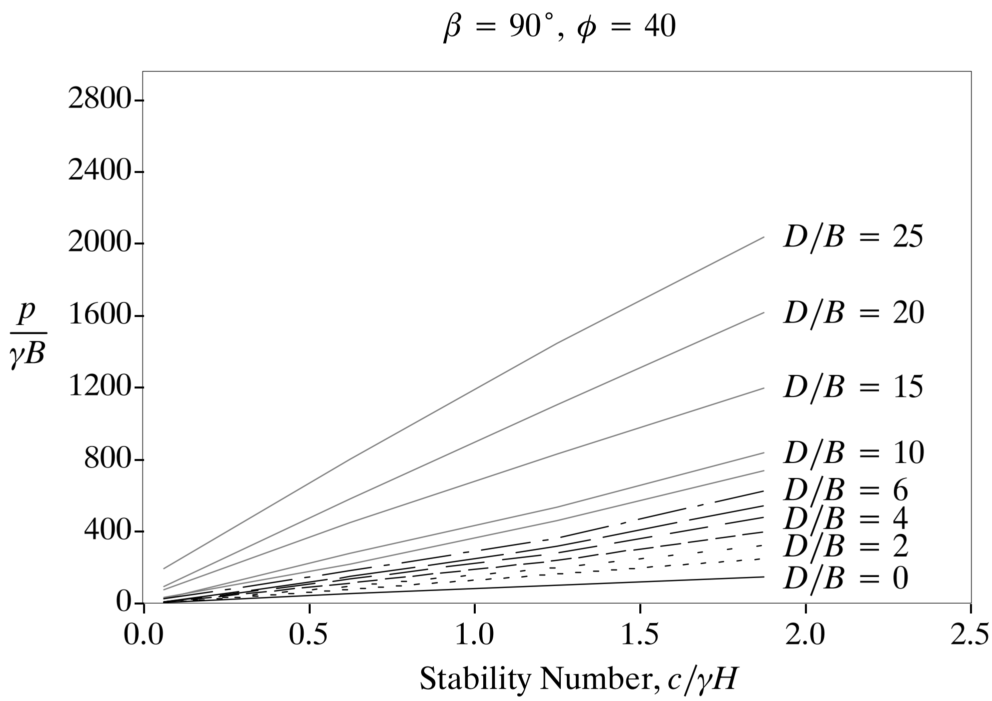

Figure F.40: Change in Normalised Bearing Capacity with Stability Number

8.7 Appendix G -

Data Used in Design Charts

The following tables contain the data that was used to during the numerical analysis and to create the design charts shown in this appendix.

Each table contains the data relating to one slope height, with all the other parameters that were varied (footing distance ratio, dimensionless strength ratio, internal friction angle) contained within each table.

90 Degree slopes	c/φ soils	qrB=0	Normalised Capacity			
H on B	D on B	SR	φ=10	φ=20	φ=30	φ=40
0	X	1	10.68	21.69	55.32	210.18
0	X	10	101.14	180.84	383.06	1069.99
0	X	20	198.14	351.53	724.77	1907.85
0	X	30	296.39	521.84	1062.31	2746.19

Table G.1: Data for H/B = 0

90 Degree slopes	c/φ soils	qrB=0	Normalised Capacity			
H on B	D on B	SR	φ=10	φ=20	φ=30	φ=40
1	0	1	3.02	4.37	8.51	28.37
1	1	1	6.42	11.72	26.25	100.18
1	2	1	8.78	15.77	35.63	128.53
1	3	1	10.17	18.51	41.25	143.53
1	4	1	10.88	20.57	45.30	151.75
1	5	1	10.89	21.19	48.71	226.10
1	6	1	10.29	17.99	36.76	96.73
1	8	1	10.05	18.33	37.95	98.13
1	10	1	11.14	21.19	50.85	187.53
1	15	1	10.14	21.16	50.93	186.91
1	20	1	9.95	18.32	50.87	185.26
1	25	1	10.14	18.34	50.91	186.30
1	0	10	31.71	43.69	72.49	164.40
1	1	10	62.60	99.10	189.98	533.95
1	2	10	78.73	125.69	243.44	639.24
1	3	10	89.21	142.59	265.77	689.47
1	4	10	96.12	155.96	290.02	726.35
1	5	10	96.35	166.31	307.65	730.51
1	6	10	95.74	167.24	310.63	733.07
1	8	10	95.89	167.60	323.85	775.45
1	10	10	96.31	170.57	352.37	899.80
1	15	10	95.60	170.69	352.49	944.83
1	20	10	95.71	167.60	351.83	936.07
1	25	10	95.60	167.72	352.44	945.26
1	0	20	63.75	87.29	143.02	303.33
1	1	20	125.38	195.79	371.12	999.93
1	2	20	155.91	246.19	459.73	1207.86
1	3	20	176.50	287.52	531.30	1293.74
1	4	20	180.20	304.87	554.53	1369.96
1	5	20	191.10	326.68	588.86	1417.70
1	6	20	190.60	333.35	600.99	1451.68
1	8	20	190.72	334.01	651.88	1539.60
1	10	20	191.23	337.15	686.03	1670.78
1	15	20	190.49	337.07	687.35	1771.33
1	20	20	190.40	334.00	684.05	1771.92
1	25	20	190.66	334.00	686.20	1778.64
1	0	30	96.30	131.51	213.54	438.31
1	1	30	187.86	293.65	548.93	1456.34
1	2	30	232.94	364.98	678.37	1743.80
1	3	30	263.60	411.92	752.12	1866.40
1	4	30	283.38	449.26	807.90	1949.23
1	5	30	285.12	481.10	856.44	2010.52
1	6	30	285.27	499.62	897.51	2141.94
1	8	30	285.20	500.61	979.87	2268.67
1	10	30	285.70	503.45	1016.23	2446.71
1	15	30	285.04	503.68	1016.62	2611.96
1	20	30	285.37	500.63	1016.55	2625.14
1	25	30	285.23	500.64	1017.36	2643.04

Table G.2: Data for H/B = 1

90 Degree slopes	c/φ soils	qrB=0	Normalised Capacity			
H on B	D on B	SR	φ=10	φ=20	φ=30	φ=40
2	0	1	2.98	3.82	4.70	6.77
2	1	1	5.36	7.10	10.75	23.87
2	2	1	6.86	10.12	16.72	44.52
2	3	1	8.23	12.81	22.15	59.33
2	4	1	9.20	14.61	25.49	69.27
2	5	1	10.00	16.70	28.87	73.47
2	6	1	10.13	17.40	32.46	76.48
2	8	1	10.30	18.26	36.81	85.78
2	10	1	10.15	18.40	37.96	91.94
2	15	1	10.15	18.38	38.69	100.53
2	20	1	10.16	18.33	38.71	106.24
2	25	1	10.17	18.40	38.70	106.64
2	0	10	28.42	34.08	42.42	57.45
2	1	10	50.23	65.59	95.35	165.29
2	2	10	65.49	90.03	141.85	285.58
2	3	10	77.25	111.65	179.74	377.78
2	4	10	86.96	129.58	214.04	447.87
2	5	10	94.77	142.72	241.89	503.45
2	6	10	95.58	154.63	269.12	554.54
2	8	10	95.62	167.73	291.32	647.49
2	10	10	95.64	167.77	324.70	725.48
2	15	10	95.77	167.63	340.06	807.20
2	20	10	95.67	167.72	340.54	863.71
2	25	10	95.99	167.80	343.58	866.15
2	0	20	56.59	68.24	83.85	112.89
2	1	20	99.84	130.40	189.64	315.47
2	2	20	130.60	182.06	281.82	545.49
2	3	20	153.82	221.84	362.14	733.90
2	4	20	173.80	256.15	423.67	866.59
2	5	20	188.54	283.99	472.31	978.13
2	6	20	190.60	307.53	519.10	1096.98
2	8	20	190.64	334.19	588.92	1242.25
2	10	20	190.58	333.96	646.72	1412.32
2	15	20	190.59	334.16	670.59	1633.89
2	20	20	190.53	334.08	671.18	1707.36
2	25	20	190.59	334.13	671.97	1709.22
2	0	30	84.88	101.76	125.71	167.53
2	1	30	149.34	195.95	283.17	467.30
2	2	30	196.25	271.29	435.62	808.29
2	3	30	232.64	332.13	561.40	1112.73
2	4	30	261.08	383.89	631.12	1312.67
2	5	30	282.47	426.01	709.30	1508.82
2	6	30	285.29	462.72	794.61	1627.45
2	8	30	285.32	500.35	880.53	1860.39
2	10	30	285.44	500.79	970.68	2078.86
2	15	30	285.19	500.76	1003.97	2377.19
2	20	30	285.16	500.53	1006.41	2565.53
2	25	30	285.29	500.54	1009.10	2544.20

Table G.3: Data for H/B = 2

90 Degree slopes	c/φ soils	qrB=0	Normalised Capacity			
H on B	D on B	SR	φ=10	φ=20	φ=30	φ=40
3	0	1	1.99	2.29	3.08	4.44
3	1	1	2.61	4.01	6.26	11.24
3	2	1	3.93	6.58	11.78	25.48
3	3	1	5.60	9.68	18.63	46.37
3	4	1	7.15	13.13	26.09	67.31
3	5	1	8.67	16.11	33.05	85.97
3	6	1	10.15	16.46	26.50	58.14
3	8	1	10.18	17.61	32.88	69.03
3	10	1	10.94	21.26	50.84	162.74
3	15	1	10.95	21.26	50.84	184.04
3	20	1	10.19	18.30	50.76	184.22
3	25	1	10.26	18.35	50.88	186.67
3	0	10	27.54	32.74	38.62	50.70
3	1	10	46.00	56.61	74.16	107.31
3	2	10	59.28	85.68	111.68	177.25
3	3	10	70.85	97.22	146.85	259.32
3	4	10	81.05	115.66	181.32	338.18
3	5	10	89.80	132.41	212.31	416.34
3	6	10	85.76	142.25	230.21	429.12
3	8	10	95.70	164.34	277.87	527.83
3	10	10	96.35	170.55	335.66	728.32
3	15	10	96.32	170.87	352.68	904.65
3	20	10	95.70	167.62	352.79	943.76
3	25	10	95.69	167.63	352.05	940.30
3	0	20	55.63	66.11	77.69	99.89
3	1	20	93.27	115.60	148.81	211.13
3	2	20	119.75	157.32	220.87	383.86
3	3	20	142.58	194.42	287.31	495.57
3	4	20	162.39	229.06	355.71	640.98
3	5	20	179.85	260.35	415.30	760.77
3	6	20	190.48	283.76	445.74	857.54
3	8	20	190.42	327.11	551.00	1035.63
3	10	20	191.11	336.97	626.68	1351.36
3	15	20	191.37	336.99	684.26	1619.94
3	20	20	190.48	334.18	684.43	1779.74
3	25	20	190.49	334.05	684.05	1772.38
3	0	30	84.80	100.68	116.55	148.33
3	1	30	142.29	175.96	224.95	313.83
3	2	30	182.33	237.67	331.01	510.02
3	3	30	216.11	290.89	418.56	728.32
3	4	30	245.13	341.10	517.02	915.68
3	5	30	269.48	386.20	596.81	1128.33
3	6	30	285.11	424.61	676.79	1288.71
3	8	30	285.12	489.85	791.32	1533.37
3	10	30	285.98	503.65	927.94	1928.47
3	15	30	285.87	503.78	1016.69	2384.15
3	20	30	284.96	500.47	1015.20	2628.41
3	25	30	285.19	500.61	1018.58	2652.74

Table G.4: Data for H/B = 3

90 Degree slopes	c/φ soils	qrB=0	Normalised Capacity			
H on B	D on B	SR	φ=10	φ=20	φ=30	φ=40
4	0	1	2.99	3.59	4.38	5.65
4	1	1	5.05	6.16	7.88	10.61
4	2	1	6.40	7.99	11.04	16.47
4	3	1	7.34	9.76	14.23	23.82
4	4	1	8.40	11.72	17.61	31.02
4	5	1	9.24	12.79	20.39	37.71
4	6	1	10.07	15.18	23.19	44.70
4	8	1	10.10	17.69	28.33	57.38
4	10	1	10.16	18.33	33.68	68.54
4	15	1	10.19	18.36	38.79	91.61
4	20	1	10.11	18.36	38.74	103.88
4	25	1	10.01	18.27	38.71	106.49
4	0	10	28.38	33.64	39.52	49.35
4	1	10	47.79	60.19	67.61	92.50
4	2	10	60.10	75.38	85.76	137.65
4	3	10	70.28	91.32	134.14	191.37
4	4	10	79.07	106.45	150.79	252.79
4	5	10	87.32	125.83	184.00	297.94
4	6	10	94.43	135.08	196.55	356.45
4	8	10	95.69	156.41	244.33	457.03
4	10	10	95.64	167.70	291.20	544.97
4	15	10	95.78	167.60	341.80	772.70
4	20	10	95.53	167.61	342.75	822.01
4	25	10	95.60	167.57	342.87	868.57
4	0	20	56.46	66.98	78.74	96.26
4	1	20	94.81	115.32	138.44	178.10
4	2	20	119.61	150.99	191.95	269.30
4	3	20	140.10	182.65	248.99	383.94
4	4	20	158.19	212.80	300.22	488.59
4	5	20	174.16	241.16	350.82	602.92
4	6	20	187.70	268.55	399.09	729.02
4	8	20	190.35	311.67	484.09	925.08
4	10	20	190.66	334.22	557.21	1060.77
4	15	20	190.83	333.99	671.59	1395.13
4	20	20	190.59	334.02	672.01	1586.06
4	25	20	190.77	334.09	675.31	1725.80
4	0	30	84.79	100.70	117.29	144.37
4	1	30	141.82	172.95	212.17	264.25
4	2	30	178.95	226.14	289.62	399.75
4	3	30	209.52	274.26	376.73	564.66
4	4	30	236.87	319.03	452.89	732.63
4	5	30	260.61	361.75	529.08	915.82
4	6	30	280.93	399.53	596.40	1060.34
4	8	30	285.31	466.21	733.83	1303.28
4	10	30	285.27	500.82	830.74	1566.56
4	15	30	285.29	500.48	1004.69	2087.55
4	20	30	285.08	500.62	1005.88	2396.13
4	25	30	285.19	500.62	1004.39	2556.45

Table G.5: Data for H/B = 4

90 Degree slopes	c/φ soils	qrB=0	Normalised Capacity			
H on B	D on B	SR	φ=10	φ=20	φ=30	φ=40
5	0	1	2.97	3.58	4.36	5.61
5	1	1	5.04	6.10	7.60	10.05
5	2	1	6.36	7.86	10.20	14.43
5	3	1	7.31	9.19	12.77	19.75
5	4	1	8.27	10.76	15.73	25.31
5	5	1	9.09	12.23	18.83	31.33
5	6	1	9.92	13.39	20.79	37.32
5	8	1	10.29	16.39	26.23	49.81
5	10	1	10.11	18.22	30.84	59.77
5	15	1	10.11	18.37	37.87	83.89
5	20	1	10.31	18.34	38.62	101.26
5	25	1	10.21	18.34	38.79	104.94
5	0	10	28.35	33.65	39.58	48.10
5	1	10	47.69	57.83	64.52	83.03
5	2	10	60.04	74.53	88.77	122.57
5	3	10	69.83	89.14	109.70	165.25
5	4	10	78.24	102.64	133.11	207.62
5	5	10	85.72	115.71	161.54	259.68
5	6	10	92.64	128.17	179.57	294.21
5	8	10	95.61	150.42	233.71	397.25
5	10	10	95.91	167.43	287.57	490.65
5	15	10	95.60	167.67	338.44	708.58
5	20	10	95.83	167.60	345.27	793.02
5	25	10	95.72	167.65	342.33	867.47
5	0	20	56.40	66.94	78.61	95.85
5	1	20	94.86	115.27	135.89	164.30
5	2	20	118.40	149.14	181.93	231.64
5	3	20	138.98	178.44	225.60	329.69
5	4	20	155.92	204.69	272.01	428.24
5	5	20	170.99	230.59	322.04	515.28
5	6	20	184.42	255.57	359.92	622.62
5	8	20	190.39	299.92	463.94	820.68
5	10	20	190.64	333.66	521.44	972.13
5	15	20	190.56	334.14	665.01	1330.29
5	20	20	190.73	334.17	671.22	1507.17
5	25	20	190.56	334.04	669.57	1702.22
5	0	30	84.75	100.67	118.93	143.72
5	1	30	141.94	172.64	208.84	253.33
5	2	30	178.68	223.38	277.22	352.16
5	3	30	208.14	267.29	345.11	470.20
5	4	30	233.42	306.37	415.93	618.20
5	5	30	255.90	345.15	495.15	781.09
5	6	30	276.14	382.94	548.65	900.14
5	8	30	285.44	448.80	669.93	1172.21
5	10	30	285.16	499.88	780.13	1382.64
5	15	30	285.35	500.76	999.01	1913.23
5	20	30	285.21	500.47	1005.10	2276.55
5	25	30	285.33	500.64	1004.17	2573.17

Table G.6: Data for H/B = 5

90 Degree slopes	c/φ soils	qrB=0	Normalised Capacity			
H on B	D on B	SR	φ=10	φ=20	φ=30	φ=40
6	0	1	-0.52	1.04	1.89	3.11
6	1	1	-1.80	1.00	2.81	4.49
6	2	1	-2.50	1.02	3.24	7.48
6	3	1	1.98	2.03	5.41	12.83
6	4	1	2.43	3.14	9.19	20.82
6	5	1	2.84	4.96	13.34	33.14
6	6	1	8.80	13.10	19.39	33.21
6	8	1	10.22	16.80	24.16	43.12
6	10	1	10.61	18.31	41.43	109.06
6	15	1	10.84	21.20	50.93	183.76
6	20	1	10.05	18.36	51.05	184.31
6	25	1	10.17	18.36	50.87	186.34
6	0	10	27.53	32.79	38.26	45.72
6	1	10	45.70	55.19	63.27	77.01
6	2	10	57.08	72.11	82.11	107.25
6	3	10	66.17	86.94	111.37	147.14
6	4	10	73.83	96.22	125.63	194.37
6	5	10	81.25	111.10	152.32	237.33
6	6	10	91.82	124.52	182.69	270.96
6	8	10	95.92	147.07	220.13	342.80
6	10	10	96.37	169.64	271.47	499.32
6	15	10	96.39	170.65	352.07	776.87
6	20	10	95.80	167.78	352.47	923.67
6	25	10	95.94	167.45	352.89	939.22
6	0	20	55.66	65.75	77.30	94.01
6	1	20	92.91	112.75	134.59	153.86
6	2	20	116.63	145.20	175.18	210.19
6	3	20	135.51	172.62	216.15	281.67
6	4	20	151.66	196.78	256.58	370.30
6	5	20	166.25	222.24	299.13	483.06
6	6	20	182.82	246.42	346.56	541.85
6	8	20	190.56	291.35	423.12	749.19
6	10	20	191.23	332.74	513.90	906.80
6	15	20	191.19	337.13	681.36	1384.84
6	20	20	190.54	334.15	684.12	1665.37
6	25	20	190.64	334.11	684.14	1784.76
6	0	30	83.99	99.74	117.24	142.19
6	1	30	139.86	170.23	205.80	246.46
6	2	30	176.01	219.40	271.52	323.04
6	3	30	204.64	260.69	328.92	421.30
6	4	30	228.97	297.84	393.00	548.00
6	5	30	250.74	334.91	455.45	690.32
6	6	30	273.58	372.38	517.43	793.70
6	8	30	285.20	435.81	631.59	1025.38
6	10	30	285.82	496.62	761.18	1364.54
6	15	30	285.96	503.56	1009.66	1917.41
6	20	30	285.26	500.63	1016.13	2360.03
6	25	30	285.26	500.77	1016.97	2643.71

Table G.7: Data for H/B = 6

90 Degree slopes	c/φ soils	qrB=0	Normalised Capacity			
H on B	D on B	SR	φ=10	φ=20	φ=30	φ=40
8	0	1	2.94	3.60	4.36	5.56
8	1	1	5.66	6.29	7.38	9.43
8	2	1	6.37	8.09	9.76	12.55
8	3	1	7.26	8.93	11.27	15.64
8	4	1	8.17	10.16	13.66	19.84
8	5	1	8.91	11.63	15.16	23.27
8	6	1	9.64	12.81	17.45	27.49
8	8	1	10.06	15.29	21.45	36.29
8	10	1	10.04	17.55	25.92	45.07
8	15	1	10.24	18.33	35.81	67.60
8	20	1	10.20	18.34	38.68	87.86
8	25	1	10.23	18.33	38.78	101.86
8	0	10	28.37	33.61	39.50	47.97
8	1	10	47.80	57.68	65.20	74.90
8	2	10	60.04	74.21	85.64	97.69
8	3	10	69.75	88.33	104.99	120.89
8	4	10	77.86	100.51	116.27	156.76
8	5	10	85.08	111.56	141.71	178.42
8	6	10	91.45	121.76	152.98	216.03
8	8	10	95.68	141.44	192.47	298.67
8	10	10	95.76	159.25	227.28	368.17
8	15	10	95.68	167.72	305.23	557.74
8	20	10	95.74	167.67	343.18	731.30
8	25	10	95.58	167.44	341.25	808.30
8	0	20	58.39	66.96	78.68	96.01
8	1	20	94.77	115.22	136.08	152.81
8	2	20	119.41	149.02	177.41	196.22
8	3	20	138.93	177.01	215.53	252.33
8	4	20	155.46	200.10	249.94	298.92
8	5	20	169.73	222.38	284.42	361.83
8	6	20	182.21	243.08	320.72	413.73
8	8	20	190.64	281.86	391.38	615.81
8	10	20	190.65	317.15	455.16	750.00
8	15	20	190.48	333.99	608.81	1032.95
8	20	20	190.44	334.10	671.65	1350.42
8	25	20	190.31	334.14	670.47	1555.86
8	0	30	84.72	100.65	118.44	143.78
8	1	30	141.93	172.71	208.65	240.43
8	2	30	178.80	223.13	277.19	306.40
8	3	30	208.00	264.82	333.43	376.71
8	4	30	232.72	300.30	385.87	471.46
8	5	30	254.01	333.44	435.50	560.19
8	6	30	272.73	364.18	485.62	654.05
8	8	30	285.13	421.65	594.90	854.15
8	10	30	285.43	474.81	681.90	1058.01
8	15	30	285.36	500.72	908.77	1515.16
8	20	30	285.21	500.51	1007.26	2022.11
8	25	30	285.17	500.52	1002.53	2341.62

Table G.8: Data for H/B = 8

90 Degree slopes	c/φ soils	qrB=0	Normalised Capacity			
H on B	D on B	SR	φ=10	φ=20	φ=30	φ=40
10	0	1	-0.33	-0.44	-0.16	-0.12
10	1	1	-0.26	-0.25	-0.12	0.63
10	2	1	-0.25	-0.10	0.75	1.98
10	3	1	-0.18	0.02	1.86	3.49
10	4	1	-0.19	0.16	2.31	6.07
10	5	1	-0.18	1.47	3.85	10.24
10	6	1	8.64	12.34	16.61	24.07
10	8	1	10.28	14.69	20.00	31.62
10	10	1	5.43	11.22	21.99	56.79
10	15	1	10.72	20.78	49.69	128.62
10	20	1	10.23	18.31	50.88	184.99
10	25	1	10.19	18.33	50.84	184.69
10	0	10	27.51	32.75	38.22	45.88
10	1	10	45.70	56.20	63.66	75.86
10	2	10	57.12	70.74	81.45	91.62
10	3	10	66.18	83.59	97.02	115.66
10	4	10	73.56	94.28	111.74	137.82
10	5	10	80.22	104.19	127.72	171.08
10	6	10	91.52	121.47	155.32	191.44
10	8	10	95.68	140.04	182.97	254.20
10	10	10	96.27	150.33	222.70	378.90
10	15	10	96.34	170.65	322.51	612.08
10	20	10	95.81	167.67	352.20	806.54
10	25	10	95.59	167.46	352.40	935.04
10	0	20	55.61	66.06	77.17	93.98
10	1	20	92.91	112.74	134.60	157.61
10	2	20	116.57	145.19	181.32	196.72
10	3	20	135.55	172.08	211.11	238.92
10	4	20	151.45	194.82	244.11	288.40
10	5	20	165.46	216.14	272.33	336.60
10	6	20	182.19	242.52	319.10	393.17
10	8	20	190.44	279.17	386.74	500.00
10	10	20	191.25	307.20	440.67	682.82
10	15	20	191.12	337.05	599.12	1061.11
10	20	20	190.50	334.25	685.31	1406.09
10	25	20	190.68	334.19	684.57	1702.40
10	0	30	83.96	99.77	117.11	142.73
10	1	30	140.00	170.28	206.41	242.83
10	2	30	176.00	219.44	272.52	318.49
10	3	30	204.60	260.14	328.58	369.78
10	4	30	228.89	295.78	377.09	443.29
10	5	30	250.04	327.16	422.93	536.91
10	6	30	272.77	363.38	476.12	616.74
10	8	30	285.24	417.60	563.51	810.30
10	10	30	285.85	462.38	652.84	1005.96
10	15	30	285.89	503.84	887.26	1490.48
10	20	30	285.16	500.71	1015.57	2006.05
10	25	30	285.05	500.60	1016.34	2401.73

Table G.9: Data for H/B = 10

90 Degree slopes	c/φ soils	qrB=0	Normalised Capacity			
H on B	D on B	SR	φ=10	φ=20	φ=30	φ=40
13	0	1	2.97	3.59	4.39	5.56
13	1	1	5.04	6.27	7.42	9.21
13	2	1	6.34	8.05	9.53	11.52
13	3	1	7.27	9.15	11.27	13.29
13	4	1	8.16	9.93	13.06	16.41
13	5	1	8.97	11.59	14.50	18.94
13	6	1	9.64	12.49	15.71	22.15
13	8	1	10.17	14.83	20.49	26.80
13	10	1	10.18	17.07	22.01	34.38
13	15	1	10.19	18.30	31.76	53.04
13	20	1	10.05	18.35	37.55	69.64
13	25	1	10.19	18.34	38.74	89.92
13	0	10	28.34	33.60	39.49	47.95
13	1	10	47.72	57.84	65.21	74.79
13	2	10	60.06	76.45	85.34	93.21
13	3	10	69.77	90.01	101.87	112.44
13	4	10	77.88	100.56	116.87	137.63
13	5	10	85.14	111.51	125.08	154.75
13	6	10	91.35	121.43	143.24	177.52
13	8	10	95.87	139.83	178.86	230.75
13	10	10	95.51	155.89	207.79	292.03
13	15	10	95.61	167.70	280.53	482.04
13	20	10	95.73	167.72	338.10	591.33
13	25	10	95.72	167.53	340.02	771.67
13	0	20	56.38	66.92	78.70	94.89
13	1	20	94.79	115.23	136.00	155.80
13	2	20	118.51	149.00	176.49	193.13
13	3	20	138.87	176.94	214.11	232.64
13	4	20	155.44	200.06	252.67	285.97
13	5	20	169.75	222.00	284.61	318.03
13	6	20	182.25	242.57	317.35	359.32
13	8	20	190.49	278.85	369.10	456.10
13	10	20	190.45	310.43	421.98	584.95
13	15	20	190.49	334.06	546.53	855.47
13	20	20	190.45	333.96	663.31	1126.25
13	25	20	190.58	333.99	670.00	1356.93
13	0	30	84.75	100.68	118.48	143.74
13	1	30	141.94	172.81	208.89	244.92
13	2	30	178.75	223.12	277.17	317.75
13	3	30	208.02	264.89	334.08	378.30
13	4	30	232.65	300.38	384.82	460.85
13	5	30	254.11	333.25	431.67	524.57
13	6	30	272.81	363.44	475.08	606.67
13	8	30	285.29	417.25	555.63	732.71
13	10	30	285.25	464.80	631.49	879.04
13	15	30	285.32	500.48	820.26	1284.47
13	20	30	285.13	500.54	998.91	1611.46
13	25	30	285.24	500.44	1004.18	2027.67

Table G.10: Data for H/B = 13

90 Degree slopes	c/φ soils	qrB=0	Normalised Capacity			
H on B	D on B	SR	φ=10	φ=20	φ=30	φ=40
16	0	1	-0.22	-0.20	-0.11	-0.07
16	1	1	-0.19	-0.41	-0.19	-0.13
16	2	1	-0.26	-0.24	43.09	-0.09
16	3	1	-0.52	-0.21	-0.13	1.00
16	4	1	-0.21	10.24	-0.11	1.63
16	5	1	-0.21	11.74	-0.17	2.35
16	6	1	8.73	12.89	16.36	21.01
16	8	1	10.19	15.24	19.79	26.19
16	10	1	-0.27	17.30	8.29	19.91
16	15	1	-0.18	18.28	27.34	68.30
16	20	1	10.10	18.22	40.07	85.96
16	25	1	10.09	18.36	50.94	185.68
16	0	10	27.52	32.73	38.21	46.36
16	1	10	45.63	55.15	63.64	72.47
16	2	10	57.12	70.69	82.15	89.78
16	3	10	66.13	83.52	96.84	107.04
16	4	10	73.56	94.31	110.32	129.21
16	5	10	80.27	104.09	123.81	142.99
16	6	10	91.33	121.48	140.17	176.46
16	8	10	95.75	139.92	179.87	209.99
16	10	10	96.52	139.87	187.68	272.80
16	15	10	95.86	170.59	276.83	443.49
16	20	10	95.81	167.65	332.26	574.62
16	25	10	95.66	167.61	352.48	795.43
16	0	20	55.61	66.00	77.10	93.91
16	1	20	92.86	112.73	134.59	158.36
16	2	20	116.62	145.28	177.58	195.60
16	3	20	135.55	172.11	211.25	234.68
16	4	20	151.54	194.90	245.18	276.67
16	5	20	165.41	216.16	276.62	311.06
16	6	20	182.17	242.51	317.48	357.46
16	8	20	190.41	278.14	383.89	454.02
16	10	20	191.23	299.96	404.39	528.95
16	15	20	191.31	337.28	529.74	825.46
16	20	20	190.58	334.07	663.45	1097.85
16	25	20	190.59	334.08	687.77	1441.09
16	0	30	83.97	99.80	117.15	142.19
16	1	30	139.85	170.25	206.17	243.30
16	2	30	175.99	219.42	272.40	317.76
16	3	30	204.64	260.22	328.72	393.52
16	4	30	228.85	295.75	377.17	475.51
16	5	30	249.99	327.01	422.38	539.12
16	6	30	272.76	363.42	475.21	620.21
16	8	30	285.28	417.21	555.72	731.47
16	10	30	285.76	455.91	614.76	831.62
16	15	30	285.96	503.86	798.80	1191.82
16	20	30	285.22	500.42	987.50	1610.14
16	25	30	285.20	500.68	1020.43	2031.89

Table G.11: Data for H/B = 16